P-194

CR-174707
PWA-5628-69

IN - 35 98660

DATE OVERRIDE

NASA

THIN FILM STRAIN GAGE DEVELOPMENT PROGRAM
FINAL REPORT

Contract NAS3-21262

By

H.P. Grant
J.S. Przybyszewski
W.L. Anderson
R.G. Claing

December, 1983

Prepared For

NATIONAL AERONAUTICS AND SPACE ADMINISTRATION
Lewis Research Center
Cleveland Ohio 44135

by

Commercial Engineering
Pratt & Whitney
UNITED TECHNOLOGIES CORPORATION

1. Report No. NASA CR-174707	2. Government Accession No.	3.Recipient's Catalog No.
4. Title and Subtitle Thin Film Strain Gage Development Program		5. Report Date December , 1983
		6. Performing Organization Code
7. Author(s) H. P. Grant, J. S. Przybyszewski, W. L. Anderson, and R. G. Claing		8. Performing Org. Rept. No. PWA-5628-69
9. Performing Organization Name and Address UNITED TECHNOLOGIES CORPORATION Pratt & Whitney Engineering East Hartford, Connecticut 06108		10. Work Unit No.
		11. Contract or Grant No. NAS3-21262
12. Sponsoring Agency Name and Address NATIONAL AERONAUTICS AND SPACE ADMINISTRATION Lewis Research Center 21000 Brookpark Road; Cleveland, Ohio 44135		13. Type Rept./Period Covered Contractor Report
		14. Sponsoring Agency Code 505-31-52

15. Supplementary Notes

Project Manager: Frank G. Pollack
NASA Lewis Research Center; Cleveland, Ohio 44135

16. Abstract

Sputtered thin-film dynamic strain gages of 2 millimeter (0.08 inch) gage length and 10 micrometer (0.0004 inch) thickness were fabricated on turbojet engine compressor blades and tested in a simulated compressor environment. Four designs were developed, two for service to 600K (600°F) and two for service to 900K (1200°F). The program included a detailed study of guidelines for formulating strain-gage alloys to achieve superior dynamic and static gage performance. The tests included gage factor, fatigue, temperature cycling, spin to 100,000G, and erosion. One type of gage was further demonstrated on simulated turbine blade specimens to 1100K (1500°F). The durability of gage element, insulation, overcoats, and lead films was excellent to 1100K (limit of e tests), but the fatigue life of lead-film-to-wire attachment was limited above 600K. The thin film strain gage systgems are redy for use in dynamic stress surveys in engine tests with an expected life of about 50 hours at 600K. Further development of lead-wire attachments methods is required above 600K. Since the installations are 30 times thinner than conventional wire strain gage installations, and any alteration of the aerodynamic, thermal, or structural performance of the blade is correspondingly reduced, dynamic strain measurement accuracy higher than that attained with conventional gages is expected. The low profile and good adherence of the thin film elements is expected to result in improved durability over conventional gage elements in engine tests.

17. Key Words [Suggested by Author(s)] Sputtering Compressor Blades Strain Gages Thin Film Strain Gages Turbine Blades	18. Distribution Statement ████████████████ until STAR Category 35

19. Security Class (This Rept) UNCLASSIFIED	20. Security Class (This Page) UNCLASSIFIED	21. No. Pgs	22. Price *

FOREWORD

PRECEDING PAGE BLANK NOT FILMED

TABLE OF CONTENTS

TABLE OF CONTENTS (Continued)

SECTION 1.0

SUMMARY

The development of high-temperature thin-film dynamic strain gage systems has been conducted by Pratt & Whitney under a NASA program. The objective of this program was to establish a method for measurement of dynamic strain on compressor blades to 900K in turbojet engines during engine operation without disturbing the gas flow, altering the blade strains, or disturbing the metal temperature profiles. The method was to fabricate blade-mounted resistive strain gages by sputtering thin films of insulating materials and gage materials onto the blade, rather than attach wire strain gages to the blade surface by means of layers of cement or flame sprayed ceramics.

Thin-film resistive strain gages of 2 millimeter (0.08 inch) gage length and 10 micrometer (0.0004 inch) thickness, including insulation and protective overcoat, were developed. The installations are about 30 times thinner than conventional wire strain gage installations. Accuracy better than that attained with conventional gages is therefore expected. In addition, the low profile and strong adherence of the thin film elements is expected to result in improved durability over conventional gage systems in engine tests.

The thin-film strain gage development program was divided into two phases. The first phase was designated the Components Program and the second phase the Gage Program.

In the first phase, the Components Program, candidate materials and thin-film fabrication procedures were selected and tested. The selection was made on the basis of the principles governing physical, chemical, and electrical behavior of materials to optimize stability, durability, and accuracy of strain measurements at temperatures to 600K on blades of a titanium alloy (AMS 4928) and to 900K on blades of a steel alloy (Incoloy 901).

Design curves describing the interrelationships between geometrical parameters of thin film gage systems were developed to permit selection of film thicknesses to achieve a desired gage resistance and insulation resistance.

A systematic experimental program was then carried out to complete the Components Program. All combinations of four insulating layers (Si_3N_4, Al_2O_3, HfO_2, SiO_2) and two surface finishes (smooth and roughened) were fabricated and tested on actual compressor blades of the two blade materials. The 11 best combinations were then used as substrates for each of four candidate gage materials (Ni-30%Cr, Cu-45%Ni, Pt-20%W, Pd-30%Mo) resulting in a test matrix of 44 types of thin-film strain gage system on blades. Tests of the 44 types resulted in selection of four candidates, two for service to 600K on the titanium alloy blades and two for service to 900K on steel alloy blades. The best blade surface finish in all four cases was the smooth 0.1 micrometer polish. The two final candidate 600K systems, designated Type A and Type B, utilized Ni-30%Cr gages on Si_3N_4 insulation

material, and Cu-45%Ni gages on HfO_2 insulation, respectively. The two final candidate 900K systems, designated Type C and Type D, utilized Ni-30%Cr gages on Si_3N_4 and on Al_2O_3, respectively. Eight methods for lead wire attachment were tested briefly and conductive cements were adopted for use in the program.

In the second phase, the Gage Program, the four gage types (A, B, C, D) were tested on flat test specimens of the compressor blade materials. Modified Type D gage installations (Type E) were tested on flat test specimens of MAR-M200 + Hf turbine blade material. The total number of thin film strain gages fabricated in the Gage Program was 168.

The tests in the Gage Program for each of the five gage types included measurement of gage factor versus temperature, apparent strain versus temperature, durability and drift during fifty thermal cycles (each cycle including 20 minutes at design temperature), fatigue at room temperature (10^7 strain cycles), fatigue at design temperature (10^7 strain cycles), and effect of erosion at room temperature. In addition, samples of Type A and Type C were subjected to a one-hour spin test at 100,000G at room temperature.

The durability of the gage elements, insulation, overcoats and lead films was demonstrated to be excellent, but the fatigue life of lead-film-to-lead-wire attachments was limited above 600K. The thin film strain gage systems are ready for use in dynamic stress surveys in engine tests with an expected life of 50 hours at 600K. Further development of lead-wire attachment methods is required to extend the expected life at temperatures above 600K to 50 hours or more.

On compressor blades of the titanium alloy AMS 4928 for service to 600K, the Type A thin film strain gage is recommended. After initial fabrication problems were overcome in the Gage Program, fabrication and testing of these Type A gages proceeded with no failures. For the competing Type B gages, rejection rate during fabrication remained high.

On simulated compressor blades of the nickel steel alloy Incoloy 901 for service to 900K, the Type C and Type D gages performed well, but expected service life in engine tests is limited to a few hours above 600K by the present lead-film-lead-wire attachment durability. Type C is recommended over Type D because of a much better success rate (lower cost) in fabrication.

On simulated turbine blades of the nickel-based superalloy MAR-M200 + Hf, the Type E thin film strain gages performed well to 1100K (limit of tests) and were notably free of fabrication problems, but, like Type C and D, expected service life in engine tests is limited by the present lead-wire attachment durability.

SECTION 2.0

INTRODUCTION

2.1 · BACKGROUND AND PRIOR EXPERIENCE

Compressor blade dynamic strain measurement by blade-mounted sensors is currently accomplished with strain gages embedded in layers of cement or flame-sprayed ceramics typically 0.3 mm (0.012 inch) thick on the blade surface. The uncertainty in this method of measurement cannot be readily determined in actual engine tests but can be 50 percent or more in unfavorable cases due to disturbance of gas flow and thermal profiles as well as alteration of blade stiffness and damping. As blade thicknesses are decreased in the high-pressure compressor and turbine stages, the presence of the bulky wire gages becomes more adverse both from a structural and a measurement viewpoint. It is desirable to have a surface-mounted strain sensor which is of such minimum mass and thickness that it causes no serious alternation of dynamic strain within the blade or gas flow distortion over the blade.

Using various thin film techniques (plating, vacuum evaporation, vacuum sputtering), a sensor can be formed by depositing layers of electrical insulating materials and metals whose thickness is only a few micrometers (μm). Successful surface thermocouples were obtained in this way by Burger in 1930 (Reference 1), Harris in 1934 (Reference 2), and Benderskey in 1953 (Reference 3). On metal parts the technique was limited to temperatures below 800K because adherence of deposited films of insulation materials was poor when cycled above 800K. More recently thin film thermocouples, durable and accurate to 1250K on turbine blades, were developed at Pratt & Whitney under a NASA program (Reference 4). This work and other recent thin film work at Pratt & Whitney are summarized in Table I.

The work described in column 1 of Table I was performed by Dils (Reference 5), using solid FeCrAlY test pieces oxidized in air to form an insulating layer of aluminum oxide. An additional amount of aluminum oxide was then sputtered on this grown aluminum oxide. The thermocouple legs were then sputtered on this insulator, and tests at 1350K were performed. This combination of fabrication methods and materials was able to withstand the high temperatures. Thermal electromotive force (emf) was within 1.5 percent of standard reference Type S wire thermocouple, while a 600K temperature gradient was imposed along the length of the thin film. Drift in thermoelectric emf was generally less than 0.01 percent per hour at constant temperature in air, over a period of 150 hours (Reference 6), at one atmosphere pressure.

The work described in columns 2, 3, 4 and 5 of Table I was performed by Przybyszewski (unpublished). In furnace tests on flat specimens (column 2), a typical turbine blade material (MAR-M200 plus hafnium) was coated with a typical alumina-forming protective material (NiCoCrAlY); then platinum versus platinum/10-percent rhodium thermocouples, 2 μm thick, were sputtered on a furnace-grown Al_2O_3 layer on the NiCoCrAlY coating and tested to 1250K to demonstrate the feasibility of use on standard engine hardware. Film strain gages were also tested (column 3), and film erosion samples were prepared

TABLE I

REVIEW OF PRATT & WHITNEY AIRCRAFT EXPERIENCE
WITH SPUTTERED THIN-FILM SENSORS
ON McrAlY SUBSTRATES AT HIGH TEMPERATURES

	1	2	3	4	5	6
Date	1972 - 1975	1975 - 1976	1976	1976	1977	1979 - 1982
Type of Sputtered Sensor	Thermocouples	Thermocouples	Strain gage	Erosion samples	Thermocouples	Thermocouples
Sputtered Film	Pt/Pt-10% Rh	Pt/Pt-10% Rh	Platinum	Platinum	Pt/Pt-10% Rh	Pt/Pt-10% Rh
Film Thickness	2 to 12 m	2 m	2 m	2 m	2 m	2 to 14 m
Substrate Coating	---	NiCoCrAlY	NiCoCrAlY	NiCoCrAlY	NiCoCrAlY	NiCoCrAlY CoCrAlY
Base Material	FeCrAlY	MAR-M-200 + hafnium	Hastelloy X	B1900 + hafnium	B1900 + hafnium	MAR-M-509 B1900 + hafnium IN1000 MAR-M-200 + hafnium
Lead-Wire-to-Film Connection	Strap weld	Fired platinum paste	Fired platinum paste	None	Fired paste	Hot compression bond
Configuration	Erosion bars, rods, cylinders, and airfoils	Flat bar	Strain bar	JT9D 1st-stage turbine blades	JT9D 2nd-stage turbine vanes	Flat bars and JT9D turbine blades
Test Facility	Lab combustor	Lab furnace	Lab furnace	Operating engine	Operating engine	Furnace, torch, and combustor
Time Above 1250K, Each Sensor	100 hours	170 hours	32 hours	150 hours	60 hours	60 hours
Typical Cycles to 1250K, Each Sensor	100	6	1			50
Reference Publications	(5) (6)	---	---	---	---	(4)
Remarks	20 specimens tested for proof of calibration stability	Instrumented specimen for proof of calibration stability	Strain test specimen	Engine erosion test	Metal temperature and heat transfer coefficient	Developed lead wire attachments and ran extended hot calibrations of thin film thermocouples

and tested (column 4) to further evaluate possible applications and assess potential problems. The strain gage tests demonstrated the feasibility of miniaturization of instrument sensor systems with pattern line widths down to 75 μm, and the erosion tests proved the capability of thin film metal coatings to survive under engine conditions without prohibitive deterioration. Finally, an engine test of thin film thermocouple devices was performed with sensors mounted on turbine vanes (column 5). Although problems occurred with the thin-film-to-lead-wire connections, the thin-film thermocouple sensors on the vanes survived engine operating conditions for 60 hours in most cases.

The work in column 6 of Table I was performed under the NASA program (Reference 4). Reliable lead wire attachments for the thin film thermocouples were developed, feasibility of sputtered thermocouples on four different turbine blade and vane alloys was demonstrated, and thermocouple drift of less than 0.02 percent of Fahrenheit temperature per hour was demonstrated on actual turbine blades at 1250K (1800°F) in combustor flow tests and oven tests.

2.2 OBJECTIVES

The objectives of the Thin Film Strain Gage Development Program, the subject of this document, conducted under Contract NAS3-21262, were as follows:

a. Establish the technology for producing thin film dynamic strain gage systems directly on compressor blades, with gage length and width less than 6mm and gage thickness less than 25 μm.

b. Demonstrate the performance of the strain gage systems under the following simulated compressor operating conditions:

o Temperature from ambient to 900K (1200°F);
o Steady strain to +1000 x 10^{-6} and -1000 x 10^{-6};
o Vibratory strains to +350 x 10^{-6} superimposed on a steady strain of +400 x 10^{-6};
o Centripetal acceleration levels up to 100,000G for at least one hour
o Erosion effects of high-velocity (approximately Mach 1.0) particle-laden air jet impinging on the sensors and lead films.

c. Analyze two separate classes of sensor systems, one for application to 600K (600°F) and the other for application to 900K (1200°F). Develop two most-promising sensor system candidates for each of the two temperature environments. Subject a number of specimens of each gage type to gage factor, thermal cycle, fatigue, and erosion tests. Subject selected types to a spin test.

d. In addition, apply a selected thin film strain gage system to turbine blade material specimens, and perform gage factor, thermal cycle, fatigue, and erosion tests. Extend the gage factor test to 1100K (1500°F) on the turbine blade material system.

2-3

2.3 DESCRIPTION OF PROGRAM

The program was conducted in two phases. The first phase, designated the Components Program, included an analysis of materials and procedures and a testing program to develop technology for application of thin film strain sensors to compressor blades. Two separate classes of sensor systems were analyzed, one for applications up to 600K and the other for applications up to 900K.

In the second phase, designated the Gage Program, the basic technology evolved in the Components Program was applied to the design and development of two most-promising sensor system candidates for each of two temperature environments. Flat bar specimens were instrumented with thin film strain gage systems. From the total of 168 strain gages fabricated, selected samples were subjected to gage factor, fatigue, thermal cycle, erosion and spin tests, over the range of specified test conditions. In addition, samples of one type of thin film strain gage system were applied to turbine blade material specimens and tested, with gage factor testing extended to 1100K (1500°F).

SECTION 3.0

TECHNICAL DISCUSSION OF THIN FILM STRAIN GAGE APPROACH

3.1 BASIC STRAIN GAGE PRINCIPLES

A resistive strain gage system is shown in Figure 1. The bridge circuit shown is powered from a constant voltage source, E_1. Each of the four arms of the bridge has a nominal resistance of R_0 ohms.
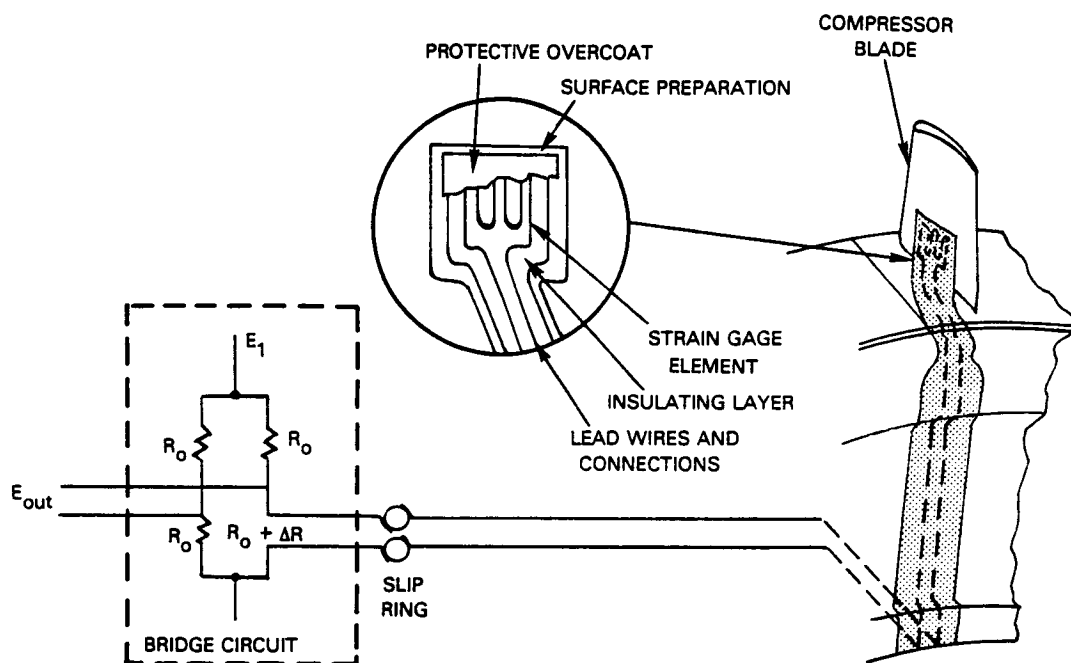
Figure 1   A Resistive Strain Gage System for Dynamic Strain Measurement.

One arm is a resistive strain gage whose unstrained resistance is also R_0 (ohms) and whose gage factor is G, defined as:

$$G = \frac{\Delta R/R_0}{\varepsilon} \tag{1}$$

where ΔR (ohms) is the resistance increment due to strain increment ε (cm/cm). The output voltage, E_{out}, from the bridge is described accurately by the following equation when the strain is less than 10 percent:

$$E_{out} = \frac{E_1 G}{4} \left[\left(\varepsilon + \frac{(\Delta R)_{other}}{GR_0} \right) \left(1 - \frac{1}{2} \frac{(\Delta R)_{other}}{R_0} \right) + \left(\frac{2}{G} \frac{(\Delta E)_{other}}{E_1} \right) \right] \tag{2}$$

3-1

In this equation, $(\Delta R)_{other}$ is any stray resistance change, in any arm of the bridge circuit, not due to strain in the strain gage. Examples of this change include resistance changes in the slip ring, lead wires, lead wire connectors, bridge resistors, or resistance changes in the strain gage itself due to temperature effects, metallurgical changes with time at temperature, or to changes in shunting resistance of insulating layers. In particular, a temperature change may affect the gage resistance itself in several ways, including change in resistivity of the gage material with temperature, change in dimension with temperature due to mismatch of expansion coefficients of gage and substrate, and drift in resistivity with time at temperature due to slow metallurgical changes.

$(\Delta E)_{other}$ is any stray voltage which may appear in any one arm of the bridge circuit, e.g., stray thermocouple e.m.f., piezoelectric voltages, magnetostrictive voltages, ground loops, electromagnetic pickup.

In designing and fabricating resistive strain gage systems, careful attention must be given to minimizing or correcting for all sources of false strain indication represented by $(\Delta R)_{other}$ and $(\Delta E)_{other}$ in Equation 2.

If the strain is unsteady (due to blade vibration or buffeting) then the total strain at any instant is the sum of the steady state component, ε_s, commonly called the static strain and the unsteady component $d(\varepsilon)$ commonly called the dynamic strain. The relationship between the unsteady component of bridge output voltage, $d(E_{out})$, and dynamic strain, $d(\varepsilon)$, is obtained by writing the first derivative of Equation 2, for constant values of $(\Delta R)_{other}$ and $(\Delta E)_{other}$:

$$d(E_{out}) = \frac{E_1 G}{4} d(\varepsilon) \left(1 - \frac{(\Delta R)_{other}}{2R_0}\right) \text{ for } \begin{matrix} (\Delta R)_{other} = constant \\ (\Delta E)_{other} = constant \end{matrix} \qquad (3)$$

It is evident from Equation 3 that in the measurement of dynamic strain the presence of a constant $(\Delta E)_{other}$ contributes no error and a constant $(\Delta R)_{other}$ contributes error only by effectively altering the gage factor. Examination of Equation 3 leads to the concept of an apparent gage factor defined by:

$$G \left(1 - \frac{(\Delta R)_{other}}{2R_0}\right) = apparent\ gage\ factor \qquad (4)$$

For example, a 10 percent change in the resistance in any one arm of the bridge results in a 5 percent change in apparent gage factor. The resistance of strain gages commonly employed for dynamic strain measurements at temperatures above 400K can easily drift by 10 percent or more. This drift occurs unless meticulous care is exercised in preliminary heat cycling of the installation to assure proper cure of cements employed and stabilization of the sensor metal alloy and lead wire junction resistances. In addition, the temperature coefficient of resistance (α) of the sensor must be below 400 ppm/K (parts per million per Kelvin) to maintain less than 10 percent change in apparent gage factor over a 500K temperature range, even assuming that the gage factor itself is constant with temperature.

In the discussion so far it has been assumed that the actual gage factor G is a constant for any given strain gage, invariant with temperature, and invariant with drift in gage resistance. In fact, the gage factor typically decreases by ten percent or more as temperature increases to 900K, and in addition probably changes with time (at high temperature) due to metallurgical changes in the gage alloy. This is to say that gage factor itself probably depends on that portion of $(\Delta R)_{other}$ which is the result of gage resistance changes with temperature and time. These effects are poorly documented in the literature. One result is that simply rebalancing the bridge by adding or subtracting resistances in another arm of the bridge does not guarantee a constant apparent gage factor and may even increase the measurement error. For this reason, in practice, the bridge balance setting is not ordinarily readjusted during the course of an engine test program.

From this discussion it is worth noting that the term "dynamic strain" as employed in the industry, and described by Equation 3, describes any sequence of strain measurements during which the rate of change of strain is large compared with the rate of change of $(\Delta R)_{other}$ or $(\Delta E)_{other}$. Equation 3 remains true even if the time period of the strain cycle or transient is long, provided that the strain change occurs nearly isothermally (so that gage resistance change due to temperature is small) and provided that all electrical quantities in the strain gage circuit are stable over the time period of the strain cycle.

If a true constant-current bridge is employed in place of the constant voltage bridge, the effects of $(\Delta R)_{other}$ and $(\Delta E)_{other}$ are reduced by about a factor of two. In practice, the bridges employed usually lie between constant voltage and true constant-current operation.

Installation of a thin-film dynamic strain gage on a compressor blade requires consideration of the following system components indicated in Figure 1:

1. Compressor blade material
2. Surface preparation
3. Insulating film
4. Strain gage film
5. Lead film
6. Overcoat film
7. Lead wire connection

Each of these system components is discussed individually in the remainder of this section, after a background discussion of the thin film fabrication process. Each must be designed for durability in the compressor environment (versus oxidation, erosion, thermal expansion stresses, fatigue, strain range, and centrifugal loading) and for stability of apparent gage factor in service. For completeness, design considerations affecting static strain measurement accuracy are also noted in the following discussions.

3.2 THIN FILM FABRICATION PROCESS

Sputtered thin film technology is the selected approach for thin film strain gage insulating layers, sensors and overcoats. Several other film deposition techniques are available including chemical plating, fired pastes, and various evaporation techniques. The sputtering technique provides the following unique advantages:

o   Thin films of virtually any material can be produced, including conductors, semiconductors, pure metals, alloys, compounds, and polymers.

o   High density films with properties approaching bulk material properties can be achieved.

o   Repeatability of surface conditions during the deposition process can be assured by sputter etching and bias sputtering, resulting in improved adherence and uniform properties from batch to batch.

By using high-resolution masking techniques, (e.g., photomasks) thin film sputtered strain gage systems with line widths as small as 10 micrometers (μm) can be achieved. Thickness of a few μm in the insulating layer, sensor, and overcoat layer or layers is achieved in a few hours of sputtering. Complex patterns, in areas less than 6 mm x 6 mm, on flat or curved surfaces, are readily produced.

The sputtering process produces thin films by continuously transferring molecule-sized particles from a source "target" to the work piece under the action of a low pressure gas plasma (ionized gas). High-energy ionized gas molecules strike a target, dislodging target material molecules. The target molecules travel at high velocity to strike the work piece and form a dense adherent film. The process can be reversed ("sputter- etching") to remove surface material from the work piece and provide an atomically clean surface. The gas may be inert or reactive, permitting many variations in the process.

The sputtering process has been studied for over 100 years, and an excellent description of the modern process is given by Vossen and O'Neill in Reference 7.

Sputtered strain-gage pressure transducers are produced commercially (Reference 8) and are notable for their excellent stability to 500K.

Sputtered thermocouples have been operated successfully to 1000K in gas turbine engines by Liebert at NASA (Reference 9) and to 1250K at P&WA on turbine blades in combustor rigs under a NASA funded development program (Reference 4).

Factors affecting stability, resistivity, and α of thin films are critical in strain gage systems and are further discussed here.

Because of the nature of the sputtering process, a thin sputtered film cannot necessarily be expected to behave like a slice of bulk material. In sputtering, high energy gas ions are used to disintegrate a bulk material target on a molecular scale to form thin film deposits. This material transfer across a gas plasma results in a severe disorganization of the material as it is deposited, and possible foreign atom contamination from the sputtering environment. Consequently, the resulting film does not initially have the orderly crystal lattice that is characteristic of a bulk material. Instead, it is thermodynamically unstable and is in a high state of stress due to large defects in the crystal structure. As a result, resistivity is high, α is low or negative, and the material is unstable as sputtered.

Low temperatures of formation of thin films generally result in the most disorganized "amorphous" structure because there is little atomic mobility at these temperatures. High temperatures of formation increases atomic mobility, and this mobility allows for rearrangement of atoms to a lower energy state, resulting in improved stability.

If sputtered at low temperatures, thin films must be aged by heating, preferably to near the recrystallization temperature of the thin film material. This procedure will rearrange the film atoms to a low state of energy and stress. Aging also results in a coarsening of film structure, i.e., grain growth, loss of occluded and adsorbed gas, lower resistivity, and higher α (near bulk properties). Film thickness must be greater than 0.1 μm to achieve the desired stability.

Finally, it is worth commenting that since a thin film represents a very small volume of material, it can be expected to reach equilibrium conditions much more rapidly than bulk material.

From this discussion, it can be concluded that adherence and survival of thin film sensors in gas turbine engines are not major problems, but that the electrical stability and low α required for strain gage applications at higher temperatures may be a major challenge.

3.3 BLADE MATERIAL PROPERTIES

Blade materials typical of modern turbine engine practice are:

a)   AMS 4928 titanium alloy for 600K service in compressors
b)   Incoloy 901 nickel steel (PWA 1003) for 900K service in compressors
c)   MAR-M 200+Hf nickel-based superalloy (PWA 1422) for service in turbines

Some pertinent properties of these materials are listed in Table II. Nearly all blades of gas turbine engines in service today are fabricated of these materials or of slight variations of them.

The large difference in temperature coefficient of linear expansion (tce) between the titanium-based alloy (9 ppm/K) and the iron and nickel based alloys (15 ppm/K) is noteworthy. A strain gage installation perfectly matched to AMS 4928 could experience a thermally induced strain of about 3600 x 10^{-6} at 900K on Incoloy 901.

TABLE II

PROPERTIES OF BLADE MATERIALS

	Material Specification		
	AMS 4928	PWA 1003	PWA 1422
Common Name	6A1-4V Titanium	Incoloy 901	MAR-M 200 + Hf
Approximate Composition	Ti Bal. Al 6% V 14% Other 0.1%	Fe Bal. Ni 42% Cr 12% Mo 5.75% Ti 2.85% Co 1.0% Cu 0.5% Al 0.35% Mn 0.5% Si 0.4% C 0.1%	Ni Bal. W 12% Co 10% Cr 9% Al 5% Ti 2% Hf 2% Cb 1% Fe 0.35% Zr 0.2% Other 0.6%
Maximum Recommended Service Temperature	700K	1000K	1300K
Maximum Heat Treat Temperature	1200K	1300K	1470K
Modulus of Elasticity (E)	97,000 MPa at 600K	160,000 MPa at 900K	145,000 MPa at 900K
tce, parts per million per Kelvin	9 ppm/K at 600K	15 ppm/K at 900K	14 ppm/K at 900K
Approximate Elastic Strain Limit, 0.2% yield	5000×10^{-6} at 600K	4300×10^{-6} at 900K	5800×10^{-6} at 900K
Fatigue, Strain Limit, smooth, 10^7 Cycles	2800×10^{-6} at 600K	1700×10^{-6} at 900K	1800×10^{-6} at 900K
Fatigue, Strain Limit, notched, 10^7 Cycles	1300×10^{-6} at 600K	1100×10^{-6} at 900K	---

3.4 SURFACE PREPARATION CONSIDERATIONS

Surface roughness specifications acceptable to blade designers may vary considerably, depending on the size of the blade, fabrication procedure, and position in the engine. However, to assure reproducible results in thin film sensor adhesion and sensor performance characteristics, surface roughness must be closely controlled.

Best adhesion of films of oxide-forming or nitride-forming materials is achieved on a highly polished surface because intimate molecular contact is achieved permitting chemical bonding to occur. In addition, sputtering tends to replicate surface defects, so the surface should be smooth to minimize film defects. However, best adhesion of chemically inactive materials is achieved on a slightly roughened surface, where mechanical interlocking and pegging is promoted.

In the present program it was planned to deposit a refractory oxide or nitride film to form an insulating layer, and then a strain gage alloy on this layer.

Best adherence of the insulating layer might be accomplished on a highly polished blade surface. However, this would result in an insulating layer with an extremely smooth outer surface perhaps not optimum for adhesion of the chemically less active strain gage materials. The alternatives were to perform additional roughening operations on the insulating layer outer surface, or to start with a compromise surface finish. In Reference 4, it was found that a compromise initial surface roughness produced acceptable results at temperatures to 1250K for noble metal sensor films on Al_2O_3. Some initial trials of surface finish treatments were, therefore, included in the components test program described in Section 4.0.

3.5 INSULATING FILM MATERIAL AND THICKNESS

The insulating material must have high resistivity and high dielectric breakdown voltage at service temperature. The candidate material must possess both an elastic strain range and a temperature coefficient of thermal expansion (tce) reasonably well matched to the blade material and sensor material.

There is a little data available on elastic strain range and tce of refractory insulating materials in thin film form, and there is much scatter in the available data. This is not surprising, since the thermal and mechanical behavior of the material depends on the internal structure, grain size and porosity which in turn depend on fabrication procedure and on the character of the substrate surface.

Table III lists the approximate properties of the only four high-resistance refractory materials for which favorable experience in thin film form has been reported: Al_2O_3 (References 10, 11, and 12); HfO_2 (in-house experience); Si_3N_4 (References 13, 14, and 15); and SiO_2 (Reference 16). All have promising electrical properties. On the basis of thermal expansion matching, all four have low reported tce, with the highest (Al_2O_3) still somewhat below the tce of the titanium blade alloy. Table IV lists values of tce for a variety of materials, for comparison with the insulating layer candidates.

TABLE III

APPROXIMATE PROPERTIES OF CANDIDATE INSULATING LAYER MATERIALS

	Al_2O_3	Si_3N_4	HfO_2	SiO_2
Resistivity at 600K, microhm-cm	10^{19}	10^{16}	10^{16}	10^{16}
Resistivity at 900K, microhm-cm	10^{15}	10^{13}	10^{12}	10^{12}
Modulus, MPa	--	70,000	--	70,000
Temperature Coefficient of Expansion (tce), ppm/K	7	3	4	1
Dielectric Breakdown, volts/cm	5×10^5	10^7	--	--
Thermal Distortion Strain:				
vs. AMS 4928, 300K to 600K	580×10^{-6}	1730×10^{-6}	1440×10^{-6}	2310×10^{-6}
vs. Incoloy 901 300K to 900K	4980×10^{-6}	7460×10^{-6}	6840×10^{-6}	8710×10^{-6}

TABLE IV

APPROXIMATE TEMPERATURE COEFFICIENT OF LINEAR EXPANSION (tce) FOR SEVERAL MATERIALS

Material	tce (ppm/K)	Material	tce (ppm/K)
MAR-M 200+Hf	14	Fe	12
AMS 4928	9	Mn	22
Incoloy 901	15	Mo	5
Al_2O_3	7	Ni	13
Si_3N_4	3	Pd	12
HfO_2	4	Pt	9
SiO_2	1	Si	3 to 7
Ag	20	Ti	8
Al	24	W	4
Cu	16	Au	14
Cr	6	Kanthal A-1	16
NiCoCrAlY	13	Ni20Cr	14
B1900	14	IN100	11
304 Stainless Steel	18	Cu45Ni	15

First-hand experience at Pratt & Whitney and United Technologies Research Center has shown that:

a. Al_2O_3 can be sputtered directly on nickel steel alloys with good adherence and durability to about 1000K, but cracks or spalls at temperatures above 1000K unless a ductile alumina-forming precoat is used such as the MCrAlY coating used on turbine blades (Reference 4).

b. HfO_2 can be sputtered directly on tungsten and is durable at 1470K on a tungsten-nickel interface.

c. Si_3N_4 can be sputtered directly on silicon and provides a dense, hard abrasion-resistant coating at room temperature, and is durable at 1470K on Si.

d. SiO_2 can be sputtered directly on tungsten and platinum alloys with good adherence and durability to about 800K, but it cracks and spalls at temperatures above 800K on these materials.

This experience confirms predictions based on tce matching, which results in an order of preference at 900K of Al_2O_3, HfO_2, Si_3N_4, and SiO_2. All four are worth trying on the blade materials of Table II.

Sputtering at an elevated temperature to prestress the thin film in the "safe" direction was considered but not attempted in this program. A number of new control problems arise in such a process. The work piece electrode temperature was typically 400K (250°F).

The insulating film must be thick enough to ensure that resistance to ground is large compared with the gage resistance to minimize shunting effects. The leakage resistance is given by:

$$R_L = \rho_2 \frac{t_2}{A} \qquad (5)$$

where ρ_2 is insulation resistivity (ohm-cm), t_2 is insulation thickness, (cm), and A is the combined area of gage film and lead films (cm^2). For example, Figure 2 shows minimum required insulation thickness, t_2, versus area, A, for $R_L = 10^5$ ohms, assuming $\rho_2 \geq 10^8$ ohm-cm. Figure 2 will be discussed further in the sections on film configurations and lead film configurations.

MINIMUM THICKNESS OF INSULATION μm (y-axis: 0, 1, 2, 3, 4, 5)

AREA, GAGE PLUS LEAD FILMS, mm² (x-axis: 0, 25, 50)
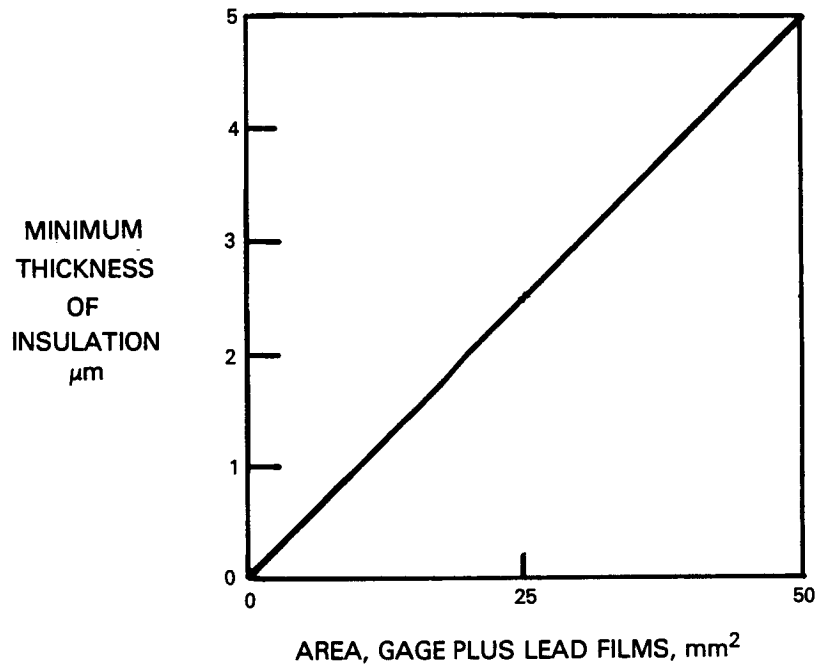
Figure 2   Minimum Required Insulation Thickness versus Area of Gage plus Lead Film for Insulation Resistance of 10^5 ohms at Resistivity of 10^8 ohm-cm.

3.6   STRAIN GAGE FILM MATERIAL SELECTION

3.6.1   General Requirements

For survival and calibration stability the sensor material must be electrically stable at all temperatures up to operating temperature. For acceptable performance in regions of steep temperature gradients (whether or not a thermocouple or a second bridge element is incorporated for temperature compensation) the strain sensor temperature coefficient of resistance (α) must be reasonable low. These two characteristics, stability, and α are the controlling factors in the selection of candidate sensor materials.

A maximum rate of drift of electrical resistance with time at service temperature in air on the order of 0.1 percent per hour was selected as an objective, including effects of oxidation and metallurgical structure changes at constant temperature. This is the order of magnitude of stability reported in the literature for several of the better high-temperature strain gage alloys in wire form (Table V). It implies a change in apparent gage factor due to bridge imbalance on the order of 0.05 percent per hour, based on Equation 4.

TABLE V

RESISTANCE STRAIN-GAGE WIRE ALLOYS[1]

Type	Trade Names	Composition at %	ρ Resistivity Microhm cm	α 300K to 600K ppm/K	α 300K to 1000K ppm/K	Approx. Gage Factor G	M.P. K	Max. Operating Temp.(K) for Dynamic Strain	Max. Operating Temp.(K) for Static Strain	Drift at 900K, Rating (10 = best)	Fatigue Rating (10 = best)	Remarks on Static Strain Limitations
Ni-Cr	Nichrome V Tophet A	Ni20Cr	110	110	50	2	1673	1400	600	8	4	Order-disorder transformation in the 700 to 800 K temperature range results in rapid drift in apparent strain during any temperature cycle above 600 K
	Nichrome Tophet C	Ni16Cr24Fe	110	150	100	2	1623	1400	600	5	4	
	Karma Molekuloy	Ni20Cr3Fe3Al	130	±20	-	2	1620	1100	600	5	9	
	Evanohm	Ni20Cr3Al3Cu	130	±20	-	2	1620	700	600	1	-	
Cu-Ni	Constantan Cupron Advance	Cu45Ni	50	±40	-	2	1500	600	600	1	-	Oxidation rapid above 600 K
Cu-Mn	Manganin	Cu12Mn4Ni	50	±15	-	2	1300	600	600	1	-	Oxidation rapid above 600 K
Pt-W	Alloy 479 Platinum-Tungsten	Pt8W	70	240	240	4	2143	1400	600	10	7	Large Pt8W gages (2 cm) with built-in temperature compensation can be used to 900 K
Fe-Cr-Al	Kanthal A-1 BCL-3	Fe22Cr5.75Al0.5Co Fe25Cr7.5Al	150	±35	40	2	1783	1400	Note 2	8	10	Cooling rate dependence and non-linear apparent strain curve limits static strain accuracy above 600 K

Note 1: Values of all quantities listed vary widely with heat treatment and cold work. The values given are typical for wound strain gages in service.

Note 2: Kanthal A-1 has been used for quasi-static strain to 1100 K in simulated engine tests.

3-12

A maximum α on the order of 200 ppm/K (positive or negative) is a reasonable temperature sensitivity goal. From the standpoint of dynamic strain accuracy this represents a change in apparent gage factor with temperature of 100 ppm/K (from Equation 4). For example, if uncertainty in temperature were 4 percent of absolute temperature, then the uncertainty in apparent gage factor would be 0.24 percent at 600K and 0.36 percent at 900K.

Since static strain measurement is also of interest (although not the goal of this program) it should be noted that the parameter dominating the effect of α on static strain is the ratio of α to gage factor (G)*. Both α and G are listed in Table V. For the gage to be useful for static strain measurement, α/G must be below 25 ppm/K. (Of course, if temperature uncertainty could be eliminated then problems due to α would vanish, but in an operating gas turbine engine the gradients are large and time-dependent, and the uncertainty in effective temperature, averaged over the region occupied by a strain gage, is always likely to be a few percent of absolute temperature.) For example, at $/G = 25$, for an uncertainty in temperature of 4 percent of absolute temperature, the uncertainty in apparent static strain is 300×10^{-6} cm/cm at 600K and 600×10^{-6} cm/cm at 900K, which might be acceptable in some programs.

The problem of obtaining low α in a stable alloy is discussed later in this section.

A resistivity in the range of 10 to 200 microhm-cm is desired to permit fabrication of strain gages in the 100 to 1000 ohm resistance range in the desired size and thickness range. If strain gage resistance is above 1000 ohms, insulation leakage to ground becomes a serious problem. If it is below 100 ohms, lead-wire resistances and contact resistances (including slip rings) become serious problems. The 10 to 200 microhm cm range includes virtually every metal and alloy in the literature, and is a weak restraint.

Gage factor itself is not predictable using the present knowledge of electrical behavior of conductors. However, on the basis of bulk dimensional change, it can be shown that the gage factor should be 5/3 for elastic deformation with a Poisson ratio of 1/3, and should be 2.0 for constant-volume deformation (Poisson ratio of 1/2). In fact, the gage factor of ordinary alloys is found to lie between 1 and 6, and the gage factor of semiconductors is large and negative (e.g., -100). No attempt is made in this analysis to predict gage factor. Gage factor estimates are based on data obtained with wire gages in each alloy family considered, where data is available.

---

* Since $\alpha = \Delta R/R \Delta T$, then in Equation 2 the additive apparent strain due to α is

$$[(\Delta R)_{other}]/GR = \alpha \Delta T/G$$

3.6.2 600K Candidates

Identification of some promising 600K alloy families is relatively straightforward, since information is available in the literature on low-α stable resistive wire strain gages and resistor wires in this temperature range. Table V is the list of eight obvious candidates from References 17 through 28. All have been used successfully in wire strain gages and several meet the requirements of the present program at 600K. The values of resistivity and α reported vary considerably depending on heat treatment. It is common practice among strain gage manufacturers to adjust the heat treating sequence to produce a value of α which provides cancellation of thermal expansion effects in the base metal on which the gage is located.

To minimize thin-film fabrication costs, binary alloys are preferable to more complex alloys. Only two of the alloy families in Table V are binary. They are Ni-Cr family (including Ni20Cr commercially known as Nichrome V or Tophet A) and the Cu-Ni family (including Constantan, Cupron, or Advance, all Cu45Ni). Alloys in both of the two binary families meet the 600K dynamic gage objective for stability and α, and these two families were selected for evaluation. In addition, these two both meet static gage requirements at 600K (stability, and α/G below 25 ppm/K). Finally, the NiCr family is promising for dynamic gage use at temperatures up to 1400K. Neither NiCr nor CuNi offers any hope for static strain above about 700K, because of oxidation in the case of CuNi and metallurgical instability in the case of NiCr.

3.6.3 900K Candidates

To gain the most benefit from the program, it was desired to select two high-temperature alloys meeting not only the primary goal of the program, dynamic strain measurement, but also offering some promise for static strain measurement.

The literature reveals that experimental measurements of electrical properties of conductors above about 600K are limited to metals and alloys in wire form, and that none of these provide both metallurgical stability and low α. No useful information on high temperature films was found, but the above references provide data on wires of 23 pure metals with melting point above 1200K, and wires of 206 binary alloy systems involving alloys of these metals with each other or with other atomic species. These references also provide data on wires of about 100 alloys of greater complexity (ternary or higher order). Many pure metals are reported to be adequately stable, but α of all pure metals is far too high (order of 3000 ppm/K). Many wire alloys have been developed specifically to attain low α, but their properties are not stable at elevated temperatures. This instability is a result of oxidation or of metallurgical structure changes with time at elevated temperatures in these complicated alloys. Examples of these low α materials appearing in Table V are Karma (NiCrAlFe), Evanohm (NiCrAlCu), and Manganin (CuMnNi). It appears that low drift and low α tend to be mutually exclusive. This dilemna has appeared often in the annals of strain gage development over the past 30 years.

An example of the problem is shown in Figure 3, where the resistance vs. temperature of Pt8W and Ni20Cr are compared. The material with the low α is Ni20Cr, but at about 800K there is a sudden drop in its resistance; also, when Ni20Cr is cooled from a temperature above 800K, the curve becomes extremely nonlinear and the curve shape becomes dependent upon rate of cooling.
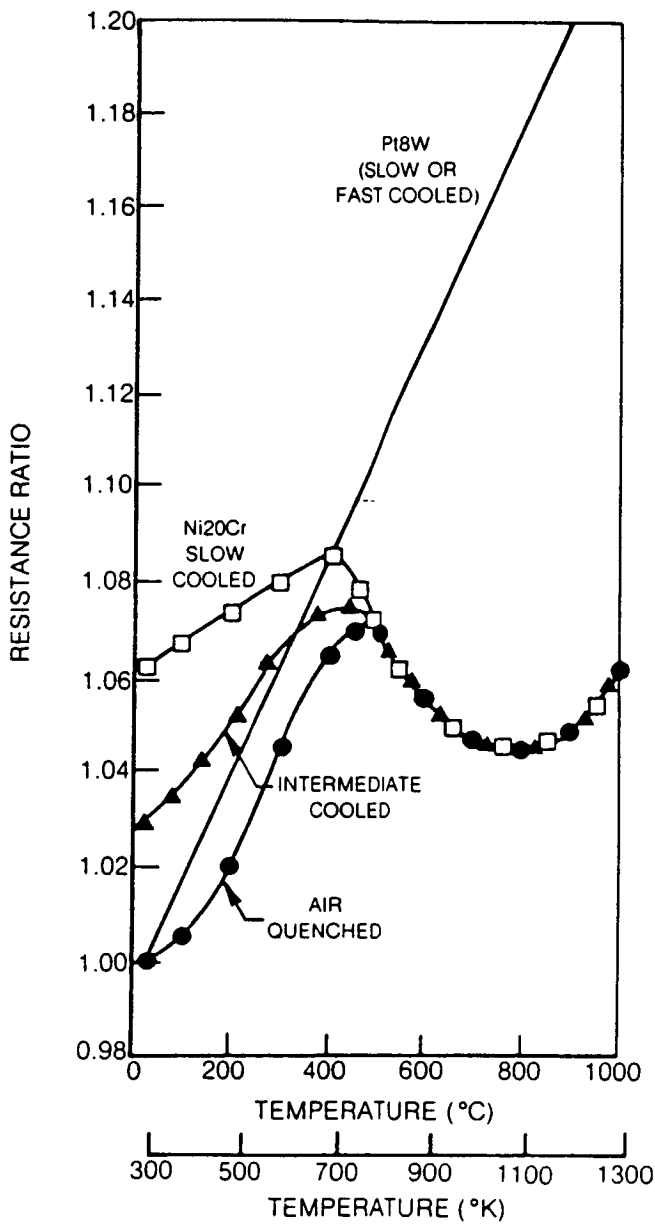
Figure 3   Resistance Versus Temperature for Ni20Cr and Pt8W.

The fact that the present program was not limited to alloys workable in wire form provided an opportunity to select candidates from a broad untested class of alloys. There are several hundred possible binary alloy systems alone that could be explored, each with an infinite number of concentrations in the 0 to 100 percent range. In order to select a promising class of candidates, the chemical, physical, and metallurgical mechanisms governing stability and were further explored and are discussed here.

The theory of electrical properties of alloys at high temperatures has not attracted much interest in the world's scientific community until recently. The theoretical problems at ordinary temperatures are staggering, involving the interrelationships governing the occupancy of the several possible energy levels in each electron shell of the atom. No proven basis exists for accurate prediction of electrical properties, particularly α, of the large number of alloys untested to date.

Certain general considerations apply. Table VI is a summary of theoretical considerations governing stability, electrical properties, and mechanical properties of pure metals and dilute alloys, from References 17, 29, and 30. First principles state that position in the Periodic Table of the Elements provides clues to behavior. All the high-melting point metals which are good conductors are found among the subset of 30 elements called the transition metals (Table VII). Every metal has a definite crystal structure with a near-perfect atomic lattice geometry within each crystal. The most common lattice structures are illustrated in Table VIII from Reference 30. The transition metals in any one column of the Periodic Table have similar atomic lattice structure (Table VIII), similar atomic radius (see Appendix 1) and similar mechanical and electrical properties (Table VII). Strength, hardness, melting temperature, α, and stability all increase toward the bottom of each column and toward the middle of each row. Stability of all properties vs. time at high temperature is highest in those elements which possess only a single atomic lattice structure at all temperatures ("monomorphic"), and is highest of all when this structure is face-centered cubic (fcc). Because electrical properties are stable only if mechanical properties are stable, the search for stable strain gage materials begins with the eight face-centered cubic transition metals which are in Group 8 in the middle of the Periodic Table, Table VIII.

Theories of dilute alloys (Table VI) predict correctly that adding <u>any</u> alloying second metal to a first metal increases the hardness, fatigue life, and electrical resistivity (ρ), and decreases α.

TABLE VI

GUIDELINES TO ELECTRICAL BEHAVIOR OF
PURE METALS AND DILUTE ALLOYS

Pure Metals

<u>Periodic Table of the Elements</u>: Elements in the same column tend to behave alike; stability is better near bottom of column.

<u>Crystal Lattice</u>: All metals have definite crystal structure (mostly bcc, fcc, hpc) at a given temperature. Some change structure at certain temperatures ("polymorphic"). Avoid for best stability. fcc is most stable.

<u>High-Melting Metals</u> are more stable (or change more slowly), are harder, stronger, have higher modulus of elasticity, higher fatigue life. Some are chemically active (bad).

<u>Mechanical and Electrical Properties are Related</u>: Phase changes, order-disorder changes in lattice, grain growth, outgassing, creep, or any alteration in metallurgical structure also alter α and ρ. The material must be mechanically stable to be electrically stable.

<u>The Transition Metals</u> are all the B groups in the Periodic Table; they are the elements of primary interest for strain gages.

<u>Actinides</u> (90-103) are all radioactive.

<u>Lanthanides</u> (58-70) are nearly inseparable from each other and relatively active: MCl_3.

<u>Metalloids</u> (semiconductors) B, Si, Ge, As, Sb, Te, have high ρ and negative α. This is a clue.

Dilute Alloys

<u>Matthieson's Rule</u>

Resistivity $= \rho_0 + \rho_T$
ρ_T is temperature dependent resistivity due to lattice-vibration scattering.
ρ_0 is temperature independent resistivity due to defects, presence of alloy element.

<u>LeChatelier-Guertler's Rule</u>

Temperature coefficient of resistance, α, of alloy is lower than α of pure metal. (This follows from Matthiesen's Rule.)

<u>Dellinger's Rule</u>

Product of α and ρ tends to be constant in an alloy system as composition is changed. Choose an alloying element which increases ρ a lot in order to decrease α a lot.

<u>Linde's Rule</u>

For dilute alloys, $\rho \propto V_x^2$. Choose high V_x; V = Valence, x = alloying element.

<u>Norbury's Rule</u>

For dilute alloys in any one period of the Periodic Table, $(N-N_x)^2 \propto \rho$, where N is atomic number. Choose x for high $(N-N_x)$.

<u>Oxidation of Alloys</u>

Oxidation rate of an alloy tends to be like that of the principal (host) element.

<u>Exceptions to Rules</u>

There are exceptions to every rule.

TABLE VII

PERIODIC TABLE OF PHYSICAL PROPERTIES (TRANSITION METALS)

SYMBOL
AT. NO
m.p. (K)
E (MPa)
α (ppm/K)
ρ (μΩ-cm)

GROUP	3b	4b	5b	6b	7b		8		1b	2b
SERIES 4	Sc	Ti	V	Cr	Mn	Fe	Co	Ni	Cu	Zn
	21	22	23	24	25	26	27	28	29	30
	1812	1993	2153	2163	1517	1807	1768	1728	1356	692
	—	120	—	248	158	200	200	200	110	—
	2800	—	—	3000	—	6200	6000	4800	4000	4000
	61	42	26	13	185	9.7	6.2	6.8	1.1	5.9
SERIES 5	Y	Zr	Nb	Mo	Tc	Ru	Rh	Pd	Ag	Cd
	39	40	41	42	43	44	45	46	47	48
	1768	2113	2683	2898	2470	2773	2239	1825	1233	594
	—	75	—	345	—	—	290	120	75	55
	2700	4400	—	4700	—	4600	4600	3800	4100	—
	57	41	13.1	5.2	—	8	4.5	10.8	1.6	6.8
SERIES 6	Lu	Hf	Ta	W	Re	Os	Ir	Pt	Au	Hg
	71	72	73	74	75	76	77	78	79	80
	1193	2423	3273	3683	3453	3300	2727	2043	1336	234
	—	—	180	370	—	550	517	145	83	—
	2200	3800	380	4500	4000	4200	4200	3900	3900	—
	6	35	12.4	5.5	19	9.5	5.3	9.8	2.2	94.1

SERIES 6
SERIES 5
SERIES 4

m.p. (K)
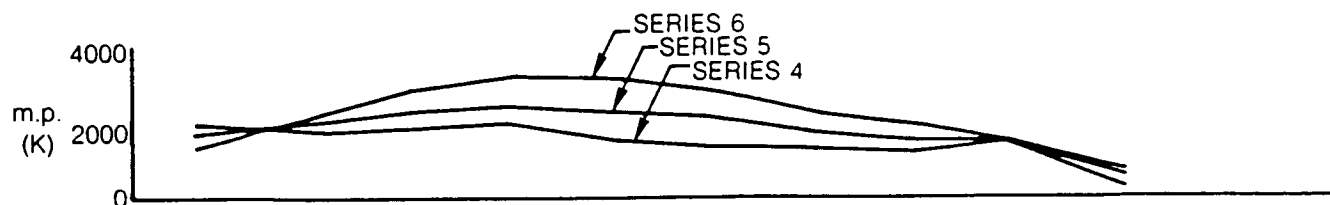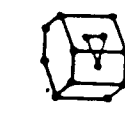
TABLE VIII

PERIODIC TABLE OF LATTICES*

TYPE OF STRUCTURE

○ BODY-CENTERED CUBIC

□ FACE-CENTERED CUBIC

⬡ CLOSE-PACKED HEXAGONAL

○ MOLECULAR STRUCTURE

(⌒) STRUCTURE WHERE C N = (8-N)

(⌒) OTHER STRUCTURES

NOTE: WHERE MORE THAN ONE CRYSTAL STRUCTURE IS SHOWN,
THE SPECIES IS POLYMORPHIC, i.e., POSSESSES DIFFERENT CRYSTAL
STRUCTURES AT DIFFERENT TEMPERATURES.

* REPRODUCED FROM REFERENCE 25.

TRANSITION ELEMENTS

LANTHANIDES

ACTINIDES

GROUPS

SERIES

1a 2a 3b 4b 5b 6b 7b 8 1b 2b 3a 4a 5a 6a 7a 0

The PtW alloy family is a typical example of dilute alloy behavior. Figure 4 illustrates α as a function of percent W in the alloy, and shows that decreases from 3900 ppm/K (at 0%W) to 145 ppm/K (at 10%W). There is no electrical data in the literature beyond 10%W because the alloys with higher W content are too hard to be mechanically workable in wire form. The scatter band in Figure 4 is the effect of different heat treatments employed by different investigators. Similar curves are found for all dilute alloys, differing only in quantitative detail.

FD 184818
791511
gn1-485
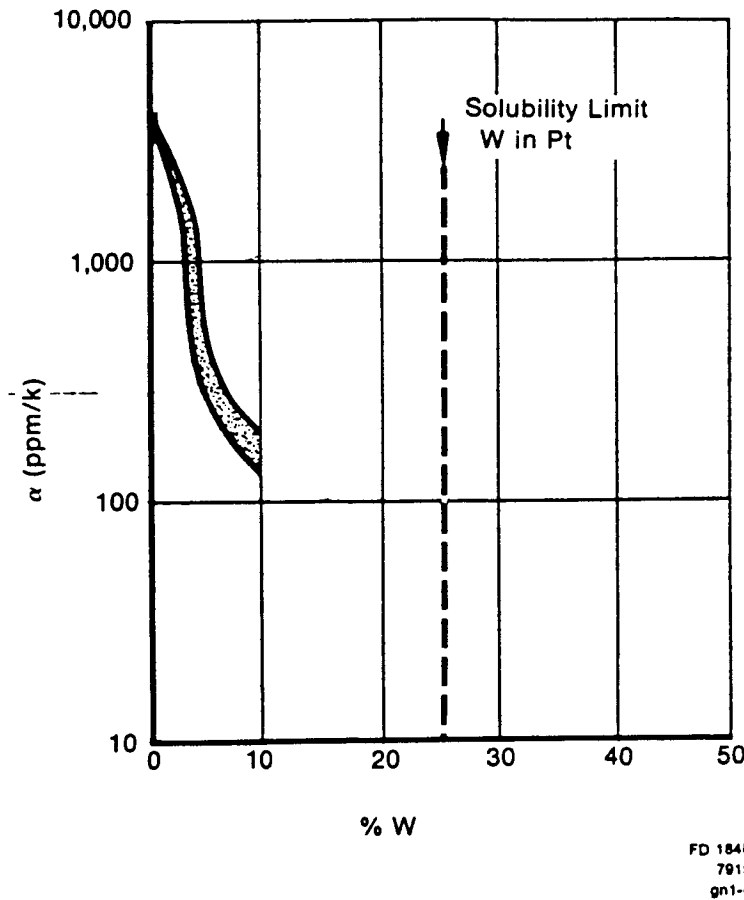
Figure 4   Temperature Coefficient of Resistance (α) versus Percentage Tungsten in a Platinum-Tungsten Alloy Wire.

In fact, a general rule for dilute alloys, called Dellinger's rule in Table VI, states that the $\alpha\rho$ product tends to be constant as alloy concentration is changed. This implies that α could not be expected to approach zero for an alloy of reasonable maximum resistivity, although fairly low α values might be attained if the harder, more concentrated, alloys were used.

The physical model on which predictions such as Dellinger's Rule are based is the perfect lattice arrangement of atoms in the metal crystal. At low temperatures, the atoms are nearly stationary in their lattice sites, and the structure is practically transparent to conduction electrons. The electrical resistance is low (free flow of electrical current). At high temperatures the atoms vibrate more vigorously about their mean locations, resulting in increased scattering of electrons passing through the structure. The electrical resistance is higher, resulting in the large positive value of α for all pure metals (good conductors). Adding any alloying metal results in defects in the lattice structure, since no two metals have exactly the same atomic radius or lattice spacing. The defects increase the resistivity by producing additional scattering. This added resistivity due to alloying is independent of temperature (Mathiessen's Rule) because it does depend upon atomic vibrations. The product of α and ρ tends to be roughly constant (Dellinger's Rule) because the increase in ρ due to alloying is a result of a temperature independent mechanism.

This model did not explain the existence of zero and negative values of α in alloys such as Evanohm, Cupron, Fe-Al, and high-resistance semimetals (metalloids or semiconductors). The model does show that low values of α can be associated with a highly defective lattice structure. Since structures with many defects often are unstable at high temperature (in some cases changing from an ordered to a disordered state over a period of time), the model throws some light on the low α vs. stability question. One requirement for a strain gage is a stable defective structure.

A series of papers published in the early 1970's by J. H. Mooij and summarized in his 1973 paper (Reference 31) discusses zero and negative values of α . Mooij's work is based on examination of a large body of experimental data on low α alloys and provides rules for selection of low α alloys.

Mooij's most startling observation concerns the behavior of disordered concentrated alloys. (In a disordered alloy, the atoms of the different species do not form a regular periodic lattice, as they would in a chemical compound, but instead are jumbled together randomly. A solid solution is usually a disordered alloy. Solid solutions can be quite stable.) He observed, for alloys containing at least one transition metal plus at least one atomic species from some other column of the Periodic Table than that occupied by the first species, that not only is α much lower and ρ much higher than in the first species, but in addition, α is a universal function of ρ , with α passing through zero at ρ of about 125 microhm-cm.

The α - ρ correlation is shown in Figure 5, reproduced from Reference 31. Data on Figure 5 are from 27 different binary alloy systems and 3 ternary systems. Several different compositions within some systems are represented, and the data cover a wide range of temperatures for some particular alloys.
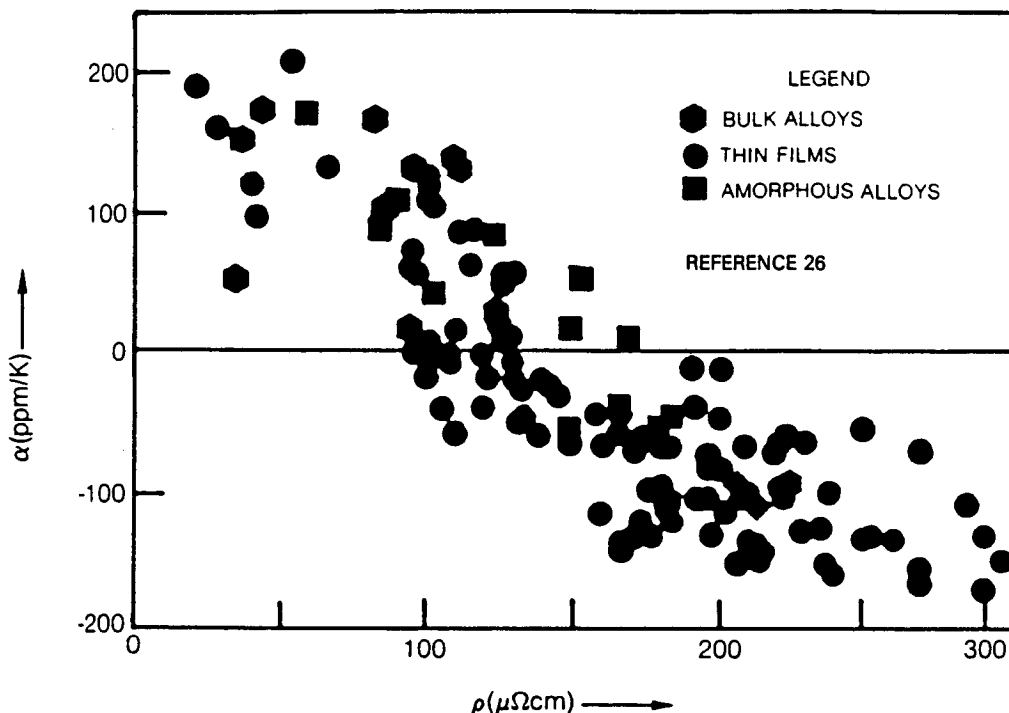
Figure 5   Temperature Coefficient of Resistance versus Resistivity for Bulk Alloys.

Mooij surmises that the lattice structure in each of these concentrated disordered alloys is saturated with defects even at low temperatures. This results in a resistivity so high that increased vibration of the lattice has no significant additional effect on α .

To explain the negative values of α , Mooij suggests that in these concentrated alloys there can be thermally activated releasing sites where electrons are liberated at high temperatures.

The Mooij alloy systems are prime candidates for thin film strain gages. It is interesting that every one of the strain gage wire alloy systems of Table V is a Mooij alloy system including the binary systems Pt-W, Ni-Cr, and Cu-Ni. In the case of Pt-W the data does not extend beyond 10%W where α = 145 ppm/K and ρ = 70 microhm-cm. The Mooij argument suggests that at higher W content α could approach or pass through zero, provided only that ρ rises above 100 microhm-cm.

The guidelines to be used for selection of candidate binary alloy systems may now be summarized, combining the rules for alloy stability (Table VI) and the Mooij rules for low α. These guidelines are as follows:

o The first atomic species in the alloy to he a monomorphic face centered cubic transition metal (Table VIII) with:

   o melting temperature above about twice the service temperature (K), and

   o high oxidation resistance (at least when in solution with second species below).

o The second atomic species in the alloy to be from a different column of the period table with:

   o large difference in atomic radius,

   o large difference in valence,

   o a range of solid solutions (no ordering or formation of phases or compounds with first species) at all temperatures to service temperature, and

   o high oxidation resistance when in solution with the first species.

As a starting point, a list of 41 high-melting binary alloy systems was compiled (Table IX). This list includes all of the 27 binary systems considered by Mooij in 1973 (Reference 31) plus 14 others for which some data on α and ρ were available in strain gage papers by Easterling in 1963 (Reference 19), Bertodo in 1968 (Reference 18), and Masumoto, et al in 1978 (Reference 32). All fit the Mooij model.

A further study of the Periodic Table will suggest many more possibilities, but the data available on other possibilities is so limited that a massive experimental investigation beyond the scope of this program would be required.

Table IX lists the following information for the 41 alloys:

   Column 1: Melting point (K) of end members A, B

   Column 2: Solid solution ranges (A in B and B in A), plus other pertinent information from phase diagrams (References 24, 33, 34, 35, and 36) that would indicate any stability problem below 900K.

   Column 3: Oxidation rating of A, B, A in B, B in A, for those alloy systems not already rejected in Column 2.

3- 23

Column 4: Alloy composition (%A or %B) within the solid solution range, for which the highest ρ was found in the literature, and the value of ρ and α reported. In the case of starred (**) items, ρ and α were reported for all compositions in the solid solution range, and the ρ reported is then the highest possible in this alloy system and the reported α is the lowest possible.

Column 5: Overall rating as a strain gage alloy candidate:

        A: should be tried
        B: could be tried
        C: should not be tried

The screening of the 41 candidates in Table IX proceeds from left to right across the table and reduces the number of candidates to four which offer some hope of the desired $\alpha <$ 200 ppm/K (and α /G < 25 ppm/K). These candidates are:

Ni-30Cr	600K
Cu-45Ni	600K
Pt-20W	600K and 900K
Pd-30Mo	600K and 900K

All four of these candidates were also judged as excellent from the point of view of erosion resistance, fatigue life (based on hardness, high tensile strength*), thermal expansion coefficient match with compressor blade materials, and adherence potential at 100,000G. All form some oxides and, therefore, are expected to bond well to oxide and nitride insulating layers.

---

*   See References 37, 38, and 39 for comments on how fatigue life increases with tensile strength and hardness.

TABLE IX

FORTY-ONE CANDIDATE ALLOYS FOUND IN THE LITERATURE

Alloy No.	Alloy Components A	B	1 Melting Point (K) A	B	2 Max. At. % for Solid Solution with no Anomalies between 73K and Stated Temp (K) B in A	A in B	3 Oxidation Threshold (K) A	B	3 Rating at (At. %) B in A	A in B	4 α ppm/K	4 ρ Microhm-cm	4 ρ(293K) At. %	5 Rating 600K	5 900K	Notes
BULK ALLOYS (Mooij)																
1	Ag	Pd	1233	1825	0-100	0-100	500	1000	A (50)	A (50)	380**	42	60 Pd	B	B	4 Pd40Ag
2	Al	Fe	933	1807	0	0-23 (900)	800	600		A (10)	500**	80	18 Al	B	B	4 Fe18Al
3	Al	Ti	933	1993	0	Limited	800	800		B						2
4	Al	V	933	2153	0	0-41 (770)	1000	700		B (40)						3
5	Cr	Ni	2163	1728	0-2	8-33 (700)	500			A	23**	120	29 Cr	A	C	3 Ni30Cr
6	Cu	Mn	1356	1517	0-7	0	500	700	C	B						
7	Cu	Ni	1356	1728	50-100 (1400)	0-50 (1400)	500	1000	C	B (50)	35**	52	50 Ni	B	C	3 Cu50Ni
8	Cu	Pd	1356	1825	0-8	0-40	500	1700	B	C						3
9	Cu	Pt	1356	2043	0-2 (670)	0-7 (670)	800	1700	B	C						2, 3
10	Ir	Pt	2727	2043	0-100	0-100* ***		1000	C	B						2, 3
11	Mn	Ni	1517	1728	0-3	***	500	800	B	C						3
12	Mn	Pd	1517	1825	0-25	0-25	500	300	B	C						3
13	Mo	Ti	2898	1993	0-85 (870)	0-2	600	800	C	C						3, 5
14	Mo	U	2898	1406	0-2	0-1	1700	600	C	C						3
15	Nb	Ti	2683	1993	0-3	0-3	800	700	A	C						3
16	Pt	W	2043	3683	0-25 (2000)	0-30	1700	600	C	A	145	60	8 W	A	A	3 Pt20W ?
17	Ti	V	1993	2153	0-3	0-1	800	700	C	C						3
18	U	Zr	1406	2113	0-25	0-25	300		C	C						3, 5
THIN FILMS (Mooij)																
19	Al	Nb	933	2683	0	0-8	800	600	C	C						
20	Al	Ta	933	3273	0	0-8	800	700	C	C						3
21	Ag	Mn	1233	1517		0	500		B	B						3
22	Au	Cr	1336	2163	0-14	0-7 (1170)	1300	1000	B	B						2, 3
23	Cr	Pd	2163	1825	0-23* (1170)	0-5 (1470)	1000	1000								2, 3
24	N	Ta	2163	3273	0-5	0-4		700		C						3
AMORPHOUS (Mooij)																
25	Pd	Si	1825	1713	0	0	1000			B						
26	Au	Ge	1336	1209	0-3	0	1300			B						2, 3
27	Cu	Ge	1356	1209	0-9	0	500			C						2, 3
OTHER ALLOYS (Bertodo)																
28	Pt	Pd	2043	1825	0-100	0-100	1700	1000	A	A	1050**	23	40 Pd	C	C	4 Pt40Pd
29	Pt	Rh	2043	2239	0-100 (2000)	0-100 (1270)	1700	900	A	A	1400**	21	20 Rh	C	C	4 Pt20Rh
30	Pt	Ru	2043	2773	0-40 (1270)	0-100	1700	800	A	A	380**	46		B	B	4 Pt35Ru
31	Pt	Ni	2043	1728	0-20*	0-100	1700	800	B	A (20)						2
32	Pt	Co	2043	1768	0-10*	0-100	1700		B	A						2
33	Pt	Cr	2043	2163		0	1700	1000	A	A	401**	86		B	B	4 Pt8Cr
34	Pt	Mn	2043	1517	0-10	0-100	1700		C	A						6
35	Pt	Os	2043	3300	0-10	0-100	1700	300	C	C						3
36	Pd	Ru	1825	2773	5-10# (1370)	5-10# (1370)	1700	300	C	B						2, 3
37	Pd	H	1825	3683	0-21 (1270)	0-21 (1270)	1000	800	B	B						3
38	Pd	Fe	1825	1807	0-10	0-1 (770)	1000	600	B	C						3
39	Pd	Mo	1825	2898	0-36 (1070)	0-4 (1270)	1000	500	B	C	135	104	20 Mo	A	A	2, 3 Pd30Mo ?
40	Ru	Mo	2773	2898			800	500	B	C						3, 6
41	Os	W	3300	3683			300	600	C	C						3, 6

Notes:
Col. 2, 3, and 4 = See Col. 2, 3, and 4;
5 = Radioactive
6 = Toxic

Ratings: A Should be tried.
B Could be tried.
C Should not be tried.

*   Ordering ?
**   Minimum in solid solution range.
*** Magnetic transformation.
\#   Immiscible at low temperature.
Decomposed by water.

Figure 6 shows the α vs. %B (composition) data on which the α values in Column 4 of Table IX are based, for the four final candidate alloy systems and for two other of the ten finalists, Pd-Ag and Pt-Rh. The remaining four finalists are omitted in Figure 6 for clarity, but absolute minimum α values for all four of these are reported in Table IX and all are too high. Finally, the α vs. %Ti curve for Al-Ti is presented in Figure 6 to show a classic zero α case in a simple binary Mooij alloy. This alloy was judged a poor candidate in the present program because of its highly questionable stability in the concentration required for zero α, which is beyond the solid solution range.

The phase diagrams for the seven alloy systems of Figure 6 are presented in Appendix A. The periodic behavior of atomic species is quite evident in the phase diagrams and the α vs. %B curves.
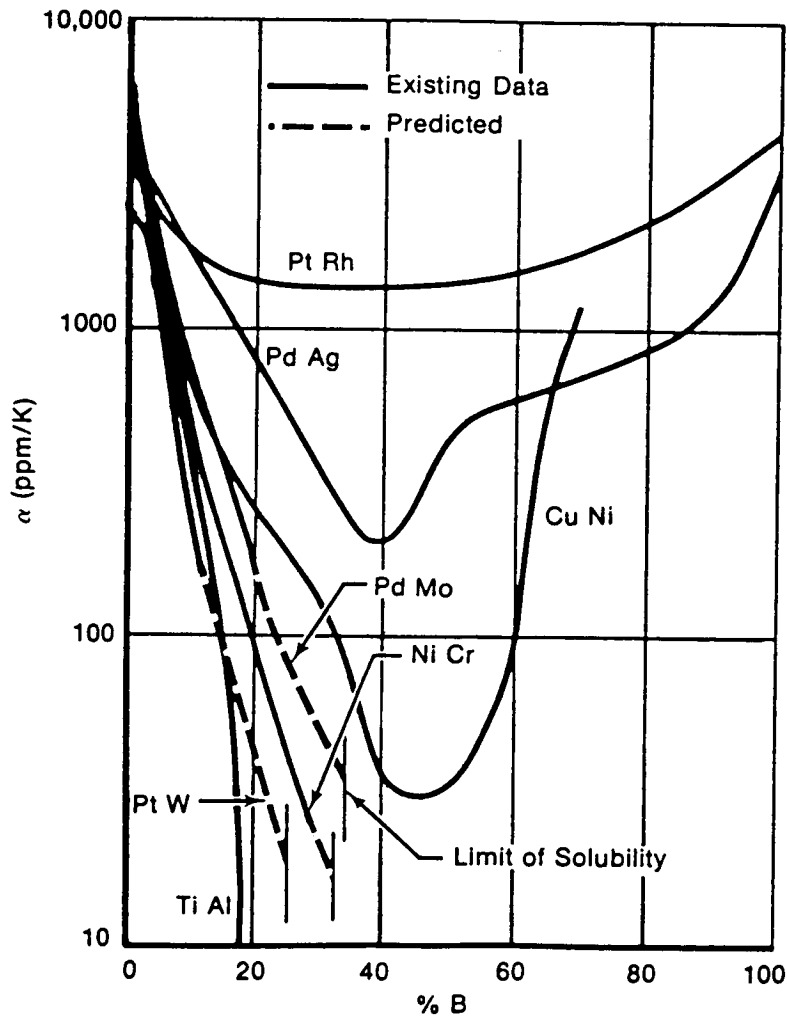
Figure 6   Temperature Coefficient of Resistance (α) versus Composition (% B) for Seven Binary Alloys.

Another approach to achieving low α would be the use of a thin layer of a positive-α alloy on a negative-α material. This approach was investigated by Lemcoe (Reference 23) using Pt on BCL-3 wire and by Weise, et al (Reference 22) using Pt on Kanthal A-1 wire. While the results were promising, it appears that control of the stability and α of the end product is difficult.

3.7 THIN FILM STRAIN GAGE CONFIGURATION SELECTION

The following five geometrical parameters define the configuration of the usual resistive strain gage grid (Figure 7): The number of lines in the grid (n), the line width, the spacing between lines, the line thickness (film thickness, t_1), and the line length (gage length, L). From these parameters, two other geometrical parameters of interest which can readily be calculated are the gage film area (needed in selecting insulation film thickness, (Figure 2) and the ratio of gage film surface area to volume (useful in predicting oxidation effects). A nondimensional parameter, Y, was used to quantify this last ratio, where Y is the ratio of gage film surface area to volume, normalized by the ratio of surface area to volume of a 25.4 μ m (0.001 inch) diameter wire. Thus the resistance drift due to oxidation of a film with Y greater than 1 is expected to be greater than that for a 25 μm strain gage wire of the same material. If the edge surfaces of the thin film are ignored, then Y is inversely proportional to film thickness and is given by:

$$Y = \frac{6.25}{t_1} \quad \text{(where } t_1 \text{ is in } \mu\text{m)} \tag{6}$$

In the present program, an overall gage grid size about 2 mm x 2 mm was desired, with gage resistance of about 200 ohms, using a gage alloy with a resistivity of about 10^{-4} ohm-cm, and with line width equal to line spacing.
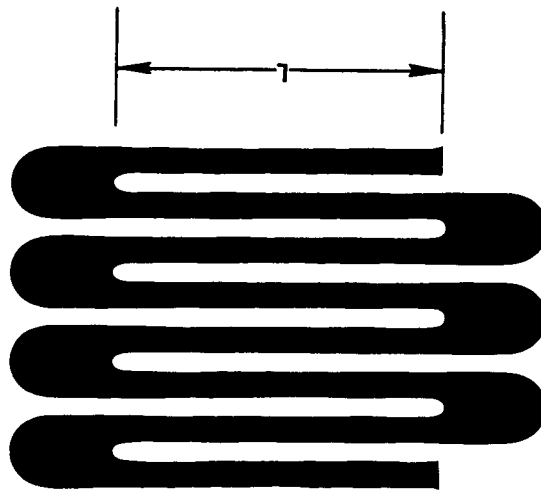
Figure 7   Thin Film Strain Gage Grid Model for Analysis.

With these constraints, specifying any one of the geometrical parameters fixes the values of all the rest. The relationships are derived in Appendix B. The result is the design curve shown in Figure 8. Two examples are marked on Figure 8 and are discussed here.
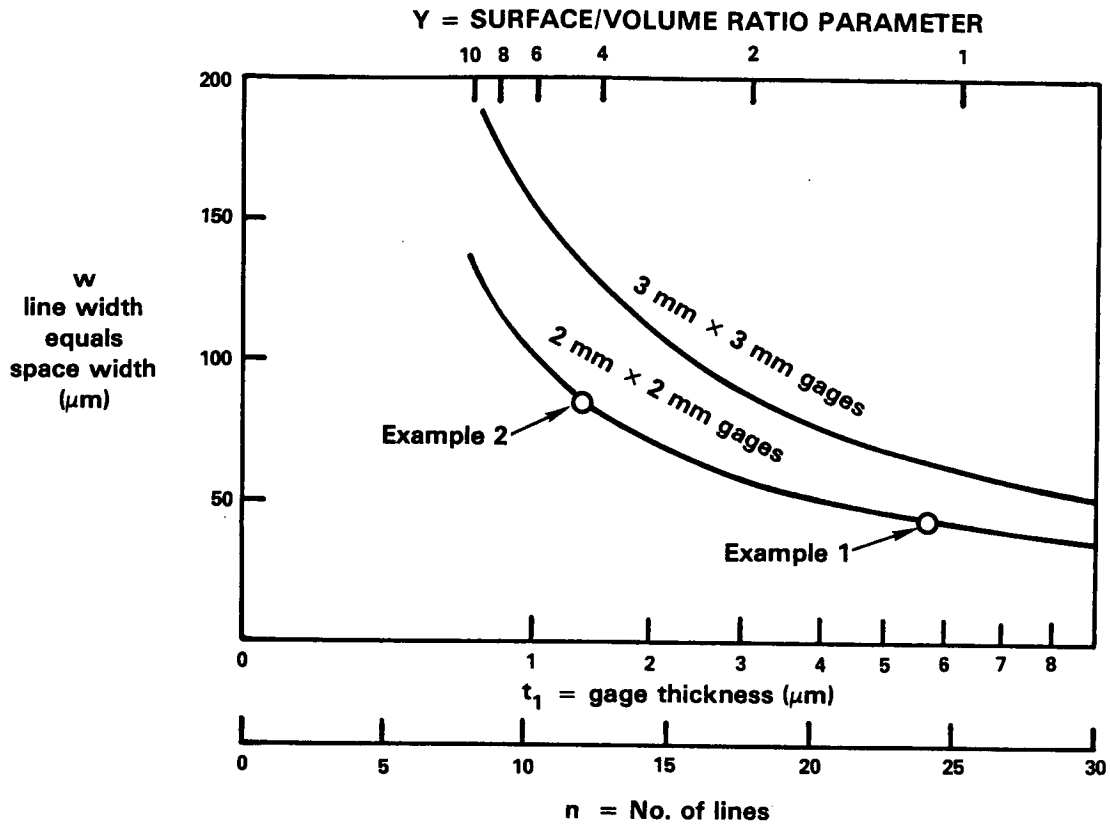
Figure 8 Design Curves for Thin Film Strain Gages, for R = 200 ohms and ρ_1 = 10^{-4} ohm-cm.

In example 1, a gage thickness between 5 and 6 μm is selected to provide a low ratio of surface area to volume. The result from Figure 8 is a pattern of 24 lines, each about 40 μm wide. The risk in this design is the small line width. Any slight imperfection in the blade surface, or any dust contamination during photomasking of the gage pattern, could result in an open gage or poorly adherent gage.

In example 2, a 12-line pattern of wider lines was selected to reduce fabrication risk. The result is a line width of about 80 μm, thickness of about 1.3 μm, and surface-to-volume parameter Y nearly four times higher than in example 1. A design based on example 2 was used throughout the program. The risk in this design is the large surface to volume parameter, requiring careful attention to protective overcoatings to limit oxidation susceptibility.

3-28

3.8 LEAD FILM MATERIAL AND CONFIGURATION

In an installation on an engine blade, sputtered thin lead films will extend from the gage to a low-stress area on the blade (or blade platform) where lead wires can be attached for maximum durability, minimum aerodynamic interference, and minimum buildup on the airfoil surfaces.

To avoid thermocouple junction effects, the lead film should ideally be of the same material as the sensor. For example, the 40 V/K thermoelectric voltage produced by a chromel (Ni-10Cr) vs. alumel (Ni-Al-Si) couple would result in an apparent static strain output of 288×10^{-6} from the strain gage bridge if the temperature gradient between lead films at the strain gage were 4 percent at 900K, with a 5V bridge (Equation 2). Of course, if the temperature gradient across the lead films is steady, then there is no apparent dynamic strain output due to thermoelectric effect.

Lead film resistance, and resistance change with temperature, must also be maintained reasonably small. If the material and thickness of the lead film and gage element are the same, then to keep each lead film resistance below 3 percent of the resistance of the 12-line sensor of Figure 7, the lead film length-to-width ratio must be less than $(0.03)(12)(2000)/80 = 9$. For example, if the lead is 10 mm long, the width must be at least 1.1 mm. This could present a spatial problem in installations involving multiple strain gages on a blade, and the use of thicker, narrower films or lower resistivity materials would be required.

The lead film surface area must be taken into account when calculating the insulation layer thickness required for high resistance to ground (Figure 2). For the 2 mm x 2 mm gage configurations of Figure 8, the gage area is approximately 2 mm^2 (i.e., about half of the 2 mm x 2 mm gage envelope area). For comparison, note that the two 10 mm x 1.1 mm leads found reasonable for lead resistance have an area of 22 mm^2. The sum of film and lead area must be used when calculating resistance to ground (Equation 5).

In engine installations on blades or vanes, the lead film will probably pass through regions of sharp curvature and complex geometry. For this reason, photographic masking of lead films will not be practicable. Tape masking procedures will be used, since this procedure was found entirely satisfactory in Reference 4 on complex surfaces for line widths over 0.4 mm. The lead film can be masked at the same time as the sensor since the tape mask for lead films and optical photoresist mask for gage elements can be used simultaneously. The lead film can then be sputtered at the same time as the sensor if the same thickness is acceptable..

3.9 OVERCOAT FILM MATERIAL AND THICKNESS

During engine test exposure of strain gages on blades or vanes, corrosion due to hot high-pressure gases and erosion due to impact of particulate matter are to be expected. Erosion alone is not expected to be a dominating influence in thin film strain gage life. For example, in the Reference 4 thin film thermocouple program, 2 μm platinum films survived without overcoating for over 150 hours of engine testing on JT9D first-stage turbine vanes, with only local damage in a few high-erosion areas. In another test, the erosion rate of 130 μm thickness of sputtered platinum on several JT9D first-stage turbine blades was determined in a nonrotating combustor rig during a carbon erosion test program at Pratt & Whitney. Near the blade leading edge, in the highest erosion area, the platinum film was lost from 0.1 to 0.3 percent of the leading edge stagnation line per hour with the clean burner configuration. In most other areas of the blade the loss of platinum material was negligible during 30-hour tests. It seems probable that an effect less than 0.01 percent per hour may be expected in an engine due to erosion.

Corrosion (and oxidation in particular) poses a more serious threat to thin film strain gage measurement stability. The large surface-to-volume ratio of the gage configuration selected (Figure 8) suggests that oxidation will produce about five times more drift than would be experienced by the usual wire strain gages (using 25 μm wire), for the same gage material and protection. Wire gages are normally buried beneath a protective layer of cement or flame-sprayed Al_2O_3 more than 100 μm thick. It is, therefore, to be expected that the thin film strain gages will require overcoating for oxidation protection. The overcoat must be electrically nonconducting, adherent on the gage material, and provide some degree of barrier to oxygen penetration. The most reasonable material for initial trial is the material found most suitable for the insulating layer under the gage, with thickness to be decided by trials. A composite overcoat consisting of an insulating layer plus a metal layer was a second alternative considered since the dense metal layer could provide a better oxygen barrier and could serve in a sacrificial role. Composite overcoat layers involve additional complication in fabrication, however, and were beyond the scope of the present program.

3.10 LEAD-WIRE MATERIAL AND CONNECTION TO LEAD FILM

To minimize the thermocouple effects discussed in Section 3.8 the lead-wire alloy and lead film alloy should have nearly the same thermoelectric properties. However, the lead-wire alloy must be readily workable (and available) in wire form and preferably should be an alloy of proven durability in engine leadwire installations. To meet all of these requirements, reasonable choices are chromel (Ni-10Cr) wire for use with Ni-Cr thin film gages, and platinum wire with noble metal gages. If the two leadwire junctions for each gage are close together, to keep temperature gradients below 50K, then the thermoelectric effect on static strain output will be less than 50 microstrain with these material combinations.

At the point of connection to the lead film, the lead-wire diameter should be small to minimize stresses during fabrication of connections and local loads during engine operation. Pigtail leads with diameter of 76 μm have been found satisfactory in previous thin film work (Reference 4). At a short distance from the connection to the lead film, extension lead wires of larger diameter can be spliced to the pigtails safely.

There are several candidate techniques for connection of lead wires to thin films (which are on thin film insulating layers) for service to high temperatures. Brush plating, oven brazing, flame-spray metallic coating, resistance welding, laser welding, ultrasonic welding, hot compression bonding, and fired conductive paste coating all offer some promise. Each has recognized or suspected problems as follows:

Brush plating, oven brazing, and flame-spray involve complex masking and fixturing to restrict the bonding material to the desired area.

Resistance welding, laser welding, and ultrasonic welding all tend to result in damage to the thin-film insulating layer under the metal film. Of these three, ultrasonic welding had shown the most promise in preliminary trials. Control of the energy delivered to the bond site is a problem with all three. Excessive energy results in electrical or mechanical breakdown of the insulation. Insufficient energy results in weak bonds.

Hot compression bonding of fine wires to thin films has been successful only with noble metals (gold, platinum, rhodium, and their alloys) easily deformed for intimate contact at the junction, and not prone to form surface oxides (which interfere with the bonding) at the elevated temperatures required for bonding.

Fired conductive pastes available on the market (such as Hanovia platinum or silver-bearing epoxies) have little mechanical strength above 600K.

Each of these techniques required study and additional trials with specific thin-film strain gage and lead film systems.

SECTION 4.0

COMPONENTS PROGRAM FABRICATION AND TEST PROCEDURES

4.1 FABRICATION AND TEST MATRIX

In the components program, preliminary screening tests were conducted on candidate materials and configurations for each of the seven components of the thin film strain gage system (Section 2.0) and on combinations of components. Table X is a listing of the materials and configurations tested for each component. These candidates were selected on the basis of the consideration presented in Section 3.0, Technical Discussion of Thin Film Strain Gage Approach. Table XI is a summary listing of the independent parameters involved in fabricating the test pieces, and the number of values tested for each parameter. The sputtering parameters (gas pressure, applied power, sputtering distance) are not listed in Table XI but were established on the basis of past experience and were checked in preliminary calibration runs using glass slides as substrates.

The following methodology was adopted, resulting in fabrication of components on 103 test blades, including many repeats to confirm principal results.

For insulating film evaluation, involving parameters 1 through 4 of Table XI (two blade materials, two surface finishes, four insulating film materials, two insulating film thicknesses), a full factorial fabrication matrix (32 test blades) plus four repeats was utilized. Eleven candidate combinations of the first four parameters were retained in the program after the testing of these samples was completed including at least one combination involving each insulating material on each blade material. Thirty-six blades were utilized in this sequence.

For evaluation of gage systems, involving parameters 5 and 6 of Table XI (four gage materials, two gage thickness), strain gage elements of all four materials of Table X were sputtered on newly prepared specimens of the 11 candidate combinations which had survived the insulation evaluations. Then, the second selected values of gage thickness were fabricated and tested for selected cases, gage systems on five blades were overcoated and tested, and repeats were fabricated and tested. Eighty-seven gage systems were fabricated on 55 blades in this sequence.

For parameter 7 of Table XI (lead wire connections), lead wire connections trials were conducted for all four strain gage materials, each on one insulating material. A total of 12 additional blades were utilized in this sequence.

Test items, fabrication procedures, and test procedures are described in the following sections.

TABLE X

CANDIDATE MATERIALS AND CONFIGURATIONS·

Compressor Blades:

600K Material	AMS 4928 (Ti-6A1-4V)
600K Configuration	Figure 9
900K Material	Incoloy 901 (PWA 1003)(Fe-42Ni-12Cr)
900K Configuration	Figure 9

Surface Preparation
1. Polish, 0.12 μm (5 microinch)
2. Roughen with light grit blast

Insulating Film:

Materials:
1. Al_2O_3; aluminum oxide
2. HfO_2; hafnium oxide
3. Si_3N_4; silicon nitride
4. SiO_2; silicon dioxide

Thicknesses:
1. 2.5 μm
2. One other thickness if required

Strain Gage:

Configuration   Figure 10

Film Materials:
1. Ni-30Cr; nickel-chromium
2. Cu-45Ni; copper-nickel
3. Pt-20W; platinum-tungsten
4. Pd-30Mo; palladium-molybdenum

Film Thicknesses:
1. 1.25 μm
2. One other thickness if required

Lead Film;

Configuration   Figure 10

Materials   Same as strain gage

Thicknesses   Same as strain gage

Overcoat Film:

Material   Same as insulating film

Thicknesses   Same as insulating film

Lead Wire:

Materials:
1. Ni-10Cr (Chromel) for gages of Ni-30Cr
2. Cu-45Ni (Constantan) for gages of Cu-45Ni
3. Pt (platinum) for gages of Pt-20W and Pd-30Mo

Diameter   76 μm (0.003 inch)

Connection Method
1. Brush Plating
2. Braze
3. Flame Spray
4. Resistance Weld
5. Laser Weld
6. Ultrasonic Weld
7. Hot Compression Bond
8. Conductive Cement

TABLE XI

INDEPENDENT PARAMETERS IN COMPONENTS PROGRAM

Parameter Number	Parameter Description	Number of Parameter Values
1	Blade Material	2
2	Surface Finish	2
3	Insulating Film Material	4
4	Insulating Film Thickness	2
5	Gage Film Material	4
6	Gage Film Thickness	2
7	Lead Wire Connection Method	8

4.2 DESCRIPTION OF TEST BLADES

Used blades from a high-pressure axial-flow compressor were used as substrates throughout the components fabrication and test program. Strain gage components for 600K service were fabricated on the AMS 4928 titanium alloy blades shown in Figure 9a. Components for 900K service were fabricated on the Incoloy 901 steel alloy blades shown in Figure 9b. Sample blades were analyzed to verify that composition was within commercial tolerances for each blade material. All surface preparation and component fabrication were performed on the concave side of the blade (pressure side) only. Insulation layers were sputtered over the entire airfoil surface on this concave side.

4.3 SURFACE PREPARATION PROCEDURES

The following two surface treatments were investigated:

o A 0.12 μm (5 microinch) arithmetric average (AA) polish.

o A 0.12 μm polish followed by a light grit blast using aluminum oxide 320-grit at 280 kPa (40 psi) gage pressure at a distance of 10 cm, and an angle of 90+20 degrees, for about 1 minute to produce a uniform dull appearance. The roughness of this surface is on the order of 0.12 m AA but the peening action of the grit blast produces a reticulated surface character that is more conducive to adherence of some films.

All blades were polished by hand in an engine parts finishing shop using high speed cloth wheels charged with either ferric oxide (rouge) or silica abrasives. Since the blade surfaces were smooth, prepolishing operations, such as grinding, were not required. Only the concave surfaces of blades were polished. The polished surfaces were microscopically examined and those having deep scratches were repolished. The final surface finish produced was measured with a laboratory profilometer employing a traversing mechanical stylus (2.5 μm tip radius) with optical readout.

1 CM

A   B
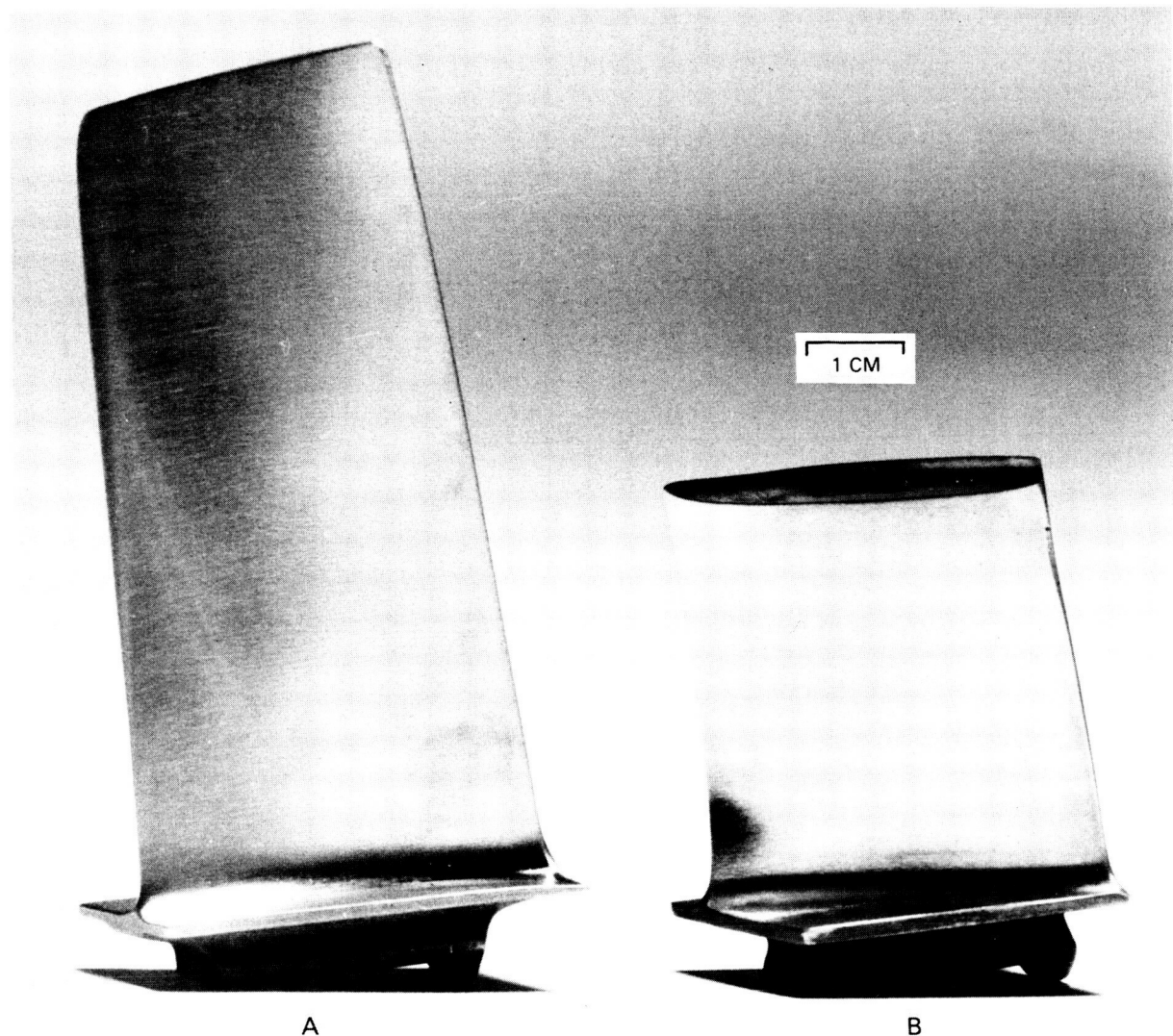
Figure 9   Compressor Blades Used in the Components Program.   (A) AMS 4928
            titanium alloy blade for service to 600K.   (B) Incoloy 901 nickel
            steel alloy blade for service to 900K.

After polishing, the blades were cleaned in a hot ultrasonic bath of strong
detergent mixed with deionized water. The cleaning was continued until the
polished surfaces passed a water break test. In the water break test, any
breakup or beading of a water film on the surface indicates unacceptable
contamination.

The blades were rinsed several times in 90°C deionized water, blown dry with
high purity nitrogen gas, and stored in a dessicating cabinet after cleaning.
The Incoloy 901 and titanium blades were baked in air at 900K and 600K,
respectively, for 1 hour to decompose any organic contamination. Blades that
were stored for more than a day after baking were hot freon vapor cleaned just
prior to sputtering of the insulating film.
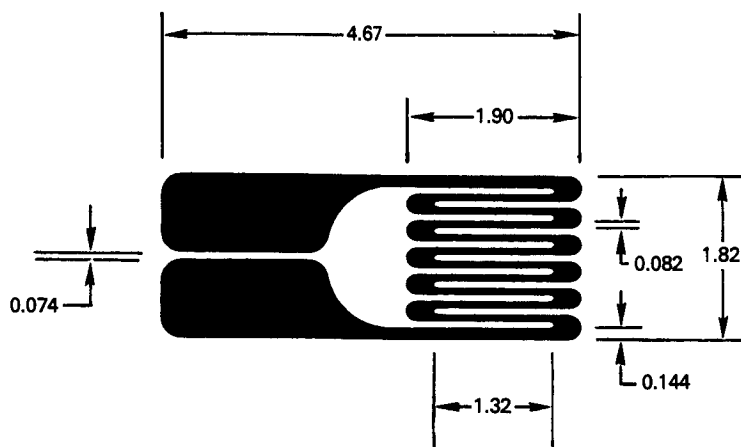
ALL DIMENSIONS IN MILLIMETERS

Figure 10 Component Program Gage Configuration.

4.4 SPUTTERING PARAMETERS

The two sputtering facilities used in the current contract program, described previously in Reference 4, are specifically designed for r-f sputtering of metals and dielectrics. One facility is a small planar unit, using 15-cm diameter flat disk targets, providing moderate sputtering rates and providing uniform sputtering over a working area of 10-cm diameter at a height of about 7.5 cm from the target. The other facility is a large magnetron S-gun unit, using complex (more expensive) conical targets, providing high sputtering rates and providing uniform sputtering over an annular working area of about 10-cm width and 25-cm mean diameter at a sputtering height of about 15 cm from the target. Experience in several programs, including the present contract program, indicates that the quality and structure of thin films produced in the two units are identical when appropriate sputtering parameters are used. The sputtering parameters used in the present contract program are listed in Table XII. Targets of aluminum oxide (Al_2O_3), silicon (Si), and silicon dioxide (SiO_2) were already available in both planar and S-gun configurations; either sputtering unit was used to sputter films requiring these target materials depending upon which sputtering unit was unoccupied at the time. Targets of the other materials needed were not available in the S-gun configuration; the planar unit was therefore used for all sputtering of these other materials to avoid the higher cost of acquiring special targets in the S-gun configuration.

The target material in most cases was the desired film material in cast bulk form with a purity of better than 99.99 percent. Exceptions, noted in Table XII, were as follows:

TABLE XII

SPUTTERING PARAMETERS

Sputtered Material	Target Material	Target Type	Target Self Bias (DC Volts)	Gas Composition	Gas Pressure (Pascal)	Sputter Height (cm)	Sputter Rate (μm/hr)
Al_2O_3	Al_2O_3	S-Gun	800	Ar-5%O_2	0.33	15	0.21
Al_2O_3	Al_2O_3	Planar	1100	Ar-5%O_2	0.66	7.5	0.12
Si_3N_4	Si	S-Gun	400	N_2	0.33	15	0.21
Si_3N_4	Si	Planar	1500	N_2	0.66	7.5	0.12
SiO_2	SiO_2	S-Gun	900	Ar	0.33	15	0.66
SiO_2	SiO_2	Planar	1100	Ar	0.66	7.5	0.14
HfO_2	HfO_2	Planar	1100	Ar-50%O_2	0.66	7.5	0.10
Pd-30Mo	Composite	Planar	900*	Ar	0.66	7.5	0.60
Pt-20W	Composite	Planar	900*	Ar	0.66	7.5	0.45
Ni-30Cr	Ni-30Cr	Planar	900*	Ar	0.66	7.5	0.32
Cu-45Ni	Cu-45Ni	Planar	900*	Ar	0.66	7.5	0.32

* Input power limited by maximum working temperature of photoresist masks.
Note: 1 Pascal = Torr x 133.32.

o Silicon nitride was reactively sputtered from pure silicon in a pure nitrogen atmosphere.

o Noble metal alloys (Pd-30Mo and Pt-20W) were sputtered from composite planar targets fabricated in-house. A pure planar target of the low-cost material (Mo or W) was masked and sputtered with islands of the pure noble metal (Pd or Pt). After removal of the masking material, this composite was then used as a target to sputter the desired films. The exposed area of each atomic species was adjusted by trial until the desired composition was obtained.

4.5 INSULATING FILM TEST PROCEDURES

Thickness

Film thickness, t_2, in initial runs was determined after sputtering by measurement with an optical interferometric microscope on sample glass slides sputtered simultaneously with the test blades. Glass slides were included in the first few runs of each new material sputtered. After a repeatable calibration curve of thickness versus sputtering time under standard operating conditions had been established, the slides were omitted, and thickness was assumed to correspond to sputtering time.

Adherence

A length of adhesive tape (Connecticut Hard Rubber Co., Type TV, or equal, teflon tape with pressure sensitive silicone polymer adhesive) was applied, adhesive side down, to the surface of the test piece and firmly pressed down to ensure intimate contact with the entire sputtered film area. The tape was left in place for 30 to 60 seconds and then removed by pulling one end normal to the test surface until entirely removed. Both the tape adhesive and the test surface were visually examined during and after tape removal for indications of sputtered film or its removal. Tape adhesive residue on the test surface was removed by ultrasonic solvent cleaning prior to further testing. If film removal was observed over more than 1 percent of the film area, the test piece was rejected.

Hardness

Hardness and probe penetration of sputtered insulation layers were measured by hand pressing a chromium plated steel test probe, with a tip diameter of 0.64 mm, into the insulation-layer surface until an electrical short was produced. Load was not measured during the individual hardness tests, but a calibration indicated that "easy penetration" was in the load range of 2N (0.5 lbf) and "very hard" was in the range of 70N (15.8 lbf).

Chemical Composition

The electron microprobe technique was used to determine chemical composition of sample films as sputtered on glass slides.

Surface Morphology

An optical microscope (10X to 100X) was used to examine the surface structure of sample films as sputtered on actual blades.

Resistivity as Sputtered

The resistivity ρ_2 was determined from resistance measurements (R, ohms), using 0.1 cm^2 patches of conductive silver paint, and the known thickness (t_2, cm), using the relationship

$$\rho_2 = 0.1 \frac{R}{t_2} \qquad (6)$$

A low voltage source (1.35 volts) ohmmeter (Data Processor 175) was used for each resistance measurement to avoid premature electrical breakdown of the insulating film. One terminal of this ohmmeter was connected to the 0.1 cm^2 patch and the other terminal to the bare base metal of the test piece. The resistivity was measured at six locations randomly selected on the blade surface. The contact with the blade surface was made on the reverse (uncoated) side of the blade in a region which was first abraded to obtain a clean metal surface.

Dielectric Breakdown as Sputtered

Dielectric breakdown voltage was determined by connecting an adjustable low voltage, D.C. power supply across the insulating film (with +voltage supplied at film surface) through a series 4900 ohm resistor. A digital voltmeter (DVM) monitored the voltage across the insulating film. Another DVM was connected across the series resistor to determine when breakdown occurred. The test began by slowly increasing the power supply voltage until a sharp increase in the voltage across the series resistor occurred. The highest voltage observed across the insulating film (before breakdown) was used to calculate the dielectric breakdown strength in volts per cm based on earlier film thickness measurements.

Resistivity After Four Cycles to Service Temperature

The resistivity measurements were repeated at room temperature after four thermal cycles to the planned service temperature (600K for AMS 4928 blades, 900K for Incoloy 901 blades). A thermal cycle consisted of placing the blade into an oven preheated to planned service temperature, soaking until the blade reached oven temperature, soaking for a further 1 to 5 minutes, removal from the oven, and air cooling. The temperature of the blade was monitored by a wire thermocouple attached to the reverse (convex) side. The insulating layers were then visually examined, and, in some cases, the hardness and adherence tests were repeated.

4.6 GAGE FILM MASKING PROCEDURE

The gage alloy configuration used in the components program consisted of one or more strain gage patterns (Figure 10) and, on some blades, two test stripes. The test stripes were 13mm long and 2mm wide located about 1 cm from the gage. The gage pattern of Figure 10 is a 12-line grid slightly smaller than the 2 mm x 2 mm design of Figure 7, Example 2. Lead films length to width ratio is about 2, to keep total resistance of both lead films at about 2% of gage resistance.

Two types of masking were used to produce the test pattern. The strain gage was masked with a photographic mask on which the image of the strain gage was clear on an opaque background. The test stripes were masked by applying 3M Company no. 218 tape, cut to size, directly to the insulation surface.

The masking procedure began by tape masking the test stripes on a blade that had a sputtered insulating film. The blade was then dipped tip first into a container of Shipley No. AZ-1350-J positive working photo resist. After drying in air for 30 minutes, the tape was removed and the blade was baked at 90°C in air for 30 minutes with a heat gun to dry the photoresist. After cooling, the strain gage photographic mask was clamped to the concave, resist-coated, surface of the blade. The assembly was exposed to a 200 watt collimated ultraviolet light source for about 7 minutes. The mask was removed and the strain gage pattern developed in Shipley, AZ developer, mixed 1:1 with deionized water. The developing process removed the resist that had been exposed through the clear portion of the photomask. The result was that the surface of the blade was uncovered in the form of the clear pattern on the photomask. Development time was 1-2 minutes. After development, the blade was rinsed for 1 minute in deionized water with agitation, blown dry with pure nitrogen gas and inspected with a 70X microscope. If the photoresist pattern was unacceptable, the photoresist was stripped in a solvent and the blade was recleaned and remasked. If accepted, the blade was then baked at 100° - 120°C and installed in the sputtering system for sputtering of the strain gage alloy.

After sputtering of the strain gage alloy was completed, the remaining (unexposed) portions of the resist coating were stripped form the surface of the blade by soaking in an agitated solvent. The stripping solution used was either A. C. 3 grade acetone or Shipley 1112A remover mixed 1:1 with deionized water and heated to 80°C. Stripping times required were highly variable and could extend to an hour or more because the unexposed resist was covered with a sputtered film of strain gage alloy. Blades stripped in remover were given a hot (80°C) water rinse and blown dry with pure nitrogen gas. The blade was then stored in a dessicating cabinet.

4.7 GAGE FILM TEST PROCEDURES

The following sequence of tests was performed, in the order given, on selected thin film strain gages.

Thickness

Thickness of gage material films was determined by the optical interferometer on sample glass slides sputtered simultaneously with test blades. After a calibration curve of thickness versus sputtering time under standard operating conditions was established, the glass slides were omitted and thickness was assumed to correspond to sputtering time.

Adherence

The first test of gage adherence was survival of the gage film during removal of photoresist, a procedure involving agitation in hot solvents. On some blades the adhesive-tape test described in Section 4.5 was also used to characterize the adherence of sputtered gage films which survived photoresist removal, using the test strips of gage material sputtered adjacent to the gage pattern. The tape test was carried out on one test strip in the as-sputtered condition and on the other test strip after completion of gage testing at maximum service temperature.

Composition

The electron microprobe technique and wet chemical techniques were used to determine chemical composition of sample gage material films sputtered on glass slides. In selected cases, the film composition was surveyed for uniformity over large areas by Energy Dispersive Analysis with Y-Rays (EDAX). This technique permits mapping the distribution of selected atomic species over a surface area up to several hundred micrometers square. By adjustment of applied energy, the depth of the layer sampled could be adjusted from 0.5 microns to several microns.

Pesistance as Sputtered

As-sputtered gage resistance was measured with the low-voltage-source ohmmeter, using test prods to make contact with the lead films.

Insulation Resistance Under Gage

Resistance of the insulating film under the gage was measured at room temperature with the low-voltage-source ohmmeter, using test prods to make contact with the lead film and the blade surface. The contact with the blade surface was made on the reverse (uncoated) side of the blade in a region which was first abraded to obtain a clean metal surface.

Resistance After Thermal Cycles to Service Temperature

Each sputtered strain gage was then heat treated by a series of one-hour exposures in air at the planned service temperature. The gage resistance and resistance to ground were measured at room temperature after each hour, using test prods and the low-voltage source ohmmeter.

In addition, some of the noble-metal alloy gages were vacuum heat treated for various periods at service temperature before exposure to air at service temperature. These heat treatments are described for each gage in the discussion of results.

Resistance at Service Temperature

If the gage survived the cycles to service temperature described above, temporary lead wires were then mechanically clamped to the gage lead films and to the blade metal surface (ground) for final high-temperature testing. Lead wire materials were those listed in Table X. Lead wire diameter for these tests was typically 250 μm, the length typically 30 cm., and resistance typically as follows:

Ni-10Cr	:	4.3	ohms
Cu-45Ni	:	2.9	ohms
Pt	:	0.6	ohms

The gage resistance and resistance to ground were then monitored during a temperature cycle to service temperature.

Approximate Gage Factor

After the thermal cycle tests, the approximate gage factor at room temperature was determined by applying a bending load to the blade. A reference commercial foil strain gage was mounted on a spare blade at the same location to determine the strain with the same loading applied. The resistance of the sputtered gage was measured with the low-voltage-source ohmmeter with a resolution of 0.1 ohm. This sensitivity was adequate to measure gage factor with a resolution of 0.25 for a gage resistance of 200 ohms and 2000 microstrain. One edge of the blade was clamped in a vise and a force large enough to produce between 1000 and 2000 microstrain was applied to the free edge. The strain cycle was repeated four times to determine repeatability. The gage factor test was applied to each candidate sensor alloy at least one time.

Apparent Strain Due to Temperature

Approximate apparent strain due to temperature (microstrain per Kelvin) was calculated from the equation:

$$\text{Apparent Strain} = \frac{10^6 \, (R_2 - R_1)}{R_1 G \, (T_2 - T_1)} \tag{7}$$

where R_2 and R_1 are resistance values measured respectively at planned service temperature, T_2, and at room temperature, T_1 (during the tests of resistance at service temperature), and G is the approximate gage factor measured at room temperature.

Erosion

The objective of the erosion test was to determine the relative durability of thin film strain gages under conditions of erosion by a hard abrasive material. Base line for the erosion tests was the rate of erosion of a 2 m sputtered platinum - 10% rhodium strip on an oxidized NiCoCrAlY coated MAR-M 200 + Hf substrate. This combination of materials is representative of sputtered films that have been successfully operated in an engine hot section environment for 150 hours.

The erosion tests were performed in an S.S. White industrial air abrasive unit using S.S. White No. 1 Al_2O_3 (27 μm particle size) at a nominal pressure of 40 psi. The nozzle was located about 10 cm from the sensor surface at an angle of about 30 degrees from the normal. The size of the particulate stream at the blade surface was approximately 6 mm x 6 mm. Initial tests of the reference platinum - 10% rhodium films in this apparatus indicated that measurable erosion (and sometimes failure) occurred in a minute or less. The standard test sequence arbitrarily adopted was then a series of 9-second exposures of the thin film gage to the particulate stream. After each 9-second exposure the stream was turned off and the gage resistance and resistance to ground were measured with the ohmmeter (four significant figure resolution) using test prods to contact the lead films and the blade. Photographs of erosion damage were obtained in selected cases.

4.8 OVERCOAT TRIAL PROCEDURES

The purpose of the overcoat trials was to determine to what extent oxidation protection and erosion protection could be provided by applying a sputtered overcoat of the same material as the insulating film.

Two of the insulating materials (Al_2O_3 and Si_3N_4) were selected for trial. Thin film gage systems on five test blades were overcoated. The lead films were masked before sputtering of overcoats, so that lead films remained uncoated. The sputtering parameters of Table XII were used. The thickness of the overcoat was approximately equal to the thickness of the insulating layer. The five samples included gage systems with Al_2O_3 and Si_3N_4 on polished AMS 4928, Al_2O_3 on polished Incoloy 901, and Si_3N_4 on roughened Incoloy 901.

Each of these overcoated gage systems was subjected to at least two thermal cycles to planned service temperature and five strain cycles to a level between 1000 and 2000 microstrain at room temperature. A thermal cycle consisted of placing the blade into an oven preheated to planned service temperature, soaking until the blade reached oven temperature, soaking for a further 1 to 5 minutes, removing from the oven, and air cooling. The temperature of the blade was monitored by a wire thermocouple attached to the reverse (convex) side. A strain cycle consisted of one application and removal of the load previously used during gage factor testing (Section 4.7)

At the end of each thermal cycle and each strain cycle, the sputtered films were visually examined for cracking and spalling, gage resistance was measured, and resistance from gage to blade was measured. The resistance was measured with the low-voltage-source ohmmeter using test prods to contact the uncoated lead films and the blade.

After the thermal cycles and strain cycles were completed, overcoated gage systems were subjected to the erosion test described in Section 4.7.

4.9 LEAD WIRE CONNECTION TRIAL PROCEDURES

Eight methods for lead wire connection were investigated. Table X summarizes the lead wire materials and connection methods. Insulation layers plus thin film gages and strips of gage film material were sputtered on extra blades for these trials (except where otherwise noted). The gages and strips were sometimes heat treated before lead wire attachment. It was expected that the most reliable connections would be obtained on gage material surfaces not previously subjected to high temperatures and possible surface oxidation.

The strength of bond achieved was measured where appropriate by using a force gage attached to the lead wire. Peel strength (wire pulled at 90 degrees to the plane of the film until peeling began) was the primary measurement. Electrical resistance of the wire to film connection and of the insulating layer under the film was measured with the low voltage source ohmmeter. Tests were performed before and after cycles to planned service temperature.

The following procedures and equipment were used in the lead wire connection trials in the components program. Each procedure began by clamping or taping a clean lead wire in position on the surface, with the lead wire extending across the lead film.

Brush Plating

For connection of Ni-10Cr lead wires to NiCr lead films, one electrode (positive) of a plating current supply was connected to a platinum wire inside an applicator brush and the second electrode (negative) was connected to the part to be plated (wire, film, or both). Commercially available nickel-plating solutions were applied to the parts by brushing, with plating current turned on. Variables investigated were brush geometry, electrical current level, electrical connection geometry, composition of the plating solution, and cleaning procedures.

The applicator brushes were shory lengths of flexible, porous, woven glass fiber tubing 0.5 mm to 1 mm diameter (Varflex Corp., R9me, N. Y. 13440, Class H NEMA electrical insulation sleeving) in straight and looped forms. Plating currents from 1 ma to 40 ma were employed. Second electrode connection to lead film alone, lead wire alone, and both simultaneously were tried. The plating solutions used were No. SPS 5630 Special Nickel and No. SPS 5650 Neutral Nickel (products of Selectron Ltd., 137 Mattatuck Hts. Rd., P.O. Box 115, Waterbury, CT 06720). In some trials, the wire and film were cleaned by a two step procedure recommended by the supplier of the plating solutions: application of No. SCM 4100 cleaning solution followed by No. SCM 4200 activator solution. In other trials, cleaning was accomplished by ultrasonic agitation in a detergent bath followed by deionized water rinse.

Oven Braze

This technique was investigated for connection of Ni-10Cr lead wires to Ni-30Cr lead films on high-temperature (900K) blades only. The junction was coated with a silver solder paste of American Welding Society (AWS) Specification BAg4, with a solidus temperature of 944K (1240°F) and a liquidus temperature of 1052K (1435°F). The assembly was placed in a furnace and the temperature was increased until the braze material was observed to melt and flow. To avoid oxidation of the wire and film during brazing, some trials were conducted in an argon-filled furnace and in a vacuum furnace.

Flame Spray

Tape masking was applied to leave exposed only a small region around the junction area between lead wire and lead film (typically 1 mm x 0.3 mm). A flame-sprayed coating of Metco ^{TM} 443 NiCrAl powder was applied using a hand-held flame-spray gun. This procedure was identical with that commonly used for application of NiCrAl precoats for high temperature wire strain gage installations on airfoils.

Parallel Gap Pesistance Weld

A small commercial parallel gap welding head (Unitek^{TM}) was used to apply an adjustable constant contact pressure, by a spring load, to a pair of welding electrodes 0.46 mm (0.018 inch) wide, spaced 76 μm (0.003 inch) apart. A variable transformer provided adjustable 60 Hertz alternating current flow through the electrodes and through the 76 μm lead wire between the two electrodes. With current turned off, an initial spring load was selected to provide firm contact. Current ws then increased until the lead wire attained a high temperature (typically cherry red), and then the current was held constant for a selected dwell time. Flattening and deformation of the lead wire was observed during this period. The variables investigated included contact load, current, and dwell time.

Laser Weld

A survey of vendors of laser welding equipment was conducted. Two vendors were found willing to attempt welds of 76 μm platinum 10% rhodium wire to platinum 10% rhodium films, materials being already used in a related in-house

program. Film samples were prepared consisting of 2 μm sputtered platinum films on 2 μm Al$_2$O$_3$ layers on flat plates of NiCoCrAlY coated Hastelloy X. Ten film samples were submitted to each vendor for trial. The objective was to identify commercially available laser welder equipment with a potential for further trail in thin film applications.

Ultrasonic Weld

A commercial ultrasonic welding unit (Sonobond^{TM}) successfully used in the past for wire-to-wire bonds in the wire diameter range of 76 μm to 127 μm was used for trials of wire to thin film connection. This unit provided an adjustable constant preload to a single electrode typically 1.6 mm (0.063 inch) wide, with adjustable dwell time and adjustable power ultrasonic agitation at 100 kHz. Flattening and deformation of the lead wire occurred when power was turned on. The variables investigated were preload, dwell time, and power.

Hot Compression Bond

Clamping pressure was applied to reduce the wire diameter by 20 to 50 percent and the test piece held at 50K above planned service temperature until a successful bond occurred or film damage occurred, or until 8 hours was reached, whichever happened first. Insulation resistance was monitored to determine whether the clamping pressure applied damaged the sputtered insulating layer in the strain gage system.

Conductive Cement

Four candidate conductive cements were applied to trial junctions, as follows:

o Walsco^{TM} 36-1 silver-filled butyl acetate cement, a conductive cement used in printed circuit repair work, requiring only air drying at room temperature.

o Walsco^{TM} 36-1 plus Ceramadip^{TM} No. 518 thinner. The thinner is a ceramic cement, added to promote improved adherence at high temperatures. This combination was air dried at room temperature for 1 hour and then baked at 350 K (170°F) for 4 hours to cure the ceramic thinner.

o Silver-filled polyimide, consisting of equal volumes of 1 μm silver powder (from Consolidated Astronautics Corp. of Hauppauge, New York) and polyimide resin (Denex^{TM} No. 8), purchased from Dentronics Inc., of Hackensack, N. J.). A small drop of cement is applied to the lead film so that the lead is covered. The paste cure schedule is: one houre at room temperature one hour at 390K (250°F) and one hour at 480K (400°F). Joints are not clamped during the cure.

o Nickel-filled ceramic, consisting of two parts 5 μm nickel powder (from Consolidated Astronautics, Happange, N.Y.) to one part Cerama-Bind No. 542 (from Aremco Products, Inc., of Ossining, N.Y.). A small drop of cement is applied to the lead film so that the lead is covered. The joint is clamped using Teflon tape and a silicone rubber pad. The cure schedule is: one hour at room temperature, one hour at 370 (200°F) and one hour at 480K (400°F).

4-15

SECTION 5.0

GAGE PROGRAM FABRICATION AND TEST PROCEDURES

5.1 OVERVIEW

Four of the thin-film strain gage system designs evolved in the Components
Program for use on compressor blades were selected for extensive fabrication
and evaluation in the Gage Program. The four systems selected were designated
Type A, Type B, Type C, and Type D, and are described in Table XIII. The
principle features are tabulated below:

Type	Compressor Blade Material	Service Temperature	Insulation Layer and Overcoat Material	Gage Material
A	AMS 4928	600K	Si_3N_4	Ni-30Cr
B	AMS 4928	600K	HfO_2	Cu-45Ni
C	Incoloy 901	900K	Si_3N_4	Ni-30Cr
D	Incoloy 901	900K	Al_2O_3	Ni-30Cr

A fifth thin film dynamic strain gage type, designated Type E, also described
in Table XIII, was designed for service to 1100K on PWA 1422 (MAR M200 + Hf
superalloy) turbine blade material. The Type E gage design uses the same
insulating layer (Al_2O_3), gage material (Ni-30Cr) and overcoat (Al_2O_3)
as the Type D system, but this entire sputtered gage system is applied over
the grown (Al_2O_3) layer produced by the method of Reference 4, involving
1300K heat treatment of an alumina-forming coating (NiCoCrAlY) applied to the
turbine blade material. This process produces an Al_2O_3 film known to be
adherent and durable to at least 1300K. The process is not applicable to
compressor blade materials because of the high temperature required in the
alumina-forming heat treatment.

The five types of thin film strain gage systems were fabricated on flat bars
of the appropriate blade materials and were subjected to lead wire attachment
tests, gage factor tests, thermal cycle tests, and fatigue tests. In addition,
Type A and Type C systems were spin tested to 100,000 G, and, Type A, B, C,
and E systems were erosion tested.

The remainder of this section describes the gages, bars, test configurations,
fabrication procedures, and test procedures.

5.2 GAGE PROGRAM GAGE DESIGNS

The strain gage system materials, finishes, film thicknesses, and lead-wire
connection method used in the final fabrication of Types A, B, C, D, and E
gages are listed in Table XIII. During some initial trials of fabrication of
gages on the flat bars, some variations in finishes, thicknesses, and lead-
wire connection were explored. These variations and their effects are
described in Section 7.0, Gage Program Results.

TABLE XIII

GAGE DESIGNS FOR THE GAGE PROGRAM

	Gage Type				
	A	B	C	D	E
Surface Finish	Polished 0.12 μm	Polished 0.12 μm	Polished 0.12 μm	Polished 0.12 μm	Roughened See Ref. 4
Insulating Layer:					
Material	Si_3N_4	HfO_2	Si_3N_4	Al_2O_3	Al_2O_3
Thickness (μm)	4.5	4.5	4.5	4.0	3 (Note 1)
Gage Pattern	Fig. 11	Fig. 11	Fig. 11	Fig. 11	Fig. 11
Gage:					
Material (atomic %)	Ni-30Cr	Cu-45Ni	Ni-30Cr	Ni-30Cr	Ni-30Cr
Thickness (μm)	1.2	1.2	1.2	1.2	1.2
Lead Film:					
Material (atomic %)	Ni-30Cr	Cu-45Ni	Ni-30Cr	Ni-30Cr	Ni-30Cr
Thickness (μm)	1.2	1.2	1.2	1.2	1.2
Overcoat:					
Material	Si_3N_4	HfO_2	Si_3N_4	Al_2O_3	Al_2O_3
Thickness (μm)	2	2	2	2	2
Lead Wire:					
Material (atomic %)	Ni-10Cr	Ni-10Cr	Ni-10Cr	Ni-10Cr	Ni-10Cr
Diameter (μm)	76	76	76	76	76
Attachment Method	Note 2	Note 2	Note 3	Note 3	Note 3

Note 1: Sputtered on Oxidized NiCoCrAlY (PWA 270) on MAR-M 200 + Hf (PWA 142?) Turbine Blade Material, per Reference 4.
Note 2: Silver-filled polyimide cement.
Note 3: Nickel-filled ceramic cement.

The gage configuration employed throughout the gage program is shown in Figure 11. The gage grid is the same 12-line, 2 mm x 2 mm pattern used in the Components Program (Figure 10), but the lead films are wider and spaced farther apart to facilitate lead-wire connection. The lead-film length-width ratio of 18 assured that the total resistance of the two lead films would be less than 3% of the gage resistance as discussed in Section 3.8. The overcoating, as noted in Figure 11, covers all of the gage grid and part of the lead film, but most of the lead film is left bare for connection of lead wires. A thin protective overcoating of cement is later applied over the lead wires and lead films, as described in Section 5.4.
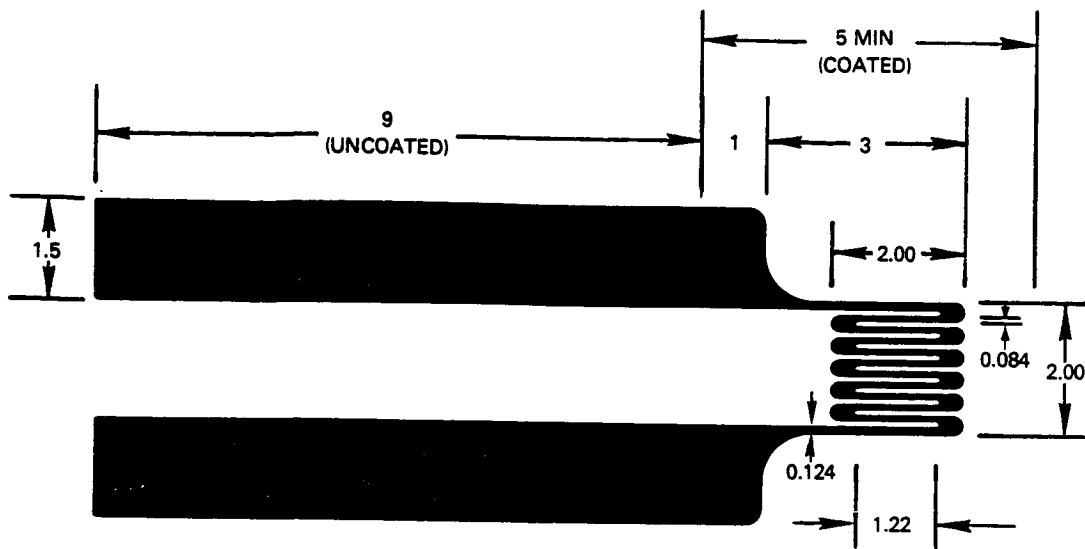
ALL DIMENSIONS IN MILLIMETERS

Figure 11 Gage-Program Gage Configuration. (83-A1352-003)

5.3 DESCRIPTION OF TEST BARS

Thin film strain gage systems were fabricated on flat test bars of three different sizes as follows:

o Static test bars 16.75 cm x 3.50 cm, Figure 12, used for gage factor tests, thermal cycle tests, and fatigue tests by the contractor.

o Special bars 16.5 cm x 3.5 cm, Figure 13, for delivery to NASA.

o Spin test bars, 9.62 cm x 0.95 cm, Figure 14, used for 100,000 G spin testing and for erosion testing by the contractor.

Two thin film strain gages were fabricated on each test bar. The thin film gage locations are shown in Figures 12, 13 and 14.

The static test bars and the special NASA bars were designed for constant bending strain over the tapered section of uniform thickness, near the center of the bar, when the large end of the bar is clamped and the small end of the bar is deflected by applying a load at the point where the two tapered edges would meet if extended beyond the end of the bar. The fixture used by the contractor to apply loads to the static test bars of Figure 12 is described in Section 5.5.

On the static test bars and on the special NASA bars, a reference commercial foil strain gage and a Chromel-Alumel thermocouple were also mounted as shown in Figure 12. The reference gage was a Micromeasurements™ WK-60-062-AP-350 with option B-87 (76 μm nickel clad copper leads attached), a 1.57 mm (0.062 inch) nickel-chromium alloy gage with glass-film reinforced epoxy-phenolic resin carrier for short-term service to 670K. The commercial gage was used to verify applied strains during initial tests on each test bar, as described in Section 5.5. The thermocouple provided surface temperature data.
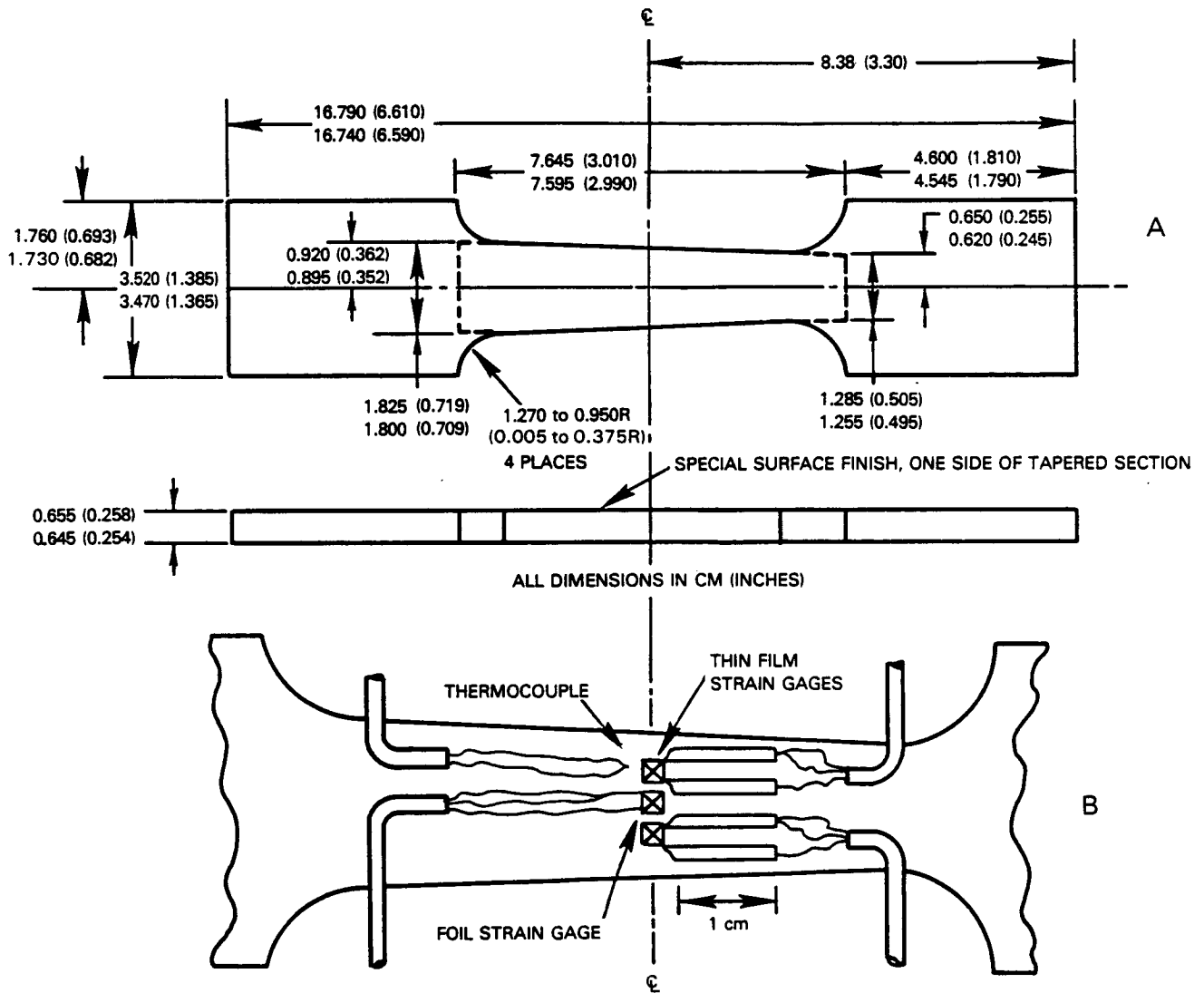
Figure 12   Static Test Bar Design.   (A) Dimensions of Test Bar.   (B) Layout of Instrumentation on the Test Bar.

The static test bars and special NASA bars were fabricated in each of the three materials used in the gage program (AMS 4928, Incoloy 901, and MAR-M200 + Hf). Spin test bars were fabricated only in AMS 4928 and Incoloy 901, since spin testing of MAR-M200 + Hf bars was not planned.

AMS 4928 and Incoloy 901 test bars were machined from commercial bar stock produced by consumable electrode or induction vacuum melting, heat treated to compressor blade material specification. MAR M200 + Hf (PWA 1422) test bars were machined from billets cast in-house (vacuum melted, vacuum cast) and solution heat treated to MAR-M200 + Hf turbine blade material specification, but without directional solidification.

The composition and properties of the three alloys were presented in Section 3.3 and Table II. Composition of samples of each batch of the materials used during fabrication were verified by wet chemical analysis and found to be within specified tolerances.

ALL DIMENSIONS IN CM (INCHES)

Figure 13 Special Test Bar for Delivery to NASA.

1.30 (0.510)
1.25 (0.490)

0.025 to 0.090R
(0.010 to 0.035R)

4.60 (1.810)
4.55 (1.790)

1.130 (0.445)
1.105 (0.435)

2.430 (0.956)
2.415 (0.951)

8.38 (3.30)

℄ GAGES

9.65 (3.810)
9.60 (3.790)

ALL DIMENSIONS IN CM (INCHES)

Figure 14   Spin Test Bar. Note that the spin test bar is a modification of the static test bar which is defined by the dashed lines.

The test bars were machined to shape washed in hydrocarbon solvents, and then were baked in air for at least three hours at service temperature (600K for AMS 4928, 900K for Incoloy 901 to vaporize remaining traces of organic contaminants such as cutting oils. Then the top and bottom surfaces were surface ground to a finish of approximately 0.38 μm AA (15 microinches). Polishing procedures described in Section 5.4 were then used to prepare the surface on the central tapered portion of each test bar for thin film strain gage deposition.

5.4   GAGE SYSTEM FABRICATION PROCEDURES

Overview of Type A, B, C, and D Gages

The sequence of fabrication operations listed in Table XIV was performed on each test bar of compressor blade material to fabricate a type A, B, C, D, or E thin film strain gage:

The procedures finally used in each operation were based on the techniques evolved during the Components Program, described in Section 4.0, with some significant alterations which were found necessary during the Gage Program. The alterations stemmed partly from the different starting condition of the bar material compared with actual finished blades (requiring special polishing of the bars) and partly from the discovery of problems with long-term adherence of some sputtered films on the bar materials as well as chemical incompatibility of Al_2O_3 with alkali stripping agents (which had not been obvious during the Components Program). During trials of fabrication of each gage type on the test bars, some variations in finishing, stripping, and cleaning procedures were explored to overcome such problems. These variations and their effects are described in Section 7.0, Gage Program Results.

5-6

The final fabrication procedure for the Type A gage system is described first in detail below. The final fabrication procedure for the Type B, C and D gage systems was the same as for Type A, with some exceptions. The exceptions are described briefly after completing the Type A description. Table XIV is a summary of the final fabrication procedures for each gage type. The table provides a cross reference for the following narrative descriptions of procedures.

Type A Gage

Surface Preparation

One side of each bar was polished at the United Technologies Research Center with a Strasbauch Model RZR-1 polishing machine. The polishing process began with No. 120 grit silicon carbide abrasive paper and continued using the following, successively finer, grades of abrasive: No. 600 grit silicon carbide, 6 μm diamond paste, 1 μm diamond paste and finally, 0.3 μm alpha alumina. Polished bars were stored in a dessicating cabinet to minimize the accumulation of surface moisture.

When test bars were scheduled for fabrication of thin film strain gages, the bars were cleaned by ultrasonic agitation in a bath of hot detergent solution and rinsed in hot (350K) deionized (DI) water until the polished surfaces passed the water break test. After a final rinse in hot DI water, the bars were blown dry with pure, dry nitrogen gas, baked at 600K in air for one hour, and while still warm <u>immediately</u> installed in the sputtering system for sputter etching. (Cleaned bars which were not used immediately were stored in a dessicating cabinet. Bars stored for more than a few days were recleaned. All cleaned bars were handled with rubber gloves.)

Each bar was then sputter etched (by using the bar as the sputtering target) for 15 minutes in argon at a target potential of 1.5 kV.

Insulating Film

When the sputter etching was completed, the sputtering system was opened and the test bars were repositioned for sputtering of the insulating film. The correct sputtering target was installed. Both the target and test bars were blown clear of dirt particles using dry nitrogen gas (small hand-held pressurized gas cans). The sputtering system was pumped down to the low 10^{-4} Pa (10^{-6}torr) range and then back-filled with the appropriate sputtering gas (Table XII). Sputtering of the insulating film was initiated, using the sputtering parameters of Table XII.

The completed insulating films were microscopically examined at 70X magnification, and films showing poor adherence or cracking were rejected and the bar was reprocessed.

Gage and Lead Film

Test bars having acceptable insulating films were masked for sputtering of strain gages. All masking steps described below, except baking of the resist, were performed on a laminar-flow clean bench.

Masking for strain gage patterns began by dusting the test bar with nitrogen gas and then dipping it into a container of positive working photoresist. The bar was withdrawn slowly from the container and placed in a vertical position on a paper towel to allow excess resist to drain. The resist coating was air dried at room temperature for 30 minutes and then baked at 360K in air for 30 minutes with a heat gun.

The bar and a strain gage photographic mask (clear image on opaque film) were dusted with nitrogen gas and the mask was positioned on the bar. The assembly was exposed to a 200 watt collimated ultraviolet light source for 6.5 minutes. The mask was removed and the strain gage pattern was developed by agitating the bar in the photoresist developing solution for 1 to 2 minutes. After development was complete, the bar was given a prolonged rinse with DI water and blown dry with nitrogen gas.

The two strain gage patterns on the bar were examined at 70X. If they were acceptable, the bar was immediately installed in the sputtering system. The proper gage alloy sputtering target was installed, and the strain gages were sputtered. (Rejected photoresist masks were stripped from the insulation film surface with the hot alkali remover per Note 3 in Table XIV. After rinsing and drying, the bar was remasked.)

After sputtering, the photoresist was stripped in a solution of hot alkali remover in an ultrasonic cleaner. When stripping was complete, the bar was rinsed in hot DI water and blown dry with nitrogen gas. The strain gages were examined at 70X. If the gages were well defined, well adhered and complete, the gage resistances and their resistances to ground (bar) were measured. If the measured values were within acceptable bounds (described in Section 7.0 Gage Program Results) then the gages were accepted for overcoating. Otherwise the gages were rejected and the bar was reprocessed.

Overcoat

Accepted bars were masked with photoresist for overcoating of the strain gages using the same technique described for masking of the strain gage patterns. The photographic mask in this case was a piece of opaque material covering the strain gage lead film region during exposure to the ultraviolet lamp. When the resist was developed, the lead films remained covered with resist. The resist mask was examined at 70X and if satisfactory, the bar was sputtered with the same material used for the thin film insulation. The resist mask was then stripped from the lead film area using the hot alkali remover, and the bar was rinsed and dried. Measurements of gage resistances and resistances to ground were made. If the resistance readings were acceptable, the completed bar was stored in a dessicating cabinet until required for installion of lead wires and testing.

Lead Wire Attachment

To prepare the test bar for lead wire attachment, the bar was sputter etched (by using the bar as the sputtering target) for 15 minutes in argon at a target potential of 1.5 kV. Since the entire bar and gage system except for the lead films was protected by the hard overcoat, the only significant effect of the sputter etching was to roughen the bare lead film surface slightly producing a surface finish more conducive to adherence of the conductive cements used for lead wire attachment.

5-8

The lead wires of 76 μm Chromel (Ni-10% Cr) were connected to the lead films using the silver-filled polyimide cement. The cement and procedure are described in Section 4.9.

Extension cable of three conductor, 28 AWG, Ni clad Cu with glass fiber insulation was attached to the bar with epoxy cement and spliced by brazing with 944K (1240°F) silver solder. Epoxy cement was applied under and over the splice. The epoxy cement was GA-61 and the silver solder (mixed with paste flux) was 1240-FPA, both purchased from Micro-Measurements of Raleigh, NC.

Type B Gage

Some procedures for fabrication of Type B bars were different from those described for Type A bars. These differences occurred because fabrication of Type B bars was completed earlier in the gage program while fabrication of other types continued to develop.

There were two significant differences which are noted in Table XIV:

1. Method of polishing.

2. Solvent used for stripping of the strain gage photoresist mask.

The Type B bars were polished by hand using a metallurgical polishing wheel. Polishing began with No. 400 silicon carbide abrasive paper and continued using the following successively finer grades of abrasive: No. 600 grit silicon carbide, 3 micron silicon carbide, and 0.3 micron alpha alumina.

Photoresist masks on Type B bars were stripped in a container of continuously stirred, room temperature A.C.3. grade acetone, rather than in the alkali remover. At this point in the program, the alkali remover and acetone had been used interchangeably for photoresist removal on all gage systems.

Type C Gage

The fabrication procedure for Type C bars was identical to that described for Type A bars, except for the lead wire connection procedure as noted in Table XIV.

The lead wires were connected to the lead films using a the nickel-filled ceramic cement. The cement and procedure are described in Section 4.9.

Extension cable of three conductor, 28 AWG Ni clad Cu with glass fiber insulation was attached to the bar with ceramic cement and spliced by brazing with 944K (1240°F) silver solder. Ceramic cement was applied under and over the splice. The ceramic cement was GA-100 and the silver solder (mixed with paste flux) was 1240-FPA, both purchased from Micro-Measurements of Raleigh, NC.

Type D Gage

The final fabrication procedure for Type D gage systems was identical to that described for the Type A systems except for the solvent used for stripping of photoresist masks, and the procedure for lead-wire attachment, as noted in Table XIV.

TABLE XIV
SUMMARY OF GAGE FABRICATION PROCEDURES

Fabrication Step	Gage Type				
	A	B	C	D	E
Surface Preparation					
Polish	Std	9	Std	Std	Std
Vapor Hone					8
Electron Beam Vapor Deposit NiCoCrAlY					8
Dry Glass-Bead Peen					8
Polish					8
Grit Blast					8
Heat Treat, 1350K, 4 hours in vacuum					8
Oxidize, 1300K, 50 hours in air					8
Clean	Std	Std	Std	Std	
Bake	Std	Std	Std	Std	
Sputter Etch	Std	Std	Std	Std	
Insulating Film					
Sputter Insulation Material	Std	Std	Std	Std	Std
Gage and Lead Film					
Mask for Gage and Lead Film Pattern	1	1	1	1	1
Sputter Gage and lead Film Material	Std	Std	Std	Std	Std
Strip Mask Material	3	4	3	5	5
Clean	Std	Std	Std	Std	Std
Overcoat					
Mask for Overcoat Material	1	1	1	1	2
Sputter Overcoat Material	Std	Std	Std	Std	Std
Strip Mask Material	3	4	3	5	5
Clean	Std	Std	Std	Std	Std
Lead Wire Attachment					
Sputter Etch	Std		Std	Std	
Install Lead Wires	6	6	7	7	7

NOTES:

Std Standard procedure used on all gage types, and described in text for Type A gages.
1 Ultraviolet exposure for 6.5 minutes.
2 Ultraviolet exposure for 1.25 minutes.
3 Hot alkali solvent (50% Shipley 1112A in DI water, 350K)
4 Room temperature stirred acetone.
5 Hot acetone in Soxhlet extractor followed by 10% solution of hot alkali solvent.
6 600K lead-wire installation.
7 900K lead-wire installation.
8 Special procedure described in text.
9 Hand polish.

In order to avoid prolonged exposure of the Al_2O_3 films to the alkali stripper (which readily dissolves Al_2O_3), the stripping was carried out in two steps. First, the bulk of the photoresist was removed with hot acetone (a chemically neutral solvent), using a Soxhlet extractor distillation loop which continually supplies clean hot acetone. The bar was then briefly dipped in 10% solution of alkali remover to remove the last traces of photoresist. The bars were rinsed in hot DI water and blown dry with nitrogen gas before proceeding to the next step.

The lead wires and the extension cables were installed by the same techniques used for Type C gages, described above, using the special high-temperature conductive cement to connect the 76 μm chromel lead wires to the lead films, and high temperature ceramic cement to bond the extension cable to the test bar.

Turbine Blade System (Type E Gage)

The following sequence of preliminary fabrication operations was performed on each test bar of turbine blade material to initiate fabrication of a Type E thin film strain gage.

> Polish
> Vapor hone
> Electron beam vapor deposit NiCoCrAlY, 125 $\pm$25 μm
> Dry glass-bead peen
> Polish
> Grit Blast
> Heat Treat, 1350K; 4 hours in vacuum
> Oxidize, 1300K; 50 hours in air.

As noted in Table XIV, this sequence replaced the first three steps (polish, clean, sputter etch) of the sequence used in fabricating gages on compressor blade materials. The details of these preliminary operations are described in Reference 4. The result of these preliminary operations is an adherent grown Al_2O_3 layer about 1 μm thick on a 125 μm layer of an alumina forming alloy (NiCoCrAlY). The surface texture of this Al_2O_3 is slightly grainy and reticulated (dull matte appearance rather than highly reflective) even though its measured surface roughness is about the same as the polished surfaces.

The next step in Type E gage fabrication was to sputter the layer of Al_2O_3 over the grown Al_2O_3. The fabrication procedure from this point on (Table XIV) was as described for Type D strain gages after sputtering of the Al_2O_3 insulating layer. The final result was a Ni-30Cr strain gage on Al_2O_3, overcoated with Al_2O_3, with lead wires and the extension cables installed by the same techniques used for Type C and D gages.

5.5 GAGE FACTOR TEST

The gage factor of Type A, B, C, D, E gages was measured at room temperature and at elevated temperatures.

Gage factor was determined by the cantilever bending method of ASTM E251-67, using a Budd^{TM} fatigue testing machine (Figure 15) to apply bending stress to the test bars of Figure 12. Maximum load capability of the machine used is 30 kg and maximum deflection is 5 cm, peak to peak. A heated environment is provided by a split Marshall oven fitted over the test bar mounted in the fatigue machine, as shown in Figure 15. The oven is capable of 1250K operation and has an 8-cm diameter cylindrical interior 30 cm long. Special end fixtures are used to isolate the region of high strain. Previous tests have shown that room temperature strain is uniform within 5 percent and that temperature is uniform within 5K (at temperatures to 1100K) over the center 6-cm active portion of a test bar with the static test bar shape of Figure 12. The amplitude of deflection is determined by the eccentricity of the motor-driven crank arm shown in the figure. The eccentricity is manually selected before each test and is repeatable within ±1 percent.

Strain gage data were acquired through a precision ungrounded (floating, battery-powered) Wheatstone bridge circuit connected to each gage, as diagrammed in Figure 16, using the three-wire gage connection method to minimize the effects of lead-wire resistance. A constant voltage power source was used (1.5 V). The adjustable resistor R_1, was set equal to the gage resistance at the beginning of each gage factor test. Since gage resistance was generally over 100 ohms, gage current was less than 7.5 milliamps. Power dissipation was below 2 milliwatts per square millimeter of gage grid area. Current density in thin film gages was less than 75 amperes per square millimeter of film cross section area.

The recorder indicated in Figure 16 is a desktop computer based digital data acquisition system providing acquisition and storage of bridge output voltage and power source voltage on manual command, and subsequent automatic data reduction and output of tables and plots of calculated gage factor versus applied strain and temperature.

Thermocouple data were acquired by the same digital data acquisition system through an interface module providing a reference cold junction and providing translation to engineering units through the standard Type K thermocouple curve.

End-to-end accuracy of gage factor determinations were estimated to be within ±3 percent, including uncertainty in reference gage strain indication at room temperature, uncertainty in test bar strain variation with temperature (due to oven temperature gradients, at constant bar deflection), bridge circuit repeatability, and data acquisition uncertainty. Accuracy of temperature determination was estimated to be within 3°F.

Before the start of gage factor testing, each test bar was aged for five hours at a temperature approximately 25K above planned service temperature.

The gage factor measurement procedure was as follows: For each strain level and temperature, the bar was deflected (strained) twice in each direction (tension and compression) in a 0, +, 0, -, 0, +, 0, -, 0 sequence. The sequence was run first at a 500×10^{-6} strain level and then at a 1000×10^{-6} strain level. This test was conducted at room temperature, midway between room and service temperature, service temperature, and room temperature (repeated). In addition, the test was carried out at 1100K (1500°F) for two Type E gages. At each temperature, when the strain sequence was completed, the bar was held at $+1000 \times 10^{-6}$ strain for 15 minutes. For each strain gage, an average gage factor was calculated for each direction, strain level, and temperature based on four measurements (from the deflection sequence). The standard deviation was also calculated for the four measurements. Additional repeats of selected test points were acquired in some cases. The gage resistance drift in 15 minutes was also calculated.

5.6 THERMAL CYCLE TEST

Gages of Types A, B, C, D, and E mounted on the test bars of Figure 12 were subjected to a sequence of fifty thermal cycles to service temperature. A thermal cycle consisted of placing the test bar into an oven preheated to planned service temperature, soaking until the bar reached oven temperature, soaking for a further 2 to 5 minutes, removing from oven, and air cooling to near room temperature.

The temperature of the bar was indicated by the wire thermocouple attached to the bar (Figure 12). The resistance of each thin film strain gage was monitored with a low-voltage-source ohmmeter with an analog voltage output available for recording. A switching arrangement permitted measurement of insulation resistance to ground with the same ohmmeter.

The laboratory digital data system was used to acquire, store, process, and print out temperature and resistance data. The data system was programmed to acquire and store sample measurements of temperature and gage resistance once every 10 seconds, compare the temperature reading with the previous reading, stop sampling when the temperature value changed less than 1K between readings, and then sound on audible alarm to call a test operator. The test operator, after verifying that temperature equilibrium was established at the desired level, then commanded acquisition of a final end point reading (temperature, gage resistance, insulation resistance, cycle no., time) and moved the test bar into or out of the oven to begin the next temperature transient.

Accuracy of gage resistance measurements was 0.2 ohms, insulation resistance measurement 2 percent, and temperature 2K in these tests based on combined uncertainty of instrument calibrations and data system resolution.

5.7 FATIGUE TEST

Gages of Types A, B, C, D and E, mounted on the test bars of Figure 12, were subjected to fatigue tests at room temperature and at service temperature. Each test extended to 10^7 cycles or failure, whichever came first. Failure was defined as an open circuit or a signal-to-noise ratio of less than one. The strain level for fatigue testing was $+300 \times 10^{-6}$ mean strain $+ 450 \times 10^{-6}$ alternating strain. In some initial tests, strain levels up to $+1000 \times 10^{-6}$ mean strain $\pm 1500 \times 10^{-6}$ alternating strain were imposed.

An electrodynamic shaker (Ling Model A300-B) was used for fatigue testing at room temperature, and of Type A and B bars at 600K. The fixturing used on the shaker is shown in Figure 17. One end of the bar was clamped between plates that were bolted to the table of the shaker. The other end was held by set screws in a C-fixture, also bolted to the table. By adjustment of the set screws, a 300×10^{-6} steady strain was applied. The stiffener shown in the figure was used to control strain distribution so that the maximum steady strain and dynamic strain occurred at the location of the strain gages (at the center). A small rectangular-section oven was used to heat the bar during 600K testing. The oven rested on the surface of the shaker table but was not bolted down. (The soft insulation in the oven walls acted as a vibrator isolator between the table and the heater coils.)

Bar temperature was measured using the thermocouple located at the center of the bar (Figure 12). Strain was measured using the reference strain gage (Figure 12). The bar was vibrated by the shaker in the fixed-pinned mode, at the resulting natural frequency in the range of 1100 to 1300 Hertz. The shaker force was increased to produce alternating strain of $\pm 450 \times 10^{-6}$ on the bar. During the test, the shaker force was adjusted, if necessary, to maintain the proper dynamic strain level. Each test of 10^7 cycles could be completed in less than three hours in this apparatus. To keep the shaker table base plate temperature well below a specified safe upper limit of 340K, the highest test bar temperature permitted in this arrangement was 600K.

For high-temperature fatigue testing at 900K (required for Types C, D, and E gages) the high-temperature fatigue machine (Figure 15) described in Section 5.5 was used. The maximum cycle rate provided by the motor-driven crank arm in this machine is 30 Hertz. Each test of 10^7 cycles at 900K therefore required about 90 hours of testing.

The temperature of the bar, using the reference thermocouple, was monitored on a digital temperature indicator. Steady strain was measured at the start (and in the room temperature and 600K tests, also at the finish) of each test with the reference foil gage using a portable strain indicator incorporating the static strain circuit of Figure 16. Dynamic strain of the bar at temperatures to 600K was measured using the reference foil strain gage in a standard half bridge dynamic strain circuit with a 500 ohm dummy resistor and 4 V d-c excitation. The signal wave form was observed on an oscilloscope and the

A

| 10 cm |

B
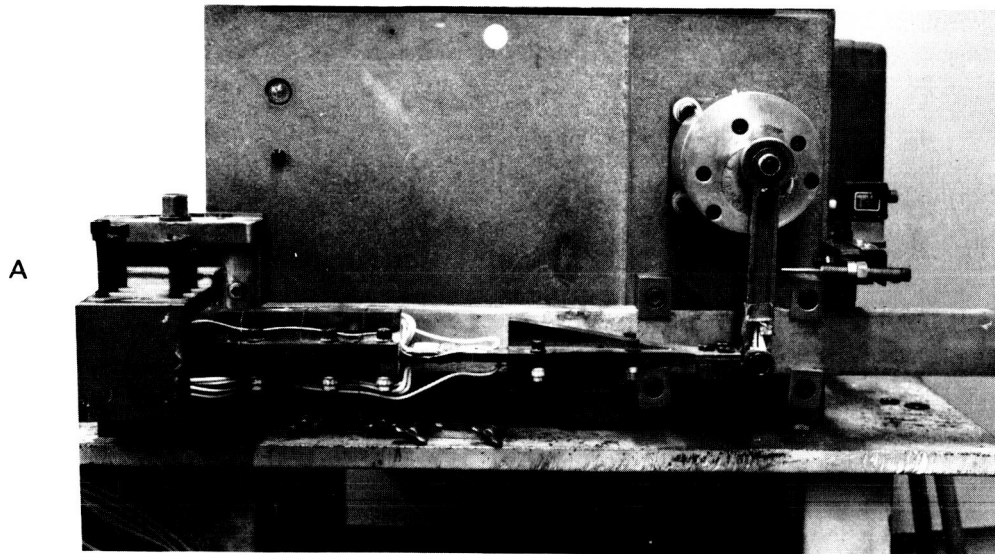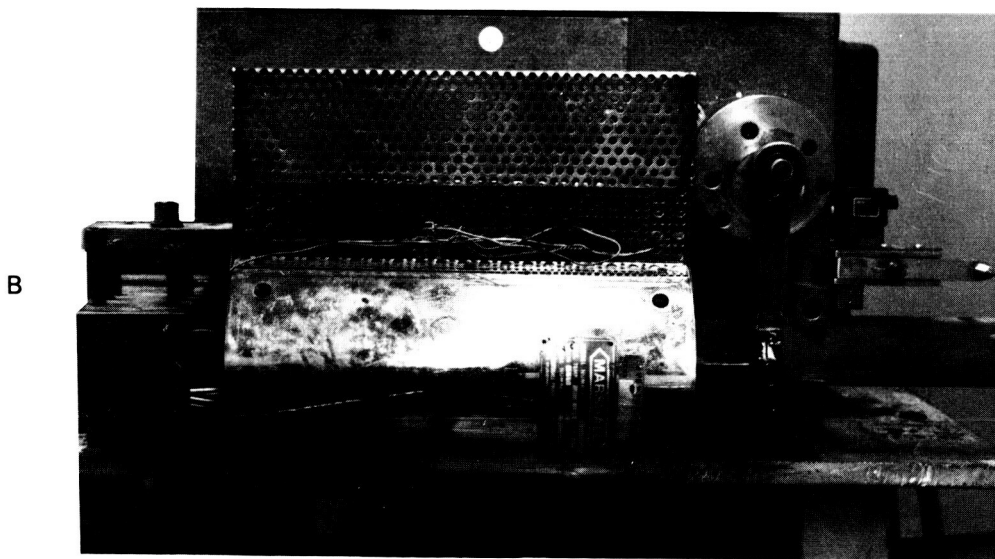
Figure 15 Fatigue Machine Shown (A) with Oven Removed, and (B) with Oven
Installed. This apparatus was used for gage factor testing and for
900K fatigue testing.   (78-444-4019-A)
                                                           (78-441-4019-B)
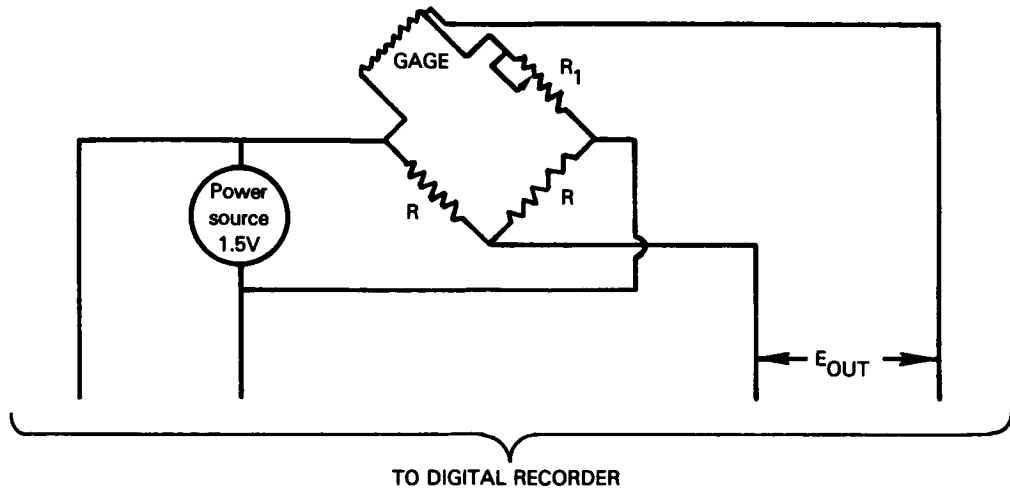
Figure 16 Strain Gage Bridge used for Gage Factor Testing.
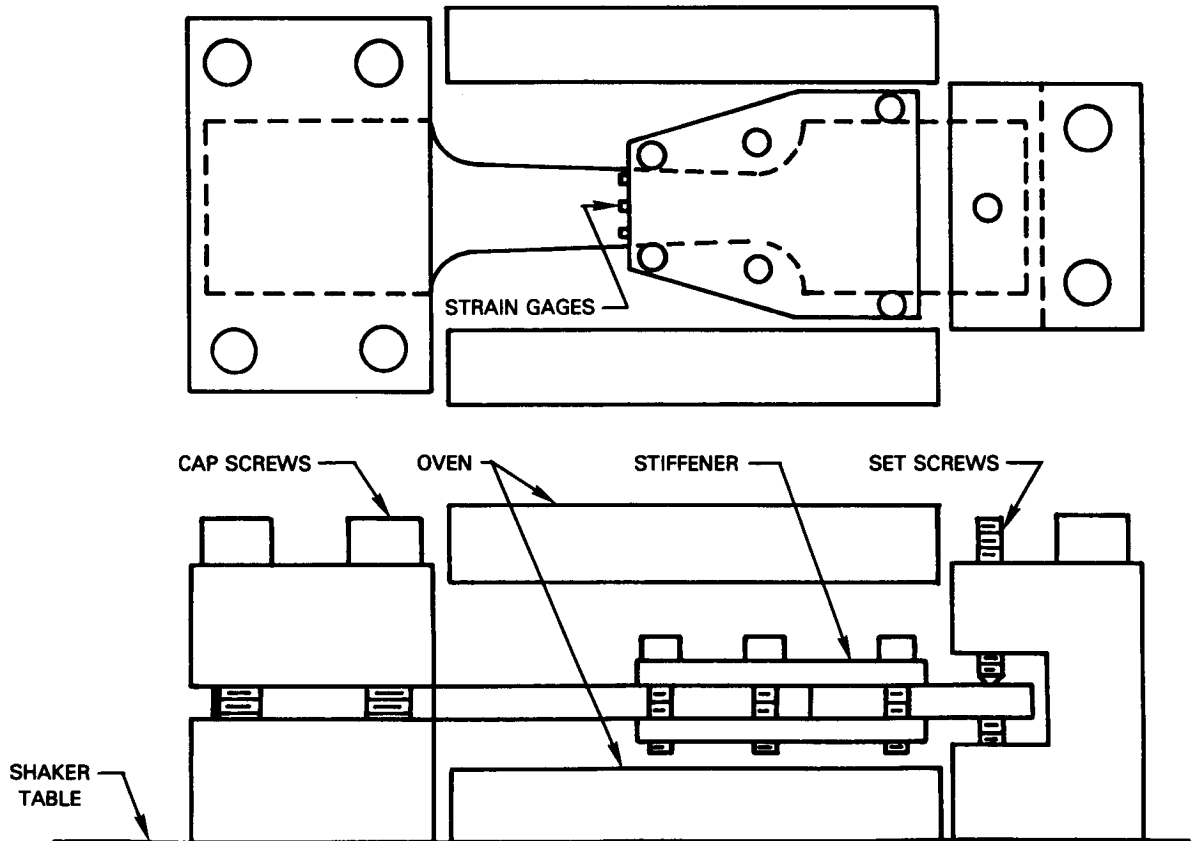
Figure 17 Fatigue Testing Fixture on Electrodynamic Shaker.

amplitude was measured with an a-c voltmeter. Measurements of thin film dynamic strain signals were made using the same method. Thin film strain gage and insulation resistance measurements were made using a digital ohmmeter. In the 900K tests the static and dynamic strain of the bar was established first at room temperature using the deflection adjustment on the fatigue machine and the reference foil gage. The deflection was then maintained throughout the high temperature tests.

During room temperature and 600K tests, on the electrodynamic shaker, readings of temperature, strain signal, and resistance were recorded on the data sheets from 5 to 15 times during the 3-hour tests. During 900K tests, on the fatigue testing machine, readings were recorded on the data sheets from 10 to 30 times during the 90-hour test.

Testing of each bar continued until both thin film strain gages experienced either an open circuit or a signal-to-noise ratio of less than one. Signal quality was based on observation of oscilloscope signals. In some cases, open circuit or high noise was due to lead wire distress and repairs allowed continuation of testing.

5.8 SPIN TEST

Type A and Type C gages were spin tested for one hour at 100,000G. Thin film strain gage systems were fabricated on two of the spin test bars of Figure 14 (one of each compressor blade material). The thin film gage system fabrication technique was exactly as described in Section 5.4 except that in place of the three-conductor extension cable, special extension lead wires were used because of the high-G environment. These extension leads were stranded 34 AWG copper, 0.16 mm (0.0063 inch) conductor diameter, with polyimide (Kapton) inner insulation and Teflon outer insulation of 0.53 mm (0.021 inch) diameter. The Teflon is etched for improved bonding to epoxy cement.

The instrumented spin bars were mounted 90 degrees apart on the rim of a spin disk, using a special clamp (Figure 18) for each bar. Dummy bars were mounted at 180 degrees from each instrumented bar for mass balancing. The orientation of strain gages was normal to and away from the direction of rotation, as shown in the figure. The routing of the lead wires is also shown in the figure. The lead wires were cemented to the clamp and disk surfaces, with cement under and over the lead wires, over the entire length from gage to hub. Photographs of the completed assembly on the spin disk, mounted in the spin rig, are shown in Figures 19 and 20. The strain gage leads extend through the hollow shaft, on which the spin disk is suspended, and then through the slip ring (Figure 20) to monitoring instruments in the control room.

The resistance of each gage circuit (gage plus lead-wire plus slip ring resistance) and the insulation resistance from each gage lead film to the spin test bar were measured before and after the spin test, using a low-voltage-source ohmmeter. During the one-hour spin test the resistance of each gage circuit was measured and recorded manually every five minutes, using the ohmmeter and a selector switch.

Standard spin pit instrumentation provided gas temperature (stationary thermocouple suspended below the spin pit cover), gas pressure, and disk rpm.

The spin rig was operated at 17,510 rpm to impose a centripetal acceleration of 100,000G at the gage location (29.2 cm radius). The spin pit pressure was 0.1 atmosphere during spin tests. The disk was at room temperature at the start of the spin test and near 350K at the end of the spin test.

5.9 EROSION TEST

Erosion tests were performed on Type A, B, C, and E systems which had been fabricated on test bars. The erosion tests were conducted after all other testing was completed.

The apparatus used for erosion testing was the same as that used for erosion testing in the Components Program, as described in Section 4.7. After each nine-second exposure, the stream was turned off and the gage resistance and resistance to ground were measured with the low voltage source ohmmeter (with resolution of four significant figures) through the lead wires attached to the lead films on these test bars. In addition, post-test photographs of erosion damage were obtained.
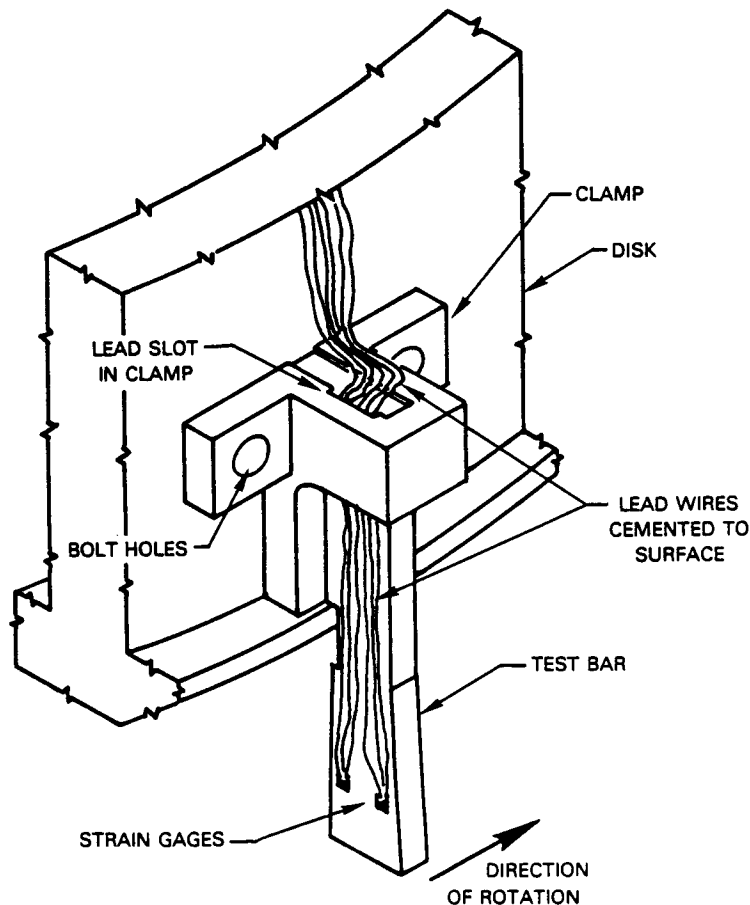
Figure 18   Installation of Spin Test Bar on Spin Disk.
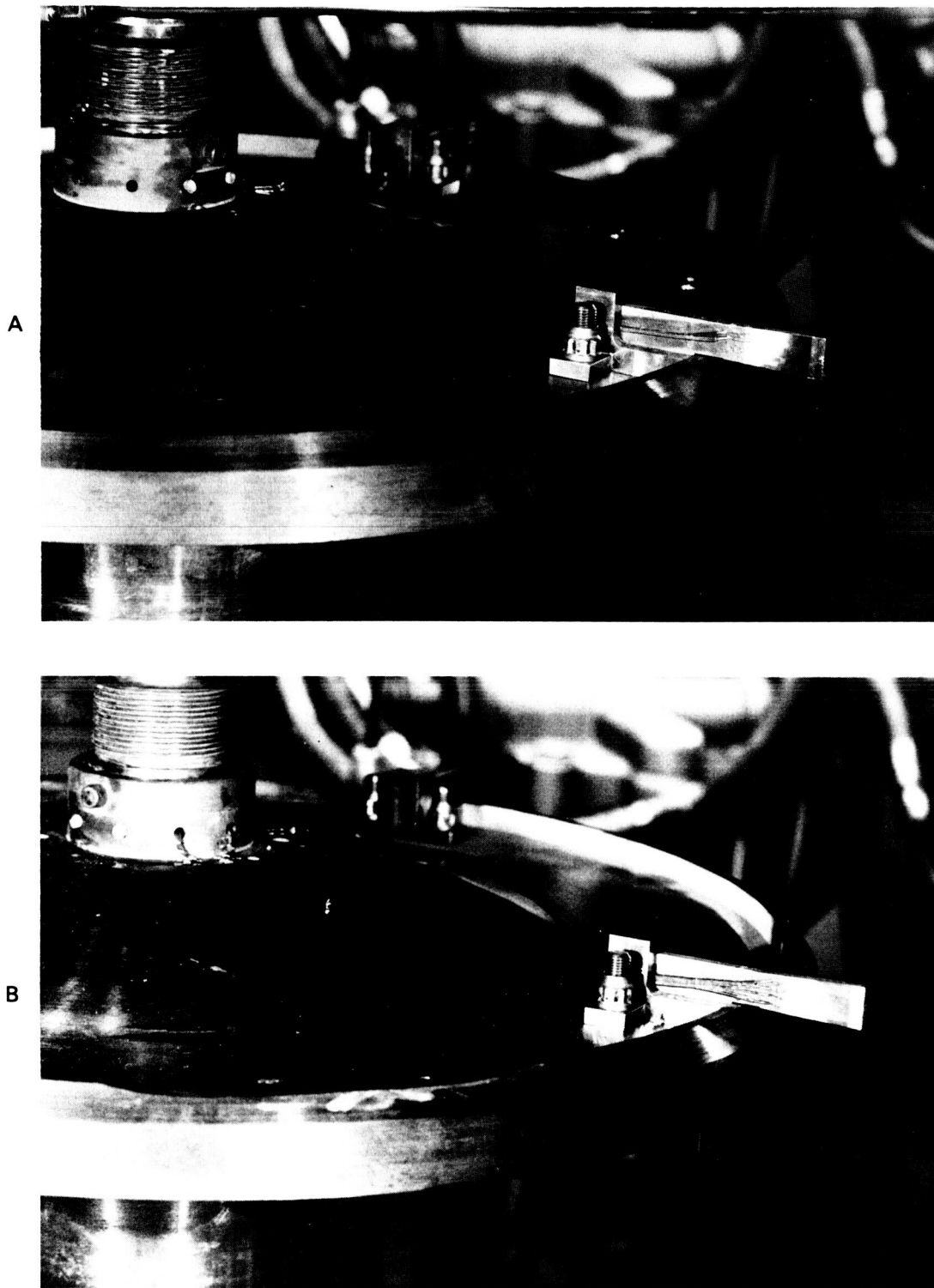
Figure 19 Spin Disk with Spin Test Bars Installed. (A) Bar A-3 in Foreground,
Bar C-19 in Background. (B) Bar C-19 in Foreground, Dummy Bar in
Background.   (83-C0734-0003)
                                                        (83-C0734-0002)

5-19

SLIP RING

SPIN PIT COVER

SPIN DISK
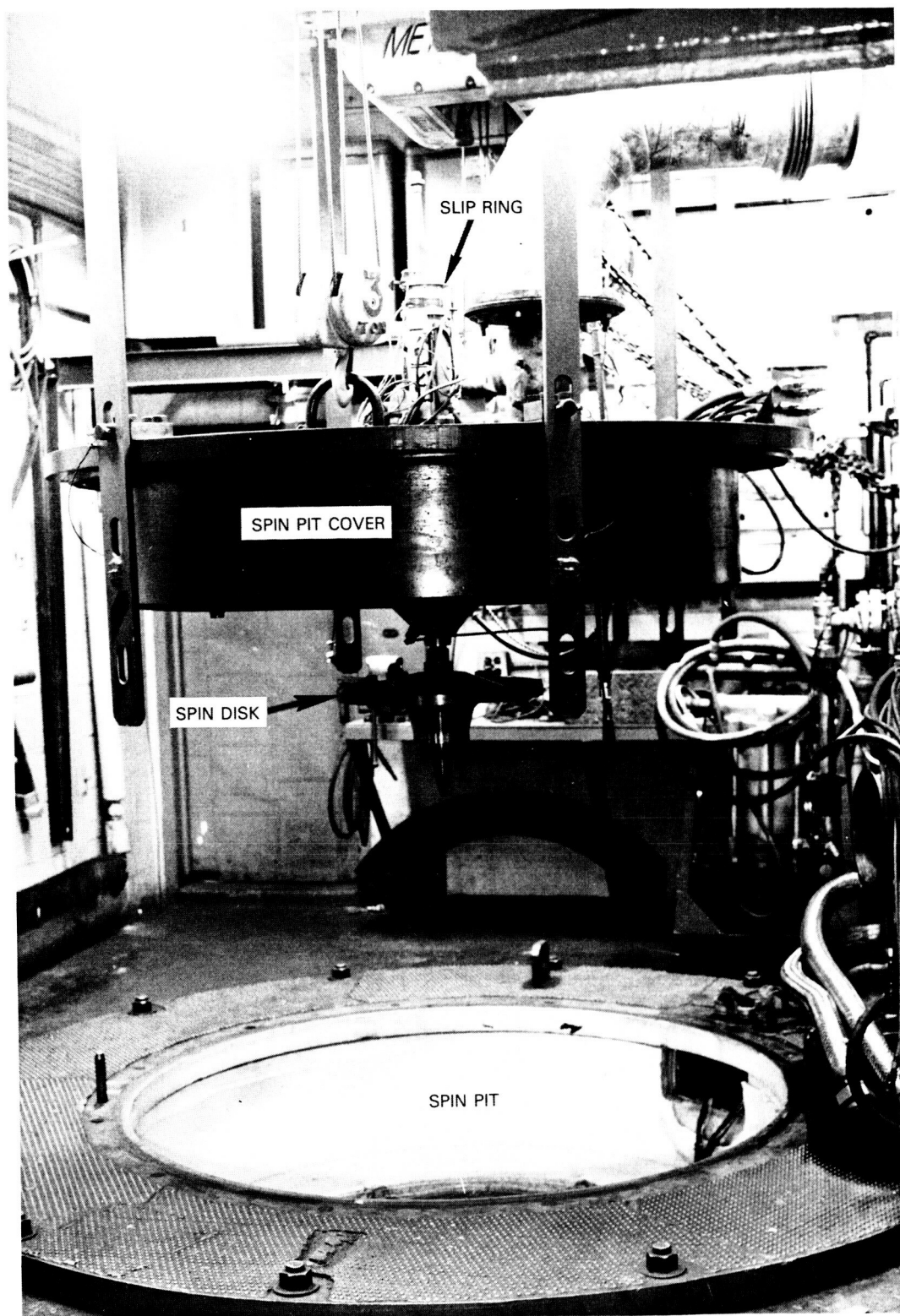
SPIN PIT

Figure 20 Spin Rig Mounted on Spin Pit Cover, before Lowering into Spin Pit.
(83-C0734-0001)

SECTION 6.0

COMPONENTS PROGRAM RESULTS

6.1 INSULATING FILM EVALUATIONS

Resistivity versus Blade Material, Surface Preparation, and Film Thickness

Table XV is a summary of measurements of insulating film resistivity (presented as Log_{10} ρ_2, where ρ_2 is the resistivity in ohm-cm) for the sixteen candidate insulating film systems fabricated on compressor blades. The sixteen systems are all the combinations of four insulating materials (Al_2O_3, Si_3N_4, HfO_2, and SiO_2), two blade materials (AMS 4928 and Incoloy 901), and two surface roughnesses (polished and roughened) prepared as described in Section 4.0. Film thicknesses from 0.6 to 4.5 µm were tested in selected systems, as indicated in the table. The electrical resistance of the insulating film was measured at six locations on each blade, using a 0.1 cm^2 contact area at each location, as described in Section 4.5. The measurements were performed at room temperatures before and after the blade with film system had been subjected to four thermal cycles to its service temperature (600K for systems on AMS 4928 blades, 900K for systems on Incoloy 901 blades). Since there was no significant difference in measurements obtained before and after temperature cycling, the table presents only the final measurements, after temperature cycling.

The table lists the largest and smallest of the measured values of Log_{10} ρ_2 at six locations for each film system.

The table shows that there was considerable scatter in the six measurements of insulation resistance on each blade, probably because of variations in film thickness in the vicinity of local peaks and valleys in the surface finish. Since a fixed value of film thickness was assumed, the resulting determinations of resistivity on each blade also show considerable scatter.

Very thin films of Al_2O_3 (0.6 µm) and SiO_2 (1.5 µm) were the first to be fabricated and tested. The results shown for these films in the table indicate reasonable resistivity on the polished surfaces, but a high incidence of short circuits on roughened surfaces. Thicker films (3 µm) of all four insulating materials were then fabricated on additional blades. The table shows that at this thickness Si_3N_4 and HfO_2 were satisfactory on polished surfaces, but none of the materials yet was satisfactory on roughened blades. Still thicker films (4 to 4.5 µm) were fabricated on additional blades. The table shows that enough of these thicker film systems were satisfactory on roughened surfaces so that in all there were two or three promising insulating film materials demonstrated on each of the four kinds of blade surface (polished surfaces of each blade material, roughened surfaces of each blade material).

As noted in the table, five of the sixteen insulating film systems were eliminated from the components program at this stage, on the following basis:

Al_2O_3 was unsatisfactory on roughened surfaces:

- o   4.5 μm film shorted at all locations on roughened AMS 4928;
- o   4.5 μm film had lowest maximum ρ_2 on roughened Incoloy 901.

HfO_2 was unsatisfactory on roughened AMS 4928:

- o   4.0 and 4.5 μm film shorted at all locations.

SiO_2 was ranked slightly lower than other films on polished surfaces:

- o   1.5 μm film had lowest maximum ρ_2 on polished AMS 4928;
- o   1.5 μm film on Incoloy 901 was the only film on any polished blade to develop short circuits to ground.

TABLE XV

RESISTIVITY OF SPUTTERED INSULATING FILM SAMPLES

Blade Material	Film Thickness t_2 (μm)	Range of Log_{10} ρ_2 (See Notes 1 and 6)							
		Al_2O_3		Si_3N_4		HfO_2		SiO_2	
		Polished[d2]	Roughened[3]	Polished	Roughened	Polished	Roughened	Polished	Roughened
AMS 4928	0.6 1.1 1.5	7-11	X[4,7] X					7-8	X
	3.0 4.0 4.5	10-13	X X	7-13	*[5] 0-11	6-14	X X		X 0-11
Incoloy 901	0.6 1.1 1.5	9-11	X X					0-10	X
	3.0 4.0 4.5	10-13	X 6-7	7-8	0-12 0-10	7-13	X 7-10		X 0-8

NOTES:

1. Range of Log_{10} of measured ρ_2, where ρ_2 is resistivity (ohm-cm), at a minimum of six locations after four oven cycles to service temperature.
2. Polished = polished surface before sputtering insulating layer.
3. Roughened = grit blasted surface before sputtering insulating layer.
4. X = all locations shorted to ground (blade material).
5. * = one or two locations shorted to ground. At least four locations measured 10^7 ohm-cm or higher.
6. Resistivity (ρ) was measured between 0.1 cm^2 electrodes of conductive paint on the surface and ground.
7. ////// = candidate dropped from program on the basis of these tests.

The order of magnitude of maximum measured resistivity (Table XV) generally coincides with the predictions of Section 3.5, (Table III) for each material. These measured values are discussed further at the end of this section (6.1), under the heading "Summary by Insulation Film Type".

The remaining eleven of the sixteen insulation film systems were retained in the program, for evaluation with each of the four candidate strain gage materials.

Other Properties

The most surprising result of the insulating film evaluations was the mechanical survival of all films after four temperature cycles to 900K on Incoloy 901, despite thermally induced stresses due to mismatch of tce (Table III, Section 3.5).

Adherence of all the insulating films was generally excellent, both as-sputtered and after four cycles to service temperature. The tape tests described in Section 4.5 resulted in no observable loss of insulation material. After storage, some spontaneous spalling and delamination of one 4.5 μm Si_3N_4 film began to occur near the blade trailing edge, but the spalling never progressed beyond 2 percent of the blade surface area.

Information on the long-term adherence of the eleven insulating film systems retained in the program was obtained on the later set of 44 blades (four of each kind, not included in Table XV) on which gage systems were fabricated. The results are discussed later in Section 6.2, Gage Film Evaluations. It is worth noting here that after two years of bench testing and storage, the insulating layers on these 44 blades generally remained in good condition.

Hardness of the insulating films of Table XV, as determined by the 0.64-mm diameter steel stylus penetration tests, is summarized in Table XVI. The table shows that hardness was in the "very hard, no penetration" range for the thickest films of all sixteen candidate systems, and even for some of the thinnest films on polished surfaces. The corresponding stylus pressure was approximately 2×10^5 N/m^2 (30,000 psi). The table also shows that hardness was in the "easy penetration" range for some thinner films on roughened surfaces. The stylus pressure in this range was only about 6×10^3 N/m^2 (900 psi). It would appear that the films remained intact unless the supporting substrate material surface became plastically deformed. Local deformation could occur readily at asperities in the roughened surfaces.

Chemical composition of a sample of each of the four insulating materials, sputtered on glass slides, was measured by the electron microprobe technique. The concentration of each atomic species was found to be correct, within the 5 percent uncertainty of this technique. This, together with the resistivity measurements already described, was considered sufficient evidence that the desired chemical compounds had been achieved (Al_2O_3, Si_3N_4, HfO_2, and SiO_2). It is probable that the Al_2O_3 films were of phase rather than the harder and more stable α phase which generally can be formed only by high temperature (1200K) heat treatment.

TABLE XVI

HARDNESS OF SPUTTERED INSULATING FILM SAMPLES

Blade Material	Film Thickness t_2 (μm)	Al_2O_3		Si_3N_4		HfO_2		SiO_2	
		Polished	Roughened	Polished	Roughened	Polished	Roughened	Polished	Roughened
AMS 4928	0.6	B	E						
	1.1		A					A	E
	1.5								
	3.0		A	A	A	A			D
	4.0	A		A			A	A	
	4.5		A		A		A		A
Incoloy 901	0.6	A	D						
	1.1		C					A	E
	1.5								
	3.0		D	D	A	A			A
	4.0	A		A			A	A	
	4.5		A		A		A		A

LEGEND

Code	Description
A	Very hard, no penetration at 70 N (15 pound force).
B	Very hard, penetration.
C	Hard.
D	Moderate.
E	Easy penetration at 2 N (0.5 pound force).

All hardness measurements after four thermal cycles to service temperature.

The surface structure of each blade was examined before and after sputtering each insulating film. An optical microscope was used at 10X to 100X magnification with oblique lighting at an incidence angle of about 45 degrees. In this magnification range, the surface structure of the sputtered films appeared identical with the blade surface structure before sputtering. The surfaces were essentially featureless, with faint indication of a grain structure in the 1 to 10 μm size range, and occasional larger scratches and inclusions. The Incoloy 901 surfaces were distinctive in that larger inclusions of a darker color were fairly common. These inclusions were of irregular shape, with dimensions up to 20 microns. Materials experts who examined these inclusions stated that they were typical of Incoloy 901 blade structure, and in the past have been identified as titanium carbides formed during casting and heat treatment.

The dielectric breakdown voltage was measured at room temperature by the technique of Section 4.5 at sample locations for each of the 14 insulation systems in Table XV which were off ground. (The systems not tested for dielectric breakdown were, therefore, Al_2O_3 on roughened AMS 4928, and HfO_2 on roughened AMS 4928, since all locations on these systems were shorted to ground.) Only the thickest film of each type was tested. The measurements were made at two or three of the conductive patch locations on each blade, and only at locations where resistivity was at least 10^7 ohms. Since this test was potentially destructive, it was performed after all other testing was completed (after temperature cycling to service temperature and final resistivity measurements).

The breakdown voltages varied widely, from 7 volts to 100 volts, probably again as a result of local thickness variations. In no case did breakdown occur at a voltage difference of less than 7 volts across any film tested. Measurements did not correlate clearly with the average thickness, the measured resistivity, the blade material, the insulation material, or the blade surface roughness. A conservative conclusion is that for any one of the systems tested the dielectric breakdown strength is above 10^4 volts/cm (based on 7 volts across a 4.5 μm film). This value is well below the 10^5 volts/cm reported in the literature (Table III, Section 3) for bulk Al_2O_3 and 10^7 volts/cm reported for bulk Si_3N_4, but the difference is not surprising since the measurements on thin films can be strongly affected by microscopic pinholes, surface asperities, or local contamination of the film.

Summary by Insulation Film Type

Al_2O_3

Al_2O_3 films were fabricated in four thicknesses (0.6, 1.1, 3.0 and 4.5 μm) on roughened blades of AMS 4928 and Incoloy 901, and in two thicknesses (0.6 and 4.0 μm) on polished blades of AMS 4928 and Incoloy 901. All of the Al_2O_3 films were adherent both before and after four temperature cycles to blade service temperature (600K for AMS 4928, 900K for Incoloy 901). After temperature cycling, the hardness (penetration), resistivity, and dielectric breakdown voltage were measured. It was found that the 0.6 μm films were easily penetrated with a steel stylus, but all thicker films were hard and not penetrated at 2×10^5 N/m^2 (30,000 psi) stylus pressure. Electrical resistivity was also higher for the thicker films, and approached the predicted value for bulk Al_2O_3 (10^{13} ohm-cm) in the 4 μm films on polished surfaces. On roughened blades, shorts to ground were found at every location on every blade except for the case of the thickest film on Incoloy 901. On this roughened blade, the resistivity of all locations was in the range of 10^6 to 10^7 ohm-cm. Dielectric breakdown voltage was above 7 volts (that is, above 10^4 volts/cm). The combinations of Al_2O_3 and the roughened surface of either AMS 4928 or Incoloy 901 were dropped from the program.

Si$_3$N$_4$

Si$_3$N$_4$ films were fabricated in two thicknesses (3.0 and 4.5 μm) on roughened blades of AMS 4928 and Incoloy 901, and in one thickness (3.0 μm) on polished blades of AMS 4928 and Incoloy 901. All of the Si$_3$N$_4$ films were adherent both before and after four temperature cycles to blade service temperature (600K for AMS 4928, 900K for Incoloy 901), although a small amount of spontaneous spalling of one sample (3 μm film on polished AMS 4928) was observed near the blade leading and trailing edges. After temperature cycling, the hardness (penetration), resistivity, and dielectric breakdown voltage were measured. It was found that all of the Si$_3$N$_4$ films were hard and not penetrated at 2 x 10^5 N/m^2 (30,000 psi) stylus pressure, except for one sample (3 μm film on polished Incoloy 901) which was penetrated moderately easily. Electrical resistivity on polished blades was above 10^7 ohm-cm at all locations measured; a few locations showed higher values, near the predicted value for bulk Si$_3$N$_4$ (10^{10} ohm-cm). On roughened blades, shorts to ground were found at one or two locations on each blade, but resistivity was above 10^7 ohm-cm at all other locations and some locations showed values as high as 10^{12} ohm-cm. Dielectric breakdown voltage was above 7 volts (that is, above 10^4 volts/cm). All combinations of Si$_3$N$_4$ with both blade materials and both surface finishes were retained in the program.

HfO$_2$

HfO$_2$ films were fabricated in two thicknesses (4.0 and 4.5 μm) on roughened blades of AMS 4928 and Incoloy 901, and in one thickness (3.0 μm) on polished blades of AMS 4928 and Incoloy 901. All of the HfO$_2$ films were adherent both before and after four temperature cycles to blade service temperature (600K for AMS 4928, 900K for Incoloy 901). After temperature cycling, the hardness (penetration), resistivity, and dielectric breakdown voltage were measured. It was found that all of the films were hard and not penetrated at 2 x 10^5 N/m^2 (30,000 psi) stylus pressure. Electrical resistivity on polished blades was above 10^6 ohm-cm at all locations and was as high as 10^{14} ohm-cm, (far above the predicted value of 10^{10} ohm-cm for bulk HfO$_2$) at some locations. On roughened blades of AMS 4928 every location was shorted to ground, even in the case of the 4.5 μm film thickness. On roughened blades of Incoloy 901, every location was shorted to ground in the case of the 4.0 μm film thickness, but there were no shorts to ground in the case of the 4.5 μm thickness. Here the resistivity at all locations was in the range of 10^7 to 10^{10} ohm-cm. Dielectric breakdown voltage was above 7 volts (that is, above 10^4 volts/cm). The combination of HfO$_2$ with roughened AMS 4928 was dropped from the program.

SiO$_2$

SiO$_2$ films were fabricated in three thicknesses (1.5, 3.0 and 4.5 µm) on roughened blades of AMS 4928 and Incoloy 901, and in one thickness (1.5 µm) on polished blades of AMS 4928 and Incoloy 901. All of the SiO$_2$ films were adherent both before and after four temperature cycles to blade service temperature (600K for AMS 4928, 900K for Incoloy 901). After temperature cycling, the hardness (penetration), resistivity, and dielectric breakdown voltage were measured on most of these blades. It was found that on the polished surfaces the films of both thicknesses were hard and not penetrated at 2×10^5 N/m^2 (30,000 psi) stylus pressure, but that on the roughened surfaces only the thickest films were not penetrated at this stylus pressure. Electrical resistivity on polished AMS 4928 was 10^7 to 10^8 ohm-cm at all locations, somewhat below the predicted value of 10^{10} ohm-cm for bulk SiO$_2$. On polished Incoloy 901, shorts to ground were found at two of the six locations tested. (SiO$_2$ was the only film material which developed short circuits to ground on any polished blade surface.) On roughened blades with 1.5 or 3.0 µm films, every location was shorted to ground. On roughened blades with 4.5 µm films, one or two locations were shorted to ground on each blade, but at other locations the resistivity was 10^7 to 10^{10} ohm-cm. Dielectric breakdown voltage was above 7 volts (that is, above 10^4 volts/cm). The combinations of SiO$_2$ and the polished surface of either AMS 4928 or Incoloy 901 were dropped from the program.

6.2 GAGE FILM EVALUATIONS - FIRST GENERATION

Composition, Adherence, and Resistance as Sputtered

Initial sample strain gages were sputtered on polished glass slides and roughened glass slides using the gage mask configuration of Figure 10 and each of the candidate gage alloys of Table X (NiCr, CuNi, PtW, PdMo). These initial samples were used to determine composition as sputtered, the gage configuration as sputtered, and to verify the sputtering rate parameters of Table XII. The NiCr and CuNi gages were adherent on the polished glass, permitting measurement of gage resistance as sputtered and gage resistance after several thermal cycles to 600K. All other samples were poorly adherent, some portions breaking loose during photoresist removal.

The compositions as determined by wet chemical techniques are summarized in Table XVII.

TABLE XVII
COMPOSITION OF STRAIN GAGE FILMS
(a/o = Atomic Percent)

Alloy Description Code	Nominal Composition	Measured Composition
NC	Ni-30 a/o Cr	Ni-29 ±2 a/o Cr
CN	Cu-45 a/o Ni	Cu-43 ±2 a/o Ni
PW	Pt-20 a/o W	Pt-17 ±2 a/o W
PM	Pd-30 a/o Mo	Pd-25 ±2 a/o Mo

In the case of the PtW and PdMo alloys, two sputtering trials were required, with adjustment of composite target area ratios, to arrive at the composition shown in the table, acceptably close to the desired alloys. It was found that the atomic percent of W (or Mo) in the sputtered gages was about half of the percent of target area of exposed W (or Mo).

The gage materials showed a bright metallic luster as sputtered.

A surface profile across the NC gage sample (Figure 21) using a mechanical profilometer with optical readout shows gage line width of about 69 μm, space width of about 95 μm, end line width of about 133 μm, thickness of about 0.6 μm, and sharp definition of all edges.

The resistance of this sample NC gage was 616 ohms as sputtered. The gage was then heat treated in air at 600K for seven hours. The resistance, (measured at room temperature after each hour of exposure at 600K) dropped slowly and finally stabilized at 571 ohms after the fourth hour. The gage retained its bright luster.
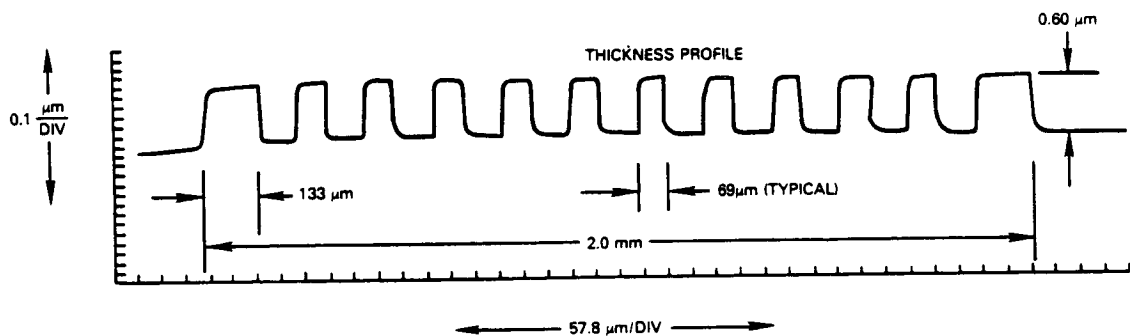
Figure 21 Thin Film Strain Gage Thickness Profile for NC Gage on a Polished Glass Slide. The profile shows that the applied strain gage pattern was sharply defined.

A sample CN gage 0.6 μm thick was also heat treated at 600K in the same way. Resistance was 362 ohms as-sputtered and increased more and more rapidly in each hour of exposure at 600K, reaching 480 ohms after the third hour. Bubbling and discoloration (yellow and blue areas) were observed. Testing of this preliminary sample was discontinued.

Insulating films and thin film strain gages were then sputtered on 44 compressor blades (one gage on each blade), providing one sample of each of the four gage alloys on each of the eleven acceptable candidate insulating film systems shown on Table XV. These 44 gages were called the "first generation" gages. The matrix of samples is presented in Table XVIII. The four-digit "blade number" in the table is the identifying serial number etched on the blade. The first two digits indicate the blade material (06XX for AMS 4928, 12XX for Incoloy 901).

The sputtered insulation was approximately 4.5 μm thick on all blades. The thickness of sputtered gage material was varied from one sputtering run to another on the basis of gage resistance measurements for each material obtained on the glass slides and gage resistance measurements on the first blades sputtered with each material. The objective was gage resistance between 100 ohms and 1000 ohms. The thickness of gage material on each blade is noted in Table XVIII. Thickness varied from 0.65 to 1.3 μm.

TABLE XVIII

MATRIX OF 44 THIN FILM STRAIN GAGE SYSTEMS
FABRICATED ON COMPRESSOR BLADES

Blade Material	Gage Materials	Blade Number and Gage Thickness (m)							
		Al$_2$O$_3$		Si$_3$N$_4$		HfO$_2$		SiO$_2$	
		Polished	Roughened	Polished	Roughened	Polished	Roughened	Polished	Roughened
AMS 4928	NC	0609 1.0	Al$_2$O$_3$ Ruled Out	0621 0.65	0638 0.65	0613 0.65	HfO$_2$ Ruled Out	SiO$_2$ Not Continued	0634 0.7
	CN	0610 0.8		0622 0.8	0639 1.3	0627 0.8			0635 0.8
	PW	0611 0.7		0642a 0.8	0640 0.8	0628 0.7			0636 0.8
	PM	0612 0.8		0642b 0.8	0641 0.7	0629 0.8			0637 0.8
Incoloy 901	NC	1209 1.0	Al$_2$O$_3$ Ruled Out	1221 0.65	1242 0.7	1213 0.65	1247 0.8	SiO$_2$ Not Continued	1238 0.8
	CN	1210 0.8		1222 0.8	1243 1.3	1227 0.8	1248 1.3		1239 1.3
	PW	1211 0.7		1223 0.8	1237 1.0	1228 1.0	1249 1.0		1240 1.0
	PM	1212 0.8		1230 0.8	1236 0.8	1229 0.8	1250 0.8		1241 0.8

NOTES:

1. Insulation thickness is approximately 4.5 m.
2. Gage configuration, See Figure 10.

To describe the gage system on each blade in the following discussions, additional suffixes shown in Table XIX were appended to the blade number. Blade 0609P-AO-NC, for example, is an AMS 4928 blade with a polished surface, Al_2O_3 insulation, and a Ni-29 a/o Cr gage.

TABLE XIX

NOMENCLATURE FOR GAGE CODE NUMBER
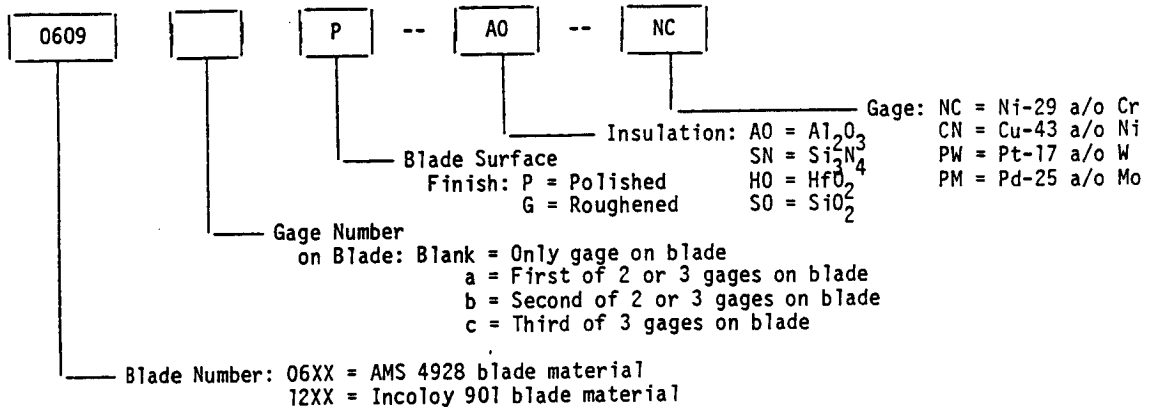
Gage adherence data and typical gage resistance as sputtered on the 44 blades are presented in Table XX.

In this table, the term "poor initial adherence" (symbol a') indicates that the gage survived photoresist removal but showed slight delamination along portions of the pattern edges, not affecting electrical continuity. These gages were retained in the program. The term "not adherent - open" indicates delamination across the width of at least one gage line before or during photoresist removal, resulting in loss of electrical continuity. These gages were then dropped from the program. (Some "not-adherent - open" gages were later subjected to temperature cycles to service temperature to determine whether adherence improved; there was no improvement. The results are included in a later final summary table.)

Of the 44 types, ten were not adherent, and seven others had "poor initial adherence".

Among the 34 adherent types, eleven were characterized as "shorted" in that the measurements showed only a few ohms resistance through the insulation layer to the blade material and only a few ohms resistance across the gage.

The remaining 23 adherent, and not shorted, gage systems had gage resistances between 200 and 2000 ohms, and insulation resistances above 10^7 ohms.

6-10

TABLE XX

ADHERENCE AND GAGE RESISTANCE AS SPUTTERED
OF 44 THIN FILM STRAIN GAGE TYPES
(One Gage of Each Type)

Blade Material	Gage Materials	Shorted	Gage Resistance (Ohms) 0	500	1000	1500	2000	Not Adherent (Open)
AMS 4928	NC	0634G-SO		0609P-AO 0621P-SN 0613P-HO	0638G-SN			
	CN	0610P-AO (a') 0639G-SN 0635G-SO		0622P-SN (a') 0627P-HO (a')				
	PW				0640G-SN 0636G-SO			0611P-AO 0642aP-SN 0628P-HO
	PM				0642bP-SN 0641G-SN	0637G-SO		0612P-AO 0629P-HO
Incoloy 901	NC	1247G-HO		1209P-AO 1221P-SN (a') 1213P-HO	1242G-SN 1238G-SO			
	CN	1210P-AO (a') 1243G-SN 1248G-HO 1239G-SO		1222P-SN 1227P-HO				
	PW	1237G-SN			1249G-HO 1240G-SO			1211P-AO 1223P-SN 1228P-HO
	PM	1212P-AO (a')		1236G-SN	1250G-HO	1241G-SO (a')		1230P-SN 1229P-HO

Summary:

10 Gages Not Adherent
34 Gages Adherent (but 11 shorted)
44 Gages Total

Legend:

a' Poor Initial Adherence

The results in the table indicate that the adherence and resistance were strongly dependent on the combination of surface finish and gage material, and to a smaller degree dependent on insulation material and blade material. These results are summarized in the following two paragraphs; gage systems on polished surfaces are discussed first. Gage systems on roughened surfaces are then reviewed.

On polished surfaces, among the 20 gage types fabricated, the poor adherence of PtW and PdMo was the major result; in fact, ten of the twelve PtW or PdMo gage types did not adhere on polished surfaces. The PtW and PdMo gage systems on polished surfaces accounted for all of the ten initially nonadherent gage types in the components program. NiCr gages were adherent on all polished surfaces, and gage resistance was several hundred ohms. CuNi gages were adherent on polished HfO_2 and polished Si_3N_4 (although in the "poor" class on both) and gage resistance was several hundred ohms. CuNi gages were adherent on polished Al_2O_3 (although "poor" on both blade materials), but were shorted.

On roughened surfaces, all 24 gage types fabricated were adherent. The major problem was of the opposite kind, that is, shorting of two NiCr gage types, all five CuNi gage types and one PtW gage type. It is particularly notable that all ten PtW and PdMo gage types were adherent as sputtered on roughened surfaces, whereas only two types of PtW or PdMo gage had been adherent on polished surfaces.

Gage resistances of adherent gages tended to be much higher on roughened surfaces than on polished surfaces. This effect was attributed to a longer effective gage line length due to the irregular surface, and possibly to thin spots in the gage material at local asperities in the surface.

Adherence and Resistance After Cycling to Service Temperature

The 34 best gage types of Table XX (all of those which were adherent as sputtered, including ten which were shorted) were then subjected to a series of one-hour exposures at service temperature in air. After each temperature cycle, the gage was visually examined for delamination, and gage resistance and insulation resistance were measured at room temperature. The procedure was described in Article 4.7.

The chronological order in which the temperature cycling tests of PtW and PdMo gages was conducted (dictated by availability of gage systems) had an effect on the outcome. The first noble metal alloy gages tested were the PdMo candidates on Incoloy 901 (to 900K). Severe oxidation was noted, as described in more detail later. The next happened to be the PtW candidate on AMS 4928 (to 600K), one PdMo system on AMS 4928 (to 600K), and one PtW system on Incoloy 901 (to 900K). Again severe oxidation was noted. Before further testing, the remaining noble metal alloy gage candidates were vacuum heat treated for periods of 50 to 100 hours at service temperature before exposure to air at service temperature. Vacuum heat treatment at temperatures above 1250K is recommended in Reference 12 to stabilize such alloys. The temperature of vacuum heat treatment here was limited to the maximum service temperature of the gage system.

Approximate gage resistance after temperature cycling is presented in Table XXI, comments on final visual appearance and other pertinent characteristics are presented in Table XXII, and the detailed history of resistance versus cycle number is presented in Figure 22 and Table XXIII. Figure 22 and Table XXIII will be discussed in detail after the following general comments on the outcome of the testing.

In Table XXI, the five items underlined with a solid line were the best performers. The seven items underlined with a dashed line were mechanically durable although electrically shorted; these were not ruled out for further evaluation. The remaining 22 items were rated as failed under test (either open circuit or continuous drift in gage resistance); these items were then dropped from the program.

TABLE XXI

RESISTANCE OF 34 ADHERENT THIN FILM STRAIN GAGE TYPES
AFTER CYCLING (x) TIMES TO SERVICE TEMPERATURE

Max. Test Temp.	Blade Material	Gage Materials	Shorted	Gage Resistance (Ohms) 0	500	1000	1500	2000	Not Adherent (Open)
600K	AMS 4928	NC	0609P-AO (1) 0638G-SN (2) 0634G-SO #(5)		0621P-SN (5) 0613P-HO (5)				
		CN	0610P-AO #(5) 0639G-SN #(5) 0635G-SO #(5)		0622P-SN (5) 0627P-HO (5)				
		PW					0640G-SN (6) 0636G-SO (6)		
		PM				0641G-SN **(5)	0642bP-SN (5) 0637G-SO *(5)		
900K	Incoloy 901	NC			1209P-AO (5) 1221P-SN (5)	1242G-SN (5)			1213P-HO (2) 1247G-HO #(1) 1238G-SO (1)
		CN							1210P-AO #(1) 1222P-SN (1) 1227P-HO (1) 1243G-SN #(1) 1248G-HO #(1) 1239G-SO #(1)
		PW	1249G-HO ***(2)		1237G-SN ***(5)				1240G-SO (1)
		PM							1212P-AO #(1)! 1236G-SN (1)! 1250G-HO (1)! 1241G-SO (1)!

Summary:

- 14 Gages Failed (Open Circuit)
- 8 Gages Had Significant Drift
- 5 Gages Stabilized
- 7 Gages Not Ruled Out
- 34 Gages Total

Legend:

- * Vacuum Heat Treated for 50 hours at 600K
- ** Vacuum Heat Treated for 100 hours at 600K
- *** Vacuum Heat Treated for 50 hours at 900K
- # Shorted as Sputtered
- ! Open, but still adherent

The behavior of the gage systems correlates strongly with the combination of gage alloy and maximum temperature of exposure during cycling. It must be borne in mind that all gage systems exposed to the higher temperature were mounted on Incoloy 901 blades. The thermal coefficient of expansion (tce) of Incoloy 901 is high , compared with AMS 4928. The possible influence of tce matching will be examined further after a summary of the principal results.

The durability and failure modes of the gage systems as presented in Table XXI and Table XXII are summarized in the following two paragraphs. Gage systems cycled to 600K (on AMS 4928) are discussed first. Gage systems cycled to 900K (on Incoloy 901) are then reviewed.

TABLE XXII

HISTORY OF THE 44 FIRST-GENERATION THIN FILM STRAIN GAGES

Blade Material	Gage Materials	Blade Number and History							
		Al_2O_3		Si_3N_4		HfO_2		SiO_2	
		Polished	Roughened	Polished	Roughened	Polished	Roughened	Polished	Roughened
AMS 4928	NC	0609 m m 5 Bright 1		0621 0 i 5 Bright 1	0638 m m 2 Dull 1	0613 0 i 5 Bright 1			0634 d d 5 Dull 2
	CN	0610 d a' d 5 Blue 1	Al_2O_3 Ruled Out	0622 4 a' c 5 Blue 1	0639 d d 5 Blue/Gray 1	0627 c a' i 5 Brown 1	HfO_2 Ruled Out	SiO_2 Acceptable but not	0635 d d 5 Brown 2
	PW	0611 a Ⓐ 0 a 2		0642a a Ⓐ 0 a 1	0640 5 c 6 Blue 2	0628 a Ⓐ 0 a 1		Continued in Program	0636 13 c 6 Blue 2
	PM	0612 e Ⓐ b 5 Black 1		0642b 17 c 5 Blue 1	0641 10 b c 6 Blue/Grn 1	0629 e Ⓐ 0 Bubbled 1			0637 38 b c 5 Blue/Grn 2
Incoloy 901	NC	1209 7 c 5 Dull 2		1221 0 a' i 5 Bluish 4	1242 3 c 5 Bluish 2	1213 e Ⓔ d 3 Bubbled 3	1247 j d Ⓙ 1 Dull 1		1238 e c Ⓔ 5 Blk/Blue 2
	CN	1210 i a' Ⓙ d 1 Black 1	Al_2O_3 Ruled Out	1222 i Ⓙ 1 Black 1	1243 i d Ⓙ 1 Black 1	1227 i Ⓙ 1 Black 2	1248 i d Ⓙ 1 Black 2	SiO_2 Acceptable but not	1239 i d Ⓙ 1 Black 2
	PW	1211 a Ⓐ 0 a 2		1223 a Ⓐ 0 a 1	1237 0 b h i 14 Dull 1	1228 a Ⓐ 0 a 1	1249 m b m 2 Dull 2	Continued in Program	1240 e b Ⓔ k 1 k 2
	PM	1212 e a' Ⓔ 1 Wrinkled 1		1230 e Ⓐ 0 a 1	1236 e Ⓔ 4 Gray 1	1229 e Ⓐ 0 Dark 1	1250 e Ⓔ 3 Greenish 1		1241 e a' Ⓔ 1 Dark 2

Legend:

Z	T
Y	X
W	U

Z = Blade Number
T = Drift Rate (ohms/hour) at End of Test
Y = Performance Notes
X = Number of 1-hour Cycles to Service Temperature
W = Final Appearance of Gage
U = Final Appearance of Insulating Layer:
    1 = Clear   3 = Dark Spalling
    2 = Discolored   4 = Slight Crazing

24 Candidates Ruled Out (the Circled Note, Ⓞ, Indicates the Principal Reason for Rejection of the Candidate).

Note Code:

a' = Poor Initial Adherence
a = No Initial Adherence
b = Vacuum Heat Treated
c = Significant Drift at Service Temperature
d = Shorted (Less than 10 ohms) as Sputtered
e = Open (More Than 10^4 ohms)

f = Damaged; Not Ruled Out
h = Became Stable After Vacuum Heat Treat
i = Working Strain Gage
j = Disintegrated at 900K
k = Gage Spalled after Storage
m = Shorted at Test; Not Ruled Out

Of the 15 gage types cycled to 600K, all proved durable (Table XXI); no gages deteriorated seriously or became open-circuited. The four types which had been shorted as-sputtered (symbol a in Table XXI) remained shorted throughout the temperature cycles to 600K. One additional NiCr gage (0609P-A0-NC) shorted during the first cycle, and another NiCr gage (0638G-SN-NC) shorted during the second cycle. The insulation resistance for all other gages

remained above 10^7 ohms. Gage resistance generally changed by several percent during the first cycle or two, and then more slowly during subsequent cycles; the gage resistance readings versus cycle number (Figure 22) are discussed in detail later. Finally, the appearance of the insulating films and gages tested to 600K remained generally good (Table XXII). In particular, the insulating films either remained transparent or showed slight color changes or mottling. The appearance of the gages, which were all initially characterized by a bright metallic luster as sputtered on polished surfaces or a dull gray as sputtered on roughened surfaces, generally became darker and slightly discolored, suggesting that some oxidation had occurred during temperature cycling to 600K. The darkening and discoloration of the gage alloy was particularly noticeable in the three noble metal alloy systems, which had not been vacuum heat treated (two PtW system and one PdMo system). These three gages darkened drastically and acquired a blue tinge. Darkening and discoloration was slightly less pronounced in the two PdMo gages which had been vacuum heat treated, still less pronounced in the CuNi gages, and practically nonexistent in the NiCr gages.

Of the 19 gage types cycled to 900K, 13 types failed completely (open circuit) during the first cycle, including one (1240G-SO-PW) which delaminated at room temperature after a 50-hour vacuum heat treatment. In addition, one gage (1249G-HO-PW) was damaged by accident (shorted while clamping temporary lead wires to the gage) after a 50-hour vacuum heat treatment and one (1213P-HO-NC) developed an open circuit during the second cycle. The remaining four candidate systems survived the five cycles to 900K in good condition, with gage resistance stabilizing to various degrees. (The gage resistance readings versus cycle number are presented in Figure 22 and are discussed in detail later). The first-cycle open-circuit failures at 900K included all six CuNi systems, all four PdMo systems, two of the six NiCr systems, and one of the three PtW systems. The four survivors which neither opened or shorted were three NiCr systems and one PtW system. The final appearance of all gages can be summarized by gage alloy as follows:

All of the six CuNi gages were apparently severely oxidized during the first 900K cycle and essentially vanished, leaving traces of a dark residue. The four PdMo gages (none of which had been vacuum heat treated) were also apparently severely oxidized, the material becoming dark in color, and, nonconducting (although still adherent). The six NiCr gages became duller and discolored, one (1238) showing a blue tint suggestive of oxidation of chromium, another (1221) showing a slight indication of crazing, and another (1213) showing some bubbling on polished HfO_2, although test stripes of NiCr on these blades survived tape tests of adherence after the temperature cycling). The three PtW gages which had been vacuum heat treated retained a metallic gray color including the one which delaminated after the vacuum heat treatment.

Possible Effect of tce Mismatch

Effects of tce mismatch on gage adherence at 900K are difficult to separate from chemical (oxidation) and mechanical surface finish effects. The relative estimated tce's are as follows (from Table IV):

Incoloy 901	15 ppm/K
Insulating films	1 to 7 ppm/K
PtW	9 ppm/K
NiCr	10 ppm/K
PdMo	12 ppm/K
CuNi	15 ppm/K

Adherence was good for the NiCr and PtW gages. It is therefore suggested that tce matching between the gage and the insulating layer (with which the gage is in contact) may be as important as tce matching between the gage and the blade. Computer programs are available to predict stress distributions in layered systems. An analysis would be of interest.

Survival of Gages with Poor Initial Adherence

Gages with "poor initial adherence" did not differ in type of eventual failure mode from other gages. The three CN gages with "poor initial adherence" on AMS 4928 all survived the five cycles to 600K and demonstrated fair-to-good stability of resistance. Three of the four on Incoloy 900 (one CN and two PM) with "poor initial adherence" all failed at 900K along with all other CN and PM gages on Incoloy 900, while the fourth gage (NC) survived the five cycles to 900K and demonstrated good stability, like other NC gages on Incoloy 900.

Gage Resistance and Insulation Resistance Versus Cycle Number

In preparing to select candidate thin film gage systems for a second round of fabrication and testing, the details of resistance stability during thermal cycling of the first-generation gages were reviewed. The following discussion of the resistance measurements results will center on Figure 22 in which gage resistance versus cycle number is plotted for each of the 34 adherent first-generation gages. Reference will occasionally be made to Table XXIII in which both the gage resistance and insulation resistance measurements are presented for each cycle.

In Figure 22 it is evident that each gage alloy displays a characteristic drift trend. All five surviving NiCr gages (as well as the sample on a glass slide, also plotted in Figure 22) drifted downward in resistance in each cycle. The drift was less in each succeeding cycle. The total drift was -3 to -5 percent in five cycles. For three of these gages the drift rate reached zero in the fifth cycle. (Gage resistance is reported to the nearest ohm.) Insulation resistance (Table XXIII) remained above 20 megohms throughout the five cycles for four of these five gages and was not a factor influencing drift. In the fifth gage system (1242G-SN-NC) the insulation resistance dropped from its initial value of 20 megohms to 40 kilohms by the fourth cycle and then remained stable. This particular gage had an initial measured resistance of 1500 ohms and final measured resistance of 1460 ohms. The reduction in measured insulation resistance (increased shunting) therefore apparently accounted for about two-thirds of the -2.7 percent change in measured gage resistance.
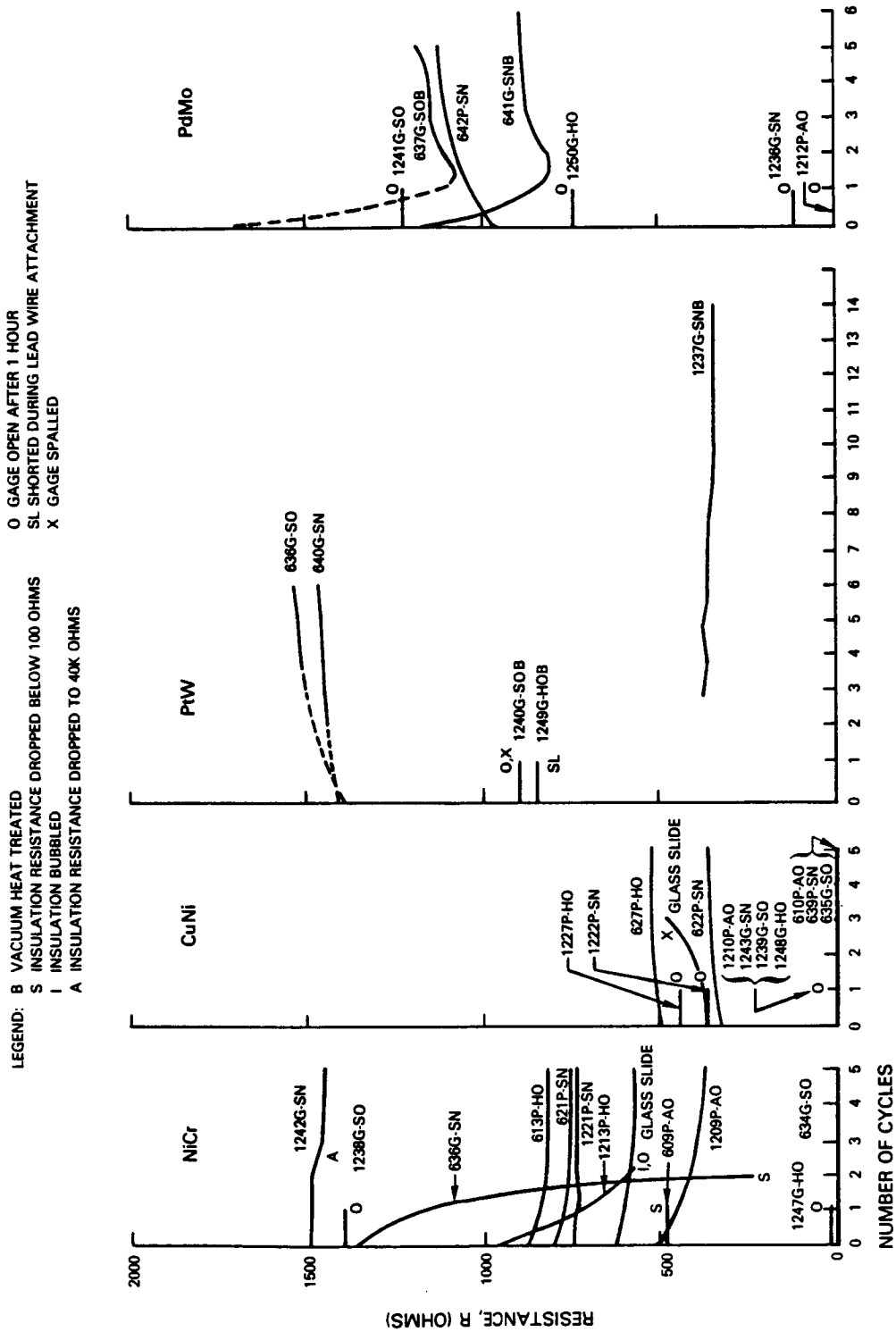
Figure 22 Gage Resistance at Room Temperature versus Number of Cycles to Service Temperature for the 34 Adherent First-Generation Strain Gages.

TABLE XXIII

GAGE AND INSULATION RESISTANCES AS SPUTTERED AND AFTER EACH TEMPERATURE CYCLE* FOR 44 FIRST GENERATION THIN FILM STRAIN GAGES

| Gage Serial Number | As Sput-tered | Gage Resistance, Ohms (First Line)/Insulation Resistance, Ohms (Next Line) Cycle Number | | | | | | | | | | | | | |
		1	2	3	4	5	6	7	8	9	10	11	12	13	14
0609P-AO-NC	487 / 20M	0 / 0	0 / 0	0 / 0	0 / 0	0 / 0									
0634G-SO-NC	0 / 0	0 / 0	0 / 0	0 / 0	0 / 0	0 / 0									
0621P-SN-NC	786 / 20M	760 / 20M	752 / 20M	748 / 20M	744 / 20M	744 / 20M									
0638G-SN-NC	1355 / 20M	1144 / 20M	245 / 58												
0613P-HO-NC	862 / 20M	833 / 20M	818 / 20M	815 / 20M	815 / 20M	815 / 20M									
1209P-AO-NC	502 / 20M	439 / 20M	412 / 20M	399 / 20M	384 / 20M	377 / 20M									
1238G-SO-NC	1500 / 8.7M	937	473	360K	1.85M	3.9M									
1221P-SN-NC	745 / 20M	733 / 20M	735 / 20M	735 / 20M	735 / 20M	735 / 20M									
1242G-SN-NC	1500 / 20K	1496 / 335	1490 / 90K	1465 / 50K	1468 / 40K	1460 / 40K									
1213P-HO-NC	934 / 20M	705 / 20M	583 / 20M	Test Discontinued Due to Bubbling of Insulating Film.											
1247G-HO-NC	Strain Gage Had Low Resistance to Ground, As Sputtered. Strain Gage Disintegrated After 1 hour at 900K.														
0610P-AO-CN	0 / 0	0 / 0	0 / 0	0 / 0	0 / 0	0 / 0									
0635G-SO-CN	0 / 0	0 / 0	0 / 0	0 / 0	0 / 0	0 / 0									
0622P-SN-CN	318 / 20M	337 / 10M	347 / 10M	352 / 10M	353 / 10M	357 / 10M									
0639G-SN-CN	0 / 0	0 / 0	0 / 0	0 / 0	0 / 0	0 / 0									
0627P-HO-CN	490 / 10M	509 / 10M	523 / 10M	525 / 10M	528 / 10M	528 / 10M									
1210P-AO-CN	0 / 0	Strain Gage Disintegrated After 1 hour at 900K.													
1239G-SO-CN	0 / 0	Strain Gage Disintegrated After 1 hour at 900K.													
1222P-SN-CN	352 / 10M	Strain Gage Disintegrated After 1 hour at 900K.													
1243G-SN-CN	0 / 0	Strain Gage Disintegrated After 1 hour at 900K.													
1227P-HO-CN	437 / 10M	Strain Gage Disintegrated After 1 hour at 900K.													
1248G-HO-CN	0 / 0	Strain Gage Disintegrated After 1 hour at 900K.													
0611P-AO-PW	Strain Gage Detached from Surface During Photoresist Removal.														
0636G-SO-PW	1406 / 2M	-- / --	-- / --	1451 / 2M	1520 / 2M	1526 / 2M	1539 / 2M								
0642aP-SN-PW	Strain Gage Detached from Surface During Photoresist Removal.														
0640G-SN-PW	1414 / 20M	-- / --	-- / --	1451 / 20M	1455 / 20M	1463 / 20M	1468 / 20M								
0628P-HO-PW	Strain Gage Detached from Surface During Photoresist Removal.														
1211P-AO-PW	Strain Gage Detached from Surface During Photoresist Removal.														
1240G-SO-PW	884 / 20M	Gage was Vacuum Heat Treated and then Spalled During Storage.													
1223P-SN-PW	Strain Gage Detached from Surface During Photoresist Removal.														
1237G-SN-PW	-- / 170	-- / --	-- / --	371 / --	363 / --	373 / 2M	365 / 2M	362 / 2.2M	360 / 2.5M	357 / 2.5M	355 / 3.0M	355 / 3.0M	355 / 3.0M	354+ / 3.0M	354 / 2.8M
1228P-HO-PW	Part of Strain Gage Detached from Surface During Photoresist Removal.														
1249G-HO-PW	872 / 20M	Strain Gage Shorted to Ground During Vacuum Heat Treat with Clamped Leads.													
0612P-AO-PM	/ 20M		20M	20M	20M	20M									
0637G-SO-PM	1700 / 20M		1100 / 20M	1142 / 20M	1147 / 20M	1185 / 20M									
0642bP-SN-PM	956 / 20M	1040 / 20M	1074 / 20M	1097 / 20M	1105 / 20M	1122 / 20M									
0641G-SN-PM	1139 / 20M	846 / 20M	807 / 20M	856 / 20M	865 / 20M	870 / 20M	880 / 20M								
0629P-HO-PM	Part of Strain Gage Detached from Surface During Photoresist Removal.														
1212P-AO-PM	0 / 0	193K / 5.0M	693K / 2.7M	1.6M	1.0M	1.0M									
1241G-SO-PM	1221 / 20M	1.75M / 20M	2.67M / 20M	2.91M / 20M	2.481M / 20M										
1230P-SN-PM	Part of Strain Gage Detached from Surface During Photoresist Removal.														
1236G-SN-PM	111 / 60	384K / 20K	337K / 20K	318K / 20K	329K / 20K										
1229P-HO-PM	Part of Strain Gage Detached from Surface During Photoresist Removal.														
1250G-HO-PM	739 / 1221	303K / 304K	545K / 20K	700K / 20K											

* NOTE: In each temperature cycle, the gage was heated to service temperature, soaked for one hour, and cooled to room temperature.
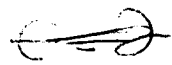
The two surviving CuNi gages drifted upward in resistance during each cycle, progressively more slowly in each cycle, reaching a total change of about 8 to 12 percent in five cycles. For one gage the drift rate reached zero in the fifth cycle. Insulation resistance remained above 10 megohms throughout the tests and therefore was not a factor influencing drift. The CuNi gage on a glass slide, also plotted in Figure 22, drifted upward and bubbled in the third cycle.

In the case of PtW gages, the behavior of gages which had not been vacuum heat treated was different from the behavior of the one surviving gage which had been vacuum heat treated.

The two surviving PtW gages which had not been vacuum heat treated drifted upward in each cycle, progressively more slowly, reaching a total change of +4 to +10 percent in six cycles. The rates of drift were still substantial in the sixth cycle (5 and 13 ohms/hr.). The insulation resistance was very low (rated as "shorted") during the first two cycles, but increased in the third cycle and remained above 2 megohms thereafter and did not appear to be a factor influencing drift during the third through sixth cycle..

The surviving PtW gage which had been vacuum heat treated (at 900K) drifted slowly downward by 5 percent. This gage was cycled 14 times. The drift was zero during the tenth through fourteenth cycles. The insulation resistance was very low (rated as "shorted") during the first four cycles, but increased to two megohms in the fifth cycle and remained above 2 megohms thereafter and did not appear to be a factor influencing drift during the fifth through fourteenth cycle.

Vacuum heat treatment also altered the drift characteristic of PdMo gages but in a different way. The surviving PdMo gage which had not been vacuum heat treated drifted upward in each 600K cycle, progressively more slowly, reaching a total change of +10 percent in five cycles. The drift was 17 ohms during the fifth cycle. Insulation resistance remained above 20 megohms and was not a factor influencing drift.

The two surviving PdMo gages which had been vacuum heat treated (at 600K) behaved quite differently from all other gages. The two gages drifted downward by 50 percent in the first two 600K cycles, then upward by 10 percent during the next several cycles, progressively more slowly in each cycle. The rates were still substantial during the final cycle (+10 and +38 ohms/hour). Insulation resistance remained above 20 megohms and was not a factor influencing drift.

In evaluating all these results, it is notable that upward drift in gage resistance was observed only in the CuNi systems and in the PtW and PdMo systems not vacuum heat treated. These systems were expected to be the most strongly affected by oxidation, and were visually observed to be most darkened and discolored by the end of testing. It would appear that oxidation increased the resistance through progressive replacement of one constituent in the alloy with its oxide, reducing the cross section area available for conduction. Such a conclusion must be viewed with extreme caution, however, since oxidation could produce the opposite effect on gage resistance if the mechanism was removal of one alloying metal, leaving a single pure metal of

low resistivity. In the case of the PtW systems, this question was later investigated further, and the PtW case is discussed in a later section. No further information on the CuNi or PdMo drift behavior was obtained.

Downward drift in gage resistance was observed in all NiCr systems. This gage alloy was least darkened or discolored by thermal cycling and therefore thought to be least affected by oxidation. The drift in this case could be the result of slow change in metallurgical lattice structure from a partially disordered state as sputtered to a more disordered state (Reference 19), or it could be the result of some oxidation mechanism.

Approximate Gage Factor

After the thermal cycling tests were completed, the gage factor (G) of sample gages was measured at room temperature. One gage of each stable alloy (NiCr, CuNi, PtW) was tested using the procedure described in Section 4.7. The measured gage factors are listed in Table XXIV.

TABLE XXIV

APPROXIMATE GAGE FACTOR MEASURED ON BLADES

Gage Alloy	Gage Number	Gage Factor (G)
NC	0621P-SN-SC	1.9 $\pm$ 30%
CN	0627P-HO-CN	2.1 $\mp$ 30%
PW	1237G-SN-PW	1.8 $\mp$ 30%

The measured gage factors lie in the range expected (Table V) for conventional wire gages, except in the case of the PtW, where the measured gage factor is lower than expected by a factor of two.

Resistivity, #, and Insulation Resistance at Service Temperature

Gage resistance and insulation resistance were measured at service temperature for sample gages, using the procedure described in Section 4.7. The tests provided data at temperatures to at least 600K for at least one sample of each insulation material (Al_2O_3, Si_3N_4, HfO_2, SiO_2) and at least one sample of each stable gage material (NiCr, CuNi, PtW). The gage resistance measurements were used to calculate α. No corrections were applied for the differences in coefficients of expansion between gage insulation and blade materials. These differences (Table IV), are believed to account for no more than 10 percent of the observed apparent strain due to temperature. Table XXV lists the results, along with the apparent strain α/G (based on the measured gage factor, G), the insulation resistance at temperature, and the calculated gage resistivity at room temperature (based on the nominal gage dimensions of Figure 10 and measured resistance and thickness).

The large value of α (3420 ppm/K) for the PtW gage was startling, since a value below 100 ppm/K was hoped for (see Figure 6).

The insulation resistance measurements were encouraging and did not rule out any of the insulation materials.

The calculated resistivities were of the expected order of magnitude.

TABLE XXV

RESISTIVITY, TEMPERATURE COEFFICIENT OF RESISTANCE (α), APPARENT STRAIN, AND INSULATION RESISTANCE FOR SAMPLE GAGES

Gage No.	Gage Alloy Calculated Resistivity at 300K (μohm-cm)	α (ppm/K)	Apparent Strain, α/G (ppm/K)	Measured Insulation Resistance (Ohms)		
				at 300K	at 600K	at 900K
0621P-SN-NC	150	101	53	10^7	10^7	
0627P-HO-CN	130	88	42	10^7	10^7	
1237G-SN-PW	110	3420	1900	10^7		229K
0610P-AO-CN				10^7	10^7	

The Tungsten Segregation Problem

Because the α of the PtW sample (gage 1237G-SN-PW) was surprisingly high, the structure of the sputtered PtW material was examined using electron microscope techniques. Several regions were scanned on a sample strip of the PtW gage material sputtered at the same time as gage 1237G-SN-PW and exposed to the same test history. The structure (Figure 23) was generally uniform and fine-grained (grain size below 5 μm) with scattered larger amorphous islands. The average composition as determined by electron microprobe was about the same as the composition determined by the wet chemical analysis (Pt-17a/o W). Detailed mapping of the distribution of Pt, W, and O_2 (Figure 24) revealed that the large islands were nearly 100 percent tungsten and that the surrounding sea was nearly 100 percent platinum. The maps in the figure were obtained by Energy Dispersive Analysis with X-Rays (EDAX). A light area indicates a high concentration of the labeled species. The energy could be adjusted to sample to depths of 0.1 to 0.5 μm. Several regions were scanned, at 0.1 μm depth and 0.5 μm depth. The results were always the same, showing that virtually all of the tungsten was segregated in the large isolated islands (20 to 50 μm size). In these islands the platinum was absent. A small amount of oxygen was detected everywhere. (This technique does not indicate whether the tungsten was in the form of an oxide.)

The observed value of α (3400 ppm/K, Table XXV) for this segregated PtW material is extremely high like that of pure platinum (3900 ppm/K) or pure tungsten (4800 ppm/K). The low drift rate at 900K (Figure 22) is alos typical of pure platinum. On the other hand, the resistivity (110 μohm-cm) is far above that of platinum (10 μohm-cm) or tungsten (5 μohm-cm), and near that of Pt-10 a/o W in Reference 18. The gage factor (1.8) is much lower than expected for pure Pt or its dilute alloys (Ref. 18). The behavior of this material has not been explained, but it is probably related to the observed segregation of the tungsten.
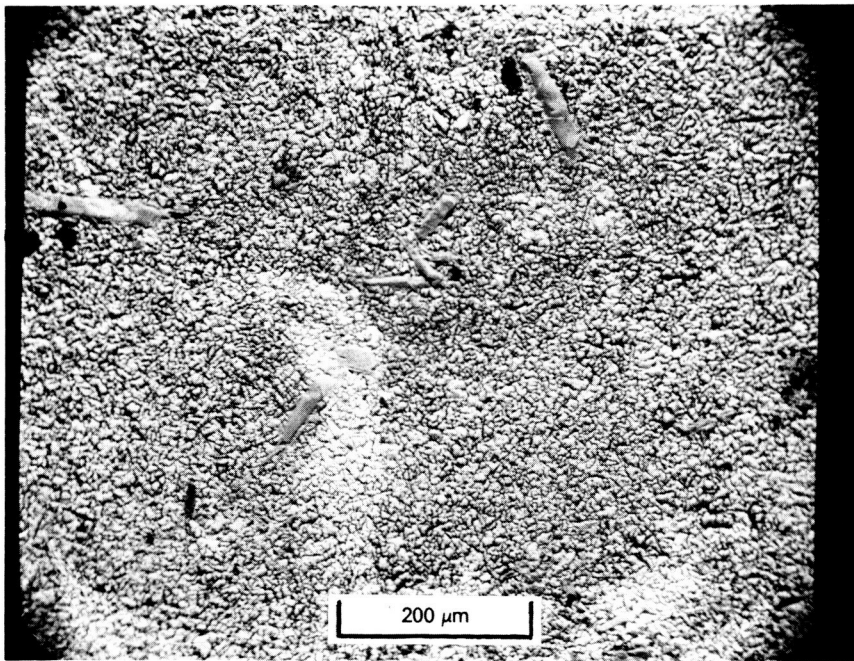
A
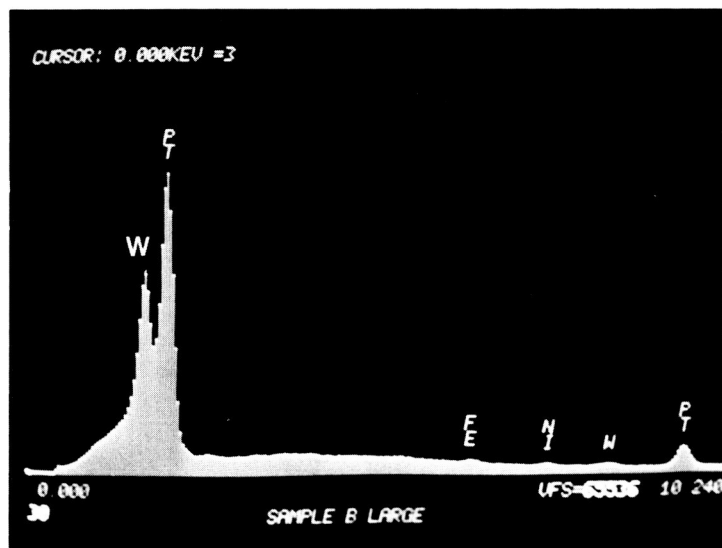
B

Figure 23 PtW Gage Material Surface Structure (A) and Electron Microprobe
Composition Spectrum (B).
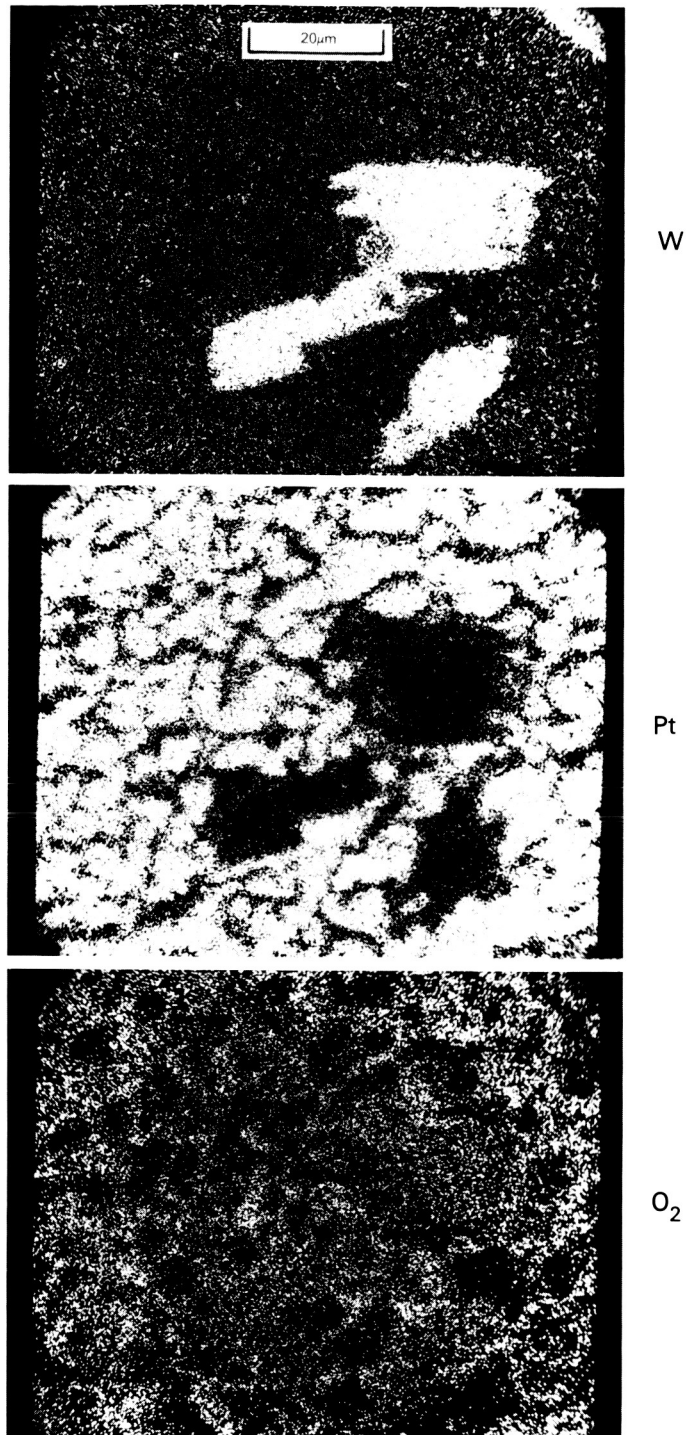
Figure 24   X-Ray Maps of W, Pt, and O_2 Over a 70 μm by 80 μm Region of PtW
Film.   A light area indicates a high concentration of the
identified species.   The same area is shown in each photo.   The
islands are rich in tungsten and contain almost no platinum.   The
oxygen is randomly distributed.

The segregation of the tungsten has not been explained, but it is conjectured to be related to the configuration of the composite sputtering target used. In a later program, the size of each individual area of exposed tungsten on the target surface was reduced tenfold, and the segregation did not occur. The result was not available in time to be of use in the present contract program.

Candidates Ruled Out by the First-Generation Results

On the basis of the results of testing the first generation of thin film strain gages, 24 of the 44 types were dropped from the program (shaded areas in Table XXII), as follows:

On AMS 4928:	No. of Types	Reason
PtW on polished surfaces	(3)	no adherence
PdMo on polished Al_2O_3 or HfO_2	(2)	no adherence

On Incoloy 901:		
NiCr on HfO_2 and SiO_2	(3)	infinite resistance at 900K
CuNi (all samples)	(6)	disintegration at 900K
PtW on polished surfaces	(3)	no adherence
PtW on SiO_2	(1)	spalled during storage
PdMo on polished Si_3N_4 or polished HfO_2	(2)	no adherence
PdMo on other surfaces	(4)	infinite resistances at 900K

Total 24

The other 20 types remained as candidates for further evaluation (unshaded areas in Table XXII).

6.3 GAGE FILM EVALUATIONS - SECOND GENERATION

Overview

After completing the evaluation of the first generation of strain gage film elements, a second generation was fabricated and evaluated. The objectives were to determine gage-to-gage repeatability in fabricating quantities of selected types, and to increase the data base to be used in selecting two final candidates for service to 600K and two for service to 900K.

From the 20 most promising first-generation systems (unshaded area in Table XXII), six were selected for the second generation strain gage systems. Six to nine gages of each kind were fabricated, for a total of 48 gages in the second generation, as listed in Table XXVI (Parts A and B).

Selection Process

The systems were selected on the basis of the data of Table XXII and other data from the literature.

TABLE XXVI-A

TEST RESULTS FOR SECOND-GENERATION GAGES ON AMS 4928 BLADES

Proto-type Blade Number	Second-Generation Gage Number	Insulation Run No.	Insulation Thickness (μm)	Gage Run No.	Gage Thickness (μm)	Adherence* as Sputtered	Adherence* after Service Temp. Exposure	Gage Resistance (ohms) as Sputtered	Gage Resistance (ohms) after Stabilization	Insulation Resistance Room Temp. as Sputtered	Insulation Resistance Room Temp. after Stabilization	Insulation Resistance at Service Temperature	Drift (ohms) at Service Temp.	Gage Factor at Room Temp.	Apparent Strain (με/K)
0609	0659aP-AO-NC	101	4.0	108	1.1	S	S	359	261	20M	0		2		
	b					S	S	369	280	20M	440		-6		
	0660a					S	S	330	270	19K	0		-4		
	b					S	S	322	212	20M	250		-46		
	0661a					S	S	354	299	20M	1600		1		
	b					S	S	350	281	20M	400	0	0		
	0662a					S	S	382	272	0	0	0	-2		
	b					S	S	374	118	0	120		-185		
0621	0667aP-SN-NC	102	4.0	105	1.1	S	U	526	515	20M	20M		--	2.2	30
	b					S	S	349	330	20M	20M	20M	0		
	0668a					S	S	325	310	20M	20M	20M	2	2.1	73
	b										20M		1		
	0669a					S	S	300	294	20M	20M		1		
	b					S	S	303	296	20M	20M	20M	1		
	0670a					S	S	350	337	20M	20M		1		
	b					S	S	278	270	20M	20M		0		
0610	0671aP-AO-CN	106	4.0	109	1.1	S	S	152	146	20M	0	0	0	2.0	12
	b					S	S	144	146	20M	19K	12M	0		
	0672a					S	S	149	137	20M	1300		0		
	b					S	S	151	144	20M	10K		-2		
	0673a					S	S	139	137	20M	250		3		
	b					S	S			--	--		--		
0627	0663aP-HO-CN	100	4.5	107	1.1	S	S	593	522	82K	2K		-8		
	b					S	S	276	256	20M	20M		--		
	0664a					S	S	255	256	3M	0		3		
	b					S	S	244		13M	260		-5		
	0665a					S	S	175	172	9K	20M	20M	8		
	b					S	S	210	191	.2M	210		-8		
	0666a					S	S	211	245	20M	1300		51		
	b					S	S	218	219	20M	20M	20M	6	2.1	42

* S = Satisfactory Rating
U = Unsatisfactory Rating

GAGE LOCATIONS
a
b

TABLE XXVI-B

TEST RESULTS FOR SECOND-GENERATION GAGES ON INCOLOY 901 BLADES

Proto-type Blade Number	Second-Generation Gage Number	Insulation Run No.	Insulation Thickness (μm)	Run No.	Gage Thickness (μm)	Adherence* as Sputtered	Adherence* after Service Temp. Exposure	Gage Resistance (ohms) as Sputtered	Gage Resistance (ohms) after Stabilization	Insulation Resistance at Room Temperature as Sputtered	Insulation Resistance at Room Temperature after Stabilization	Insulation Resistance at Service Temperature	Drift (ohms) at Service Temp.	Gage Factor at Room Temp.	Apparent Strain (με/K)
1209	1251aP-A0-NC	103	4.0	111	1.1	S	U			20M	0		--		
	b					S	S	433	338	20M	670		-10		
	c					S	U	459		20M	4M		--		
	1252a			112	1.1	S	S	273	283	20M	20M		-14		
	b					S	S	272	277	20M	20M		-78		
	c					S	S	299	333	20M	20M		-20		
	1253a			112	1.1	S	S	261	275	20M	20M		-20	2.2	70
	b					S	S	262	287	20M	20M		9		
	c					S	S	278	292	20M	20M		0		
	1254a			112	1.1	S	S	281	288	20M	20M		-14	2.1	47
	b					S	S	289	298	20M	20M		2		
	c					S	S	308	327	20M	20M		1		
1237	1255aG-SN-PW	104	4.0	110	1.0	U	S	666	317	.2M	20K	20K	3		SHORTED
	b					S									
	c					U									
	1256a					U									
	b					U									
	c					U									
	1257a					U									
	b					U									
	c					U									
	1258a					U									SHORTED
	b					U									
	c					S	S	812	361	20M	300K	230K	-12		

* S = Satisfactory Rating
  U = Unsatisfactory Rating

GAGE LOCATIONS (a, b, c)

6-26

Referring to Table XXII, on AMS 4928 blades the most promising gage alloys were NiCr and CuNi. On these blades the insulating layers in the only entirely successful systems were Si_3N_4 and HfO_2. In addition, the Al_2O_3 insulating layers showed some promise (although one shorted at test and one shorted as-sputtered). The SiO_2 insulating layers were least promising (both were shorted as-sputtered and discolored after temperature cycling). A final consideration was that, in the literature, Al_2O_3 was clearly the best insulator at elevated temperature. To be sure that Al_2O_3 was given a thorough evaluation, both of the two Al_2O_3 systems in Table XXII were selected (0609P-AO-NC and 0610P-AO-CN). One Si_3N_4 system was selected, the choice being obvious (0621P-SN-NC). One HfO_2 system was selected. In this case choice between two stable systems of Table XXII was difficult, the final selection being 0627P-HO-CN to provide equal numbers of NiCr and CuNi samples on AMS 4928.

On Incoloy 901 the gage materials not ruled out were NiCr and vacuum-heat-treated PtW. With NiCr gages the insulating film candidates were Si_3N_4 and Al_2O_3. With PtW gages the insulating film candidates were Si_3N_4 and HfO_2. The final selections were 1209P-AO-NC and 1237G-SN-PW. This selection provided further experience with two insulating layers and two gage materials on Incoloy 901.

Results

For each gage type selected, two or three gage systems were fabricated on each of four blades. The gage mask configuration of Figure 10 was used. Insulation thickness and gage thickness are noted in Table XXVI.

Figure 25 shows photographs of the resulting gages on one blade for each of the six gage systems as sputtered. There were no significant variations in appearance from blade to blade of the same gage system type. For example, the only serious adherence problem was that experienced with PtW, typified by the gages on blade 1255 in Figure 25.

Test results are listed in Table XXVI. The first several columns list adherence ratings, gage resistances, and insulation resistances measured for each gage. Each of these quantities was determined in the as-sputtered condition and again after five one-hour exposures at service temperature.

The test of adherence as sputtered was the photoresist removal process. The test of adherence after temperature exposure was a tape test. A satisfactory adherence rating (S) was assigned if only local edge delamination was observed (not affecting gage continuity). An unsatisfactory rating (U) was assigned if delamination extended across a gage film line (usually affecting continuity).

The remaining columns of Table XXVI list measurements of drift at service temperature, gage factor (G) at room temperature, and apparent strain. These quantities were measured on a few selected gage samples only. The drift is the change in the room-temperature gage resistance due to the fifth hour of exposure at service temperature.
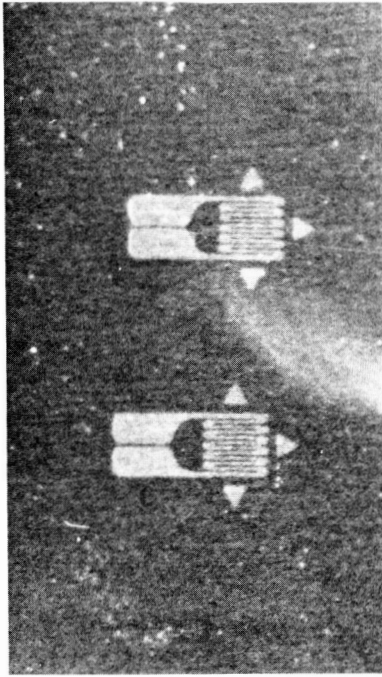
0659P-AO-NC
(81C0631-001)
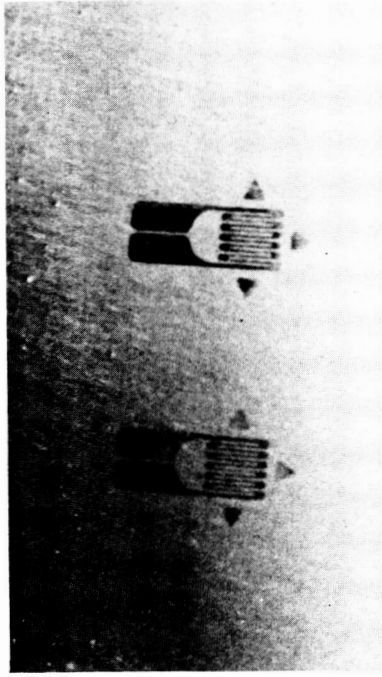
0664P-HO-CN
(81C0631-002)
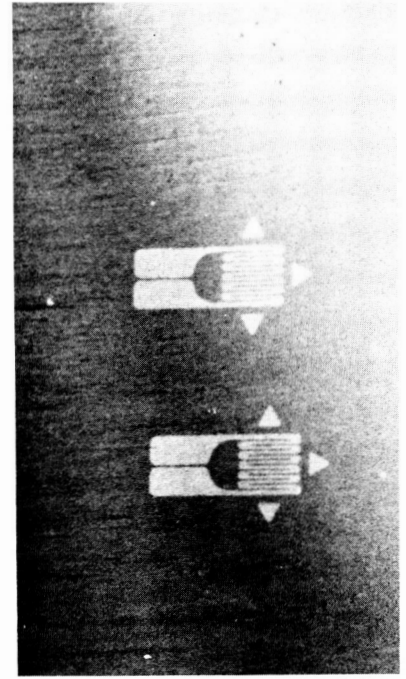
0668P-SN-NC
(81C0631-003)
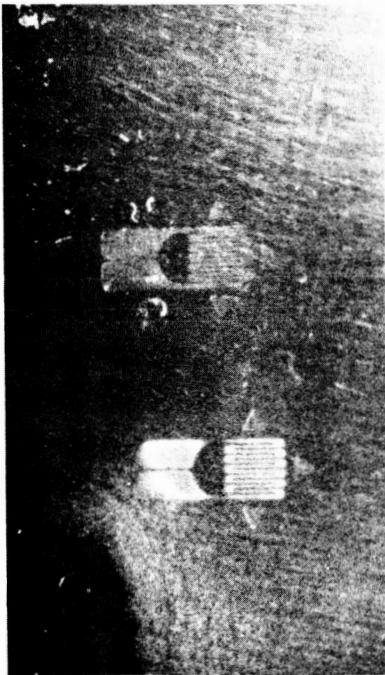
0673P-AO-CN
(81C0631-004)
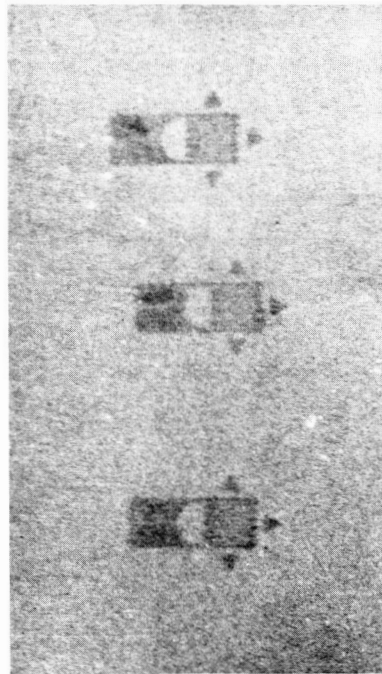
1254P-AO-NC
(81C1050-001)
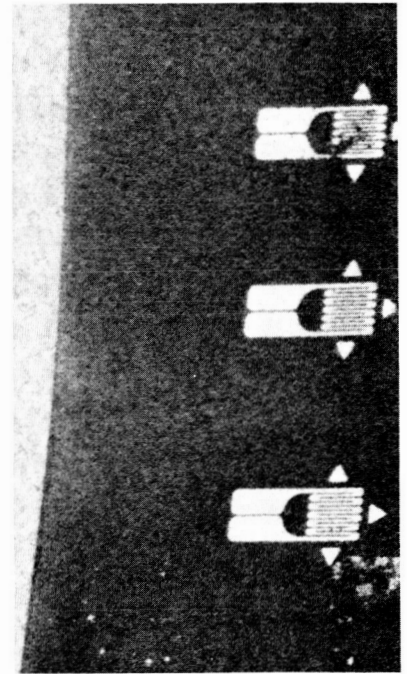
1255G-SN-PW
(81C0837-001)

Figure 25   Second-Generation Thin-Film Strain Gage Systems on Blades.   One
sample blade of each of the six types is shown, as sputtered.

It is evident in Table XXVI that three of the six systems exhibited serious shortcomings. Specifically, the two Al_2O_3 systems on the AMS 4928 blades (06XXP-AO-NC and 06XX-AO-CN) were plagued by poor insulation resistance after the high-temperature exposure, and the PtW gage films on the Incoloy 901 blades (12XXG-SN-PW) were generally not adherent as sputtered.

The other three systems (06XXP-SN-NC, 06XXP-HO-CN, and 12XX-AO-NC) exhibited good to outstanding properties and good repeatability from gage to gage.

The gage resistance drift trends due to exposure at service temperature were similar to those observed in first-generation gage tests (Figure 22) with the exception that six of the 14 CuNi gages drifted downward by as much as 5 percent rather than upward.

The results of Table XXVI for all the second-generation gages are further reviewed in Section 6.7, Final Candidate Systems, where the final scoring of all first-generation and second-generation systems is presented.

6.4 OVERCOAT TRIALS

Selection Process

To evaluate the effect of protective overcoats in reducing oxidation and erosion, eleven thin film gages of four kinds on five blades were overcoated by sputtering a film of the same material and thickness as the insulation material (Al_2O_3 or Si_3N_4) over the sputtered gages. The procedure was previously described in Section 4.8, Overcoat Trial Procedures. The four kinds overcoated were NiCr on AMS 4928 with Al_2O_3, NiCr on AMS 4928 with Si_3N_4, NiCr on Incoloy 901 with Al_2O_3, and CuNi on Incoloy 901 with Si_3N_4.

Table XXVII lists the specific blade and gage code numbers and the resistance values measured before and after overcoating, after two thermal cycles, after two strain cycles, and after erosion testing. The erosion results with and without overcoating are discussed in detail in a later section. The resistance measurements after erosion testing are presented here to identify the test sequence for each overcoated gage. Some gages were thermal-cycle tested and strain-cycle tested before erosion testing and some after erosion testing, as shown in the table.

Samples of the first three of the four kinds to be overcoated were readily available from the second generation group of gages listed in Table XXVI. As noted in Table XXVI, some of these gages were overcoated before any testing and some were overcoated after the completion of the testing described in Section 6.3.

Gages of the fourth kind (on Incoloy 901 with Si_3N_4) were not available from the second-generation tests since the candidate in this category had employed the PtW gage material which proved to be generally not adherent as sputtered. To provide the fourth kind, CuNi gages were sputtered on a spare Incoloy 901 blade with Si_3N_4 insulation and Si_3N_4 overcoat. The CuNi gage material was selected for this category to provide a gage known to be severely affected by oxidation at 900K when uncoated.

TABLE XXVII

TEST RESULTS FOR OVERCOATED THIN-FILM STRAIN GAGES

Blade and Gage Number	Gage Resistance, ohms, and (Insulation Resistance, ohms)					
	Before Overcoat	After Overcoat	After Erosion Test as-Overcoated	After Thermal Cycles	After Strain Cycles	After Post-Strain Erosion Test
0675aP-AO-NC	X	326 (54)	433 (54)	Open (53)	Open (60)	N.A.
b	X	96 (8)	N.A.	95 (11)	96 (14)	N.A.
0676a	X	179 (14)	N.A.	178 (116)	178 (119)	N.A.
b	X	32 (14)	34 (14)	51 (21)	51 (20)	N.A.
0668aP-SN-NC	330 (20M)	329 (20M)	329 (20M)	329 (20M)	329 (20M)	N.A.
b	310 (20M)	310 (20M)	310 (20M)	309 (20M)	310 (20M)	N.A.
1253aP-AO-NC	275 (20M)	315 (20M)	N.A.	318 (20M)	325 (20M)	357 (20M)
b	287 (20M)	276 (20M)	N.A.	273 (15M)	272 (16M)	N.A.
c	292 (2)	296 (2)	N.A.	287 (2)	288 (2)	N.A.
1259aG-SN-CN	X	254 (13)	364 (13)	*	N.A.	N.A.
b	X	123 (11)	N.A.	*	α	N.A.

Legend:

* Uncoated Lead Films Disintegrated.
α 50 percent of Overcoat Spalled in Gage Film Area.
X These Gages were Overcoated Before any Testing; Resistance Before Overcoating was not Measured.
N.A. Not Applicable.

Overcoat Adherence and Durability

The Si_3N_4 and Al_2O_3 overcoat films were adherent as sputtered on all four kinds of strain gage system. The overcoat films on ten of the eleven gages remained adherent, hard, and transparent throughout all subsequent testing. The one exception was the Si_3N_4 overcoat on one CuNi gage on Incoloy 901 (1259bG-SN-CN) which spalled and delaminated over 50 percent of the gage area during strain cycling at room temperature after surviving thermal cycling to 900K.

Resistance Stability and Durability of Overcoated Gages

The first kind of overcoated gage (0600P-AO-NC, four samples) displayed very low insulation resistance before overcoating, like many of the second-generation gages of this type. No significant change occurred as a result of overcoating and all subsequent testing, except for the small effects of the erosion testing to which two of these gages were exposed. (Erosion tests are described in detail in a later section.)

For the second and third gage types overcoated (0600P-SN-NC and 1200P-AO-NC) the gage resistance stability, insulation resistance stability, and durability were outstanding. Table XXVII shows that the thermal cycles and strain cycles produced no significant changes in the five samples of these gages tested. Erosion resistance was also excellent. (The details of erosion tests of coated and uncoated gages are presented and described in detail in a later section.)

The fourth kind of overcoated gage (1200G-SN-CN, two samples) also displayed very low insulation resistance before overcoating, like the first generation gage of this type. No significant change occurred as a result of overcoating. The effect of erosion testing of one of these gages was small. (Erosion test results are described in detail in a later section.) The thermal cycle tests of this gage type demonstrated dramatically the potential benefits of the Si_3N_4 overcoat, in that the uncoated CuNi lead films darkened and disintegrated completely at 900K (like all uncoated CuNi gages in the first-generation tests of Table XXIII), while the coated grid portion of CuNi gages retained a bright metallic luster throughout the thermal cycles to 900K. Finally, as mentioned previously, during strain cycling, the Si_3N_4 overcoat delaminated from 50 percent of the area of one CuNi gage.

All of these results are further reviewed later in Section 6.7, Final Candidate Systems, where the final scoring of all first-generation and second-generation gage systems is presented.

6.5 EROSION TESTS OF UNCOATED AND COATED GAGES

Six of the overcoated gages on blades (Table XXVII) and twelve uncoated gages on blades were erosion tested by the method described in Section 4.7. (The erosion was produced by a controlled high-speed stream of Al_2O_3 powder. Gage resistance is measured once every few seconds.)

The gage films tested, Table XXVIII, were NiCr and CuNi gages on several blade-substrate combinations, coated and uncoated, and one PtW gage on Si_3N_4, uncoated.

Plots of gage resistance versus time during erosion testing show a wide scatter in the behavior of uncoated gages (Figure 26), but excellent stability and durability for all overcoated gages (Figure 27).

The standard of comparison for erosion durability was the behavior of a $2\mu m$ platinum-10-percent-rhodium film sputtered on Al_2O_3 insulating film, produced by the method of Ref. 4, on a turbine blade of MAR-M-200 + Hf superalloy. This type of film routinely survives for at least 50 hours on rotating first-stage turbine blades in engine tests. The result of subjecting this reference film to the standard erosion test procedure is also shown in Figure 26. The electrical resistance of the reference film increased slowly and steadily during erosion testing, reaching 20 percent change in one minute.

TABLE XXVIII

EROSION TEST MATRIX AND RESULTS

Gage Material	Insulation Material	Uncoated Gage		Coated Gage	
		Gage Number	Resistance Change, 1st minute (Δ)	Gage Number	Resistance Change, 1st minute (Δ)
NiCr	Al_2O_3	0659bP-AO-NC	-57	0675aP-AO-NC	0
		0660bP-AO-NC	-100	0676bP-AO-NC	0
		1254aP-AO-NC	+4	1253aP-AO-NC	+3
		1252aP-AO-NC	+2		
	Si_3N_4	0670bP-SN-NC	+25	0668aP-SN-NC	0
		1221 P-SN-NC	+100	0668aP-SN-NC	0
CuNi	Al_2O_3	0672bP-AO-CN	-100		
	HfO_2	0627bP-HO-CN	+		
		0666aP-HO-CN	+		
		0666bP-HO-CN	+		
		0663aP-HO-CN	+		
	Si_3N_4			1259G-SN-CN	+1
PtW	Si_3N_4	1258bG-SN-PW	+		

Most of the uncoated gage films show poorer durability than the reference film (Figure 26). In fact, all of the uncoated CuNi films as well as the uncoated PtW film developed open circuits within the first nine seconds. Some of the uncoated NiCr films surprisingly developed very low resistance during the first 20 to 40 seconds. A few of the uncoated NiCr films showed a gradual increase in resistance with time, much like the reference film.

All of the overcoated gage films show much better durability than the reference film (Figure 27). In fact only one showed any significant gage resistance change during the first minute of testing, and the best performer (0600-SN-NC) showed no measurable resistance change after 33 minutes.

Typical post-erosion-test photographs in Figure 28 show the obvious damage inflicted on uncoated CuNi gages and the excellent condition of a NiCr gage overcoated with Si_3N_4.

Numerical results are summarized in the right-hand columns of Table XXVIII where the percent change in gage resistance in the first minute of erosion testing is listed. These numerical results are utilized later in Section 6.7, Final Candidate Systems, where the final scoring of gage systems is presented.
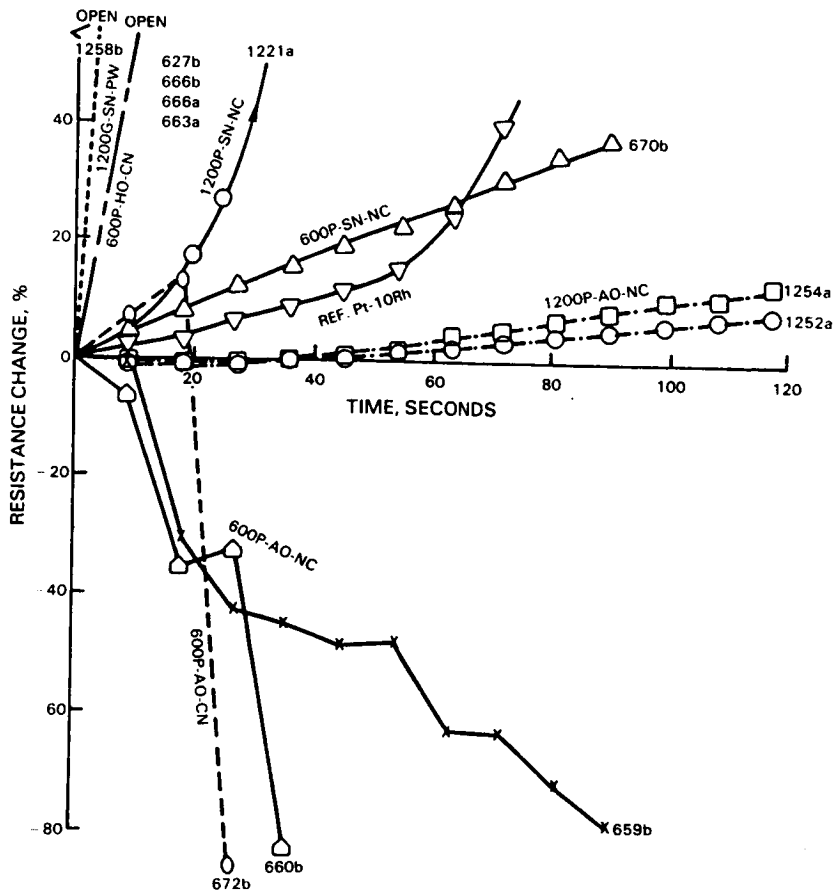
Figure 26 Erosion of Uncoated Thin-Film Strain Gages; Resistance Change versus Time.
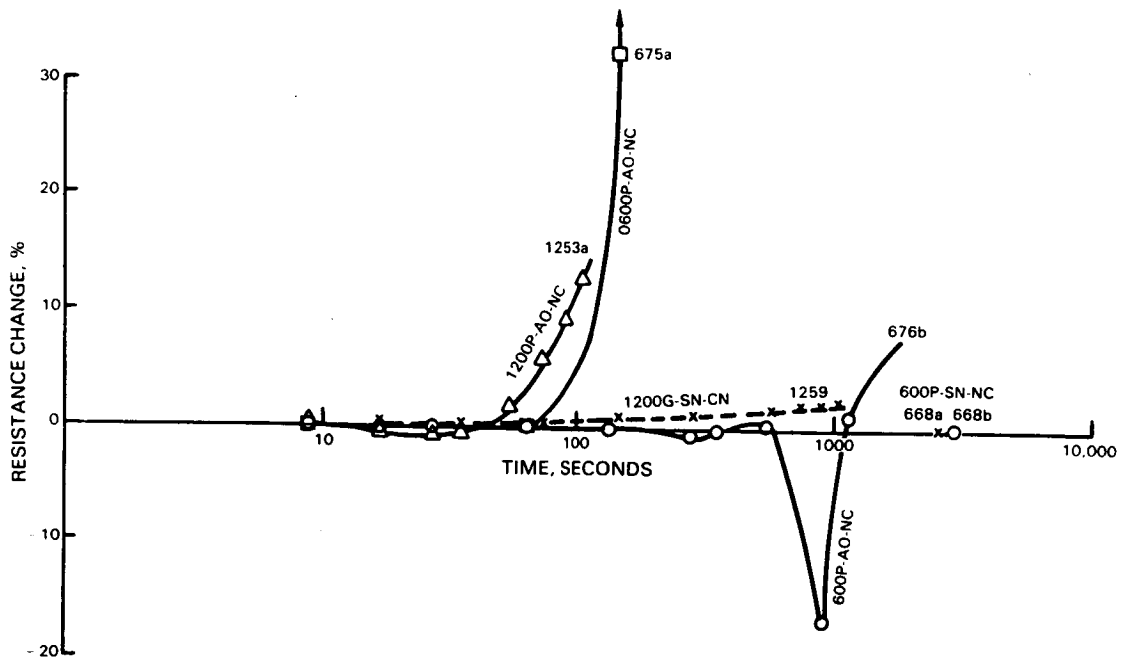
Figure 27 Erosion of Coated Thin-Film Strain Gages; Resistance Change versus Time.
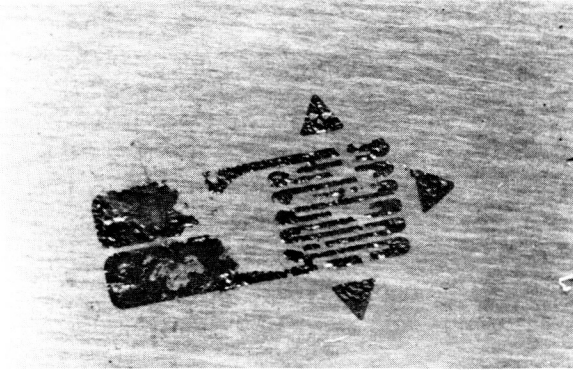
GAGE NO. 0666aP-HO-CN, UNCOATED
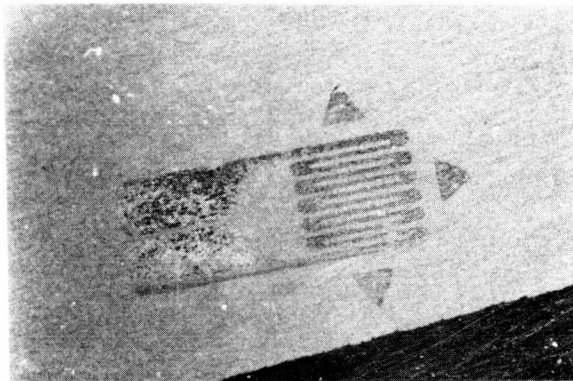
GAGE NO. 0663aP-HO-CN, UNCOATED
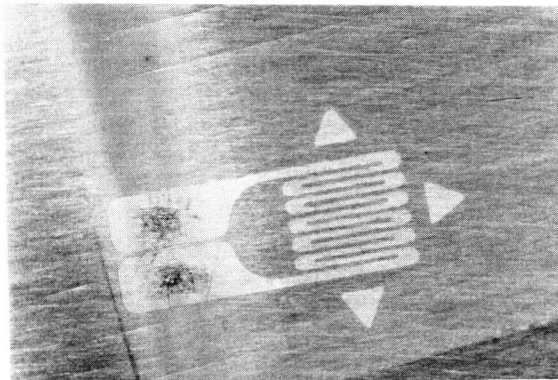
GAGE NO. 0668aP-SN-NC, OVERCOATED WITH Si_3N_4

Figure 28   Thin-Film Strain Gages after Erosion Testing.   The overcoated gage (bottom) is in excellent condition.

6.6 LEAD-WIRE CONNECTION RESULTS

Overview

A summary of results of trials of the eight methods described in Section 4.9 (and listed in Table X) for attachment of lead wires to lead films is presented below in Table XXIX.

Experiments with some of the lead-wire connection methods were conducted on some of the test bars in the Gage Program as well on the blades in the Components Program. The results described here include the work accomplished during the Gage Program on improvement in lead wire connections.

The table indicates that brush plating, resistance weld, and oven braze were generally unsuccessful and showed little promise; the fourth and fifth methods laser weld and ultrasonic weld were unsuccessful but showed considerable promise; and the other three methods (flame spray, hot compression bond, and conductive cements) produced best initial results although each has special limitations.

TABLE XXIX

LEAD-WIRE CONNECTION RESULTS

Method	Film Material	Film Thickness (m)	Lead-Wire Material	Lead-Wire Diameter (m)	Success Rate in Final Trials (%)	Potential for Future Development (%)	Remarks
Brush Plating	NiCr	1 to 2	Ni-10Cr Ni-20Cr	76+3	10	10	Plating achieved; bonding not achieved.
Oven Braze	NiCr	1 to 2	Ni-10Cr	76+3	0	10	Adherence poor and films buckled.
Flame Spray	NiCr	5	Ni-10Cr	127+3	30	60	Good bonds achieved; poor control (repeatability).
Resistance Weld	NiCr CuNi	1 to 5	Ni-10Cr	127+3	10	10	Bonding achieved, but gage films and insulating films damaged.
Laser Weld	PtRh	1 to 2	Pt-10Rh	76+3	0	70	Excellent bonding, but all samples shorted to ground.
Ultrasonic Weld	NiCr CuNi	1 to 2	Ni-10Cr	127+3	0	10	No bonding in air or argon.
	NiCr CuNi	5	Au	76+3	0	90	Gold sputtered on lead films. Gold-to-gold bonding good, but gold film delaminated later.
Hot Compression	NiCr	1 to 2	Ni-10Cr	76+3	0	0	No bond at 600K or 900K.
	CuNi	1 to 2	Cu-45Ni	76+3	0	0	No bond at 600K.
	PdMo	1 to 5	Pt	127+3	0	0	No bond at 600K.
	PtW	1 to 5	Pt	127+3	90	90	Excellent for PtW, 900K.
Conductive Cements:							
Ag Polyimide	NiCr CuNi	1 to 5	Ni-10Cr	76+3	70	10	Good at 600K, but cement crumbles and delaminates at 900K.
Ni Ceramic	NiCr CuNi	1 to 5	Ni-10Cr	76+3	70	70	Good at 900K. High-cycle fatigue life is marginal.

The conductive cement methods were adopted for use in the Gage Program. Further investigation of the laser weld and ultrasonic weld methods was recommended.

Results are summarized by method in the following paragraphs.

Brush Plating

Adherent metallic nickel plating was achieved on lead wires and lead films using the brush plating methods and materials described in Section 4.9. Optimum plating current range was 5 to 10 milliamperes. At the higher current levels, bubbling of the plating solution and delamination of lead films occurred. No bonding between the plated films and plated wires was achieved, after many trials of all parameters. The nickel plating growing at the lead film surface under the lead wire lifted the wire off the surface without producing bonding to the nickel plating on the wire.

Oven Braze

Some bonding was attained using the procedure described in Section 4.9 but, as noted in Table XXIX, the bonds were weak and the lead films were almost invariably damaged during the heating and cooling cycle in the presence of the braze material.

Problems associated with maintaining a clean surface without oxidation (even in the inert gas experiments), and controlling the braze material flow on this microscopic scale, were not overcome.

Flame Spray

The flame-spray technique described in 4.9 was successful in initial trials on 5 μm lead films. The photograph at right in Figure 29 shows that the flame-sprayed Ni-Al formed a fine-grained coating over the lead wire and film, bonding them firmly together. The lead film and underlying insulating film were not damaged. Bond strength exceeded wire strength. Later trials revealed that the technique is sensitive to minor variations in flame spray parameters, and operator technique. Success rate dwindled to about 30 percent. In the photograph at left in Figure 29, the flame-spray application was stopped when the lead film became shorted to ground, before the flame-spray layer was sufficiently complete to provide a reliable low-resistance bond.

Resistance Weld

Occasional good bonding was attained, but in these cases the underlying insulating layers were irreversibly damaged. Control and repeatability of the process at the required low energy levels (2 to 4 watt seconds) was poor. It is doubtful that further development effort in this area would be fruitful.
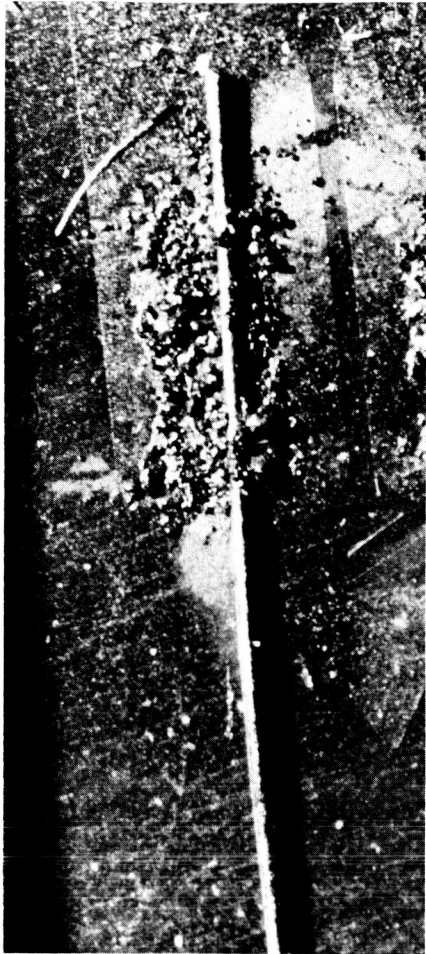
Figure 29 Flame-Spray Bonds of 76 μm Wires (Ni-10Cr) to 5 μm Films
(Ni-30Cr). A - Partially completed installation. B - Another
installation, completed.

Laser Weld

The demonstration welds performed by two vendors of sharp-focus low-energy
laser welders invariably resulted in irreversible damage to the underlying
Al_2O_3 insulation layers. One of the two laser systems, a YAG laser with
spot size as small as 15 μm diameter, repeatable energy output at low levels
(less than 1 joule), and precise positioning with an integral microscope,
produced excellent bonds on 2 μm lead films, (Figure 30) with pull strength
exceeding wire strength.

In the top two photographs in Figure 30, the lead wire was first flattened and then clamped to the film using a glass slide to maintain intimate contact. The laser beam was directed through the glass. The bond was excellent. There is evidence of glass remelt on the wire on either side of the weld.

In the bottom two photographs in Figure 30, the wire was first bent (and not flattened) and kept in contact through spring force of the wire. These bonds were also strong.

Further development of the laser technique is recommended, using thicker lead films and varying the geometry of the interface of film and wire to avoid damage to the underlying insulating film.

Ultrasonic Weld

Ultrasonic weld techniques are used in the electronics industry for bonding soft pure metal lead wires to lead pads of the same metal (typically gold to gold). Manufacturers of ultrasonic welding equipment provided detailed procedures which have proved successful for those applications. There is little information available on bonding of hard alloys such as NiCr and CuNi.

Several series of trials were conducted, under the present contract program, using an available ultrasonic welder described in Section 4.9, and special grooved electrodes to provide firm contact with the 76 μm lead wires and 127 μm lead wires.

In the first trials, welding of 127 μm Ni-10 percent Cr leads directly to the films was attempted, using a variety of combinations of electrode force and excitation power. No bonding was achieved, and at the higher forces the lead films and underlying insulation films were destroyed.

In a second set of trials, gold films 5 μm thick were first sputtered on the NiCr and CuNi lead films. Gold leads (76 μm) were ultrasonically welded to the gold films. The gold-to-gold bonding was excellent, but the gold films readily delaminated from the lead films after welding, either spontaneously or under very light normal pull force. Though success was not achieved in this series of trials, the technique appeared promising and further development, using other soft metal thick films, is recommended.

Hot Compression Bond

Excellent bonds of Pt wire to the 5 μm PtW lead films were achieved at 900K using the hot compression bond procedure described in Section 4.9 without damaging the underlying insulation layer. (With 1 to 2 μm PtW lead films, shorting sometimes occurred during hot compression bonding.) The procedure is nearly identical to that described in Reference 4 for platinum and platinum-10 percent rhodium wire-to-film bonds in sputtered thin film thermocouple systems used successfully in an engine hot section environment (1250K).
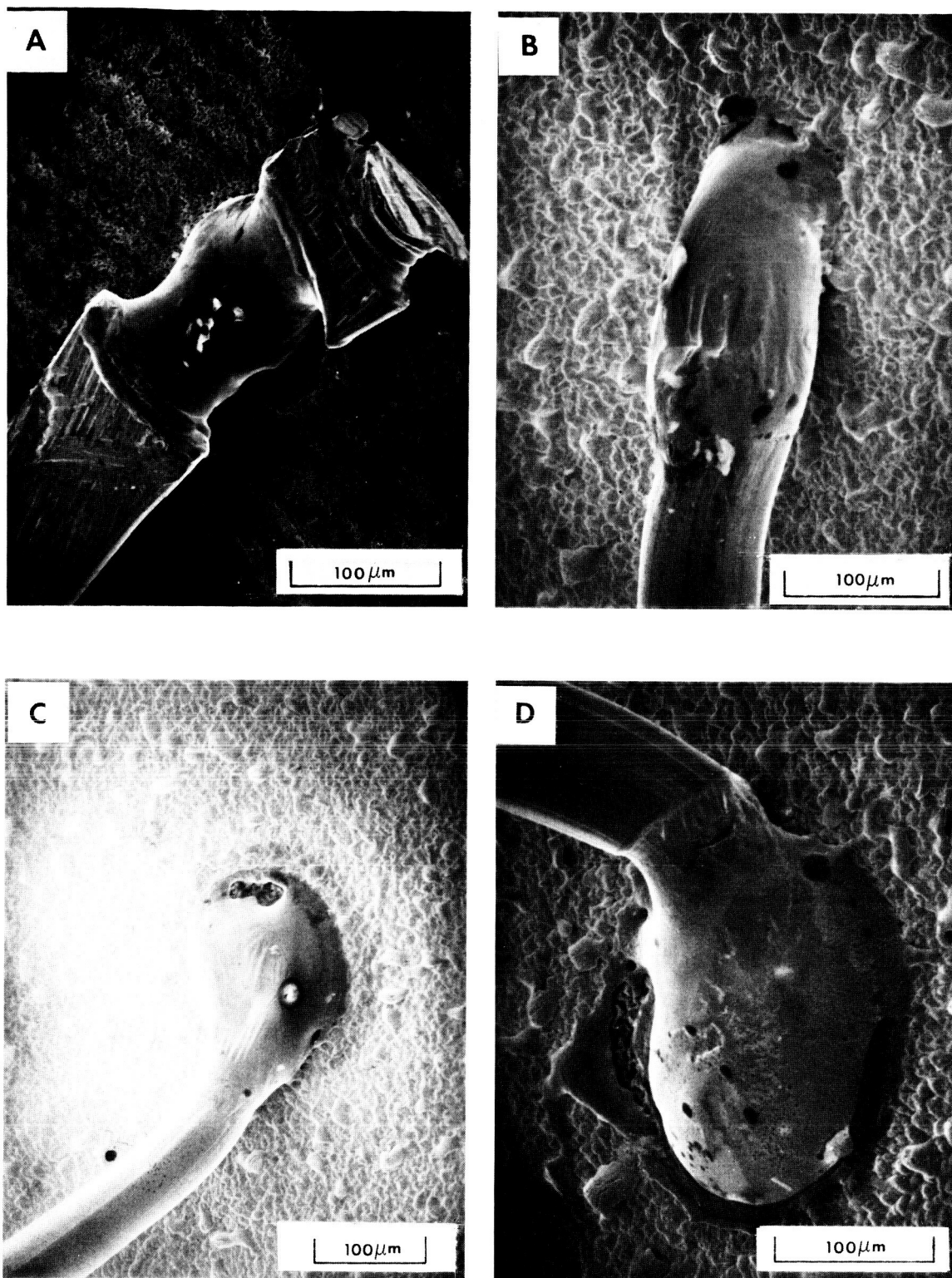
Figure 30 Laser Welds of 76 μm Wire (Pt-10Rh) to 2 μm Film (Pt-10Rh) on Al$_2$O$_3$ Insulating Film. A and B were clamped under a glass slide during welding. All bonds were strong, but the underlying Al$_2$O$_3$ films were damaged.

Weak bonds of 76 μm Ni-10Cr wire to 5 μm Ni-30Cr films were achieved by clamping for 24 hours at 980K. The bonds were too weak to support the weight of the 5 cm lengths of wire during normal handling. Figure 31 shows some film surface characteristics after the wire became debonded, including regions where no strong bonding occurred even though the clamping force was sufficient to leave an imprint of the wire in the film (Photo A) or even to crush the film (Photo B).

A   B
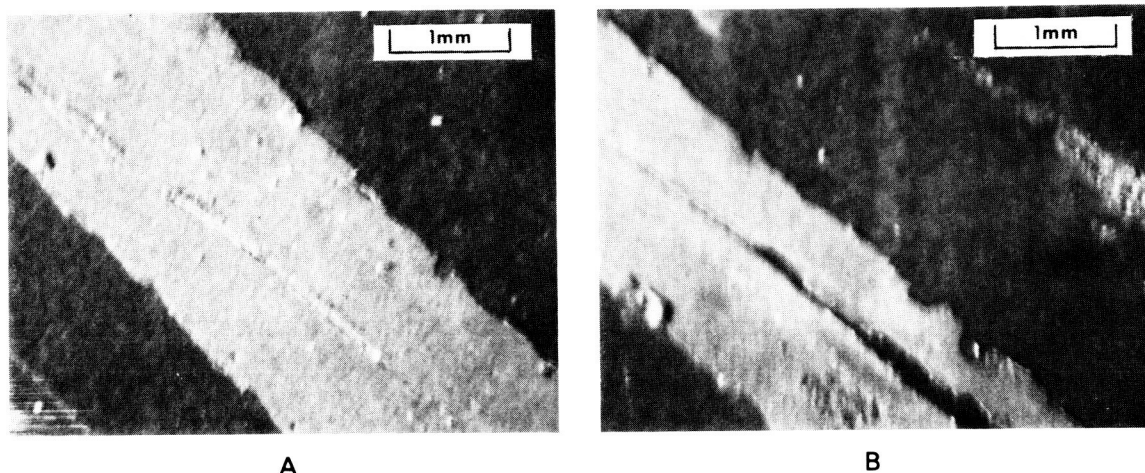
Figure 31   Surface of 5 μm Ni-30Cr Films After Attempts to Bond 76 μm Ni-10Cr Wires to the Films by Clamping for 24 hours at 980K. A - Shows an imprint of a wire. B - Shows crushing and delamination of a film in a region where a wire was clamped.

No success was achieved in several trials of hot compression bonding wire leads to CuNi, or PdMo lead films. This is not surprising since these materials, like NiCr, are hard and, in addition, the bonding temperature was necessarily limited to 600K to avoid oxidation of these materials. At this temperature the diffusion rate across the interface between wire and film was apparently two slow to produce significant bonding in a reasonable time.

Conductive Cements

The conductive cements provided a straightforward means for obtaining low-resistance electrical connections of good initial mechanical strength, with least risk of damage to lead films or underlying insulating films. The four cements and the cure cycles used are described in Section 4.9. The first (Walsco™ 36-1), a commercial product intended for room-temperature use only, crumbles and delaminates at high temperatures (after a few minutes at 600K, for example). It was used only for temporary connection of lead wires for room temperature testing. The second, third, and fourth were evolved

under the contract effort during both the Components Program and Gage Program. The second (Walsco plus ceramic thinner) provided some improvement in durability at 600K and was superseded by the third (silver powder in polyimide) which increased durability at 600K by an order of magnitude, surviving fatigue tests of 10^7 strain cycles at 600K in the Gage Program.

Figure 32 is a photograph of typical silver-filled-polyimide cement lead-wire connections used on the 600K test bars of the Gage Program.

None of the first three cement formulations proved to be durable at 900K. Discussion with vendors led to the fourth formulation, a nickel powder in a silicon-free ceramic thinner.

This fourth cement proved to have sufficient durability at higher temperatures to permit completion of fatigue tests at 900K (10^4 to 10^6 strain cycles between repairs), gage factor tests at 900K, and gage factor tests at 1090K. Because of the limited fatigue life at 900K, this lead wire connection, although the best available to date at 900K on NiCr, is not recommended for extended use in the engine environment.

6.7 FINAL CANDIDATE THIN-FILM STRAIN GAGE SYSTEMS

Scoring System

In order to select as objectively as possible the two best candidate systems for service to 600K on AMS 4928 blades and the two best candidates for service to 900K on Incoloy 901 blades, a numerical scoring procedure was used to evaluate the results of the Components Program Tests.

Each candidate system was scored on a scale from zero to one in the following five performance categories: adherence, insulation resistance, gage drift rate, apparent strain due to temperature, and erosion rate.

The product of the five scores was taken as the overall score. The range of overall scores was therefore also zero to one. (The product was taken in order to rule out candidates poor in any one category.)

To arrive at a numerical score, a performance variable and a normalizing scoring equation were defined for each category (Table XXX). In the last four of the categories the scoring equations are of exponential form. This form was chosen because the acceptable range of the performance variables in these categories could cover several orders of magnitude. The exponential rating equation results in a sharp reduction in rating (to below 0.37, or e^{-1}, where e is the base of natural logarithms) only if the value of the performance variable fell on the wrong side of a selected cutoff level, shown in the table. Specifically, the rating is below 0.37 if the insulation resistance was below 0.2 megohms, or drift in final hour of testing was more than 5 percent, or apparent strain was more than 200 ppm/K, or erosion rate in the standard erosion test was more than 20 percent in one minute. Performance three times better than the cutoff level produces a score of 0.75; ten times better, 0.90; and 100 times better, 0.99.
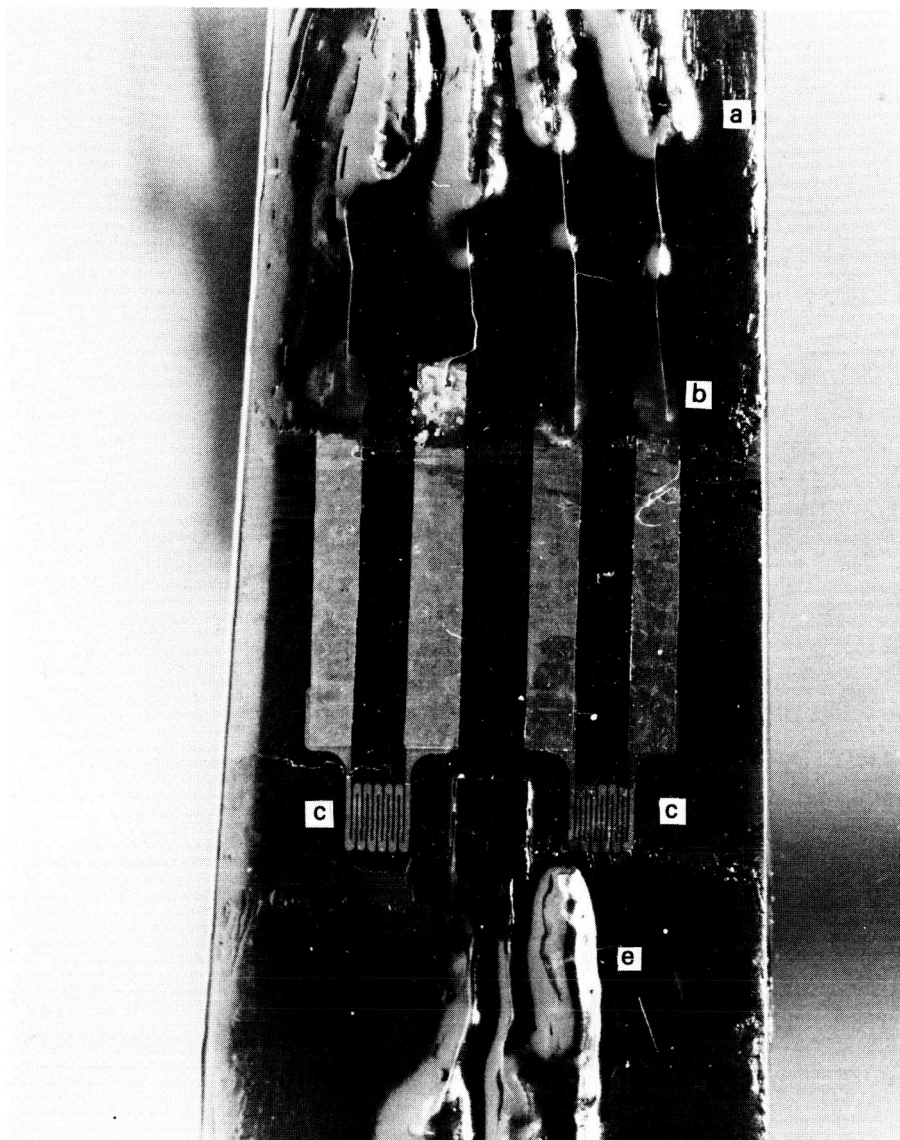
Figure 32   Thin Film Strain Gage Installation on AMS 4928 Bar 7.   Details shown include: a) - Connection of sheathed extension wire to 76 μm Ni-10Cr lead wire, b) - Connection of lead wire to 1.3 μm Ni-30Cr lead film, c) - Ni-30Cr thin film strain gages, d) low- temperature reference foil gage, and e) - reference thermocouple.   Sputtered insulation and overcoat is Si_3N_4. Photo No. 81C3373-002

TABLE XXX

SCORING SYSTEM FOR THIN-FILM STRAIN GAGES

Category	Performance Variable	Cutoff Value (for score = 0.37)	Score	Range of Score
Adherence	Ratio of the number satisfactory to the number tested.	0.37	$\dfrac{\text{Number Satisfactory}}{\text{Number Tested}}$	0 - 1
Insulation	R_I (megohms); the average value, for gages tested, of insulation resistance at room temperature after the final hour at service temperature.	0.2 megohms	$\exp(-0.2/R_I)$	0 - 1
Gage Drift	d (%); the average value, for gages tested, of the percent change in room temperature resistance due to the final hour of exposure at service. temperature.	5%	$\exp(-d/5)$	0 - 1
Apparent Strain	α/G (ppm/K); average value for gages tested.	200 ppm/K	$\exp(-\alpha/200G)$	0 - 1
Erosion	x (%); the average value, for gages tested, of percent resistance change in one minute in the standard erosion test.	20%	$\exp(-x/20)$	0 - 1
Overall			Product of Above Scores	0 - 1

Results

The test data, the scores in each performance category, and the overall scores are summarized in Table XXXI for the 20 candidate thin-film strain-gage systems not ruled out by the first-generation tests. The table summarizes data from the first-generation and second-generation gage tests of 73 gages of the 20 kinds. The final overall numerical score for each of the 20 gage types appears in the far right hand column of the table.

Since not every gage type was tested in every category of performance, some of the category scores in the table are estimated values (enclosed in brackets in the table). These estimated values are based on the results of tests of closely similar gage systems in the table. For example, it was assumed that all NiCr gages on AMS 4928 blades would have α/G of about 53 ppm/K at 600K, based on three samples tested.

Final Four Candidates

The two gage systems with highest overall scores in Table XXXI on each blade material were selected for further evaluation in the Gage Program portion of the contract effort, as follows:

Blade Material	Gage Type	Overcoat	Gage System Type
AMS 4928	0600P-SN-NC	SN	A
AMS 4928	0600P-HO-CN	HO	B
Incoloy 901	1200P-SN-NC	SN	C
Incoloy 901	1200P-AO-NC	AO	D

These four gage system types are henceforth designated A, B, C, and D respectively for brevity.

The two systems on Incoloy 901 (Types C and D) were forced choices since they were the only two with good overall scores on Incoloy 901. Both scored well in every category of performance as dynamic strain measuring systems to 900K. It is interesting to note that neither could be regarded as a good candidate as a static strain measuring system to 900K since the apparent strain in the NiCr gage material is undoubtedly cooling-rate dependent (see Figure 3 in Section 3.6.3 and see Reference 19).

The two final systems on AMS 4928 (Types A and B) were selected from the four with good overall scores on AMS 4928 in Table XXXI. The Type A system (0600P-SN-NC) scored much higher than all others and was a clear choice. The Type B system (0600P-HO-CN) tied for second place in scoring with 0600P-SN-CN, and both scored only slightly ahead of 0600P-HO-NC. The differences between these three were so small that the decision finally hinged on a desire to retain as many different gage materials and insulation materials as possible in the gage program. Selection of the Type B system provided an opportunity for further evaluation of the CuNi gage material and the HfO_2 insulation material, neither of which was present in the other three final candidate systems selected.

TABLE XXXI

TEST DATA AND SCORES FOR THE 20 ADHERENT AND DURABLE
CANDIDATE THIN-FILM STRAIN GAGE SYSTEMS

DATA | **SCORES (1.00 = Best)**

Remarks on First-Generation Strain Gage Performance	Strain Gage Type	Adherence** as Sputtered S	U	Adherence** after Stabilization S	U	Gage Resistance (ohms) as Sputtered	after Stabilization	Insulation Resistance (ohms) as Sputtered	after Stabilization R_I	at Service Temp.	Gage Drift (%) in Last Hour at Service Temperature Uncoated	Coated d	Gage Factor G	Apparent Strain (ppm/K) α/G	Erosion Rate (%) in 1 minute Uncoated	Coated P	Adherence (after Stabilization) S/(S+U)	Insulation Resistance exp. $-0.2/R_I$	Gage Drift (Coated) exp. $-d/5$	Apparent Strain exp. $-/200G$	Erosion Rate (Coated) exp. $-P/20$	Overall Score
Drifted Less Than 4% in Final Temperature Cycle.	*0621P-SN-NC	9	0	8	1	347 (7)	336 (7)	20M (9)	20M (9)	20M (3)	0.2 (8)	0 (2)	1.9 (3)	53 (3)	25 (1)	0 (2)	0.89 (9)	0.99 (9)	1.00 (2)	0.76 (3)	1.00 (2)	0.67[A] (9)
	*0627P-H0-CN	9	0	9	0	273 (8)	266 (7)	11M (9)	8M (9)	20M (2)	0.6 (8)	--	2.1 (1)	42 (1)	100 (4)	--	1.00 (9)	0.97 (9)	[0.94]	0.81 (1)	[0.75]	0.55[B] (9)
	0613P-H0-NC	1	0	1	0	862 (1)	815 (1)	20M (1)	20M (1)	--	0 (1)	--	--	--	--	--	1.00 (1)	0.99 (1)	[0.94]	[0.76]	[0.75]	0.53 (1)
	0622P-SN-CN	1	0	1	0	318 (1)	357 (1)	20M (1)	10M (1)	--	1.1 (1)	--	--	--	--	--	1.00 (1)	0.98 (1)	[0.94]	[0.81]	[0.75]	0.55 (1)
	0640G-SN-PW	1	0	1	0	1414 (1)	1468 (1)	20M (1)	20M (1)	--	0.3 (1)	--	--	--	--	--	1.00 (1)	0.99 (1)	[0.94]	0	[0.75]	0
	0636G-S0-PW	1	0	1	0	1406 (1)	1539 (1)	2M (1)	2M (1)	--	0.8 (1)	--	--	--	--	--	1.00 (1)	0.90 (1)	[0.94]	0	[0.75]	0
	0642P-SN-PM	1	0	1	0	956 (1)	1122 (1)	20M (1)	20M (1)	--	1.5 (1)	--	--	--	--	--	1.00 (1)	1.00 (1)	[0.94]	--	[0.75]	---
	0641G-SN-PM	1	0	1	0	1139 (1)	880 (1)	20M (1)	20M (1)	--	1.1 (1)	--	--	--	--	--	1.00 (1)	1.00 (1)	[0.94]	--	[0.75]	---
	0637G-S0-PM	1	0	1	0	1700 (1)	1185 (1)	20M (1)	20M (1)	--	3.2 (1)	--	--	--	--	--	1.00 (1)	1.00 (1)	[0.94]	--	[0.75]	---[C]
	1221P-SN-NC	1	0	1	0	745 (1)	735 (1)	20M (1)	20M (1)	--	0 (1)	--	--	--	100 (1)	--	1.00 (1)	0.99 (1)	[0.94]	[0.76]	[0.75]	0.53[C] (1)
	*1237G-SN-PW	3	10	3	10	739 (2)	339 (2)	10M (2)	1M (3)	229K (1)	1.4 (3)	0.3 (3)	1.8 (1)	1900 (1)	100 (1)	3 (1)	0.23 (13)	0.82 (13)	[0.94]	13	[0.75]	0.51[D] (13)
	*1209P-A0-NC	12	1	11	2	296 (10)	300 (1)	20M (13)	13M (13)	--	5.5 (11)	--	2.1 (2)	58 (1)	3 (2)	--	0.85 (13)	0.98 (13)	0.94 (3)	0.75 (1)	0.86 (1)	0.51[D] (13)
	1242G-SN-NC	1	0	1	0	1500 (1)	1460 (1)	20M (1)	40K (1)	--	0.2 (1)	--	--	--	--	--	1.00 (1)	0.01 (1)	[0.94]	[0.76]	[0.75]	0.01 (1)
Shorted During Temp. Cycles	*0609P-A0-NC	9	0	9	0	355 (8)	249 (8)	13M (9)	1K (9)	1K (2)	5.2 (5)	0.2 (2)	--	--	80 (2)	0 (2)	1.00 (9)	0 (9)	0.96 (2)	[0.76]	1.00 (2)	0 (9)
	0638G-SN-NC	1	0	1	0	1355 (1)	--	20M (1)	0 (1)	--	--	--	--	--	--	--	1.00 (1)	0 (1)	[0.94]	[0.76]	[0.75]	0 (1)
	1249G-H0-PW	1	0	1	0	842 (1)	--	20M (1)	0 (1)	--	--	--	--	--	--	--	1.00 (1)	0 (1)	[0.94]	0	---	0 (1)
Shorted as Sputtered	0633G-S0-NC	1	0	1	0	0 (1)	0 (1)	0 (1)	0 (1)	--	--	--	--	--	--	--	1.00 (1)	0 (1)	[0.94]	[0.76]	[0.75]	0 (1)
	*0610P-A0-CN	7	0	7	0	147 (5)	141 (5)	17M (7)	5K (6)	12M (1)	0.9 (4)	--	2.0 (1)	12 (1)	100 (2)	--	1.00 (7)	0 (6)	[0.94]	0.94 (1)	[0.75]	0 (7)
	0639G-SN-CN	1	0	1	0	0 (1)	0 (1)	0 (1)	0 (1)	--	--	--	--	--	--	1	1.00 (1)	0 (1)	[0.94]	[0.81]	0.95 (1)	0 (1)
	0635G-S0-CN	1	0	1	0	0 (1)	0 (1)	0 (1)	0 (1)	--	--	--	--	--	--	--	1.00 (1)	0 (1)	[0.94]	[0.81]	[0.75]	0 (1)

NOTES:
1. Where two numbers appear in a box, the number at the right is the quantity of gages tested.
2. * Indicates that second-generation gages also were fabricated and evaluated.
3. ** S indicates satisfactory adherence; U indicates unsatisfactory adherence.
4. A,B Indicates the two systems recommended on AMS 4928 blades to 600K.
5. C,D Indicates the two systems recommended on Incoloy 901 blades to 900K.
6. [α] Indicates estimated score based on applicable data from related gage types.
7. Drift rate and erosion rate of coated CN gages estimated from data from special gage 1259aG-SN-NC, not listed in this table.

2 FOLDOUT FRAME

1 FOLDOUT FRAME

SECTION 7.0

GAGE PROGRAM RESULTS

7.1 FABRICATION PROCESS MODIFICATION ON TEST BARS

Overview

In the Gage Program (conducted after completion of the Components Program), gage systems of the five types (A, B, C, D, E) were fabricated in pairs on flat test bars. The test bars were of three basic shapes suitable for gage factor tests and spin tests. The gages and the test bars are described in Section 5.0. As previously noted, gage types A, B, C, D are the types selected for compressor blades as a result of the Components Program testing (described in Section 6.0.) and gage Type E is the type designed for turbine blades.

The final fabrication procedures used in the Gage Program have already been described in Section 5.0. These final procedures differed in some significant details from the procedures used in the Components Program. The development of these modifications is described in this section.

The fabrication modifications stemmed partly from the different starting condition of the bar material compared with actual finished blades (requiring special polishing of the bars), and partly from the recognition of additional critical factors as a result of experience in fabricating large numbers of complete gage systems (particularly the effects of alkali attack on Al_2O_3, oxidation of metal surfaces during baking, and enhancement of adherence by sputter etching).

In the course of this further development of fabrication procedures, 84 fabrication trials (with two gages per trial on each test bar) were carried out on test bars in the Gage Program to achieve 43 acceptable thin film strain gages. The 43 strain gages included 33 tested at P&WA, and 10 delivered to NASA. Early in the Gage Program the fabrication success rate of gage Types A, B, C, and D on test bars was below 25%, with a high incidence of shorted and open gages. By the end of the program, the success rate of Types A and C gages had improved to better than 60%. The success rate for Type E was above 75% throughout the program.

The following acceptance criteria were established for gages fabricated on test bars. Gages meeting these criteria were accepted for use in the planned main test program, or for delivery to NASA:

o Reasonable gage resistance and insulation resistance as sputtered.
   (Detailed resistance values are presented in a later section).

o Electrical stability and absence of any significant indication of delamination or distress in the films during and after final overcoating, lead wire attachment by conductive cement, and a 5-hour bake at service temperature. (The bake was performed sometimes before and sometimes after lead wire attachment.)

There were some gages damaged in lead wire attachment trials using alternative techniques. These gages are not rated as either successes or failures according to the above criteria. In the tabulated results of all gages fabricated in the gage program, (discussed later in this section) they are listed in a special category, "durability undetermined", to indicate that no failure occurred during the fabrication process through and including overcoating and subsequent storage prior to special tests of lead wire attachment.

The fabrication history for each of the 84 pairs of trial gages is presented in Table XXXII.

The three columns at left in the table list bar number, bar shape, and trial run number on each bar. (Each trial run was an attempt to fabricate a pair of gages on a bar.)

The columns in the center of the table present notes on the fabrication procedure used in each of the five major steps in fabricating a pair of gages, as follows:

    o   Surface Preparation
    o   Insulating Film
    o   Gage Films and Lead Films
    o   Overcoat Films
    o   Lead Wire Attachment

Fabrication notes in the table indicate which of four different surface polishing procedures was employed, and where heat treatments (bakes), sputter etching, variation in insulation thickness, variation in lead film thickness, variation in photoresist stripping solvent, or variation in overcoat thickness were employed. Failure notes in the table indicate the failure modes during fabrication.

The right hand columns of table XXXII present the test matrix for the 43 gages completed and tested or shipped to NASA. The test results will be discussed in later sections.

In the balance of this section the modifications and results for each of the five major fabrication steps are discussed. Table XXXII is used as a guide throughout this discussion.

TABLE XXXII-A

GAGE PROGRAM HISTORY; TYPE A STRAIN GAGES

Bar, AMS 4928   Insulation, Si3N4   Gage, Ni-30Cr

Bar No.	Bar Shape	Trial No.	FABRICATION MATRIX					TEST MATRIX					
			Surface Preparation	Insulating Film	Gage and Lead Film	Overcoat Film	Lead Wire Attachment	Gage Factor	Thermal Cycle	Fatigue	Spin	Erosion	Ship to NASA
A2A	P	1	b e		1		o	X X	X X	X X		X	
A8A	P	1	b e		1		o	X X	X X	X X		X X	
A1	P	1	a e	j u									
		2	a	u									
		3	a e		1		o y w	X		X		X	
A2	P	1	a e	j u									
		2	a	u									
		3	a e		1 w								
A3	S	1	a e	j	1 w								
		2	b e		1 v								
		3	b		1		p w						
		4	d i		k		p v				X	X	
A4	S	1	a e	j	1 w								
		2	b e		1 v								
		3	b		1 v								
		4	b i		k		p					X X	
A5	N	1	b	j	1 v								
		2	b i		k v								
		3		i	v								
		4		i	v								
		5	d i		i i v								
		6	d i		1		p						X X
A6	N	1	b e	j	1 v								
		2	b i		k		p	X X					X X
A7	P	1	a e		1 m		t	X X					
A8	P	1	a e		1 m		t						

Fabrication Notes:

a - Shop polish
b - Hand polish
c - 600 grit polish
d - UTRC polish

e - 600K bake in air
f - 900K bake in air
g - 950K bake in vacuum
i - Sputter etched (where note i is omitted, bar was not sputter etched)

j - 4 m insulation thickness
k - Stripped in 50% alkali
l - Stripped in 75% acetone
m - 3 m lead film thickness

n - 1 m overcoat thickness
o - Baked before lead attachment
p - Baked after lead aattachment

Bar Shape Code:

P - P&WA
S - Spin
N - NASA

X - Column-head test conducted

Failure Code:

t - Durability undetermined
u - Bad insulating film
v - Gage adherence failure
w - Gage shorted

x - Bad overcoat
y - Overcoat spalled
z - Lead wire adherence failure

7-3

TABLE XXXII-B

GAGE PROGRAM HISTORY; TYPE B STRAIN GAGES

Bar, AMS 4928   Insulation, HfO_2 Gage, Cu-45Ni

Bar No.	Bar Shape	Trial No.	Surface Prepa-ration	Insu-lating Film	Gage and Lead Film	Over-coat Film	Lead Wire Attach-ment	Gage Factor	Ther-mal Cycle	Fatigue	Spin	Erosion	Ship to NASA
B16	P	1	a e	j	1		o w	X X	X X	X		X	
B15	P	1	a e	j	1		o v y						
		2	b e			n	o v y						
		3	b										
B12	S	1	b e										
B11	S	1	a e	j u									
		2	b e										
B10	P	1	a e	j	1 v								
		2	b e		1	n	o v y						
		3	b										
B9	P	1	a e	j	1 m	v y		Bar Broke During Fatigue Trial					
B8	P	1	a										

TABLE XXXII-C

GAGE PROGRAM HISTORY; TYPE C STRAIN GAGES

Bar, Incoloy 901   Insulation, Si_3N_4 Gage, Ni-30Cr

Bar No.	Bar Shape	Trial No.	Surface Prepa-ration	Insu-lating Film	Gage and Lead Film	Over-coat Film	Lead Wire Attach-ment	Gage Factor	Ther-mal Cycle	Fatigue	Spin	Erosion	Ship to NASA
C17	P	1	a f	j u	k m w								
		2	a e		1		o w						
		3	b e		1 v								
		4	b e		1		o w						
		5	b i		1		o	X X	X	X			
C18	P	1	a f	j	k m w								
		2	a e		1 w		o w						
		3	b e		1 v								
		4	b e		1		o w						
		5	b i		1		o	X X	X X	X			
C27	N	1	b i		k		o						X X
C28	N	1	b i		k		o y v						
		2	d i		k		p z						
		3					p 1						X X
C19	S	1	a f	j u									
		2	a e		1 w								
		3	b e		1		t						
		4	d i		k		p				X X	X X	
C20	S	1	a f	j u									
		2	a e		1 w								
		3	b e		1		p w						
		4	d i		1	v w						X	
C23	P	1	a e										
		2	b g										
		3	b i		1		p	X X					
C24	P	1	a e										
		2	b i		1		p	X X	X	X		X	
C26	S	8	d i		k		p w					X X	

7-4

TABLE XXXII-D

GAGE PROGRAM HISTORY; TYPE D STRAIN GAGES

Bar, Incoloy 901   Insulation, Al$_2$O$_3$ Gage, Ni-30Cr

Bar No.	Bar Shape	Trial No.	Surface Preparation	Insulating Film	Gage and Lead Film	Overcoat Film	Lead Wire Attachment	Gage Factor	Thermal Cycle	Fatigue	Spin	Erosion	Ship to NASA
D21	P	1	a f	u				X X					
		2	a e		l v								
		3	b e		l		o						
		4	b l		k	x v							
		5	b										
D22	P	1	a f	u									
		2	a e		l v								
		3	b e		l v		o t						
		4	b g										
		5	b l		k	x v							
		6	b										
D29	N	1	b		k w								
		2	b l		k v								
		3	b l										
		4	d l		i l		z t						
		5	d l		i l w								
		6	d l		l		i w						
D30	N	1	b		k w								
		2	b l		k v								
		3	d l										
		4	d l		i l		z t						
		5	d l		l		i w						
D25	S	1	b f	u									
		2	b e		l w								
		3	b e		l w								
		4	b e		k w								
		5	b l		k u v								
		6	b l		k u v								
		7	b l		k u v								
D26	S	1	a f	u									
		2	b e		l w								
		3	b e		k u w								
		4	b e	u									
		5	b l		k u v								
		6	b l		k u v								
		7	b l		k u v								
D31	P	1	d e		k		o v x	X X	X X	X X			
		2	c e	e g	k		p						
D32	P	1	d e		k		o v x						
		2	b e	e g	k w								

TABLE XXXII-E

GAGE PROGRAM HISTORY; TYPE E STRAIN GAGES

Bar, PWA 1422   Insulation, Al$_2$O$_3$ Gage, Ni-30Cr

Bar No.	Bar Shape	Trial No.		Insulating Film	Gage and Lead Film	Overcoat Film	Lead Wire Attachment	Gage Factor	Thermal Cycle	Fatigue	Spin	Erosion	Ship to NASA
E33	P	1			l		p	X X	X X	X X			
E34	N	1			k v								
		2			l		p						X X
E35	P	1											
E36	P	1			k		p	X* X*		X		X	

* Gage Factor Test Extended to 1100K

7-5

Surface Preparation

Baking

In early trials of gage fabrication it was found that a bake in air was required after final polishing and cleaning, to attain the desired surface cleanliness (water break test). It later became evident that

the 900K bake of Incoloy 901 bars after polishing resulted in poor insulation film structure (discoloration and poor adherence as sputtered due to formation of visible surface oxides during baking). Bars C19, C20, D21, D22, D25, and D26 are noted in the table are examples of this problem. A 900K bake in vacuum was no better (Bar C23, trial 2), still resulting in visible oxides. A 600K bake in air was finally found acceptable for all bars after thorough cleaning.

In cases where the same bar was later repolished to remove defective or damaged sputtered insulating films, it was usually found that the 600K bake need not be repeated. The bake was repeated only if the desired surface cleanliness (water break test) could not be re-established by thorough cleaning after repolishing. Table XXXII indicates where baking was repeated.

Polishing

In initial fabrication trials on test bars, the bar polishing procedure was the "shop polish" procedure using high speed cloth wheels as described in Section 4.3. This was the procedure which was successful in the Components Program on blades. This procedure is denoted by Note a in Table XXXII.

In many of these initial fabrication trials short circuits developed from gage to ground through the insulating layer. For example this behavior is noted in the table for early trials on Bars A1, A2, A3, A4, C17, C18, C19 and C20. Microscopic examination and profilmometer traces of the bar surfaces revealed two problems. First on both the Type A bars (AMS 4928) and Type C bars (Incoloy 901) the shop polish procedure failed to remove some of the deeper scratches and irregularities characteristic of the original condition of the bars after machining and grinding (and not characteristic of the blades in the Components Program). Second, on the Type C bars (Incoloy 901) a large number of 5 to 20 m inclusions and pits were observed. Materials experts identified the inclusions as titanium carbide particles normally to be expected in the Incoloy 901 material. The existence of the pits indicated that some of the carbide particles had fallen out during or after polishing. It was concluded that a more gradual polishing process was required on the bars, first to remove scratches and loose carbide particles and then to level the surface, avoiding protrusion of remaining hard carbide particles (which can protrude when the surrounding softer material is polished more rapidly than the hard inclusions) and avoiding sharp edges on pits where particles have departed. To this end two additional polishing procedures were explored, denoted by notes b and d in the table, as follows:

    b. "Hand polish", using an optical polishing facility, starting with 400 grit SiC and proceeding through 600 grit SiC, 3 micrometer SiC, and 0.3 micrometer Al2O3.

    d. "UTRC polish", using the Strasbauch polishing machine as described in Section 5.4.

Surface Preparation

Baking

In early trials of gage fabrication it was found that a bake in air was required after final polishing and cleaning, to attain the desired surface cleanliness (water break test). It later became evident that

the 900K bake of Incoloy 901 bars after polishing resulted in poor insulation film structure (discoloration and poor adherence as sputtered due to formation of visible surface oxides during baking). Bars C19, C20, D21, D22, D25, and D26 are noted in the table are examples of this problem. A 900K bake in vacuum was no better (Bar C23, trial 2), still resulting in visible oxides. A 600K bake in air was finally found acceptable for all bars after thorough cleaning.

In cases where the same bar was later repolished to remove defective or damaged sputtered insulating films, it was usually found that the 600K bake need not be repeated. The bake was repeated only if the <u>desired surface cleanliness water breaktest could not be re-established</u> by thorough cleaning after repolishing. Table XXXII indicates where baking was repeated.

Polishing

In initial fabrication trials on test bars, the bar polishing procedure was the "shop polish" procedure using high speed cloth wheels as described in Section 4.3. This was the procedure which was successful in the Components Program on blades. This procedure is denoted by Note a in Table XXXII.

In many of these initial fabrication trials short circuits developed from gage to ground through the insulating layer. For example this behavior is noted in the table for early trials on Bars A1, A2, A3, A4, C17, C18, C19 and C20. Microscopic examination and profilmometer traces of the bar surfaces revealed two problems. First on both the Type A bars (AMS 4928) and Type C bars (Incoloy 901) the shop polish procedure failed to remove some of the deeper scratches and irregularities characteristic of the original condition of the bars after machining and grinding (and not characteristic of the blades in the Components Program). Second, on the Type C bars (Incoloy 901) a large number of 5 to 20 m inclusions and pits were observed. Materials experts identified the inclusions as titanium carbide particles normally to be expected in the Incoloy 901 material. The existence of the pits indicated that some of the carbide particles had fallen out during or after polishing. It was concluded that a more gradual polishing process was required on the bars, first to remove scratches and loose carbide particles and then to level the surface, avoiding protrusion of remaining hard carbide particles (which can protrude when the surrounding softer material is polished more rapidly than the hard inclusions) and avoiding sharp edges on pits where particles have departed. To this end two additional polishing procedures were explored, denoted by notes b and d in the table, as follows:

b. "Hand polish", using an optical polishing facility, starting with 400 grit SiC and proceeding through 600 grit SiC, 3 micrometer SiC, and 0.3 micrometer Al2O3.

d. "UTRC polish", using the Strasbauch polishing machine as described in Section 5.4.

Either of these procedures greatly reduced the shorting problem, as noted in the table for later trials on bars A4, A6, C17, C18, C19, C20, C23, C24, C26. Procedure "d", requiring less hand work than "b", was adopted as standard by the end of the program.

After polishing, the test bars were cleaned using the cleaning procedure described in Section 4.3.

Sputter Etching and 600 Grit Roughening

After the problem of poor insulation structure as sputtered had been reduced by limiting preliminary baking to 600K, and the problem of shorts to ground has been reduced by improved polishing, then the next major problem to occur was poor long-term adherence of insulating films on the highly polished bar surfaces and poor adherence of gage and lead films on the smooth insulating films.

Example of this adherence problems noted in the table are Bars A4 (trial 3), A6, B9, B10, B15, C17 (trial 3), C18 (trial 3) and several of the Type D bar trials.

Two further modifications of the surface preparation procedure were then explored to produce a surface texture more conducive to film adherence. The two modification are noted in the table as follows:

    c. "600 grit polish", using the same procedure as the hand polish (b) but adding a final brief polish with 600 grit SiC. This finish was intermediate between the "polished" and "roughened" surfaces used on the blades in the Components Program.

    i. "Sputter etch", using the argon ion sputter etching procedure described in Section 5.4, after completion of polishing. The change in surface texture was not obvious to the naked eye but examination with an optical microscope showed sharper delineation of surface grain structure.

Each of these two procedures was successful in improving gage system adherence, as noted in the table for Bars D31 (trial 2) in the case of 600 grit polish, and Bars A3 (trial 4), A6, C18, C27, C28, D29, D30 (and others) in the case of the sputter etch procedure. The sputter etch was adopted as standard procedure by the end of the Gage Program on Type A, C and D gage systems.

Insulating Films

The insulating film fabrication procedure described in Section 5.4 was used throughout the Gage Program without modification, for all gage types, except for a few trials of thinner insulating films described here.

The trials were conducted at the start of the Gage Program. The sputtering time for some Type A, B, and C systems was shortened to produce 4.0 m insulating films rather than the standard 4.5 μm thickness finally adopted for these systems. Note j in Table XXXII identifies the trials of thinner insulating layers.

It was during these initial trials that a high incidence of short circuits from gage to ground occurred. All subsequent insulating films in Type A, B, and C systems were sputtered to the 4.5 μm thickness. The incidence of short circuits was not significantly reduced solely by increasing the insulation thickness, as noted in Table XXXII for bar A1 (trial 3), A2 (trial 3), C17 (trial 2), C18 (trial 2), C19 (trial 2) and C20 (trial 2). It is evident that significant reduction of short circuits was finally achieved only by a combination of increased insulation thickness and improved surface preparation procedures. It is possible that the thinner (4.0 μm) insulating film would have been adequate on the carefully polished and sputter etched test bar surfaces attained by the end of the program.

Gage Films and Lead Films

Three significant modifications to the fabrication procedure for gage films and lead films were explored during the Gage Program: elimination of alkali solvents in fabricating Type D and E systems, sputter etching of insulating films to improve gage film adherence, and fabrication of thicker lead films. Only the first modification was finally adopted as an improvement over the procedure used in the Components Program.

The first modification stemmed from the discovery of destructive attack on Al_2O_3 by the Shipley 1112A remover (mixed 1:1 with deionized water and heated to 80°C) often used for stripping of photoresist strain-gage masks. During the Components Program this solvent, a strong alkali, was used interchangeably with A.C. 3 grade acetone, a neutral solution, for photoresist stripping. As noted in Section 4.6 stripping time was highly variable with either solvent because the photoresist mask was covered with a sputtered film of strain gage alloy. After several trials at different points in the Components Program, it had been concluded that the two solvents were equally effective for bulk removal and either could be used depending upon availability. During the Gage Program a continuing series of difficulties in Type D gage system fabrication was encountered, centering on adherence failure of Al_2O_3 overcoats and underlying gages and insulating films, as noted in Table XXXII for Bars D21 (trial 4), D22 (trial 5), D25 (trials 5, 6, 7), and D26 (trials 3, 5, 6, 7). The difficulties were found to correlate with extended exposure of the Al_2O_3 to the alkali remover during gage mask stripping. Review of the literature revealed that Al_2O_3 could readily be attacked by acids and alkalis. The following alkali reaction used in decomposing the Al_2O_3 in refining of aluminum from bauxite ore is one such common reaction:

$$Al_2O_3 + 2OH + H_2O \longrightarrow 2Al(OH)_4 (H_2O)_2$$
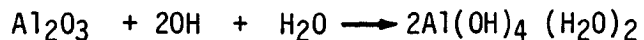
Use of the alkali solvent for photoresist removal on Al_2O_3 surfaces (Type D and E systems) was thereafter limited to a brief dip in a 10% solution to remove the last traces of photoresist after prolonged cleaning in acetone. The final procedure is described in Section 5.4. Examples of excellent results in Table XXXII using this final procedure are Bars D29, D30, E33, and E34. The literature indicates that Si_3N_4 and HfO_2 do not readily react with alkalis and acids. There was no evidence of attack by the alkali solvent on Type A, B and C systems.

The second modification in gage film fabrication explored was sputter etching of insulating film surfaces to improve adherence of gage films. It was eventually concluded that the procedure was not generally useful. Sputter etching of the polished bar surface before sputtering of insulating layers had previously been proven beneficial in promoting adherence of both the insulating film and the gage film, but sputter etching of the insulating films did not further enhance the adherence of the gage films. The procedure used was the argon-ion sputter etching procedure described in Section 5.4. On several occasions, when the routine masking and sputtering of gages resulted in incomplete or poorly adherent gages, the gages were removed by light grit blasting followed by sputter etching to clean the surface. A second masking and sputtering then sometimes resulted in acceptable (and adherent) gages. These operations are not reported as a separate trials in Table XXXII since the rework involved was minor and usually did not affect the outcome. In one case, (Bar A5, trials 3 and 4) controlled experiments of sputter etching of the insulating film were conducted. In trial 2 on this bar, the sputtered gages had been electrically acceptable, but some blistering of gage films and lead films was observed. It was decided to resputter the gages on the same Si_3N_4 insulation layer.

First most of the existing gage and film material was removed using HCl. Then the surface was sputter etched for 30 minutes. No trace of gage material remained and probing showed 20 megohms resistance to ground everywhere. Next 0.2 μm of new Si_3N_4 was sputtered on the Si_3N_4 surface. The surface was then masked for new gages, cleaned, and sputter etched for 5 minutes. The new gages were then sputtered (bar A5, trial 3). When the photoresist mask was removed, both gages delaminated from the surface. After cleaning, the bar was sputter etched for an additional fifteen minutes, remasked, and sputtered with strain gages (bar A5, trial 4). The strain gage material was again not adherent. There was no evidence that sputter etching of the hard insulating film at this stage of fabrication improved adherence. Sputter etching of the insulation film surface was therefore not incorporated as a standard procedure for any of the five gage types.

The third modification explored was sputtering of lead films much thicker (3.0 μm) than the gage grid films (1.2 μm) to reduce further the lead film resistance. The technique tried was not successful and the final procedure was to mask and sputter gage films and lead films simultaneously, of the same material and thickness. (The 1.5 mm width and 7 mm maximum length of the lead film, Figure 11, resulted in lead film resistance below 3% of gage resistance). The trials of thicker lead films are indicated by Note m in Table XXXII. Examples are Bars A7, A8, B9, C17 (trial 1), and C18 (trial 1). The procedure in the trials of thicker films was to remove the bar from the sputtering chamber after sputtering the gage film and lead film to the 1.2 μm standard thickness, strip the photoresist mask from the surface, apply a new photoresist mask over the entire bar surface except for the lead films (leaving the lead films bare), reinstall in the sputtering chamber, and oversputter with the gage alloy to the 3.0 μm thickness. In every case, the extra layer of gage alloy proved poorly adherent to the original layer of gage alloy, despite great care in cleaning between masking operations. Delamination occurred sometimes

spontaneously upon removal from the sputtering chamber, sometimes during photoresist removal, and sometimes later after storage. The failure of adherence of added lead film material was not explained and remains puzzling. The adherence of later overcoats of insulating layer materials on the gages was generally excellent, indicating that general surface contamination was not the problem.

Overcoat Films

The only modification explored in overcoat film fabrication was a trial of a much thinner overcoat film (1.0 μm) than the standard 3.0 μm thickness adopted for the Gage Program. The trial was conducted on two test bars (B10 and B15, note n in Table XXXII). The objective was to determine whether reducing the overcoat thickness would enhance adherence by reducing interface shear stresses generated by mismatch of coefficients of thermal expansion between bar material and insulation plus overcoat material. The result was negative. The thinner overcoat and underlying insulation spalled from both bars. The standard overcoat thickness of 3.0 μm, chosen for erosion and corrosion protection, was utilized on all other gages fabricated in the Gage Program. The spalling on Type B bars continured to be a problem throughout the program and was never solved.

Lead Wire Attachment

The conductive cements described in Section 5.4 (silver-filled polyimide cement for Type A and B gages, nickel-filled ceramic cement for Type C, D, and E gages) were used in attaching lead wires to all Gage Program gages which were finally accepted for static testing, spin testing, erosion testing, and delivery to NASA.

On some other spare test bars alternative techniques were explored. The results of lead wire attachment trials by all techniques explored in the Gage Program and Components Program were presented in Section 6.6, and will not be reviewed in detail here.

Two important details in the surface preparation for conductive cement installations which were explored are worthy of special mention here and are noted in Table XXXII: the deleterious effect of baking before lead wire attachment and the beneficial effect of sputter etching the lead film before lead wire attachment. These details are discussed in the next two paragraphs.

In early fabrication trials of Type A, B, C and D gages, the overcoated gages were baked (before installing lead wires) in air for one hour at service temperature (600K for AMS 4928, 900K for Incoloy 901) as a gage system stability test. Note o in the Table identifies these trials. Bars A1, B16, C17, D21 are examples. The baking produced visible oxidation of the exposed lead films (but not the overcoated gage grids). To achieve good adherence of the conductive cements it was then found necessary to scrape or abrade the oxide from the lead films. The scraping often resulted in damage to the lead films or insulating films. The bake before lead wire wire attachment was therefore eliminated from the procedure.

Late in the program, the improvement in surface finish of the bars by better polishing (already discussed) resulted in poorer adherence of the conductive cements to the lead films during lead wire attachment. A 15 minute sputter etch of the lead films (Note i in the lead wire attachment column in Table XXXII) was found to completely eliminate this problem and was incorporated in the standard procedure on the highly polished Type A, C and D bars. Bars A5, C28, D29 and D30 are examples in the table.

7.2 FABRICATION SUCCESS ON TEST BARS BY GAGE TYPE

A summary of the effect of the most critical improvements in fabrication procedures (bar surface preparation and elimination of alkali solvents) on fabrication success for all 84 pairs of gages in the Gage Program is presented in Table XXXIII. The table lists the number of open, shorted, and accepted gages for each of the five gage types (A, B, C, D, E), and within each gage type for each surface preparation method (a, b, c, d, and special NiCoCrAlY method of Reference 4). A further breakdown of Type D gage results for each of the two photoresist stripping methods (alkali and acetone) is also presented in this table.

The results for Type A and C gages, in Table XXXIII, show that the improved surface preparation procedures alone increased the fabrication success rate from below 25 percent to above 62 percent.

The results for Type D gages in the table show that the improved surface preparation plus the acetone photoresist stripping method eliminated all adherence problems. The fabrication success remained poor due to problems with electrical leakage to ground which appeared during or after lead wire attachment using the conductive ceramic cement. This problem was not overcome.

The results for Type B gages show that success rate remained below 25 percent with either shop polished or hand polished bars. Fabrication of Type B gages on bars was discontinued relatively early in the Gage Program after repeated occurrences of spalling of overcoats, underlying gage systems, and insulating films from the bar surface (discussed earlier in the section on overcoats). The severity of the problem made it unlikely that the 600 grit polish or the sputter etching procedure would have resulted in as high a success rate for Type B as for Types A, C, and D.

The success rate for Type E gages was excellent from the start, as shown in Tables XXXII and XXXIII. Four of six gages were successful on first trials (Bars E33, E34, E36) and two of two were successful on a second trial (E34). The special NiCoCrAlY surface preparation procedure of Reference 4 for turbine blade thin film thermocouples required no modification for Type E thin film strain gage fabrication.

-TABLE XXXIII

EFFECT OF IMPROVED PROCEDURES ON GAGE FABRICATION SUCCESS

Gage Type	Notes	a Shop Polish					b Hand Polish					c 600 Grit Polish					d UTRC Polish Plus Sputter Etch					Special NiCoCrAlY Surface					Total					
		No. t	No. v	No. w	No. OK	Yield	No. t	No. v	No. w	No. OK	Yield	No. t	No. v	No. w	No. OK	Yield	No. t	No. v	No. w	No. OK	Yield	No. t	No. v	No. w	No. OK	Yield	No. t	No. v	No. w	No. OK	No. Total	Yield
A		4	0	8	0	0	0	16	3	7	0.27						0	2	0	4	0.67						4	18	11	11	44	0.28
B		0	6	1	1	0.12	0	4	0	0	0																0	10	1	1	12	0.08
C		0	0	12	0	0	2	6	6	10	0.45						0	1	2	5	0.62						2	7	20	15	44	0.36
D	k						0	20	10	0	0	0	0	0	2	1.00	0	4	0	0	0						0	24	10	2	36	0.06
D	1	0	4	0	0	0	1	1	6	2	0.22						4	0	6	0	0						5	5	12	2	24	0.10
E																						0	2	0	6	0.75	0	2	0	6	8	0.75
All		4	10	21	1	0.03	3	47	25	19	0.21	0	0	0	2	1.00	4	7	8	9	0.38	0	2	0	6	0.75	11	66	54	37	168	0.24

Notes:

t = Durability undetermined

v = Gage adherence failed (open)

w = Gage shorted

OK = Gage accepted for gage factor testing

Yield = Ratio of number of gages accepted to number fabricated (omitting gages rated "t")

k = Photoresist stripped in alkali

1 = Photoresist stripped in acetone

Rev. Dec. 1983

7-13

7.3 GAGE RESISTANCE AND INSULATION RESISTANCE

Overview

As indicated in Section 7.1, among the conditions for acceptance of thin film strain gages during fabrication was reasonable gage resistance and reasonable insulation resistance. In this section, gage resistances and insulation resistances measured during fabrication are presented, the acceptance criteria are described, and the resistance trends are analyzed versus gage type and bar surface finish.

The criteria for acceptable gage and insulation resistances as sputtered were not immediately obvious and are discussed here before presentation of fabrication results.

Gage Resistance Acceptance Criteria

Two factors contributed to uncertainty in predicting gage resistance. First, it was known from the results of the Components Program that gage resistance would be sensitive to surface roughness. For example, in Section 6.2, Table XXIII, note that the resistance of gages on the standard roughened surface was about twice the resistance of gages on the standard polished surface, for the same gage thickness. Second, it was observed in the Components Program that gage resistance decreased much more rapidly than the inverse first power of thickness in the range 0.6 to 1.0 m used, indicating a decrease in resistivity with increased thickness. Since 0.6 m thickness corresponds to many thousands of atomic diameters, variation in resistivity with thickness was not expected. Variation with thickness would be expected for films of less than one thousand atomic diameters thickness (Reference 7).

Taking these factors into account, the predicted gage resistance on polished bar surfaces for the 1.2 μm gage thickness selected for the gage program was about 350 ohms for Ni-30Cr gages and 220 ohms for Cu-45Ni gages. The actual resistances of the 1.2 μm thickness gages sputtered on the polished test bars were about half these values. There were no indication of short circuits (resistances to ground were in the megohm range and the grid patterns were clearly defined, with no indication of shorted grid elements). Composition and thickness were rechecked and found unchanged within measurement tolerances. The lower value of resistance was therefore accepted and an upper limit three times higher (to account for roughness effects) was selected. The resulting acceptance resistance ranges were:

> Ni-30Cr: 150 to 450 ohms
> Cu-45Ni: 90 to 270 ohms

It will be seen later that all gages fabricated on test bars fell within these limits.

Insulation Resistance Acceptance Criteria

If there are leakage paths through the insulating film from the strain gage or lead film to the blade material then the strain measurement can be affected in two ways. First, if there is only one leakage path the indicated strain may be altered by a ground loop current flowing through lead work and a portion of the film system. Second, if there is more than one leakage path the indicated strain level can be further altered due to shunting of the gage.

The first possible effect was eliminated in the present program by using a floating-bridge circuit rather than a grounded-bridge circuit. A grounded-bridge circuit is one in which one side of the power supply is connected indirectly (for example, via the earth and the test rig) to the blade material. In a grounded-bridge circuit, the largest error occurs if a low insulation resistance develops from gage to blade material at the end of the gage which is farthest from the power supply ground. The result may be a d.c. bias plus a 60 Hertz (power line frequency) a.c. noise signal superimposed on the strain gage output.

Eliminating the second effect required limiting the number of leakage paths (or pin holes) to a maximum of one by attaining high resistance to ground everywhere else under the gage film and lead films. The situation is best described by examining the equivalent circuit for the strain gage and insulation shown in Figure 33. The quantities R, U, and T in the figure are, respectively, the three measured resistances (ohms) indicated by an ohmmeter connected as follows: 1) across the gage, 2) from one lead film to the blade material, and 3) from the other lead film to the blade material. The quantities a, b, and c in Figure 1 are, respectively, the effective resistance (ohms) of the gage itself and the effective resistances from the gage to the blade material represented by two lumped resistances, one from each end of the gage. The measured resistances R, U, and T are smaller than the corresponding effective resistances a, b and c because of shunting effects of b or c.

The rules of series and parallel lumped resistances yield Equations (1), (2), (3), and (4) in Figure 33, relating a, b, and c to R, U, and T.

In a dynamic strain gage circuit, the effect of the shunting is to reduce the gage factor by 1-0.5 (1-R/a), where, from Figure 33,

$$\frac{R}{a} = \frac{b/a + c/a}{1 + b/a + c/a}$$

It follows that there is less than a 5 percent change in indicated dynamic strain (R/a > 0.9) so long as the sum of the ratios b/a and c/a is above 9. On the basis that a 5 percent effect is marginally acceptable, and that much smaller effects (0.5 or 0.05 percent) are more desirable, the following rating scale was established for acceptability of insulation resistance in the completed strain gage systems on the test bars:

b/a + c/a	R/a	Insulating Rating
≥ 999	0.999 ≤ R/a ≤ 1.000	Good
≥ 99	0.990 ≤ R/a < 0.999	Fair
≥ 9	0.900 ≤ R/a < 0.990	Marginal
≤ 9	0.000 ≤ R/a < 0.900	Bad (unacceptable)

GAGE

BLADE
SURFACE
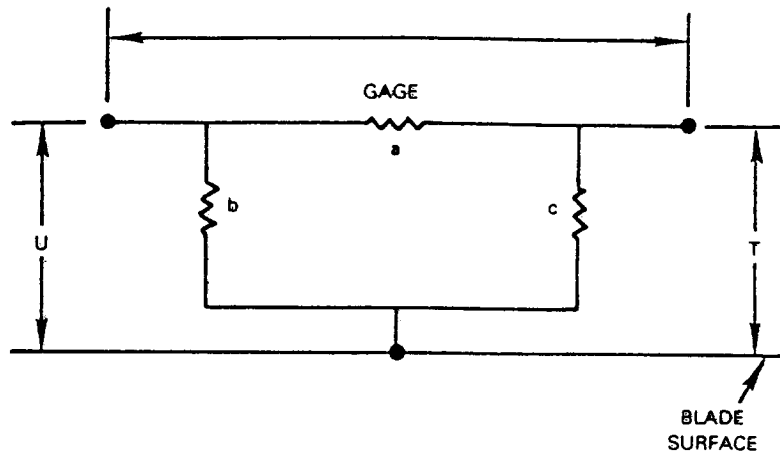
R,U, AND T ARE MEASURED RESISTANCES (OHMS). $T \geq U$. $T - U \leq R$.
a, b, AND c ARE EQUIVALENT LUMPED RESISTANCES (OHMS)

GIVEN R,U, AND T, THEN:

$$\frac{b}{a} = \frac{T + U - R}{R + T - U} \quad \text{(EQ. 1)} \qquad \frac{c}{a} = \frac{T + U - R}{R + U - T} \quad \text{(EQ. 2)}$$

AND

$$\frac{b}{a} + \frac{c}{a} = 2\frac{[(T+U)/R] - 1}{1-[(T-U)/R]^2} \quad \text{(EQ. 3)}$$

AND

$$\frac{R}{a} = \frac{b/a + c/a}{1 + b/a + c/a} \quad \text{(EQ.4)}$$

$\frac{b}{a} + \frac{c}{a}$	INSULATION RATING
> 999	GOOD
≤ 999 but > 99	FAIR
≤ 99 but > 9	MARGINAL
≤ 9	BAD (UNACCEPTABLE)

NOTE: If T = U, THEN $\frac{b}{a} + \frac{c}{a} = 4\frac{T}{R} - 2$

Figure 33   Strain Gage Equivalent Circuit and Resistance Equations.

The equivalent circuit in Figure 33 is a useful description of the strain gage and insulation system. If the insulation resistance is uniform or symmetrically nonuniform, then b = c and U = T. If the insulation is asymmetrically nonuniform, with one or more pin-holes or low-resistance paths from gage to blade, then b /≠c and U /≠T. In either case, a large value of the sum of the ratios b/a and c/a implies good insulation of the strain gage. Note that a low resistance measured from one end of the gage to the blade material is acceptable provided that the sum of the ratios b/a and c/a is large (i.e., that the resistance measured from the other end of the gage to the blade is nearly equal to the sum of resistance measured across the gage and the resistance measured from the first end to the blade).

Resistances in Fabricated Gage Systems

Table XXXIV presents measurements of the gage resistance and the insulation resistance to ground from each lead film in the as-sputtered condition immediately after removing the photoresist masking material. In addition, the table presents a second set of resistance measurements. Where appropriate, the second set is for the completed gage (after overcoating, lead-wire attachment, and 5-hour bake at service temperature). The table includes all gages which were acceptable as sputtered.

In cases where overcoating or lead wire attachment or baking were not completed, the second set is the resistances measured for the final status noted in the table. Gages not completed include those which failed or were damaged in trials of overcoating or lead wire attachment or baking even though acceptable as sputtered. The data of Table XXXIV are discussed in the balance of this section.

Gage Resistance as Sputtered

A statistical summary of the gage resistance as sputtered, from Table XXXIV, is presented in Table XXXV. For each gage type (A, B, C, D, E), average gage resistance $\bar{R}$ (ohms), standard deviation of gage resistance σ_n (percent), and number n of samples in the population are listed. In addition, for Types A, C, and D the statistics for the subset of gages which were fabricated on sputter-etched bar surfaces which had been prepared using the best polishing procedure is also presented (notes d, i in the table).

In discussing these results, it can first be observed in Table XXXV that the gage resistance behavior patterns fall into three distinct classes:

o   Nickel-chrome gages on polished bars (A, C, D)
o   Nickel-chrome gages on the specially finished turbine-blade material bars (E).
o   Copper-nickel gages on polished bars (B).

TABLE XXXIV-A

RESISTANCE MEASUREMENTS DURING FABRICATION
20 TYPE A STRAIN GAGES

Bar, AMS 4928   Insulation, Si_3N_4 Gage, Ni-30Cr

Bar No. and Gage No.	Bar Shape	Trial No. and Surface Finish	AS SPUTTERED				COMPLETED (5)				Remarks (5)
			R (Ohms) (1)	U (Ohms) (2)	T (Ohms) (3)	Insulation Rating (4)	R (Ohms) (1)	U (Ohms) (2)	T (Ohms) (3)	Insulation Rating (4)	
A2A-1	P	1 b	196	20M	20M	Good	191	20M	20M	Good	(6)
-2			192	20M	20M	Good	193	20M	20M	Good	(6)
A8A-1	P	1 b	190	20M	20M	Good	188	20M	20M	Good	(6)
-2			190	20M	20M	Good	185	20M	20M	Good	(6)
A1-1	P	3 a	171	20M	20M	Good	177	20M	20M	Good	(6)
-2			176	20M	20M	Good	24	13	12	Bad	(7)
A3-1	S	3 b	179	1.8M	1.8M	Good	178	470K	470K	Good	(8)
-2			169	.9M	.9M	Good	170	290K	290K	Good	(8)
A3-1	S	4 di	239	20M	20M	Good	240	10M	10M	Good	(6)
-2			234	20M	20M	Good	Open	20M	20M	Good	(9)
A4-1	S	4 bi	282	20M	20M	Good	284	6	284	Bad	(10)(11)
-2			256	20M	20M	Good	255	20M	20M	Good	(6)
A5-1	N	6 di	280	20M	20M	Good	282	20M	20M	Good	(6)
-2			274	20M	20M	Good	275	20M	20M	Good	(6)
A6-1	N	2 bi	247	20M	20M	Good	266	20M	20M	Good	(6)
-2			263	20M	20M	Good	290	20M	20M	Good	(6)
A7-1	P	1 a	236	20M	20M	Good	225	20M	20M	Good	(12)(13)
-2			238	20M	20M	Good	229	20M	20M	Good	(12)(13)
A8-1	P	1 a	238	20M	20M	Good	229	20M	20M	Good	(12)(13)
-2			241	20M	20M	Good	236	20M	20M	Good	(12)(13)

Notes:

(1) R = Gage resistance (Ohms)
(2) U = One lead film to ground (Ohms)
(3) T = Other lead film to ground (Ohms)
(4) Rating method is described in text
(5) After overcoating, lead wire attachment, and 5-hour bake at service temperature, unless otherwise noted.
(6) Gage accepted
(7) Overcoat spalled
(8) Shorted on spin disk
(9) Open
(10) Shorted
(11) Erosion tested
(12) Final R, U, T reported are after overcoat, before, bake or lead wire att.
(13) Gages damaged during lead wire trials.
(14) The overcoat, gage, and insulation film spalled after bake and storage, before lead wire attachment.
(15) Gage spalled
(16) Final R, U, T reported are after thick lead films spalled, before overcoating
(17) The overcoat, gage, and insulation film spalled in storage before bake and lead wire attachment

Bar Shape Code:

P = PWA
S = Spin
N = NASA

Surface Finish Code:

a = Shop polish
b = Hand polish
c = 600 grit polish
d = UTRC polish
i = Sputter etched

TABLE XXXIV-B

RESISTANCE MEASUREMENTS DURING FABRICATION
10 TYPE B STRAIN GAGES

Bar, AMS 4928   Insulation, HfO_2 Gage, Cu-45Ni

Bar No. and Gage No.	Bar Shape	Trial No. and Surface Finish	AS SPUTTERED				COMPLETED (5)				Remarks (5)
			R (Ohms) (1)	U (Ohms) (2)	T (Ohms) (3)	Insulation Rating (4)	R (Ohms) (1)	U (Ohms) (2)	T (Ohms) (3)	Insulation Rating (4)	
B16-1	P	1 a	98	20M	20M	Good	97	20M	20M	Good	(6)
-2			95	105	10	Marg.	88	88	2	Bad	(10)(11)
B15-1	P	1 a	99	20M	20M	Good	93	20M	20M	Good	(14)
-2			94	20M	20M	Good	88	105	21	Marg.	(14)
B15-1	P	2 b	118	20M	20M	Good	116	20M	20M	Good	(14)
-2			112	20M	20M	Good	110	20M	20M	Good	(14)
B10-1	P	1 a	Open	20M	20M	Good	-	-	-	-	(15)
-2			Open	20M	20M	Good	-	-	-	-	(15)
B10-1	P	2 b	104	1.8	1.8	Good	-	-	-	-	(14)
-2			108	20M	20M	Good	-	-	-	-	(14)
B9-1	P	1 a	100	20M	20M	Good	Open	99	5	Bad	(16)(17)
-2			108	20M	20M	Good	102	20M	20M	Good	(16)(17)

TABLE XXXIV-C

RESISTANCE MEASUREMENTS DURING FABRICATION
32 TYPE C STRAIN GAGES

Bar; Incoloy 901   Insulation; Si_3N_4 Gage; Ni-30Cr

Bar No. and Gage No.	Bar Shape	Trial No. and Surface Finish		AS SPUTTERED R (Ohms) (1)	U (Ohms) (2)	T (Ohms) (3)	Insulation Rating (4)	COMPLETED (5) R (Ohms) (1)	U (Ohms) (2)	T (Ohms) (3)	Insulation Rating (4)	Remarks (5)
C17-1	P	2	a	244	20M	20M	Good	61	56	110	Bad	(18)(10)
-2				237	51K	51K	Good	62	87	10	Bad	(18)(10)
C17-1	P	4	b	167	95K	95K	Good	184	23	198	Bad	(18)(10)
-2				158	284	132	Marg.	176	178	95	Bad	(18)(10)
C17-1	P	5	bi	249	20M	20M	Good	249	20M	20M	Good	(6)
-2				253	20M	20M	Good	254	20M	20M	Good	(6)
C18-1	P	2	a	235	20M	20M	Good	63	72	116	Bad	(18)(10)
-2				237	20M	20M	Good	64	114	100	Bad	(18)(10)
C18-1	P	4	b	161	20M	20M	Good	168	1.1K	1.1K	Marg.	(18)
-2				161	50K	50K	Good	166	236	86	Bad	(18)(10)
C18-1	P	5	bi	250	20M	20M	Good	267	4.7K	4.8K	Marg.	(6)
-2				250	20M	20M	Good	260	4.4K	4.2K	Marg.	(6)
C27-1	N	1	bi	253	20M	20M	Good	252	20M	20M	Good	(6)
-2				260	20M	20M	Good	259	20M	20M	Good	(6)
C28-1	N	1	bi	250	20M	20M	Good	249	20M	20M	Good	(12)
-2				257	20M	20M	Good	256	20M	20M	Good	(12)(19)
C28-1	N	3	di	247	20M	20M	Good	246	20M	20M	Good	(6)
-2				257	20M	20M	Good	257	20M	20M	Good	(6)
C19-1	S	4	di	274	20M	20M	Good	264	302K	302K	Good	(6)
-2				252	20M	20M	Good	250	1.8K	1.8K	Marg.	(6)
C20-1	S	3	b	139	20M	20M	Good	138	20M	20M	Good	(20)(8)
-2				138	20M	20M	Good	140	20M	20M	Good	(20)(8)
C20-1	S	4	di	250	20M	20M	Good	269	19	269	Bad	(10)(11)
-2				238	20M	20M	Good	Open	20M	20M	Good	(9)
C23-1	P	3	bi	207	20M	20M	Good	210	87K	87K	Good	(6)
-2				201	20M	20M	Good	215	108K	108K	Good	(6)
C24-1	P	2	bi	198	20M	20M	Good	196	31K	31K	Fair	(6)
-2				192	20M	20M	Good	190	140K	140K	Good	(6)
C26-1	P	1	di	257	20M	20M	Good	250	5	254	Bad	(10)(11)
-2				259	20M	20M	Good	251	20M	20M	Good	(6)
C19-1	S	3	b	140	2.08K	1.95K	Fair	137	2.84K	2.71K	Fair	(12)(13)
-2				135	3.43K	3.52K	Fair	133	3.99K	4.07K	Fair	(12)(13)

Notes:

(18) Final R, U, T reported are after overcoat and bake,
    before lead wire att.
(19) The overcoat and gage spalled after bake
(20) Not baked
(21) Three overcoats failed; final R, U, T reported are
    after removal of third overcoat mask
(22) Poor adherence of gage grids. Adherence of lead films
    was better.

TABLE XXXIV-D

RESISTANCE MEASUREMENTS DURING FABRICATION
25 TYPE D STRAIN GAGES

Bar, Incoloy 901   Insulation, Al_2O_3 Gage, Ni-30Cr

Bar No. and Gage No.	Bar Shape	Trial No. and Surface Finish	AS SPUTTERED R (Ohms) (1)	U (Ohms) (2)	T (Ohms) (3)	Insulation Rating (4)	COMPLETED (5) R (Ohms) (1)	U (Ohms) (2)	T (Ohms) (3)	Insulation Rating (4)	Remarks (5)
D21-1	P	3 b	188	11M	11M	Good	196	20M	20M	Good	(6)
-2			183	20M	20M	Good	187	20M	20M	Good	(6)
D21-1	P	4 bi	206	790	990	Fair	211	18K	18K	Fair	(21)
-2			199	23K	23K	Fair	205	890	850	Marg.	(21)
D22-1	P	3 b	200	20M	20M	Good	218	20M	20M	Good	(13)(18)
-2			Open	20M	20M	Good	Open	20M	20M	Good	(9)(18)
D22-1	P	5 bi	210	20M	20M	Good	214	2730	2710	Good	(21)
-2			204	17M	17M	Good	208	2360	2380	Good	(21)
D29-1	N	4 di	269	713	480	Marg.	269	926	677	Marg.	(12)(13)
-2			266	1535	1366	Marg.	268	2030	1860	Marg.	(12)(13)
D29-1	N	6 di	275	730	460	Fair	-	-	-	-	(13)
-2			272	199	454	Marg.	-	-	-	-	(13)
D30-1	N	4 di	260	3230	3270	Marg.	260	3660	3700	Marg.	(12)(13)
-2			273	740	1000	Fair	271	815	1076	Fair	(12)(13)
D30-1	N	5 di	282	30K	30K	Fair	270	8	8	Bad	(12)(13)
-2			283	357	630	Marg.	276	3	3	Bad	(12)(13)
D25-1	S	7 bi	255	20M	20M	Good	-	-	-	-	(22)
-2			234	20M	20M	Good	-	-	-	-	(22)
D26-1	S	7 bi	253	20M	20M	Good	-	-	-	-	(22)
-2			253	20M	20M	Good	-	-	-	-	(22)
D31-1	P	1 d	192	20M	20M	Good	191	700K	700K	Good	(18)(19)
-2			183	20M	20M	Good	183	20M	20M	Good	(18)(19)
D31-1	P	2 c	152	20M	20M	Good	160	5K	5K	Fair	(6)
-2			150	87K	87K	Good	161	10K	10K	Fair	(6)
D32-1	P	1 d	193	20M	20M	Good	192	200K	200K	Good	(18)(19)
-2			189	20M	20M	Good	189	9500	9500	Fair	(18)(19)

TABLE XXXIV-E

RESISTANCE MEASUREMENTS DURING FABRICATION
6 TYPE E STRAIN GAGES

Bar, PWA 1422   Insulation, Al_2O_3 Gage, Ni-30Cr

Bar No. and Gage No.	Bar Shape	Trial No. and Surface Finish	AS SPUTTERED R (Ohms) (1)	U (Ohms) (2)	T (Ohms) (3)	Insulation Rating (4)	COMPLETED (5) R (Ohms) (1)	U (Ohms) (2)	T (Ohms) (3)	Insulation Rating (4)	Remarks (5)
E33-1	P	1	338	20M	20M	Good	366	20M	20M	Good	(6)
-2			374	20M	20M	Good	392	20M	20M	Good	(6)
E34-1	N	2	376	20M	20M	Good	384	20M	20M	Good	(6)
-2			370	20M	20M	Good	374	20M	20M	Good	(6)
E36-1	P	1	323	20M	20M	Good	360	20M	20M	Good	(6)
-2			362	20M	20M	Good	429	20M	20M	Good	(6)

TABLE XXXV
GAGE RESISTANCE STATISTICS, AS SPUTTERED

Gage Type	Surface Finish	Resistance (ohms)	Standard Deviation (%)	Number of Samples, n
A	All	224.6	16.5	20
A	Notes d & i	256.8	7.8	4
B	All	103.6	7.1	10
C	All	218.9	20.2	32
C	Notes d & i	254.6	3.8	8
D	All	225.0	18.3	25
D	Notes d & i	272.5	2.6	8
E	All	357.2	5.6	6

Note d: UTRC polish.
Note i: Bar sputter-etched before sputtering insulating layer.

In the first class, each set of nickel-chrome gages on polished bars (A, C, D) shows nearly the same average gage resistance (218.9 to 225.0 ohms) and large standard deviation (16.5 to 20.2 percent). For the subset of sputter-etched, UTRC-polished Type A, C, and D bars, the standard deviation is found to be much smaller (2.6 to 7.8 percent) and gage resistance higher (254.6 to 272.5 ohms). The rougher-textured surface produced by sputter etching clearly results in higher gage resistance. Examination of the raw data in Table XXXIV shows that the rougher of the polishing procedures (note a) also generally resulted in high resistance, while the better polishing procedures (notes b and d) when not sputter etched invariably produced low gage resistance.

The second class, Type E gages, shows the highest average gage resistance (357.2 ohms) of any group examined. The standard deviation (5.6 percent) is about the same as that observed for the Type A, C, D gages on the bars with the most closely controlled surface finish (notes d, i). These results seem reasonable. The high average resistance and moderate standard deviation are not unexpected on the specially roughened surface (produced by the method of Reference 4) used on all Type E bars.

The third class, the copper-nickel gages on polished bars (Type B), show lower average gage resistance (103.6 ohms) than the nickel-chrome gages, and a rather large standard deviation (7.1 percent). These results seem reasonable. The lower gage resistance is expected, based on resistivity measurements in the Components Program. The large standard deviation is expected because surface finishes on the Type B bars fall into the poorly-controlled roughness categories (a, b, with no sputter etching employed). The raw data in Table

7-21

XXXIV again reveal a trend toward higher resistance on the Type B bars with poorer polishing procedure (note a) and lower resistance on the smoother bars (note b). These biases are lumped into the standard deviation of 7.1 percent for all Type B bars in Table XXXV.

Gage Resistance After Completion

Changes of a few percent upward or downward in measured gage resistance occurred as a result of overcoating, lead wire attachment, and 5-hour bake at service temperature (Table XXXIV). The results are consistent with small effects of aging at service temperature previously observed in the Components Program (Section 6.4). Final measurements on completed gages include the lead wire resistance, not present on gages as sputtered or gages not completed. The lead-wire resistance was generally about 1.5 percent of gage resistance.

The trends in gage resistance change were the following (excluding gages accidentally shorted):

o   Type E gage resistance invariably increased, by amounts between 2 and 19 percent.

o   Type B gage resistance invariably decreased, by amounts between 1 and 7 percent.

o   Type A, C, and D gage resistance sometimes increased and sometimes decreased, by amounts between -4 and +11 percent, with no clear correlation with surface finish.

Insulation Resistance

Insulation resistance as sputtered tended to be either good or bad, with only a few cases falling in the intermediate classes of fair or marginal defined earlier in this section. The few gages with fair or marginal insulation as sputtered were accepted for further fabrication and are included and identified in Table XXXIV, along with the gages with good initial insulation resistance. The table shows that the insulation resistance of these fair and marginal cases generally remained unchanged during subsequent fabrication steps. Among gages with insulation resistance rated good initially only about 15 percent deteriorated to fair, marginal, or bad during subsequent fabrication steps. In almost every case the deterioration was associated with a catastrohpic event, as noted in Table XXXIV, such as spalling of an overcoat film, spalling of a thick lead film, or damage during lead wire trials.

7.4 TEST MATRIX

The Gage Program test matrix has previously been presented in Table XXXII along with the fabrication details for each gage. A short-form summary of the test matrix alone is presented in Table XXXVI for quick reference during the following discussions of results of gage factor testing, thermal cycle testing, fatigue testing, spin testing, and erosion testing.

TABLE XXXVI

MATRIX OF 43 GAGES TESTED OR DELIVERED

Bar and Gage No.	Bar Shape	Gage Factor Room Temp.	Gage Factor High Temp.	Thermal Cycle	Fatigue Room Temp.	Fatigue High Temp.	Spin	Erosion	Deliver to NASA
A1-1	P	X	X			X		X	
A2A-1	P	X	X	X	X+			X	
-2		X	X	X	X			X	
A3-1	S						X	X	
A4-1	S							X	
-2								X	
A7-1	P	X*							
-2		X*							
A8A-1	P	X	X	X	X	X		X	
-2		X	X	X	X	X		X	
B16-1	P	X	X·	X					
-2		X	X·	X	X	X		X	
C17-1	P	X·	X·	X	X	X+			
-2		X·	X+						
C18-1	P	X	X	X		X			
-2		X	X	X	X·	X+			
C19-1	S						X	X	
-2							X	X	
C20-1	S							X	
C23-1	P	X	X*						
-2		X	X*						
C24-1	P	X	X·	X	X	X+		X	
-2		X·	X+						
C26-1	P							X	
-2								X	
D21-1	P	X	X+						
-2		X	X+						
D31-1	P	X	X·	X	X	X+			
-2		X	X·	X	X·	X+			
E33-1	P	X·	X	X·	X	X			
-2		X·	X	X	X	X+			
E36-1	P	X·	X[1]					X	
-2		X·	X[1]			X+			
A5-1	N								X
-2									X
A6-1	N								X
-2									X
C27-1	N								X
-2									X
C28-1	N								X
-2									X
E34-1	N								X
-2									X

X   Gage tested or delivered
1   Tested to 1100K
·   Lead wire attachment repaired
+   Lead wire attachment failed; not repairable
*   Gage grid failed

7.5 GAGE FACTOR TEST RESULTS

Gages Tested

Gage factor was measured at one or more strain levels and temperatures for 25 thin film gages using the four-increment test method at each strain level, as described in Section 5.5. The 25 gages tested are indicated in Table XXXII and also in the short-form test matrix of Table XXXVI. Seven gages were Type A, two were Type B, eight Type C, four Type D, and four Type E. The resulting gage factor test data are tabulated in Appendix 3. The data tabulated include mean gage factor and the two-standard-deviation level (2-sigma) of gage factor determinations for each gage at each temperature and each applied strain. Each entry of a mean gage factor or 2-sigma in Appendix 3 is based on four increments of strain (first increasing from zero to indicated strain level, then decreasing to zero, then repeating the increase and decrease). In addition, the drift in gage resistance in 15 minutes at 1000 microstrain at each temperature was measured and is tabulated.

Scatter and Repeatability

For about one third of all tests in Appendix 3, 2-sigma is greater than 30 percent, where 2-sigma is the two-standard-deviation level in one four-increment gage factor test.

In most of the cases of large scatter, the cause was found to be erratic changes in electrical contact resistance at the lead wire attachments to the thin films. In many of these cases, repair of the lead wire connections (by cleaning and adding fresh conductive cement) resulted in reducing the magnitude of 2-sigma in subsequent repeat tests by a factor of ten or more. In Appendix 3 the data entries are listed in chronological order within the set of entries for any one gage, and the instances of lead wire repair and subsequent improvement in 2-sigma are noted.

In some cases of large scatter, variation in leakage to ground was the suspected cause. The insulation resistance to ground was not measured during the gage factor testing, but was measured at room temperature before gage factor testing, Table XXXIV, and in most cases at room temperature and service temperature after gage factor testing, Table XL. The specific cases where large scatter is associated with a gage showing low insulation resistance are discussed in the following section, Gage Factor versus Temperature and versus Strain.

It was judged that the result of any particular four-increment gage factor test was not useful for gage factor determination if 2-sigma was greater than 30 percent. The results of such tests were discarded in analyzing gage factor trends. All remaining gage-factor test results were judged acceptable for analysis.

To summarize the trends in repeatability, Table XXXVII lists the average two-standard-deviation level for the acceptable tests, by gage type and test temperature. The table also lists the number of acceptable tests and the ratio of number acceptable to total number.

It is evident (Table XXXVII) that the repeatability of gage factor measurement was poorest at high temperatures.

TABLE XXXVII

STANDARD DEVIATION OF GAGE FACTOR MEASUREMENTS

Gage Type	300K			450K			600K			900K			1100K		
	n	$\frac{n}{N}$	$\overline{2s}_n$ Percent	n	$\frac{n}{N}$	$\overline{2s}_n$ Percent	n	$\frac{n}{N}$	$\overline{2s}_n$ Percent	n	$\frac{n}{N}$	$\overline{2s}_n$ Percent	n	$\frac{n}{N}$	$\overline{2s}_n$ Percent
A	35	0.67	6.6	15	0.62	12.6	17	0.71	15.1						
B	15	0.94	4.8	8	1.00	4.8	1	0.12	12.2						
C	62	0.72	6.6				29	0.66	9.8	3	0.09	17.9			
D	27	0.78	5.6				6	0.75	3.2	2	0.25	27.5			
E	51	0.80	7.6				7	0.44	10.3	6	0.75	12.9	1	0.12	25.3

Nomenclature

N = Number of 4-increment gage factor tests, total

n = Number of 4-increment gage factor tests in which 2s < 30%

s = Standard deviation of gage factor in one 4-increment test

$\overline{2s}_n$ = Average of two-standard-deviation level for all n

7-25

At room temperature the observed average 2-sigma level of the 4 increment gage factor tests was below 8 percent for all gage types. At 600K the 2-sigma level ranged from below 4 percent (for Type D) to 15.1 percent (for Type A). At 900K the 2-sigma level ranged from below 13 percent (for Type E) to 27.5 percent (for Type D). At 1100K the 2-sigma level was 25.3 percent for the only test conducted (Type E).

Since the analysis of the experimental procedure indicated that the precision of gage factor determination was not worse than +3 percent at any temperature, the conclusion is that the behavior of the insulating films, thin film gages, lead films, and lead wire attachments was more erratic at high temperatures.

Gage resistance drift and gage failures are discussed later.

Gage Factor Versus Temperature and Versus Strain

In analyzing the data of Appendix C for gage factor versus gage type, temperature, and strain, all tests for which 2-sigma exceeded 30 percent were first discarded. The remaining data are presented in Figure 34. For each gage type (A, B, C, D, E), the figure presents a plot of gage factor of individual gages versus temperature and a separate plot of gage factor at room temperature versus microstrain (from -1000 to +1000). Each point on each plot shows the average and total scatter of several of the tests of Appendix C. Specifically, in the plots of gage factor versus temperature, each point plotted is the average and total scatter over all strain levels (including repeats) for one gage at one temperature. In the plots of gage factor versus strain, each point plotted is the average and toal scatter over all determinations (including repeats) for one gage at room temperature at one strain level.

In Figure 34 for clairity in separating the behavior of one gage from another the points plotted for different gages at each temperature and each strain are plotted horizontally displaced from each other (along temperature and strain axes). A legend above each cluster of points indicates the temperature or strain that applies to all points in that cluster. Furthermore, open symbols identify cases in which leakage to ground is a suspected cause of bias or scatter (more than 2% leakage indicated in Table XXXIV or Table XL), solid symbols signify leakage to ground was not significant, and diagonal-barred symbols identify cases where leakage measurements were inconclusive or not available.

The trends with temperature are quite consistent from gage to gage of any one type. A straight-line trend line is drawn by eye in Figure 34 for each gage type.

For all gages the gage factor is near 2.0 at room temperature. For Type A gages the gage factor trends upward to about 2.2 at 600K. For type C gages the gage factor remains nearly constant as temperature increases to 900K. For the Type B, D, and E gages, the gage factor decreases as temperature increases.

There is no discernible distinct change of gage factor value with strain (at room temperature), within the scatter of the data in Figure 34.

The overall scatter of gage factor determinations in Figure 34 is generally about +30% around the average gage factor of all gages at any selected temperature or strain. The scatter band presented in Figure 34 for each gage (vertical line) of course includes bias shifts due to lead wire repairs from test to test or change in electrical leakage to ground from test to test. The presentation, therefore, tends to obscure the trend observed in Table XXXVII and Appendix C of lower average 2-sigma scatter during individual tests of gages at lower temperature.

In three specific cases in Figure 34 it is evident that low resistance to ground is associated with an unusually high or low gage factor or unusually large scatter of gage factor data, as follows:

> Gage A1-1, at 450K and 590K
> Gage C17-1, at 590K and 920K
> Gage E33-1, at all temperatures

In the other cases where resistance to ground was known to be low, the gage factor data showed about the same level and scatter as in the cases where resistance to ground was high.

The evidence in Figure 34 and Appendix C is that the major contribution to scatter in all of the gage factor determinations was the lead wire attachment contact resistance variability. For example, repairs to the lead wire attachments eliminated the scatter (temporarily) in the case of gages B16-2, C17-1, C17-2, C24-1, C24-2, D31-1, D31-2, E33-1, E33-2.
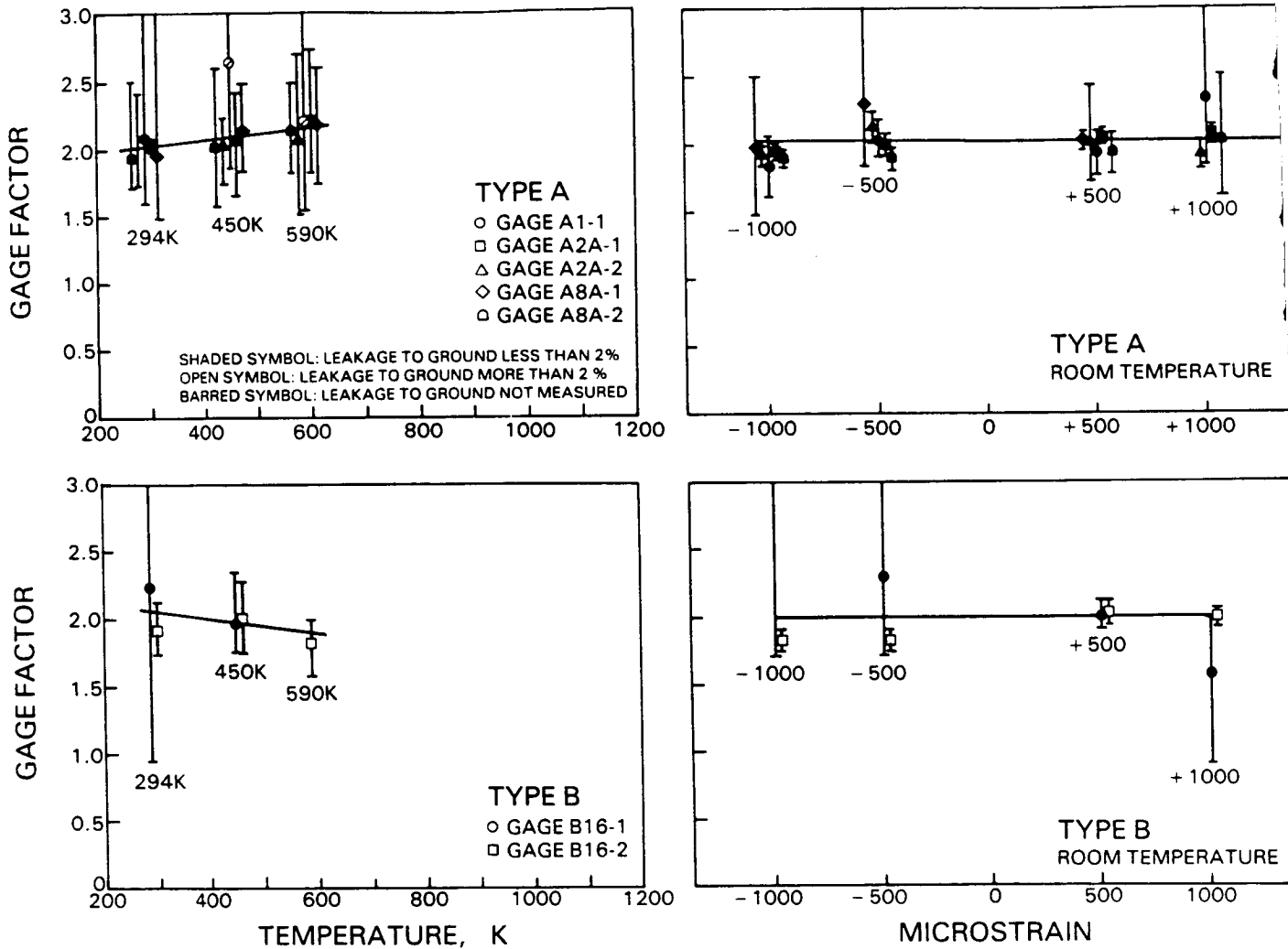
Figure 34   Gage Factor versus Temperature and versus Strain
(at room temperature).
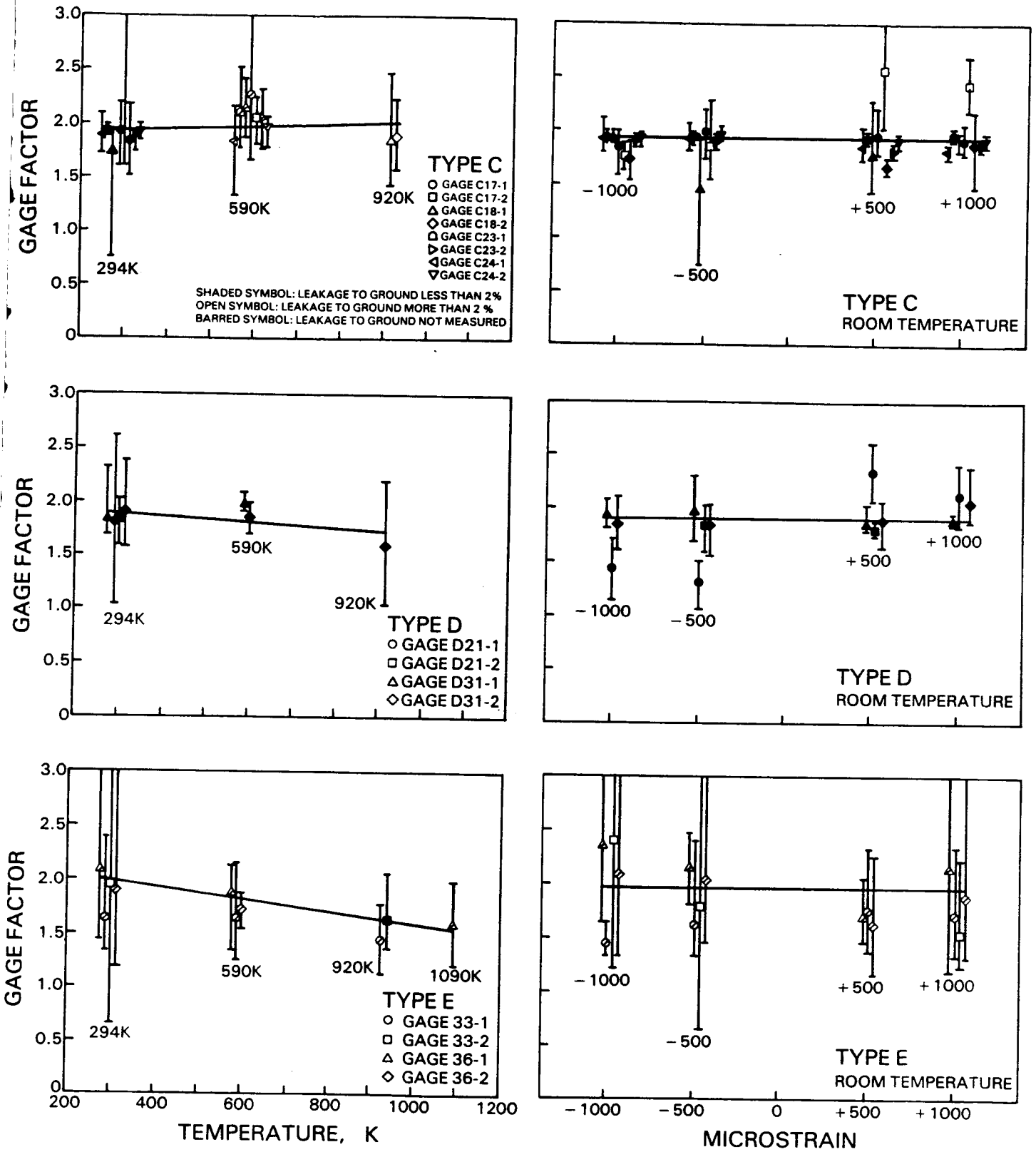
Figure 34   Gage Factor versus Temperature and versus Strain.
(at room temperature), Concluded.

Drift at 1000 Microstrain

As a part of the gage factor test sequence at each temperature, the change in gage resistance was measured during a 15-minute isothermal period while the strain was held constant at +1000 microstrain. The results are included in Appendix C and tabulated separately in Table XXXVIII. All determinations of drift are included in the table. A starred entry indicates drift measurement during any gage factor test sequence which resulted in unsatisfactory gage factor data (2-sigma greater than 30 percent) at +1000 microstrain. Notable features of the drift behavior in Table XXXVIII are as follows:

1. Drift increased as temperature increased.

2. Maximum drift at room temperature was $220x10^{-6}$ ohms/ohm.

3. Maximum drift was less than $3000x10^{-6}$ at all temperatures.

4. The largest drifts observed for any gage types at any temperature were for Type A ($2750x10^{-6}$) at 600K and Type B ($-1900x10^{-6}$) at 600K.

5. Drift for Type C, D, E gages was less than $1000x10^{-6}$ at all temperatures tested (up to 900K for Type C and D, 1100K for Type E).

6. Drift did not correlate strongly with repeatability of gage factor measurements. Large drift was sometimes associated with poor repeatability and sometimes not.

Failures During Gage Factor Testing

During gage factor testing, 8 of the 25 gage systems failed. Gage system failure in these tests was defined as irreversible increase in the 2-sigma level of gage factor determinations beyond 30 percent. In the process of failure, the gage circuit resistance measurements became progressively more erratic, culminating eventually in an unrepairable open circuit or short circuit to ground. A summary of failure mode by gage type and test temperature is provided in Table XXXIX.

TABLE XXXVIII

FIFTEEN-MINUTE DRIFT AT 1000 MICROSTRAIN

Gage No.	Drift, 10^6 x $\Delta R/R$, At Indicated Temperature					
	300K (Before)	450K	600K	900K	1100K	300K (After)
A1-1	-10	-1350*	-1840*			
A2-1	-100	80	600*			0
A2-2	-200*	-170	2750			-10
A8-1	-210*	-10	380			-220*
A8-2	0	250	1230			-190
B16-1		70	-1900*			-190
B16-2		160	-810*			-130
C18-1				0		
C18-2				0*		
C23-1	0		0	0*		
C23-2	0		0	10*		
C24-1	0		0	0*		0
C24-2	0		0	10*		
D21-1	60					
D21-2	0*					
D31-1	0		0	0*		20
D31-2	0		0*	0		0
E33-1	0		0*	0		0
E33-2	0		0*	0*		0*
E36-1					780	
E36-2					250*	

All drift readings are rounded to the nearest 10×10^{-6}

*Starred entries indicate gage factor 2s > 30% at 1000 microstrain

7-31

Four of the eight failures were due to nonrepairable deterioration of lead wire attachments to lead films in the Type C and D gage systems during testing at 900K. The lead wire attachment failures were a manifestation of the general problem of attaining and maintaining good electrical contact by the conductive cement technique. Besides the four failures, there were ten other gage systems in which repairs to lead wire attachments were accomplished during the courses of gage factor testing to restore repeatability of gage factor measurements. These ten gage systems requiring repairs are noted in Tables XXXVI and XXXIX. Included are two Type B, two Type C, two Type D, and all four Type E systems.

Four gages developed an open circuit in the gage grid during gage-factor testing. In two of these cases (bar A7) no physical damage to the gage grid was visible. In the other two cases (bar C23) obvious spalling of the overcoat and gage alloy film occurred.

TABLE XXXIX

FAILURES DURING GAGE FACTOR TESTING

Gage Type	No. of Gages Tested	No. of Failures			No. of Surviving Gages Requiring Lead Repairs		
		Open Gage at 300K	Open Gage at 900K	Unrepairable Lead Wire Attachment at 900K	at 300K	at 600K	at 900K
A	7	2					
B	2					2	
C	8		2	2			2
D	4			2			2
E	4				4		
Total	25	2	2	4	4	2	4

7-32

7.6 THERMAL CYCLE TEST RESULTS

Gages Tested

Fourteen of the thin film strain gages which had completed the gage factor testing described in the previous section were then cycled 50 times to service temperature. The test procedure is described in Section 5.6. The 14 gages tested are noted in Table XXXII and also in the short-form test matrix of Table XXXVI. Four were Type A gages, two were Type B, four Type C, two Type D, and two Type E. These tests met the objective of thermal cycling at least two gages of each type.

A sample record of temperature and gage resistance versus time for two gages on one test bar during three test cycles is presented in Figure 35. Details of the gage resistance and insulation resistance behavior during thermal cycling are discussed in the balance of this section.

Results Summary Table

The results of the thermal cycle tests are summarized in Table XL.

The table lists first the measured gage resistance, R, at room temperature and at service temperature during selected sample cycles over the course of the fifty thermal cycles for each gage. (The remaining cycles are omitted for brevity; during cycles omitted, the changes in measured gage resistance and insulation resistance from cycle to cycle were gradual and monotonic.)

The table lists next the shunting (percent of gage resistance) due to measured insulation resistances, U and T, from the two ends of the gage to ground at the time of each measurement of gage resistance. The shunting is simply the quantity 1 - R/a calculated from the measured values of U and T using the resistance equations of Figure 33. (The quantity a is the gage resistance which would be measured if U and T were infinitely large; in most cases U and T are large, 1 - R/a is close to zero, and the shunting effect is negligible.)

The table finally lists two other quantities calculated from the measured gage resistances. One is the cumulative drift in gage resistance (percent of gage resistance) referred to the first-cycle gage resistance reading. The other is the temperature coefficient of resistance, α (K^{-1}), for each cycle.

Gage Durability and Resistance Drift

The table shows that gage durability was excellent. No gage grid open circuits or delamination occurred during the thermal cycle testing.

Drift in gage resistance for the Type A and B gages (cycled to 600K) over the entire 50 cycles averaged 0.43 percent and for the Type C, D, and E gages (cycled to 900K) averaged 4.73 percent. Only one gage changed in measured resistance by more than 10 percent. This gage (C17-1) changed by 14.2 percent and was still functional at the end of testing.

TABLE XL

THIN FILM STRAIN GAGE THERMAL CYCLE TEST RESULTS

		Measured Resistances						
		At 300K			At 600 K			
Gage No.	Cycle No.	Gage Resistance R (Ohms)	Shunting Due to Insulation $100(1-\frac{R}{a})$ (Percent)	Cumul. Drift $\frac{100\,\Delta R}{R_1}$ (Percent)	Gage Resistance R (Ohms)	Shunting Due to Insulation $100(1-\frac{R}{a})$ (Percent)	Cumul. Drift $\frac{100\,\Delta R}{R_1}$ (Percent)	$10^6\alpha$ (K^{-1})
A2A-1	1	191.9	1.18	-	194.2	0.00	-	40
	2	192.1	0.00	0.10	194.5	0.00	0.15	41
	10	192.6	0.00	0.36	194.6	0.00	0.20	34
	20	193.7	0.00	0.93	195.0	0.00	0.41	22
	30	193.4	0.00	0.77	195.1	0.00	0.46	29
	34	193.3	0.00	0.72	194.9	0.00	0.36	28
	35	193.6	0.00	0.88	194.9	0.00	0.36	22
	36	193.4	0.00	0.77	194.9	0.00	0.36	26
	37	193.3	0.00	0.72	194.9	0.00	0.36	28
	38	193.3	0.42	0.72	194.7	0.00	0.26	24
	39	193.9	0.00	1.04	194.8	0.00	0.31	16
	40	193.1	2.24	0.62	194.9	0.00	0.36	31
	50	193.3	0.00	0.72	194.7	0.00	0.26	24

$$10^6\alpha \pm 2s = 28 \pm 14$$

A2A-2	1	192.8	0.00	-	190.7	0.00	-	-37
	10	192.4	0.00	-0.21	190.5	0.00	-0.10	-33
	20	191.9	0.00	-0.47	190.4	0.00	-0.16	-26
	30	190.9	0.00	-0.98	190.2	0.00	-0.26	-12
	34	192.8	0.00	0.00	190.4	0.00	-0.16	-42
	35	190.2	0.00	-1.35	190.4	0.00	-0.16	+3
	36	190.5	0.00	-1.19	190.4	0.00	-0.16	-2
	40	190.7	0.00	-1.09	190.3	0.00	-0.21	-7
	43	191.6	0.00	-0.62	190.4	0.00	-0.16	-21
	44	191.4	0.00	-0.73	190.4	0.00	-0.16	-17
	45	191.7	3.30	-0.57	190.4	0.00	-0.16	-23
	46	191.7	0.00	-0.57	190.4	0.00	-0.16	-23
	50	191.5	0.00	-0.67	190.3	0.00	-0.21	-21

$$10^6\alpha \pm 2s = -20 \pm 25 \ K^{-1}$$

A8A-1	1	186.1	0.00	-	188.7	0.00	-	47
	10	186.2	0.00	0.05	188.9	0.00	0.11	48
	20	185.7	0.00	-0.21	188.5	0.00	-0.11	50
	30	186.1	0.00	0.00	188.5	0.00	-0.11	43
	40	186.4	0.00	0.16	188.6	0.00	-0.05	39
	50	186.6	0.00	0.27	188.6	0.00	-0.05	36

$$10^6\alpha \pm 2s = 44 \pm 10 \ K^{-1}$$

A8A-2	1	191.6	0.00	-	189.0	0.00	-	-46
	10	188.7	0.00	-1.51	189.1	0.00	0.05	7
	20	188.1	0.00	-1.83	188.2	0.00	-0.42	2
	30	189.1	0.00	-1.30	188.4	0.00	-0.32	-12
	40	189.6	0.00	-1.04	188.4	0.00	-0.32	-21
	50	192.7	0.00	0.05	189.1	0.00	0.05	-63

$$10^6\alpha \pm 2s = -22 \pm 50 \ K^{-1}$$

B16-1	1	90.7	1.01	-	88.2	0.04	-	-92
	10	91.6	1.07	0.99	88.5	1.50	0.34	-114
	20	92.6	*	2.09	88.8	*	0.68	-139
	30	91.8	*	1.21	88.6	*	0.45	-117
	40	92.6	*	2.09	88.6	*	0.45	-146
	50	92.6	*	2.09	88.8	*	0.68	-139

$$10^6\alpha \pm 2s = -124 \pm 37 \ K^{-1}$$

B16-2	1	87.7	*	-	85.1	*	-	-97
	10	90.3	*	2.96	85.1	*	0	-195
	20	88.6	*	1.03	85.1	*	0	-131
	30	87.4	*	-0.34	85.1	*	0	-86
	40	88.5	*	0.91	85.1	*	0	-127
	50	90.3	*	0.68	85.5	*	0.47	-105

$$10^6\alpha \pm 2s = -124 \pm 71 \ K^{-1}$$

* Gage reported "shorted to ground", exact insulation resistance readings not recorded.

Measured Resistances

Gage No.	Cycle No.	At 300K Gage Resistance R (Ohms)	Shunting Due to Insulation $100(1-\frac{R}{a})$ (Percent)	Cumul. Drift $\frac{100\Delta R}{R_1}$ (Percent)	At 900K Gage Resistance R (Ohms)	Shunting Due to Insulation $100(1-\frac{R}{a})$ (Percent)	Cumul. Drift $\frac{100\Delta R}{R_1}$ (Percent)	10^6 (K^{-1})
C17-1	1	291.2	0.71	-	296.8	6.21	-	32
	10	299.5	0.79	2.85	309.0	5.45	4.11	53
	20	304.2	0.80	4.46	311.6	6.55	4.99	40
	30	321.0	1.07	10.23	327.0	7.83	10.18	31
	40	327.0	1.13	12.29	337.3	8.15	13.54	52
	50	332.5	1.11	14.18	342.4	8.36	15.30	50

$10^6\alpha \pm 2s = 43 \pm 18$ K^{-1}

Gage No.	Cycle No.	At 300K Gage Resistance R (Ohms)	Shunting (Percent)	Cumul. Drift (Percent)	At 900K Gage Resistance R (Ohms)	Shunting (Percent)	Cumul. Drift (Percent)	10^6 (K^{-1})
C18-1	1	274.0	0.96	-	281.9	10.86	-	48
	10	277.2	1.13	1.17	291.6	9.10	3.44	86
	20	275.6	1.06	0.58	294.0	9.04	4.29	111
	30	277.5	0.96	1.28	297.1	9.02	5.39	118
	40	278.5	1.12	1.64	300.5	8.94	6.60	132
	50	283.9	1.42	3.61	309.8	10.08	9.90	152

$10^6\alpha \pm 2s = 108 \pm 33$ K^{-1}

Gage No.	Cycle No.	At 300K R (Ohms)	Shunting (Percent)	Cumul. Drift (Percent)	At 900K R (Ohms)	Shunting (Percent)	Cumul. Drift (Percent)	10^6 (K^{-1})
C18-2	1	258.8	1.97	-	219.2	24	-	-255
	10	259.3	2.47	0.19	221.7	25	1.14	-242
	20	259.1	2.17	0.12	218.2	26	-0.46	-263
	30	259.7	2.18	0.35	215.6	29	-1.64	-283
	40	260.6	2.51	0.62	217.4	29	-0.82	-276
	50	273.9	3.46	5.83	236.0	38	7.66	-231

$10^6\alpha \pm 2s = -258 \pm 18$ K^{-1}

Gage No.	Cycle No.	At 300K R (Ohms)	Shunting (Percent)	Cumul. Drift (Percent)	At 900K R (Ohms)	Shunting (Percent)	Cumul. Drift (Percent)	10^6 (K^{-1})
C24-1	1	212.6	0.49	-	224.4	16.9	-	92
	4	205.8*	9.73	-3.20	202.8	10.68	-9.62	-24
	10	208.8	6.12	-1.79	213.7	10.12	-4.77	39
	15	219.5	0.62	3.24	237.0	8.21	5.61	133
	20	256.3	0.93	20.6	274.5	9.80	22.3	118
	30	241.0	0.81	13.4	389.9	18.9	73.8	1030
	32	528.3	0.00	148.5	383.6	18.5	70.9	-456
	33	216.0*	0.99	1.60	217.4	14.4	-3.12	11
	40	218.5	0.74	2.78	226.8	17.0	1.07	63
	50	225.1	0.76	5.88	234.8	20.8	4.63	72

$10^6\alpha \pm 2s = 49 \pm 27$ K^{-1}

Gage No.	Cycle No.	At 300K R (Ohms)	Shunting (Percent)	Cumul. Drift (Percent)	At 900K R (Ohms)	Shunting (Percent)	Cumul. Drift (Percent)	10^6 (K^{-1})
D31-1	1	Open	-	-	171.9	0.00	-	-
	6	Open	-	-	Open	-	-	-
	7	Open	-	-	Open	-	-	-
	10	181.0*	0.32	-	193.0	1.31	-	110
	20	180.5	0.33	-0.28	194.8	1.69	0.93	132
	30	179.6	0.18	-0.77	196.6	1.46	1.86	158
	40	179.3	0.00	-0.94	197.8	1.32	2.49	172
	50	179.1	0.13	-1.05	198.3	1.33	2.75	179

$10^6\alpha \pm 2s = 150 \pm 26$ K^{-1}

Gage No.	Cycle No.	At 300K R (Ohms)	Shunting (Percent)	Cumul. Drift (Percent)	At 900K R (Ohms)	Shunting (Percent)	Cumul. Drift (Percent)	10^6 (K^{-1})
D31-2	1	160.8	0.10	-	169.9	0.89	-	94
	6	162.2	0.08	-	173.5	-	-	116
	7	Open	-	-	174.2	-	-	-
	10	177.9*	0.00	-	193.9	0.71	-	150
	20	179.8	0.04	1.07	197.4	3.71	1.80	163
	30	181.3	0.01	1.91	201.8	1.74	4.07	188
	40	183.6	0.02	3.20	206.0	1.65	6.24	203
	50	185.1	0.02	4.05	209.8	1.70	8.20	222

$10^6\alpha \pm 2s = 170 \pm 42$ K^{-1}

* Lead-wire-to-lead-film attachments repaired.

Gage No.	Cycle No.	At 300K R (Ohms)	Shunting (Percent)	Cumul. Drift (Percent)	At 900K R (Ohms)	Shunting (Percent)	Cumul. Drift (Percent)	10^6 (K^{-1})
E33-1	1	397.2	x	-	416.1	x	-	79
	10	395.5	x	-0.43	416.7	x	0.14	89
	20	396.8	x	-0.10	418.2	x	0.50	90
	30	397.7	x	0.12	419.8	x	0.89	93
	33	398.0	x	0.20	420.1	x	0.96	92
	34	Open	-	-	420.1	x	0.96	-
	35	Open	-	-	Open	-	-	-
	40	Open	-	-	Open	-	-	-
	50	Open	-	-	Open	-	-	-
	51	396.0**	0.00	-0.30	422.0	x	1.42	109

$10^6\alpha \pm 2s = 92 \pm 9$ K^{-1}

Gage No.	Cycle No.	At 300K R (Ohms)	Shunting (Percent)	Cumul. Drift (Percent)	At 900K R (Ohms)	Shunting (Percent)	Cumul. Drift (Percent)	10^6 (K^{-1})
E33-2	1	464.5	17.2	-	497.6	2.3	-	119
	10	464.4	15.6	-0.02	500.6	2.3	0.60	130
	20	467.0	17.8	0.54	505.6	6.4	1.61	138
	30	469.0	17.8	0.97	510.1	7.5	2.51	146
	33	469.6	16.4	1.10	511.0	7.1	2.69	147
	34	470.0	17.8	1.18	511.2	7.8	2.73	146
	35	469.8	17.1	1.14	511.3	8.2	2.75	147
	40	470.7	16.7	1.33	512.2	7.8	2.93	147
	50	478.1	-	2.93	519.3	8.2	4.36	144

$10^6\alpha \pm 2s = 141 \pm 10$ K^{-1}

x Resistance to ground from one end of gage was less than one ohm and from other end was
R = no ohm. Shunting can not be calculated from this data.

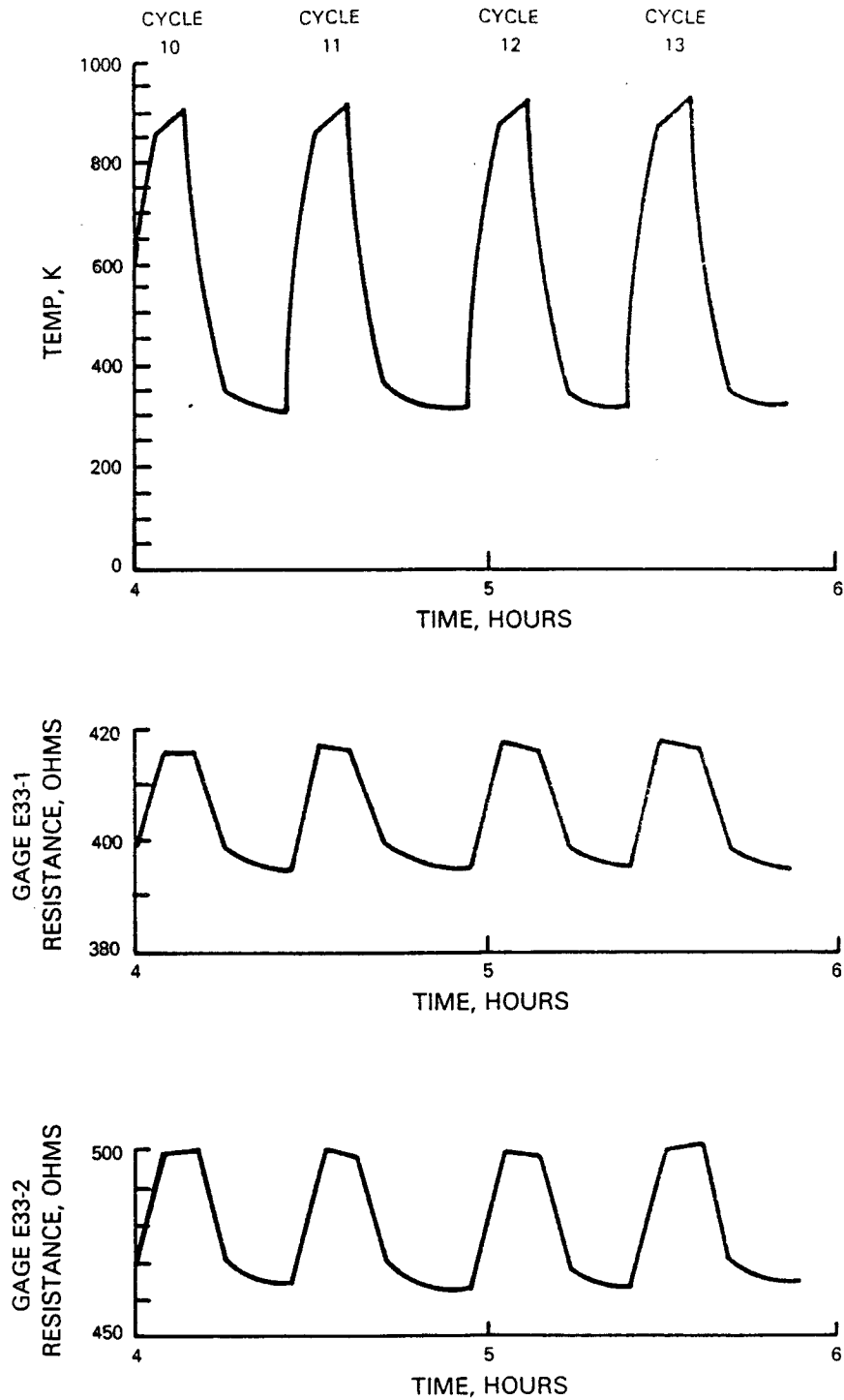** Lead-wire-to-lead-film attachment 5 repaired.

7-35

Figure 35 Sample Thermal Cycle Date. The gage resistances and temperature on test bar E33 are shown for cycle 10 through cycle 13 of the 50 thermal cycles.

The durability of the 600K lead-wire-to-lead-film connection was excellent. No repairs were required in the 600K systems.

The durability of the 900K lead-wire-to-lead-film connection was marginal. Repairs were required in four of the eight 900K systems during the course of testing, as noted in the table as follows:

Gage C24-1, after cycle no. 4 and cycle no. 32
Gage D31-1, after cycle no. 9
Gage D31-2, after cycle no. 9
Gage E33-1, after cycle no. 34

Insulation Resistance

Measured resistance from gage to ground was generally high except in the case of two Type B gages, two Type C gages, and two Type E gages. In the case of the B and one of the E gages, the symptom was a reading of less than one ohm to ground at one end of the gage and a reading equal to gage resistance reading (+one ohm) at the other end. The exact value of gage shunting becomes sensitive to precision of resistance measurements for this situation (T nearly equal to R in Figure 33), and the shunting could not be calculated for these data as noted in the table. Since the gage resistance measurements and measurements (discussed later) remained well behaved, it is assumed that shunting effects were small for these two B gages and one E gage.

In the case of the two Type C gages and the other E gage, the measured insulation resistance to ground at each end of the gage at 900K was a few dozen to a few hundred ohms. Shunting effects were unquestionably large and could be calculated accurately (38 percent for C18-2, 20.8 percent for C24-1, and 8.2 percent for E33-2). The large negative value of α ($-258 \times 10^{-6}K^{-1}$) indicated for gage C18-2 is probably the result of the resistance shunting of this gage at the 900K temperature in each cycle.

There is generally negative correlation in the table between the calculated shunting effects (based on measured resistance to ground) and changes in measured gage resistance. That is, the table shows that the gage resistances generally increased over the course of the fifty thermal cycles, and calculated percent shunting due to finite insulation resistance generally also increased (which should result in lower measured gage resistance). It would therefore appear that increases in shunting effects were more than offset by increases in gage resistance and increases in lead-wire-connection resistances as a result of temperature cycling.

Temperature Coefficient of Resistance

Calculated temperature coefficient of resistance (α) for each reported cycle of each gage is included in Table XL. There are large differences from gage to gage and even from cycle to cycle in some cases, with α generally positive (up to about $200 \times 10^{-6}K^{-1}$) but in some cases negative (to about $-200 \times 10^{-6}K^{-1}$). Within this wide range of values, there are also systematic differences from gage type to gage type, and poor agreement with the values of α measured during the Components Program. In Table XLI the values of α from the two programs are summarized for each gage type.

Scatter in α values in Table XL, within any group of the same gage type is most extreme for those groups which include some gages with low insulation resistance to ground at service temperature (gages B16-1, B16-2, C18-2, C24-1). For those groups the 2-sigma scatter of all determinations was as high as $380 \times 10^{-6} K^{-1}$, as shown in the "all gages" summary column in Table XLI. If the gages with low insulation resistance are excluded, the 2-sigma scatter within any one gage type is $71 \times 10^{-6} K^{-1}$, as shown in the "Gages Off Ground" column. This remaining scatter is small compared with the scatter of all gages, but still large compared with expected random error of measurements (about $+10 \times 10^{-6} K^{-1}$ based on the ohmeter precision). It may be concluded that additional factors such as variable and temperature dependent contact resistances at the lead-wire-to-lead-film attachments are important sources of non-repeatability in α measurements.

Of particular interest is the indication of negative values of α for at least some cycles of six of the fourteen gages in Table XL.

Four of these six gages with negative α in Table XL are the gages with low insulation resistance (B16-1, B16-2, C18-2, C24-1); three of these four show large negative values of α during every temperature cycle and the fourth shows large negatives values during some cycles. The implication is that in these four gages the shunting of the gage due to low insulation resistance can increase with temperature so much that the measured gage resistance decreases, resulting in an indicated negative α.

The other two gages with negative values of α (A2A-2 and A8A-2) had high insulation resistance. In these cases α is less strongly negative (around $-21 \times 10^{-6} K^{-1} + 40 \times 10^{-6} K^{-1}$) and not wildly different from the average of all four Type A gages ($+7 \times 10^{-6} K^{-1} + 41 \times 10^{-6} K^{-1}$, in Table XLI). It is speculated that the variations in contact resistance with temperature, which are believed to have affected the scatter of all measurements of α, resulted in these moderately negative values of α for two Type A gages.

TABLE XLI

COMPARISON OF   MEASUREMENTS IN
COMPONENTS PROGRAM AND GAGE PROGRAM

Gage Type	Values from Components Program (Table XXXI) $10^6\alpha$ (K⁻¹)	Value from Gage Program (Table XL)							
		All Gages				Gages off Ground*			
		$10^6\alpha$ (K⁻¹)	2s	n	No. of Gages	$10^6\alpha$ (K⁻¹)	2s	n	No. of Gages
A	101	7	41	38	4	7	41	38	4
B	88	-124	57	12	2	-	--	--	-
C	--	0	380	28	4	75	58	12	2
D	122	156	71	12	2	156	71	12	2
E	--	116	30	15	2	116	30	15	2

*i.e., shunting due to insulation, (1 - R/a), less than 11%

s = standard deviation (sigma)
n = number of determinations used in calculating s
"Gages off Ground" are those for which the shunting factor, 1-R/a, is less than 11%.

The α values measured on the flat bars in the Gage Program differ from the values measured on the blades in the Components Program by amounts varying from $+34 \times 10^{-6}$ K⁻¹ (for Type D) to -94×10^{-6} K⁻¹ (for Type A). These differences may be partly the result of using actual blades of complex shape in the Components Program. Thermally induced strains could occur in the blades during thermal cycling and affect the measurement.

More puzzling is the large difference in measured α from gage type to gage type in the Gage Program (Table XLI). The differences are in the direction which would be expected on the basis of mismatches of temperature coefficients of thermal expansion between gage material and bar material, but the differences are ten times larger than expected. For example, the measured α of the Type A gage system might be expected to be lower than the measured α of Type C by about 6×10^{-6} K⁻¹, because the temperature coefficient of linear expansion (σ) of the AMS4928 bar material is lower than the σ of the Incoloy 901 by about 6×10^{-6} K⁻¹, but measured α of Type A is found to be 68×10^{-6} K⁻¹ lower. Similarly, the α of Type C, D, and E gage systems should all be about the same, but in fact there is a measured difference of $+41 \times 10^{-6}$ K⁻¹ from C to E and $+81 \times 10^{-6}$ K⁻¹ from C to D.

It would therefore appear that the combinations of bar material, NiCoCrAlY layer, insulation and overcoat material, and gage material result in net values not predictable on the basis of simple linear combinations of α and σ for the gage and bar materials. A detailed analysis of the three-dimensional layered structure, using composite beam theory, would probably be useful.

In thin film gage systems intended for static strain measurement it would be important to investigate this α behavior further and to develop a model for reasonably accurate prediction of the apparent strain (α/G) due to temperature. In the present thin film gage systems intended for dynamic strain measurement, the uncertainty due to the unexpected behavior of α is small. For example, the apparent gage factor uncertainty in Equation 4 is less than +3 percent for uncertainty in α of $\pm100 \times 10^{-6}$ K^{-1} from room temperature to 900K. The results in Table XL show that uncertainty for any one of the five gage types (A, B, C, D, E) is considerably less than this.

7.7 FATIGUE TEST RESULTS

Gages Tested

Fatigue tests were performed on 14 thin film strain gages. All of these gages had previously completed the gage factor testing described in Section 7.5. All but two had also been subjected to (and had completed) the thermal cycle testing described in Section 7.6.

The 14 gages fatigue tested are identified in the fabrication and test matrix of Table XXXII and also in the short-form test matrix of Table XXXVI. Five were Type A gages, one Type B, four Type C, two Type D, and three Type E. These tests met the objective of fatigue testing of at least two gages each of Type A, C, D, and E, and one of Type B, at room temperature and at service temperature.

The fatigue test procedures are described in Section 5.7. A combination of a steady strain and an alternating strain was applied. Testing extended to 10^7 cycles of alternating strain or until failure occurred, whichever happened first. Failure was defined as a change of 10 percent in indicated amplitude of alternating strain or a signal-to-noise ratio of less than one at the strain gage bridge output.

Published fatigue data for the blade materials used indicated that 10^7 cycles of fatigue life should be attained at combined steady and alternating strains of two to three times the levels finally adopted for these tests, but in initial trials of the actual machined and polished test bars, trial test bars failed at room temperature as follows:

Bar Material	Bar No.	Microstrain	No. of Cycles to bar failure
AMS 4928	A13	1000 + 1500	0.01×10^7
AMS 4928	B9	1000 ∓ 1500	0.01×10^7
Incoloy 901	Spare	900 ∓ 450	0.10×10^7
AMS 4928	A2A	500 ∓ 750	0.87×10^7

As a result, a more conservative standard level (300 + 450 microstrain) was used throughout the balance of testing unless otherwise noted. No further failure of test bars occurred.

Results

The results of the fatigue tests are summarized in Table XLII.

The table lists the number of fatigue cycles completed and the percent increase in gage resistance (R) during testing at each temperature. Footnotes in the table identify special events and failure modes.

No gage grid open circuits or short circuits or gage-grid delamination developed during the fatigue testing. The only failures encountered were at the 900K temperature level and were traced to lead wire attachment problems.

TABLE XLII

THIN FILM STRAIN GAGE FATIGUE TEST RESULTS

Gage No.	Results at 300K		Results at 600K		Results at 900K	
	Fatigue Cycles Completed	Percent Increase in R	Fatigue Cycles Completed	Percent Increase in R	Fatigue Cycles Completed	Percent Increase in R
A1-1			1×10^7	0.6		
A2A-1	0.87×10^7#					
A2A-2	0.87×10^7#					
A8A-1	1×10^7	3.7	1×10^7	1.1		
A8A-2	1×10^7	2.0	1×10^7	0.8		
B16-2	1×10^7	1.1	1×10^7	1.3		
C17-1	1×10^7	0.3			0.070×10^7	X
C18-2	1×10^7	5.6*			0.440×10^7	X
C24-1	1×10^7	0.4			0.003×10^7	X
D31-1	1×10^7	6.1			0.077×10^7	X
D31-2	1×10^7	3.9*			0.001×10^7	X
E33-1	1×10^7	0.3			1×10^7	2.1
E33-2	1×10^7	1.9			0.370×10^7	X
E36-2					0.014×10^7+	X

Notes:
+ Previously gage factor tested at 1100K
* Lead wire attachments repaired
X Lead wire attachments failed; not repairable
Bar A2A cracked at 0.87×10^7 cycles, 500 ± 750 microstrains

R = gage resistance (ohms)
Applied strain in all tests was 300 ± 450 microstrain, except for bar A8A (300 ± 370 microstrain) and bar A2A (500 ± 750 microstrain).

The fatigue life of the 600K thin film gage systems (including the lead-wire-to-film attachments) was excellent. No repairs were required in these Type A and B systems and all six samples tested survived either to 10^7 cycles or, in the case of bar A2A, to bar failure (0.87 x 10^7 cycles) at room temperature. Four of the six samples were tested to 10^7 cycles at both room temperature and 600K, without failure.

The fatigue life of the 900K thin film gage systems was limited (at 900K) by the life of the lead-wire-to-film attachments. All samples survived 10^7 cycles at room temperature without failure (although two required repair of lead wire attachments during the course of testing) but only one (E33-1) of eight tested at 900K survived the full 10^7 cycles. In all others, the lead wire connection resistance became large and erratic after 10,000 to 3,700,000 cycles, and attempts at repair by scraping and recementing then resulted in either shorting of the lead films to ground or delamination of the lead films.

Measured gage resistance (R) of all gages increased only gradually during fatigue testing. The largest change in R over 10^7 cycles (Table XLII) was 3.7 percent for any Type A or B gage and 6.1 percent for any Type C, D, or E gage, for all cases in which lead wire attachments survived.

At 900K, the durability of lead wire attachments on Type E strain gage systems was better than on Type C or D systems. The special roughened Al_2O_3 surface in the Type E system is apparently conducive to improved fatigue life in the lead wire attachments using the conductive cement.

7.8 SPIN TEST RESULTS

Gages Tested

Three thin film strain gages on test bars (A3-1, C19-1, C19-2) were mounted on a spin disk and spin tested at 100,000G centripetal acceleration for one hour. The test method is described in Section 5.8. The gages spin tested were fabricated on the special test bars of Figure 14. These gages were not subjected to gage factor testing, extensive thermal cycling, or fatigue testing. The gages spin tested are identified in the fabrication and test matrix of Table XXXII and in the short form test matrix of Table XXXVI. These tests met the objective of spin testing sample gages designed for 600K service and 900K service.

Results

The three gages remained mechanically adherent and electrically stable throughout the one hour exposure in the 100,000G environment. Lead-wire-to-film attachments showed no deterioration. Resistance to ground remained in the high megohm range.

The only unusual occurrence was a break in one lead wire (from gage C19-2) near the disk hub after 20 minutes at 100,000G. Post-test examination showed that a 15-cm length of this lead wire had disappeared entirely leaving an empty tunnel under the cement on the disk surface. The lead wire had been routed outward from hub to rim along a straight radial path. Failure of the encapsulating cement to adhere firmly to the lead wire resulted in tensile stress in the lead wire near the hub on the order of 7×10^5 kPa (10^5 psi), exceeding the breaking strength. This type of failure can be avoided by employing a sinuous routing of lead wires (rather than direct radial routing) to increase the frictional drag of the encapsulating cement along the wire path.

The stable behavior of the gage systems in the 100,000G environment is illustrated in Figure 36 where plots of gage resistance versus temperature and temperature versus speed are presented. The data points in Figure 36 are numbered in chronological order. Figure 36a shows that the disk temperature increased from room temperature to about 335K during initial acceleration from zero rpm (point 1) to 17,450 rpm (point 2). The temperature increased further during the one hour at 17,450 rpm (points 2 through 11) and then decreased during the deceleration to zero rpm at the end of the spin test. The resistance of each of the three gages tracked the temperature changes (Figures 36b, c, d), each gage resistance changing by about 180×10^{-6} K^{-1}. Final resistance readings at room temperature were about 0.2% higher than initial readings at room temperature for gage systems A3-1 and C19-1. In the case of gage C19-2, the final reading at room temperature on the disk was not obtained due to the missing lead wire.

The steady-state strain in the thin film strain gages at the 100,000G test condition was calculated to be approximately 0.05 percent, and the expected change in gage resistance due to strain therefore about 0.10 percent, or about 0.25 ohms. This change accounts for ten percent of the change in resistance observed during the acceleration from point 1 to point 2 in Figure 36.

7.9 EROSION TEST RESULTS

Gages Tested

Fifteen thin film strain gages on test bars were subjected to accelerated erosion testing by the method described in Section 5.9. The erosion is produced by a controlled high-speed stream of Al_2O_3 powder. Gage resistance and resistance to ground are measured every few seconds.

Seven of the fifteen gages tested had previous extended exposure to +1000 microstrain and -1000 microstrain at service temperature during gage factor tests. The other eight gages tested had seen no previous high-strain testing (other than spin tests of three gages at about 500 microstrain) or high-temperature testing (other than the soak at service temperature during fabrication).
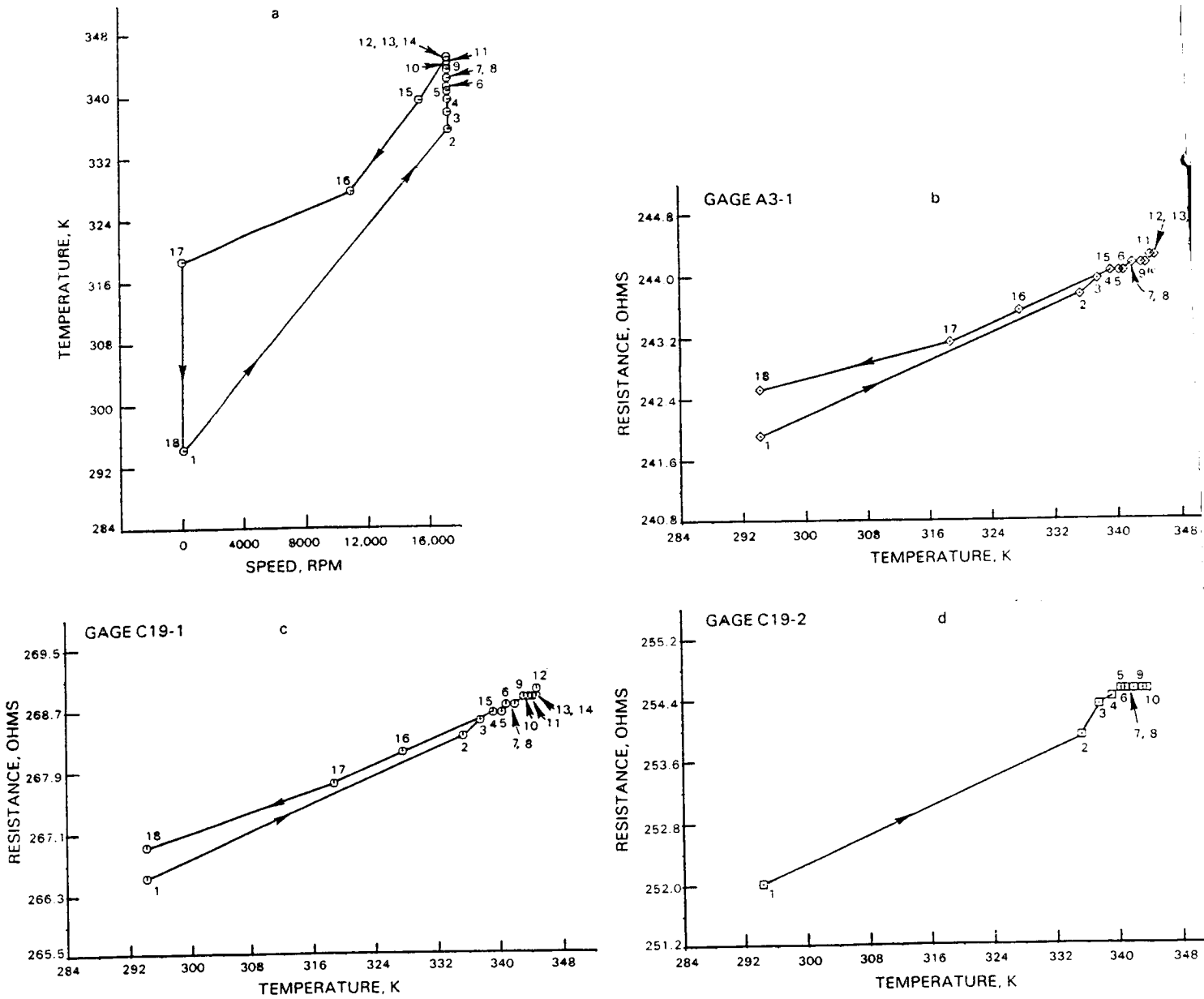
Figure 36   Spin Test Data.   (a) Temperature versus Speed;   (b), (c), (d) Gage
Resistances versus Temperature.   The three thin film strain gages
are well behaved during the spin test which includes 1 hour at
100,000G   (17,450   rpm).   The   test   points   are   numbered
chronologically.

The gages erosion tested are identified in the fabrication and test matrix of Table XXXII and in the short form test matrix, Table XXXVI. Seven gages were Type A, one was Type B, six were Type C, and one was Type E. These tests therefore met the objective of erosion testing of 600K candidates and 900K candidates.

No Type D gages on test bars were erosion tested. Several Type D gages which had been expected to be available for erosion testing (notably D22, D25, D26, and D32, in Table XXXII) were rejected in fabrication during a period when the adherence difficulties described in Section 7.1 were encountered in the fabrication of Type D gages. The adherence difficulties were later overcome, but not in time for erosion testing.

The reference base line used for erosion performance was the erosion rate of 2 μm Pt-10% Rh films on oxidized NiCoCrAlY, without overcoat, the same base line used in the erosion tests of thin film gages on blades previously described in Section 5.9. Four additional reference films were erosion tested to verify the base line. The results of all erosion tests on test bars (including the additional reference films) are presented here.

Results

Figure 37 presents plots of percent change in gage resistance versus time for the fifteen gages and four reference films during erosion testing of thin film gages on test bars. To permit ready comparison with previous results of Figures 26 and 27, erosion testing on the blades in the Components Program, the black diamond symbol marked "REF" is added in Figure 37. This symbol identifies the pass-fail benchmark established by the reference films in the Components Program: 20 percent resistance change in 60 seconds.

In Figure 37, seven of the fifteen gages tested show better durability than the reference films. A review of the test matrix in Table XXXVI reveals that these seven gages are the seven which were previously gage-factor tested.

To clarify this result, numerical erosion results are summarized in Table XLIII. Percent resistance change in the first 60 seconds is listed for each gage. The seven gages previously gage-factor tested are listed in the first column; all seven show excellent erosion durability. In fact, six of the seven show no measurable change in gage resistance in the first 60 seconds. The eight gages not previously gage factor tested are listed in the second column. All but one of these show poor erosion durability. Either shorting to ground or more than 20 percent increase in gage resistance occur within the first 60 seconds.

Further comparison of Table XLII and XXXII shows that there is no strong correlation between erosion durability and either surface finish procedure or insulation resistance rating as sputtered.

It may be concluded that Type A, B, C, or E gages which have been subjected to a few alternating strain cycles to +1000 microstrain, at service temperature, without significant drift or damage, can be expected to display excellent erosion durability. Based on this experience and on experience in the erosion tests in the Components Program, the same result can be expected for Type D gages.
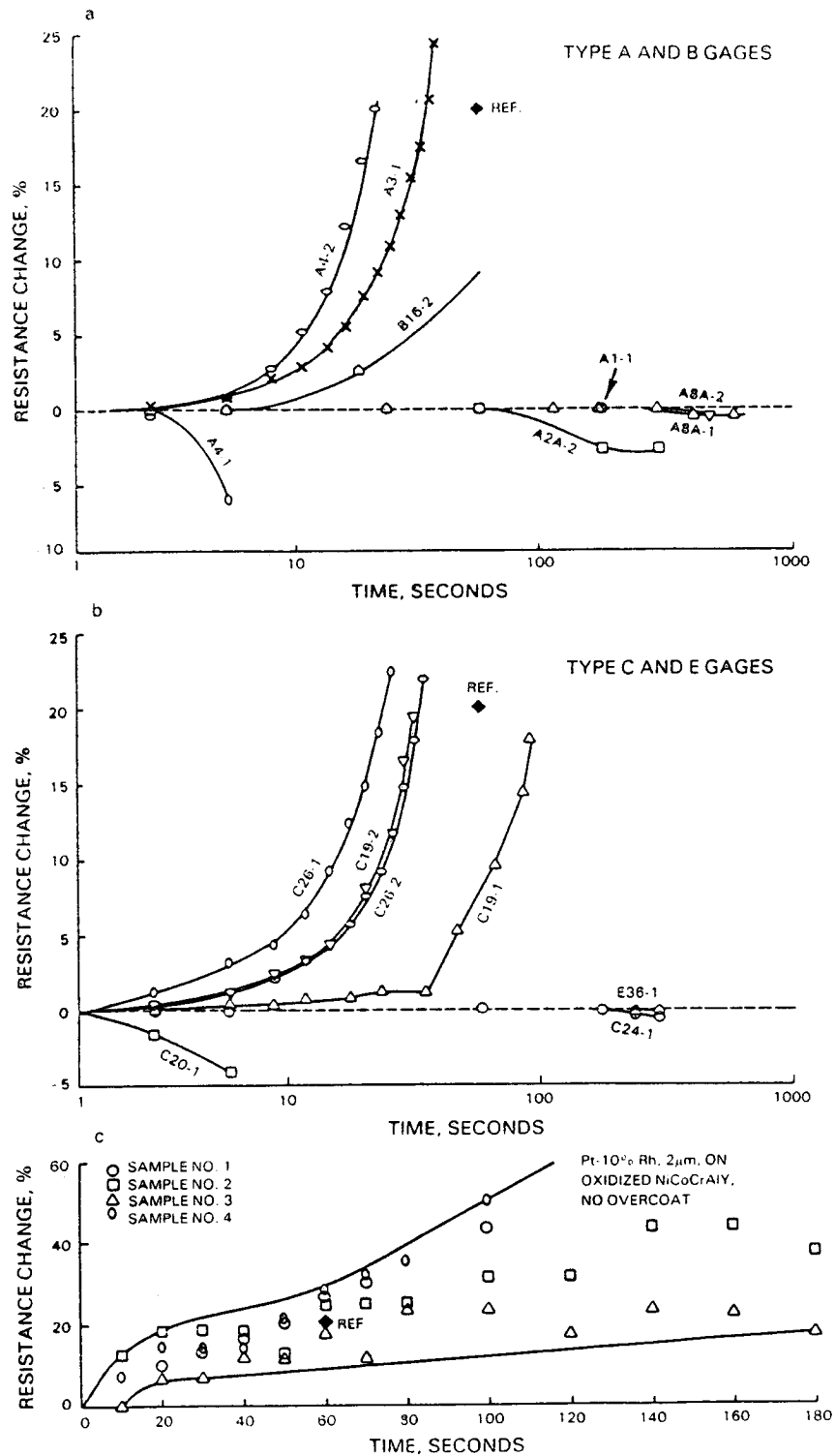
Figure 37 Erosion Test Data. (a) Type A and Type B Gages; (b) Type C and Type E Gages; (c) Reference Pt-10%Rh Films.

TABLE XLIII

EROSION TEST RESULTS

	Percent Resistance Change in 1 Minute	
Gage No.	Gages Previously Gage-Factor Tested at Service Temperature	Gages Not Previously Gage-Factor Tested
A1-1	0	
A2A-2	0	
A3-1		> 20
A4-1		Shorted
A4-2		> 20
A8A-1	0	
A8A-2	0	
B16-2	9	
C19-1		8
C19-2		> 20
C20-1		Shorted
C24-1	0	
C26-1		> 20
C26-2		> 20
E36-1	0	

There is no indication that exercising a thin film strain gage to +1000 microstrain at service temperature enhances durability, but only that the successful exercise demonstrates durability.

These results indicate further that a valid screening test for quality of fabricated gages is to apply at least two cycles of alternating strain from -1000 to +1000 microstrain, at room temperature and again at gage service temperature. Gages which survived this strain testing in the present program later demonstrated good stability through 50 thermal cycles, through 10^7 fatigue cycles at room temperature and service temperature, and through the accelerated erosion testing.

7.10 POST-TEST EXAMINATIONS

After the completion of each kind of testing (gage factor, thermal cycle, fatigue, spin, erosion), the thin film strain gage systems on test bars were visually examined with a microscope at 10X to 100X. In almost all cases the only visible signs of distress were in the region of the 900K lead-wire-to-film attachments, where cracking of the cement at 900K resulted in physical damage to the lead films. In the region of the gage grid films, the film systems were generally in excellent condition, including insulation, gage, and overcoat films (except for some erosion test damage discussed later).

Figure 38 presents post-test photographs (at the end of all tests) of all but two of the thin film strain gages tested in the Gage Program. The legend adjacent to each gage in the figure summarizes the test history for each gage (cross referencing to the test matrix in Table XXXVI). The physical appearance of the gages, insulating films, and overcoat films is generally excellent.

Four gages developed an open circuit in the gage grid during gage-factor testing (starred items). In two of these cases (bar A7) no physical damage to the gage grid is visible. In the other two cases (bar C23) obvious spalling of the overcoat and gage alloy film occurred.

In the case of the 15 gages erosion tested, erosion damage is generally visible, in the form of a sandblasted surface appearance (bars A3, A4, C19, for example) or a chipped or pock-marked surface appearance (bars A1, A8A, C20, C24, E36, for example). In the cases where high gage resistance or low insulation resistance developed during erosion testing (underlined items), the erosion damage is not generally more severe in appearance than average.

7.11 OVERALL REVIEW OF RESULTS BY GAGE TYPE

The relative performance of the five gage types (A, B, C, D, E) in the Gage Program may be assessed by focusing attention on the following three failure modes:

    a.   Low insulation resistance to ground under gages or lead films during fabrication.

    b.   Gage adherence failures during fabrication or during conditions of combined high strain and high temperature.

    c.   Deterioration of lead-wire-to-film attachments during 900K testing, leading to unrepairable open circuits or unrepairable short circuits in the lead film system.

In the Gage Program, the first of these failure modes occurred only during fabrication and the second only during fabrication or during gage factor testing. (There were no gage grid failures during thermal cycling, fatigue, spin, or erosion testing.) The third failure mode, deterioration of the lead-wire-to-film attachments, occurred during the 900K gage factor testing and extensively during 900K fatigue testing.

In the light of this experience, the potential for success in engine testing for the five gage types may be judged fairly on the basis of the performance of the bars fabricated using the methods which resulted in successful gage factor testing, plus an assessment of lead-wire-to-film attachment during 900K fatigue testing.

Of the 168 thin film strain gages fabricated during the Gage Program (Tables XXXII and XXXIII) gage-factor tests at service temperature were completed successfully on 21. The history of the particular 52 fabrication trials using the methods which resulted in these 21 successful gages is contained in Table XXXII and is summarized briefly in Table XLIV. Examination of Table XLIV leads to the following rankings, based on the highest percentages without failure listed in the right-hand column in the table.
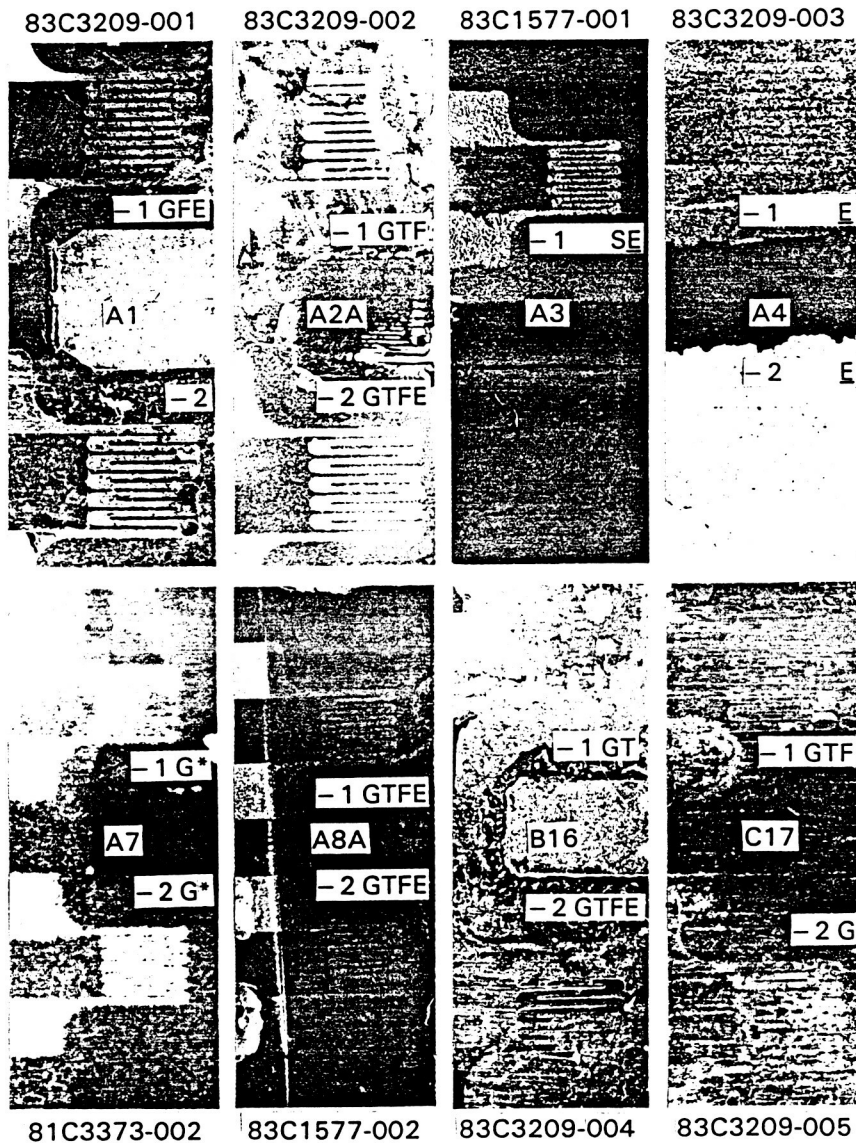
Figure 38   Post-Test Photographs of Thin Film Strain Gages, After Completion of All Tests. There are open circuits in four gage grids (starred items). Legend: G, Gage Factor Tested; T, Thermal Cycle Tested; F, Fatigue Tested; S, Spin Tested; E, Erosion Tested; E, Failed During Erosion Test.
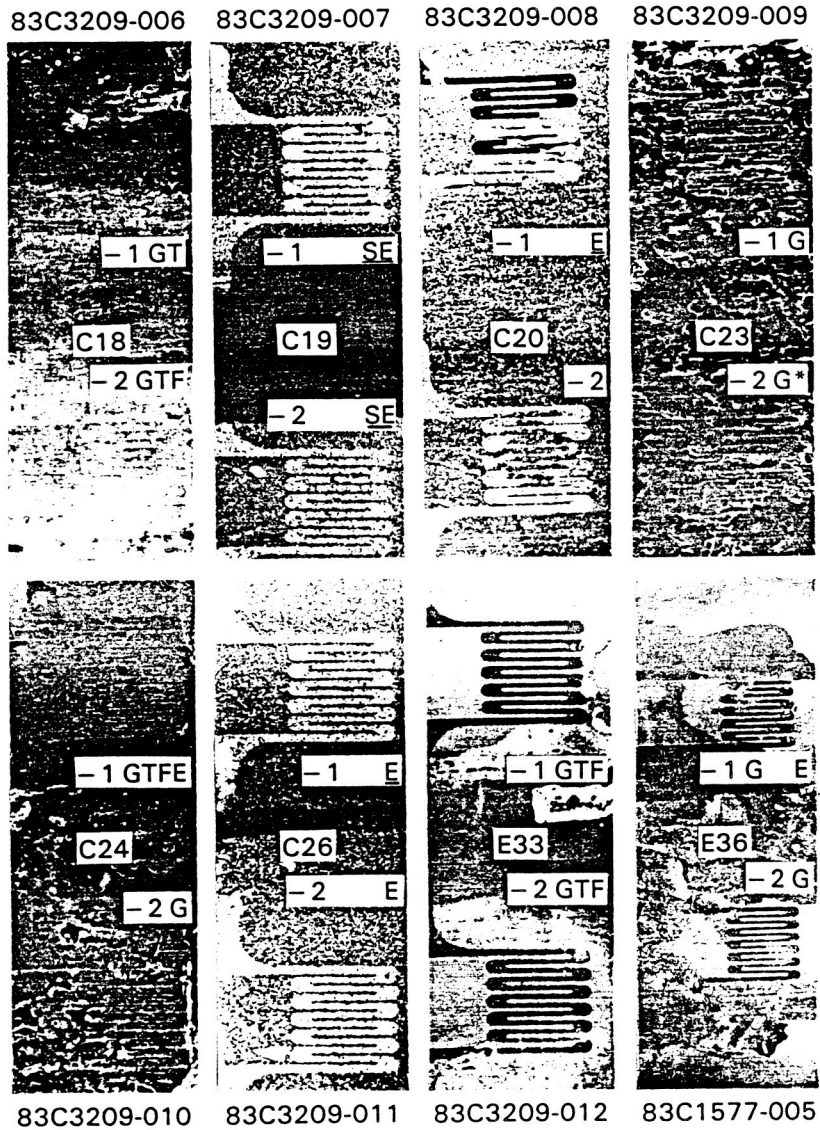
Figure 38   Post-Test Photographs of Thin Film Strain Gages, After Completion
of All Tests. There are open circuits in four gage grids (starred
items). Legend: G, Gage Factor Tested; T, Thermal Cycle Tested; F,
Fatigue Tested; S, Spin Tested; E, Erosion Tested; E, Failed During
Erosion Test.

TABLE XLIV

PERCENT WITHOUT FAILURE IN GAGE-FACTOR TESTS
BY GAGE TYPE AND BY FABRICATION METHOD

Item	Gage Type	Blade Material	Max. Test Temp. (K)	Fabrication Notes Surface Finish	Stripping Solvent	Number of Gages Sputtered	Completed Gage-Factor Test Without Failure	Principal Failure Mode	Percent Without Failure
1	A	AMS 4928	600	a		8	1	v	12
2	A	AMS 4928	600	b		4	4	None	100
3	B	AMS 4928	600	a		8	2	v	25
4	B	AMS 4928	600	b		4	0	v	0
5	C	Incoloy 901	900	b,i		8	6	v	75
6	D	Incoloy 901	900	b,c,d	k	12	2	v	17
7	D	Incoloy 901	900	b	l	4	2	w	50
8	E	MAR-M200+Hf	900	Ref. 4	l	2	2	None	100
9	E	MAR-M200+Hf	1100	Ref. 4	k	2	2	None	100
Totals						52	21		

NOTES:

a = Shop polish
b = Hand polish
c = 600 grit polish
d = UTRC polish

i = Sputter etched
k = Stripped in alkali
l = Stripped in acetone
v = Gage adherence failure
w = Gage shorted

On AMS 4928 titanium alloy compressor blades for service to 600K, the Type A gage (Ni-30Cr on Si_3N_4) can be recommended over the Type B gage (Cu-45Ni on HfO_2) without reservation. Once the fabrication problems of Type A gages (line item 1 of the table) were overcome, the fabrication and gage-factor testing of Type A gages proceeded with no failures (line 2 of the table). For the Type B gages, the fabrication problems were more complicated and were never overcome (lines 3 and 4 of the table).

On Incoloy 901 nickel steel alloy compressor blades for service to 900K, the Type C (Ni-30Cr on Si_3N_4) gages and the Type D (Ni-30Cr on Al_2O_3) gages are both reasonably good performers. Type C (line 5 of the table) has the edge. After the adherence problems of Type D gages (line 6) were overcome, the failure rate during fabrication of Type D remained at 50 percent, principally due to low insulation resistance to ground during fabrication. Further development of lead-wire-to-film attachment is recommended for the Type C and D gages. Durability of these attachments at 900K in the Type C and D gage systems tested was as little as 10 slow thermal cycles in some cases, and as little as 10^4 strain fatigue cycles in some cases.

On MAR-M 200 + Hf (PWA 1422) turbine blades the Type E gage tested (Ni-30Cr on special Al_2O_3) performed well as shown in the bottom line of the table. There were no failures in fabrication (when the approved method was used) and all samples performed well in the tests, including gage factor tests to 1100K. The durability of the lead-wire-to-film attachments was somewhat better for Type E than for the Type C and D gages, ranging upward from 33 slow thermal cycles and from 10^5 strain fatigue cycles, but further development of the lead-wire-to-film attachment is recommended.

A final brief summary of failure mode versus gage type is presented in Table XLV. The table emphasizes that there are no major problems anticipated in applying Type A thin film strain gages to AMS 4928 compressor blades in engine tests and that the only serious problems remaining in routine use of Type C gages on Incoloy 901 blades or Type E gages on nickel-based superalloy turbine blades is the limited durability of lead-wire-to-film attachments above 600K.

TABLE XLV

SUMMARY OF FAILURE MODE VERSUS GAGE TYPE

| Gage Type | Notes on Failure Modes | | |
	Shorts	Adherence	900K Lead Wire Attachment
A			
B		Unsolved Problem	
C		Occasional Problem	Improvement Needed
D	Improvement Needed		Improvement Needed
E			Improvement Needed

SECTION 8.0

CONCLUDING REMARKS

The objective of the program was to develop thin film strain gages suitable for compressor and turbine blade dynamic strain measurements in turbojet engines, with potential for higher accuracy and better durability than attained with conventional wire gages.

Thin-film resistive strain gages of 2 millimeter (0.08 inch) gage length and 10 micrometer (0.0004 inch) thickness, including insulation and protective overcoat, were developed and demonstrated on blades in bench tests. Since the installations are about 30 times thinner than conventional wire strain gage insulation, any alteration of the aerodynamic, thermal, or structural performance of the blade is correspondingly smaller. Accuracy higher than that attained with conventional gages is therefore expected. The low profile and strong adherence of the thin film elements is expected to result in improved durability over conventional gage systems in engine tests.

In the development program, candidate thin film gage systems employing combinations of two selected blade materials, two surface finishes, four gage materials, and four insulation and protective overcoat materials were fabricated and tested directly on real and simulated high-pressure compressor blades at 600K and 900K. One type of gage system was further demonstrated successfully on simulated turbine blade material specimens at 900K and 1100K. Eight different methods of lead-film-to-lead-wire attachment were evaluated briefly.

Each type of gage system developed consists of an insulating film substrate sputtered directly on the compressor blades (or over oxidized alumina-forming coatings on turbine blades), a sputtered metal film strain-sensing element, a protective sputtered overcoat film of the same material as the insulating film, sputtered lead films running from the strain-sensing element to the lead-film-to-lead-wire connection, and the lead-film-to-lead-wire connection. All films are deposited by radio-frequency sputtering.

The durability of the gage elements, insulation, overcoats, and lead films was demonstrated to be excellent to 1100K (limit of tests) but the fatigue life of lead-film-to-lead-wire attachments was limited above 600K. The thin film strain gage systems are ready for use in routine dynamic stress surveys in engine tests with an expected life of 50 hours at 600K. Further development of lead-wire attachment methods above 600K is required to extend the expected life at higher temperatures to 50 hours or more.

The thin-film strain gage development program was divided into two phases. The first phase was designated the Components Program and the second phase the Gage Program.

In the first phase, the Component Program, candidate materials and thin-film fabrication procedures were selected and tested. The selection was made on the basis of the principles governing physical, chemical, electrical, and structural behavior of materials.

The review included a detailed study of guidelines for formulating strain-gage alloys to achieve high stability (of metallurgical and electrical properties) and a low temperature coefficient of resistance, both required for good performance in a strain gage. The only promising alloys were found to be concentrated solid solutions of high-melting, face-centered cubic transition metals. Concentrated alloys of this kind are inherently hard and not workable in wire form, but are readily sputtered as thin films.

The geometrical parameters of thin film gage systems were analyzed to provide design curves for selection of film thicknesses to achieve a desired gage resistance and insulation resistance.

As a result of the review, the trial surface finishes selected were 0.1 micrometer polish, and 0.1 micrometer polish roughened with light grit blast; the trial insulating materials selected were A_2O_3, HfO_2, Si_3N_4, and SiO_2, the trial gage materials selected were Ni-30%Cr, Cu-45%Ni, Pt-20%W, Pd-30%Mo and the lead wire attachment methods selected were brush plating, resistance weld, braze, laser weld, ultrasonic weld (including ball bond), flame spray, hot compression bond, and conductive cements.

A systematic experimental program was then carried out to complete the Component Program. The sixteen combinations of insulating layers and surface finishes were fabricated and tested on actual compressor blades of AMS 4928 titanium alloy and Incoloy 901 nickel steel. The 11 best combinations were then used as substrates for each of the four candidate gage materials, resulting in a test matrix of 44 types of thin-film strain gage system on blades. Tests of the 44 types resulted in selection of four candidates, two for service to 600K on the titanium alloy blades and two for service to 900K on steel alloy blades. The best blade surface finish in all four cases was the 0.1 micrometer polish. The two 600K systems, designated Type A and Type B, utilized Ni-30%Cr gages on Si_3N_4 insulation material, and Cu-45%Ni gages on HfO_2 insulation, respectively. The two 900K systems, designated Type C and Type D, utilized Ni-30%Cr gages on Si_3N_4 and on Al_2O_3, respectively.

The experiments during the Components Program characterized the insulating films and gage alloys as described in the next paragraphs.

All four insulating film materials in the Components Program, when sputtered to a thickness of 4 μm or more, prove to be adherent, hard, and mechanically durable, surviving repeated temperature cycling to design temperature on both blade materials (600K on AMS 4928 and 900K on Incoloy 901). Some isolated cases of local minor delamination or spalling of Si_3N_4 did occur. Resistivity was above 10^6 ohm-cm and dielectric breakdown voltage above

10^4 v/cm for all films. Aging for two years had no significant effect on the films. On the roughened surfaces, local short circuits to ground were common. Increasing the film thickness helped in most cases, but in the case of Al_2O_3 (on either roughened blade material) and HfO_2 (on roughened AMS 4928) short circuits occurred even with thickest films and the use of these particular combinations of insulation film and roughened surface was ruled out.

The behavior of each gage alloy film material during the Components Program was also strongly influenced by the blade surface roughness. The noble metal gages (PtW and PdMo) were adherent only on the roughened blades. Gage resistances of all alloys were higher on roughened blades than on smooth blades by a factor of about two. Short circuits to ground were a common problem on roughened blades after sputtering of gages even though probing of the insulating film surface before sputtering of gages showed no leakage to ground. (The only short circuits experienced on smooth blades occurred with Al_2O_3 insulating films.)

Oxidation of uncoated gage films was severe at 900K. Uncoated PdMo and CuNi gages disintegrated completely due to oxidation during a one-hour exposure at 900K. Uncoated NiCr and PtW gages were visibly oxidized at 900K but stabilized after 5 hours. Overcoating with a film of the insulating material was surprisingly effective in reducing the oxidation rate. The bright metallic luster on CuNi and NiCr gage films was preserved at 900K in the overcoated areas.

Adherence of gage films was generally good as sputtered (with the notable exception of all PdMo and PtW gages on smooth surfaces) and remained good at 600K. Among gage films cycled to 900K, and not destroyed by oxidation or shorted to ground, only four combinations remained adherent, as follows: NiCr on rough Si_3N_4, NiCr on smooth Si_3N_4, NiCr on smooth Al_2O_3, PtW on rough Si_3N_4.

Segregation of the tungsten (W) in the PtW gages during sputtering resulted in an unacceptably high temperature coefficient of resistance. The PtW gages were not continued in the program, but are not ruled out for further evaluation.

The overcoat also provided excellent erosion protection.

The lead-film-to-lead-wire connection technique which produced the best results was the use of conductive cement. A silver-filled polyimide cement was developed for use to 600K, and a nickel-filled ceramic cement was developed for use above 600K. Ultrasonic welds and laser welds showed promise, but these techniques were not developed during the program to the point where results were reliable and repeatable.

In the second phase, the Gage Program, the four gage types (A, B, C, D) were fabricated, on flat test specimens of the compressor blade materials, and tested. A modified Type D gage installation (Type E) was fabricated on flat test specimens of MAR-M200 + Hf turbine blade material, and tested. The total number of thin film strain gages fabricated in the Gage Program was 168.

The tests in the Gage Program for each of the five gage types included measurement of gage factor versus temperature, apparent strain versus temperature, durability and drift during fifty thermal cycles (each cycle including 20 minutes at design temperature), fatigue at room temperature (10^7 strain cycles), fatigue at design temperature (10^7 strain cycles), the and effect of erosion at room temperature. In addition, samples of Type A and Type C gages were subjected to a one-hour spin test at 100,000G at room temperature.

Principal conclusions derived from the results of the testing are as follows:

o On compressor blades of the titanium alloy AMS 4928, for service to 600K, the Type A thin film strain gage is recommended. After initial fabrication problems were overcome in the Gage Program, fabrication and testing of these Type A gages proceeded with no failures. For the competing Type B gages, fabrication problems were never overcome.

o On compressor blades of the nickel steel alloy Incoloy 901, for service to 900K, the Type C and Type D gages performed well to 900K, but expected service life in engine tests is limited to a few hours above 600K by the current lead-film-to-lead-wire attachment durability. Type C is recommended over Type D because of a much better success rate (lower cost) in fabrication.

o On simulated turbine blades of the nickel-based superalloy MAR-M200 + Hf, the Type E thin film strain gages performed well to 1100K (limit of tests) and were notably free of fabrication problems, but, like Type C and D, expected service life in engine tests is limited by the present lead-wire attachment durability.

APPENDIX A

PHASE DIAGRAMS AND REFERENCE DATA FOR ALLOYS

Table XLVI presents the Periodic Table of Atomic Radii. Figures 29a through 39g present binary-alloy phase diagrams for Pt-Rh, Ag-Pd, Cu-Ni, Mo-Pd, Cr-Ni, Pt-W, and Al-Ti, respectively.

TABLE XLVI

PERIODIC TABLE OF ATOMIC RADII

0.32 / H / 1 ← radius (Å)

I	II											III	IV	V	VI	VII	VIII
																	0.31 He 2
1.23 Li 3	0.89 Be 4											0.82 B 5	0.77 C 6	0.75 N 7	0.73 O 8	0.72 F 9	0.71 Ne 10
1.54 Na 11	1.36 Mg 12			TRANSITION ELEMENTS								1.18 Al 13	1.11 Si 14	1.06 P 15	1.02 S 16	0.99 Cl 17	0.98 Ar 18
2.03 K 19	1.74 Ca 20	1.44 Sc 21	1.32 Ti 22	1.22 V 23	1.18 Cr 24	1.17 Mn 25	1.17 Fe 26	1.16 Co 27	1.15 Ni 28	1.17 Cu 29	1.25 Zn 30	1.26 Ga 31	1.22 Ge 32	1.20 As 33	1.17 Se 34	1.14 Br 35	1.12 Kr 36
2.16 Rb 37	1.91 Sr 38	1.62 Y 39	1.45 Zr 40	1.34 Nb 41	1.30 Mo 42	1.27 Tc 43	1.25 Ru 44	1.25 Rh 45	1.28 Pd 46	1.34 Ag 47	1.48 Cd 48	1.44 In 49	1.40 Sn 50	1.40 Sb 51	1.36 Te 52	1.33 I 53	1.31 Xe 54
2.35 Cs 55	1.98 Ba 56	1.56 Lu 71	1.44 Hf 72	1.34 Ta 73	1.30 W 74	1.28 Re 75	1.26 Os 76	1.27 Ir 77	1.30 Pt 78	1.34 Au 79	1.49 Hg 80	1.48 Tl 81	1.47 Pb 82	1.46 Bi 83	1.46 Po 84	1.45 At 85	Rn 86
Fr 87	2.20 Ra 88	Lr 103	104	105													

1.69 La 57	1.65 Ce 58	1.64 Pr 59	1.64 Nd 60	1.63 Pm 61	1.62 Sm 62	1.85 Eu 63	1.62 Gd 64	1.61 Tb 65	1.60 Dy 66	1.58 Ho 67	1.58 Er 68	1.58 Tm 69	1.70 Yb 70
2.0 Ac 89	1.65 Th 90	Pa 91	1.42 U 92	Np 93	Pu 94	Am 95	Cm 96	Bk 97	Cf 98	Es 99	Fm 100	Md 101	No 102
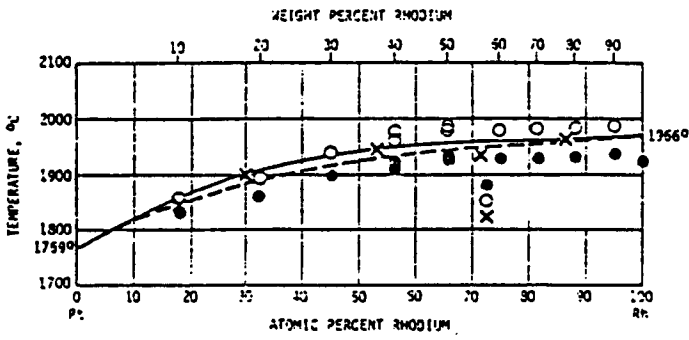
(a) Platinum-Rhodium
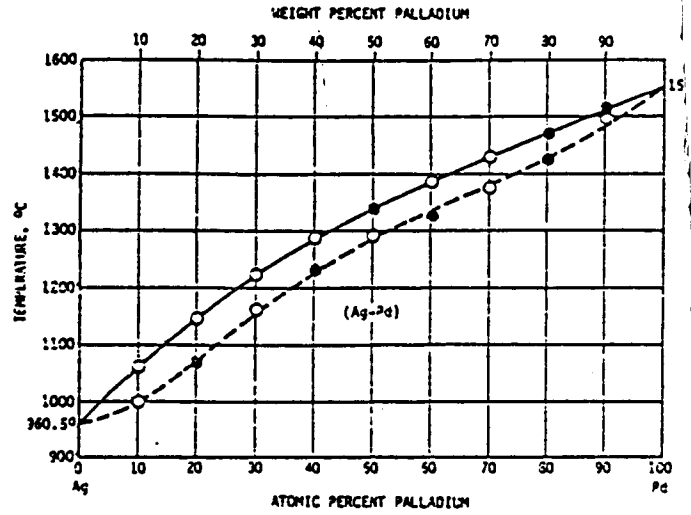
(b) Silver-Palladium
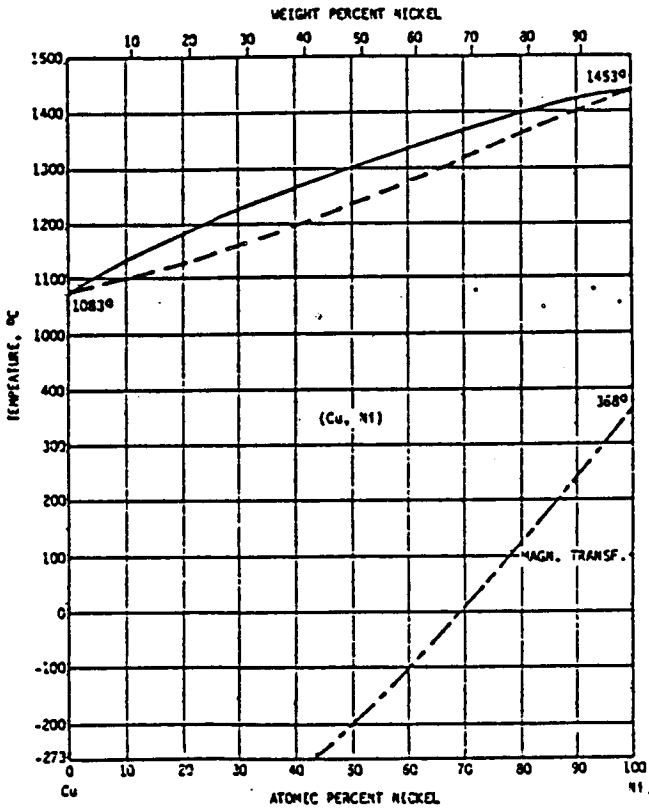
(c) Copper-Nickel
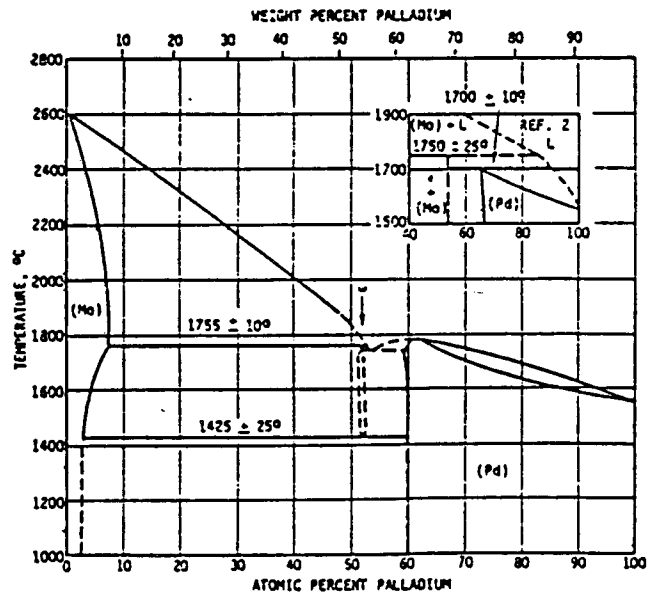
(d) Molybdenum-Palladium

Figure 39 Phase Diagrams

(e) Chromium-Nickel

(f) Platinum-Wolfram (Tungsten)

(g) Aluminum-Titanium
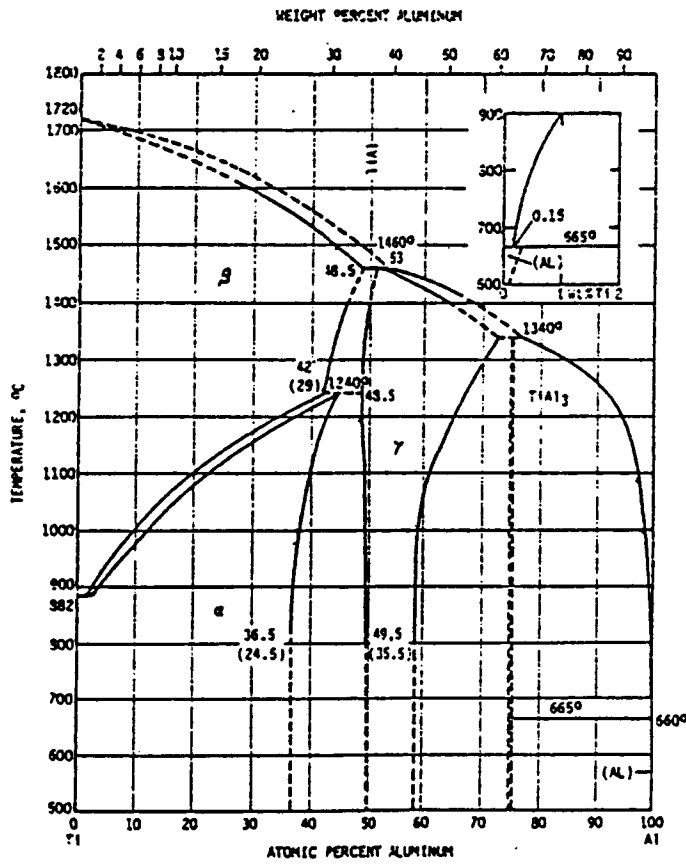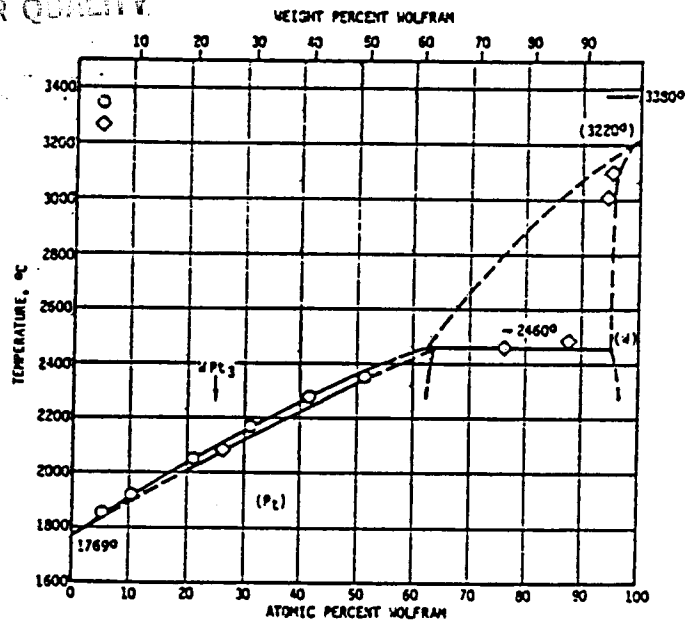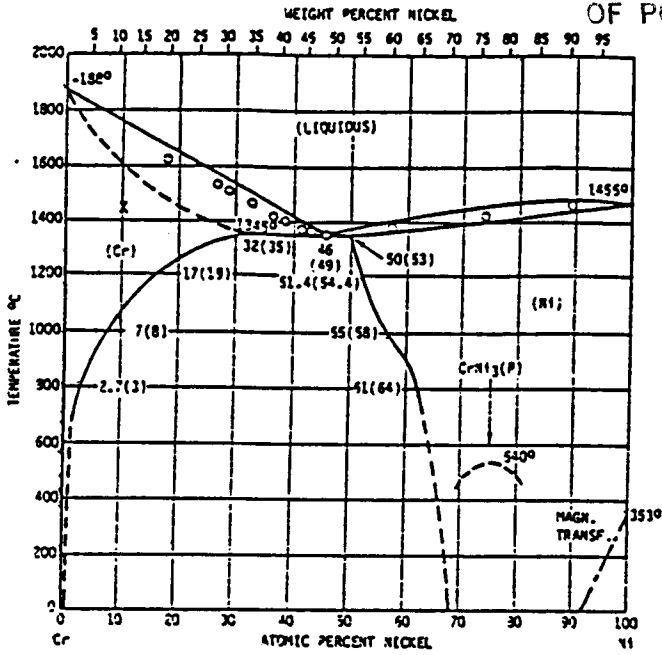
Figure 39 (Continued) Phase Diagrams

A-3

APPENDIX B

GAGE CONFIGURATION PARAMETERS

In the simplified gage pattern shown in Figure 40, the following definitions apply:

R_1 = gage resistance (ohms)
ρ_1 = gage material resistivity (ohm-cm)
n = number of lines
w = line width, equal to spacing between lines (μm)

t_1 = thickness of gage material (μm)
L = gage length, equal to gage width (μm)
Y = surface/volume ratio parameter, defined in Section 3.6 as $Y = 6.25/t_1$, where t_1 is in μm.
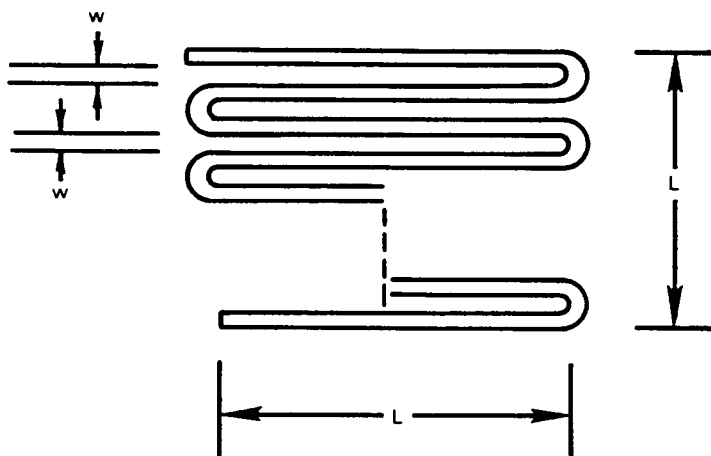
Figure 40   Strain Gage Pattern, Simplified Configuration.

A basic geometrical relationship in Figure 40 is

$$w = L/(2n-1) \qquad\qquad (B-1)$$

The definition of the surface/volume ratio parameter is

$$Y = 6.25/t_1 \qquad\qquad (B-2)$$

The definition of gage resistivity can be written as

$$t_1 = (n\rho_1 L)/wR \qquad\qquad (B-3)$$

These three relationships may be combined to yield the following convenient design equations:

$$w = L/(2n-1) \tag{B-4}$$

$$t_1 = n(2n-1) \, (\rho_1/R) \tag{B-5}$$

$$Y = [6.25/n(2n-1)] \, (R/\rho_1) \tag{B-6}$$

It is now evident that for a given gage material resistivity (ρ_1) and total resistance (R), the thickness (t_1) and surface/volume ratio (Y) depend only on the number of lines (n) and not on the gage length (L), while the line width (w) depends upon both the number of lines and gage length.

Figure 8, in Section 3.7, is a plot of w, t_1, and Y versus n (from equations B-4, B-5, and B-6) for two cases, as follows:

o   R = 200 ohms, $\rho_1 = 10^{-4}$ ohm-cm, and L = 3000 μm;

o   R = 200 ohms, $\rho_1 = 10^{-4}$ ohm-cm, and L = 2000 μm.

A striking feature of Figure 8 is the nearly square-law increase in gage thickness (and nearly square-law decrease in surface/volume ratio) as n increases. This condition results because as n increases, the gage film total length (nL) increases and gage film width [L/(2n-1)] decreases, requiring thickness to increase as n(2n-1) for a constant value of R.

APPENDIX C

GAGE FACTOR TEST DATA

GAGE NUMBER A1-1

Temperature (K)	Strain (x 10^5)	Gage Factor	2σ (Percent)	Drift μΩ/Ω
249	500	2.70	34	
	-500	3.52	189	
	1000	2.79	10.5	
	-1000	4.87	308	
450	500	14.2	179	
	-500	19.5	45	
	1000	19.9	137	
	-1000	18.5	122	
590	500	2.29	163	
	-500	1.71	112	
	1000	2.29	28.2	-626
	-1000	2.12	26.3	
294	500	1.93	8.1	
	-500	2.04	7.1	
	1000	1.87	1.7	-10
	-1000	1.83	12.1	

Reran 450K and 590K because of improved stability at 294K

450	500	2.50	46	
	-500	2.32	19.4	
	1000	1.38	57	-1353
	-1000	3.02	27	
590	500	2.80	37	
	-500	2.23	36	
	1000	1.43	116	-1838
	-1000	2.72	58	

GAGE NUMBER A2A-1

Temperature (K)	Strain (x 10^6)	Gage Factor	2σ (Percent)	Drift μΩ/Ω
294	500	2.06	0	
	-500	2.05	1.4	
	1000	2.08	0.2	-105
	-1000	1.97	1	
450	500	2.03	18.3	
	-500	1.68	55	
	1000	2.10	15.3	84
	-1000	1.74	44	
590	500	2.18	10.7	
	-500	2.13	14.2	
	1000	2.47	38	604
	-1000	2.28	20	
294	500	2.05	0.3	
	-500	1.93	0.8	
	1000	2.04	0.5	0
	-1000	1.93	0.7	

GAGE NUMBER A2A-2

Temperature (K)	Strain (x 10^6)	Gage Factor	2σ (Percent)	Drift μΩ/Ω
294	500	1.91	0.2	
	-500	1.24	286	
	1000	0.32	399	-202
	-1000	3.72	114	
450	500	2.00	9.3	
	-500	1.93	10	
	1000	2.05	5.5	-169
	-1000	2.16	3.4	
590	500	1.99	13.3	
	-500	2.06	14.3	
	1000	2.11	28.3	2748
	-1000	2.13	18.9	
294	500	2.08	16.8	
	-500	2.12	5.2	
	1000	1.92	5.1	-6
	1000	1.91	3.5	

GAGE NUMBER A7-1

Temperature (K)	Strain (x 10^6)	Gage Factor	2σ (Percent)	Drift μΩ/Ω
296	500	1.92	16.7	
	-500	1.74	7.2	
296	500	1.91	5.8	
	-500	1.72	9.8	
296	500	1.93	7.5	
	-500	1.66	13.7	

Gage grid open circuit on first cycle to 1000 x 10^-6 strain.

GAGE NUMBER A7-2

Temperature (K)	Strain (x 10^6)	Gage Factor	2σ (Percent)	Drift μΩ/Ω
296	500	6	54	
	-500	0.6	305	
296	500	22	76	
	-500	8	117	
296	500	26	80	
	-500	3	193	

Gage grid open circuit on first cycle to 1000 x 10^-6 strain.

GAGE NUMBER A8A-1

Temperature (K)	Strain (x 10^6)	Gage Factor	2σ (Percent)	Drift μΩ/Ω
294	500	2.02	3	
	-500	1.96	3.2	
	1000	1.76	36	-214
	-1000	2.00	25.7	
450	500	2.17	14.5	
	-500	2.09	4.3	
	1000	2.09	4.3	-12
	-1000	2.23	2.9	
590	500	2.17	20.2	
	-500	2.15	5.5	
	1000	2.20	8.5	375
	-1000	2.13	2.8	
294	500	1.57	89	
	-500	2.59	29.3	
	1000	0.68	176	-220
	-1000	0.88	101	

GAGE NUMBER A8A-2

Temperature (K)	Strain (x 10^6)	Gage Factor	2σ (Percent)	Drift μΩ/Ω
294	500	1.93	7.9	
	-500	1.90	0.9	
	1000	1.97	0.3	4
	-1000	1.89	0.9	
450	500	2.14	37	
	-500	2.03	28	
	1000	2.06	17.4	251
	-1000	1.99	9.1	
590	500	2.15	10.5	
	-500	2.11	8.1	
	1000	2.15	16.1	1226
	-1000	2.10	14.8	
294	500	1.99	2.1	
	-500	1.37	1.5	
	1000	2.07	21.1	-194
	-1000	2.05	41	

C-1

GAGE NUMBER B16-1

Temperature (K)	Strain (x 10^6)	Gage Factor	2σ (Percent)	Drift μΩ/Ω
294	500	2.01	4.9	
	-500	1.73	0.9	
	1000	1.98	0.6	
	-1000	1.72	0.6	
450	500	2.14	9.8	
	-500	1.80	2.6	
	1000	2.07	2.2	72
	-1000	1.80	1.2	
590	500	2.07	63	
	-500	1.90	63	
	1000	2.23	31	-1897
	-1000	2.41	68	
	*			
294	500	1.39	60	
	-500	2.88	15.4	
	1000	1.13	19.6	-187
	-1000	4.08	10.9	

GAGE NUMBER B16-2

Temperature (K)	Strain (x 10^6)	Gage Factor	2σ (Percent)	Drift μΩ/Ω
294	500	2.02	4.3	
	-500	1.82	4.3	
	1000	2.00	2.1	
	-1000	1.77	1	
450	500	2.15	6.1	
	-500	1.85	4.8	
	1000	2.11	5.4	157
	-1000	1.88	6.1	
590	500	1.75	167	
	-500	2.19	154	
	1000	1.59	152	-810
	-1000	1.77	12.2	
	*			
294	500	2.04	1.6	
	-500	1.84	1.7	
	1000	1.99	3.2	-134
	-1000	1.88	0.4	

* Lead wire attachments repaired

GAGE NUMBER C17-1

Temperature (K)	Strain (x 10^6)	Gage Factor	2σ (Percent)	Drift μΩ/Ω
294	500	1.36	33	
	-500	2.17	22	
	*			
294	500	1.83	21	
	-500	2.18	22.5	
	1000	1.85	6.1	
	-1000	1.97	5.7	
294	500	1.84	2.8	
	-500	2.01	2.4	
	1000	1.95	4.4	
	-1000	1.95	2.3	
590	500	1.99	18.1	
	-500	2.55	20.8	
	1000	2.51	33.9	
	-1000	2.80	63	
920	500	.004	115	
	-500	.008	67	
	*			
294	500	2.05	8.1	
	-500	1.97	11.6	
	1000	1.96	5	
	-1000	1.75	9.5	
590	500	2.50	14.3	
	-500	1.85	21.3	
	1000	2.27	6.8	
	-1000	2.00	11	
920	500	3.5	64	
	-500	2.9	34	
	1000	3.0	30	
	-1000	3.6	71	
294	500	1.95	1	
	-500	1.97	6.1	
	1000	1.82	2	
	-1000	1.80	2.9	

* Lead wire attachments repaired

NOTE: NO DRIFT DATA

GAGE NUMBER C17-2

Temperature (K)	Strain (x 10^6)	Gage Factor	2σ (Percent)	Drift μΩ/Ω
294	500	1.87	36	
	-500	2.15	138	
	*			
294	500	2.86	2.1	
	-500	1.64	5.3	
	1000	2.43	10	
	-1000	1.68	3.6	
294	500	2.28	10.9	
	-500	2.06	10.5	
	1000	2.44	0.8	
	-1000	1.82	2.8	
590	500	2.17	4	
	-500	1.98	9.1	
	1000	900	200	
	-1000	500	350	
920	500	140	118	
	-500	57	132	
	#			

Lead wire attachments not repairable

NOTE: NO DRIFT DATA

GAGE NUMBER C18-1

Temperature (K)	Strain (x 10^6)	Gage Factor	2σ (Percent)	Drift μΩ/Ω
294	500	1.90	1	
	-500	1.91	0.4	
	1000	1.92	2	
	-1000	1.94	3.3	
590	500	2.19	11	
	-500	2.16	0.9	
	1000	2.25	5.3	
	-1000	2.01	6.7	
920	500	1.64	15.2	
	-500	1.71	55	
	1000	2.04	21.8	< 5
	-1000	1.89	63	
294	500	1.57	9	
	-500	1.63	0.8	
	1000	1.21	33	
	-1000	1.05	98	
294	500	1.87	22.7	
	-500	0.82	3.3	
	1000	1.91	4.4	
	-1000	0.26	139	

GAGE NUMBER C18-2

Temperature (K)	Strain (x 10^5)	Gage Factor	2σ (Percent)	Drift μΩ/Ω
294	500	1.08	92	
	-500	1.71	153	
	1000	1.98	4.1	
	-1000	2.05	25.5	
590	500	1.41	136	
	-500	4.35	12.8	
	1000	2.77	38	
	-1000	1.91	110	
920	500	1.87	34	
	-500	2.10	63	
	1000	1.91	16.6	<5
	-1000	2.25	64	
294	500	1.57	4.1	
	-500	1.94	66	
	1000	1.71	13.3	
	-1000	1.72	10.8	
294	500	1.70	89	
	-500	1.33	107	
	1000	1.95	12	
	-1000	1.89	71	

GAGE NUMBER C23-1

Temperature (K)	Strain (x 10^6)	Gage Factor	2σ (Percent)	Drift μΩ/Ω
294	500	1.93	0.8	
	-500	1.92	0.8	
	1000	1.96	1.2	<5
	-1000	1.93	0.7	
590	500	2.18	16.5	
	-500	2.15	13.4	
	1000	2.07	10	<5
	-1000	2.00	10.1	
920	500	1.41	102	
	-500	1.36	87	
	1000	4.47	126	<5
	-1000	2.13	43	

**

GAGE NUMBER C23-2

Temperature (K)	Strain (x 10^6)	Gage Factor	2σ (Percent)	Drift μΩ/Ω
294	500	1.82	4	
	-500	1.89	0.1	
	1000	1.86	0.2	<5
	-1000	1.90	0.2	
590	500	1.99	10.3	
	-500	2.10	9.5	
	1000	2.02	8.9	<5
	-1000	2.03	3.8	
920	500	7.7	139	
	-500	2.59	116	
	1000	1.93	171	<5
	-1000	2.49	100	

**

** Gage grid found open after cooling

GAGE NUMBER C24-1

Temperature (K)	Strain (x 10^6)	Gage Factor	2σ (Percent)	Drift μΩ/Ω
294	500	6.5	67	
	-500	6.1	88	
	1000	4.7	224	<5
	-1000	6.1	113	
590	500	3.02	133	
	-500	2.57	167	
	1000	37	85	<5
	-1000	1.83	71	
294	500	1.67	25.1	
	-500	1.83	16.1	
	1000	2.08	19.4	<5
	-1000	1.69	3.6	
294	500	1.86	.3	
	-500	1.83	1.1	
	1000	1.86	0.7	<5
	-1000	1.84	2.9	
590	500	1.87	15.1	
	-500	1.72	22.8	
	1000	1.89	2.9	<5
	-1000	1.32	4.2	
920	500	6	89	
	-500	75	290	
	1000	5	260	<10
	-1000	4	210	
294	500	68	314	
	-500	70	92	
		*		
294	500	1.88	8.2	
	-500	2.02	2.5	
	1000	1.78	2.3	<5
	-1000	2.00	5.2	

* Lead wire attachments repaired

GAGE NUMBER C24-2

Temperature (K)	Strain (x 10^6)	Gage Factor	2σ (Percent)	Drift μΩ/Ω
294	500	1.83	3.5	
	-500	1.877	3.6	
	1000	470	346	<5
	-1000	960	197	
590	500	0.1	172	
	-500	2700	200	
	1000	0	173	<5
	-1000	1400	200	
		*		
294	500	0		
	-500	0		
	1000	0		<5
	-1000	0		
		*		
294	500	1.91	2.3	
	-500	1.98	1.4	
	1000	1.91	1.8	<5
	-1000	1.92	1.3	
590	500	1.93	6.5	
	-500	1.94	4.6	
	1000	1.94	3.9	<5
	-1000	1.98	0.9	
920	500	5	57	
	-500	1.67	106	
	1000	8	148	<10
	-1000	5	159	
		≠		

* Lead wire attachments repaired
≠ Lead wire attachments not repairable

GAGE NUMBER D21-1

Temperature (K)	Strain (x 10^6)	Gage Factor	2σ (Percent)	Drift μΩ/Ω
294	500	2.34	11.8	
	-500	1.29	17.9	
	1000	2.12	13.8	62
	-1000	1.43	19.9	
590	500	##		

GAGE NUMBER D21-2

Temperature (K)	Strain (x 10^6)	Gage Factor	2σ (Percent)	Drift μΩ/Ω
294	500	1.81	2.7	
	-500	1.82	11.8	
	1000	2.25	61	4
	-1000	.6	800	
590	500	##		

Fluctuating resistance at lead wire attachments at 590K; not repairable

GAGE NUMBER D31-1

Temperature (K)	Strain (x 10^6)	Gage Factor	2σ (Percent)	Drift μΩ/Ω
294	500	1.91	4.5	
	-500	2.00	15.6	
	1000	1.94	0.4	< 5
	-1000	1.90	0.4	
590	500	2.01	1.5	
	-500	1.95	1.9	
	1000	2.00	3.9	< 5
	-1000	1.97	2.1	
920	500	4.28	134	
	-500	3.15	182	
	1000	3.81	143	< 5
	-1000	2.99	126	
		*		
294	500	1.90	6.1	
	-500	1.73	55	
	1000	1.87	1.3	< 5
	-1000	1.90	3.5	
294	500	1.80	0.6	
	-500	1.99	1.4	
294	500	1.89	4.3	
	-500	1.99	2.4	
	1000	1.89	2	< 20
	-1000	1.99	4.1	

* Lead wire attachment repaired

GAGE NUMBER D31-2

Temperature (K)	Strain (x 10^6)	Gage Factor	2σ (Percent)	Drift μΩ/Ω
294	500	1.76	6.5	
	-500	1.88	5.7	
	1000	2.13	12.1	< 5
	-1000	1.86	13.6	
590	500	1.90	4.8	
	-500	1.80	5.3	
	1000	2.30	87	< 5
	-1000	3.94	146	
920	500	1.23	46	
	-500	1.59	84	
	1000	1.46	27.6	< 5
	-1000	1.71	27.3	
294	500	.01	149	
	-500	3500		
	1000	12	191	< 5
	-1000	37	265	
294	500	.01	148	
	-500	.02	44	
		*		
294	500	2.00	3.5	
	-500	1.80	12.9	
	1000	2.01	1.7	< 5
	-1000	1.57	50	

* Lead wire attachment repaired

GAGE NUMBER E33-1

Temperature (K)	Strain (x 10^6)	Gage Factor	2σ (Percent)	Drift μΩ/Ω
294	500	2.16	8.0	
	-500	2.14	12.3	
	1000	3.53	142	
	-1000	3.29	113	
		*		
294	500	1.86	4.3	
	-500	1.58	4.5	
	1000	2.08	12.8	< 5
	-1000	1.60	2	
590	500	1.81	19.3	
	-500	1.49	16.1	
	1000	2.11	44	< 5
	-1000	1.61	5.1	
920	500	1.50	18.3	
	-500	1.39	18.3	
	1000	1.50	14.7	< 5
	-1000	1.39	3.3	
294	500	1.61	0.5	
	-500	1.35	0.5	
	1000	1.63	8.5	< 5
	-1000	1.38	0.7	
294	500	1.39	0.7	
	-500	1.36	0.6	
	1000	1.41	5.3	< 5
	-1000	1.36	1.4	

* Lead wire attachment repaired

GAGE NUMBER E33-2

Temperature (K)	Strain (x 10^6)	Gage Factor	2σ (Percent)	Drift μΩ/Ω
294	500	2.05	120	
	-500	3.19	13.8	
	1000	3.56	105	
	-1000	4.82	148	
		*		
294	500	2.00	31	
	-500	1.84	8.2	
	1000	1.72	29.2	<5
	-1000	1.99	19.4	
590	500	3.61	55	
	-500	0.97	58	
	1000	2.67	67	<5
	-1000	1.79	67	
920	500	1.36	51	
	-500	1.71	19.7	
	1000	1.42	51	<10
	-1000	1.55	3	
294	500	1.89	98	
	-500	1.22	1.6	
	1000	1.36	1.9	<5
	-1000	1.25	2.5	
294	500	3.08	68	
	-500	0.92	29.1	
	1000	1.34	48	<5
	-1000	3.96	16.9	

* Lead wire attachment repaired

GAGE NUMBER E36-1

Temperature (K)	Strain (x 10^6)	Gage Factor	2σ (Percent)	Drift μΩ/Ω
294	500	1.92	6.8	
	-500	2.29	8.9	
	1000	2.99	21.3	
	-1000	5.83	60	
		*		
294	500	1.71	3.6	
	-500	2.34	5.9	
	1000	1.58	4.4	
	-1000	3.08	18.4	
590	500	1.88	12.8	
	-500	2.29	63	
	1000	1.89	6.6	
	-1000	2.86	74	
1090	500	1.49	55	
	-500	1.38	76	
	1000	1.60	25.3	775
	-1000	1.10	59	
294	500	1.46	1.1	
	-500	1.81	0.1	
	1000	1.66	1.5	
	-1000	1.54	0.6	
294	500	3.07	50	
	-500	2.85	44	
	1000	2.51	6.1	
	-1000	3.08	43	

* Lead wire attachment repaired

GAGE NUMBER E36-2

Temperature (K)	Strain (x 10^6)	Gage Factor	2σ (Percent)	Drift μΩ/Ω
294	500	2.05	10.1	
	-500	2.69	12.1	
	1000	3.10	25.3	
	-1000	6.69	57	
		*		
294	500	1.70	6.4	
	-500	2.47	7.4	
	1000	1.55	5.7	
	-1000	3.38	19.3	
590	500	1.70	10.1	
	-500	2.27	65	
	1000	1.72	2.2	
	-1000	2.89	80	
1090	500	1.17	62	
	-500	1.14	63	
	1000	3.10	131	250
	-1000	1.39	55	
294	500	1.19	0.5	
	-500	1.48	1	
	1000	1.35	1.7	
	-1000	1.34	0.8	
294	500	1.54	0.6	
	-500	1.54	0.1	
	1000	1.54	0.1	
	-1000	1.54	0.2	

* Lead wire attachment repaired

REFERENCES

1. Burger, H. C., and VanCitter, P. H., "Preparation of Bismuth-Antimony Vacuum Thermal Elements by Vaporization", Z. Phys., V. 66, 1930, p. 210.

2. Harris, L. and Johnson, E. A., "Technique for Sputtering Sensitive Thermocouples", Rev. Sci. Inst., 5, 1934, p. 153.

3. Benderskey, D., "A Special Thermocouple for Measuring Transient Temperatures", Mech. Engr., 1953, 75, 117.

4. Grant, H. P., Przybyszewski, J. S., and Claing, R. G., "Turbine Blade Temperature Measurements Using Thin Film Temperature Sensors", NASA CR-165201, March 17, 1981.

5. Dils, R. R. and Follansbee, P. S., "High Temperature Sputtered Surface Sensors", ISA, April, 1975, 21st International Instrumentation Symposium, Philadelphia.

6. Dils, R. R. and Follansbere, P. S., "Superalloy Sensors", presentation at the Third International Symposium on Superalloys, Seven Springs, PA, Sept. 1976.

7. Vossen, J. L. and O'Neill, J. J., "R-F Sputtering Processes", RCA Review, RCA Laboratories, Princeton, N. J., 29 (2) (1968).

8. Haag, F. K., "Development of a Sputtered Thin Film Pressure Transducer for Use Over the Temperature Range of $-320°F$ to $500°F$", ISA Instrumentation Symposium, Las Vegas, May 1977.

9. Liebert, C. H., Mazaris, G. A., and Brandhorst, H. W., "Turbine Blade Metal Temperature Measurement with a Sputtered Thin Film Chromel-Alumel Thermocouple", NASA TMX-71844 (1975).

10. Pratt, I. H., "On Al_2O_3", Thin Solid Films, 3, R23-R26 (1969).

11. Milek, J. T., "Aluminum Oxide Data Sheets", DSA AD 434173.

12. Lochman, R. E. and Dehoff, R., "Electrical Properties of Polycrystalline Ceramic Insulators", Contract N00014-75-C-0888, Florida University, (AD-A053609), Feb. 1978.

13. Milek, J. T., "Silicon Nitride for Microelectronic Applications, Part 2", Handbook of Electronic Materials, v. 6, Plenum, 1972.

14. Hu, S. M., "On Silicon Nitride" J. Electrochemical Soc., v. 113, pp. 7, 693-697 (1966).

15. Bohg, A., "Measurement of Stresses in (Si_3N_4) Thin Films on Single Crystalline Substrates", phys. stat. sol. (a) 46, 445 (1978).

16. Bowen, H. K., "Ceramics as Electrical Materials", M.I.T. Dept. of Materials Sci. and Engrg., V. 5, p. 310.

REFERENCES - (Continued)

17. Fuschillo, N. and Lindberg, P. A., "Electrical Conductors at Elevated Temperatures", ASTIA ASD-TDR-62-481, 456 pages, 1963.

18. Bertodo, P., "Platinum Metal Alloys for the Measurement of Strains at High Temperature", Engelhard Industries Tech. Bulletin, v. 9, n. 2, pp. 37-49, 1968.

19. Easterling, K. E., "High Temperature Resistance Temperature Strain Gages", British Journal of Applied Physics, 1963.

20. Bray, A. and Calcatelli, A., "Vacuum Deposited Films at High Temperatures", Instruments and Control Systems, p. 121, Nov. 1966.

21. Pitts, J. W. and Moore, D. G., "Development of High Temperature Strain Gages", NBS Monograph 26 (96).

22. Weise, R. A. and Foster, J. H., "High Temperature Strain Gage System for Application to Turbine Engine Components, AFWAL-TR-8002126, Jan. 1981.

23. Lemcoe, M. M., "Development of Electrical Resistance Strain Gage System for Use to 2000°F", ISA Paper 75-572, 1975.

24. Weast, R. C., Handbook of Chemistry and Physics, The Chemical Rubber Co., 48th Ed., p. F132, 1967.

25. Marks, L. S., Mechanical Engineers Handbook, McGraw Hill, p. 588, 1951.

26. Alloy Handbook of Electrical Resistance, Wilbur B. Driver Co.

27. Betteridge, W., Nickel and Its Alloys, MacDonald and Evans 1977.

28. Properties of Metals and Alloys, Sigmund Cohn Corporation, Technical Bulletin, 1966.

29. Woldman, N. E., Engineering Alloys, Reinhold, N.Y., 1954.

30. Savitsky, E. M., The Influence of Temperature on the Mechanical Properties of Metals and Alloys, Stanford University Press, 1961.

31. Mooij, J. H., "Electrical Conduction in Concentrated Disordered Transition Metal Alloys", phys. stat. sol. (a) 17, 521, 1973.

32. Masumoto, H., Skowkachi, S., and Michio, K., "Elinvar Properties of Mn-Pt Alloys", Trans. J. I. M., v. 19, pp. 390-394, 1978.

33. Elliott, R. P., Constitution of Binary Alloys, First Supplement, McGraw Hill Book Co., New York, 1965.

34. Hansen, M., Constitution of Binary Alloys, McGraw Hill Book Co., New York, 1958.

35. Moffatt, W. G., Binary Phase Diagrams Handbook, General Electric Co., Business Growth Services, Schnectady, New York, 1976.

36. Shunk, F. A., Constitution of Binary Alloys, Second Supplement, McGraw Hill Book Co., New York, 1969.

37. Teed, P. L., "The Influence of Metallographic Structure on Fatigue", Fatigue and Fracture of Metals: A Symposium, The Technology Press of M.I.T., 1950.

38. Gensamer, M., "General Survey of the Problem of Fatigue and Fracture", Fatigue and Fracture of Metals: A Symposium, The Technology Press of M.I.T., 1950.

39. Samons, C. H., Engineering Metals and Their Alloys, MacMillan, 1950.

END

DATE

Dec, 1987

CONTRACT REPORT DISTRIBUTION LIST

Instrumentation R&D Branch

Each addresses will receive one copy unless indicated otherwise.

NASA Lewis Research Center
21000 Brookpark Road
Cleveland, OH 44135
   Attn: Frank G. Pollack,
       M.S. 77-1
   (50) Copy #'s 1-50

NASA Lewis Research Center
21000 Brookpark Road
Cleveland, OH 44135
   Attn: Leonard W. Schopen,
       M.S. 501-11
       Copy # 51

NASA Scientific and Technical
   Information Facility
P.O. Box 8757
B.W.I. Airport, Maryland 21240
   Attn: Acquisitions Branch
   (22) Copy #'s 52-73

NASA Lewis Research Center
21000 Brookpark Road
Cleveland, OH 44135
   Attn: Library, M.S. 60-3
   (2) Copy #'s 74-75

NASA Lewis Research Center
21000 Brookpark Road
Cleveland, OH 44135
   Attn: Report Control Office,
       M.S. 60-1
       Copy # 76

General Electric Company
Aircraft Engine Group
Evendale, OH 45215
   Attn: Wayne Shaffernocker, MSH-78
       Ronald Weise, MSH-78
       William Stowell
       Copy # 77

Stanford University
Stanford, CA 94305
   Attn: Dr. R. J. Moffat
       Asst. Prof, Mech, Engr.
       Dir. Thermoscience
         Measurement Center
       Copy # 78

Air Force Wright Aeronautical
   Laboratory
Wright Patterson AFB, OH 45433
   Attn: R. Cox/POTC
       Copy # 79

Air Force Wright Aeronautical
   Laboratory
Wright Patterson AFB, OH 45433
   Attn: Everett E. Bailey/AFWAL/NASA-P
       Copy # 80

Air Force Wright Aeronautical
   Laboratory
Wright Patterson AFB, OH 45433
   Attn: William Stange/POTC
       Copy # 81

Air Force Wright Aeronautical
   Laboratory
Wright Patterson AFB, OH 45433
   Attn: M. Roquemore/POSF
       Copy # 82

UTRC/OATL
Palm Beach Gardens Facility
West Palm Beach, FL 33402
   Attn: John T. Carroll
       Bldg. 30 (MS R-23)
       Copy # 83

Lewis Engineering Company
238 Wate Street
Naugatuck, CT 06770
   Attn: C. B. Stegner
       Copy # 84

Arnold Engineering
  Development Center
Arnold Air Force Station, TN 37389
    Attn: Marshall Kingery
        Copy # 85

Hitec Corporation
Nardone Industrial Park
Westford, MA 01886
    Attn: Steve Wnuk
        Copy # 86

General Electric Company
Aircraft Engine Group
1000 Western Avenue
Lynn, MA 01910
    Attn: George Leperch, A129dD
        Copy # 87

General Electric Company
Aircraft Equipment Division
50 Fordham Road
Wilmington, MA 01887
    Attn: Ronald J. Casagrande
        Copy # 88

Allison Gas Turbine Operations
General Motors Corporation
Box 894
Indianapolis, IN 46206
    Attn: John Custer, W-16
        Copy # 89

Allison Gas Turbine Operations
General Motors Corporation
Box 894
Indianapolis, IN 46206
    Attn: Ken Cross
        Copy # 90

Allison Gas Turbine Operations
General Motors Corporation
Box 894
Indianapolis, IN 46206
    Attn: David Willis
        Copy # 91

Allison Gas Turbine Operations
General Motors Corporation
Box 894
Indianapolis, IN 46206
    Attn: Ralph Fox
        Copy # 92

Battelle Columbus Laboratories
505 King Avenue
Columbus, OH 43201
    Attn: Ross G. Luce, Energy &
              Thermal Tech. Section
        Copy # 93

Teledyne CAE
1350 Laskey Road
Toledo, OH 43612
    Attn. R. Hugh Gaylord
              Joseph Pacholec
        Copy # 94

Garrett Turbine Engine Company
P.O. Box 5217
Phoenix, AZ 85010
    Attn: N. Fred Pratt
        Copy # 95

Fluidyne Engr. Corporation
5900 Olson Memorial Highway
Minneapolis, MN 55422
    Attn: T. Matsuura
        Copy # 96

AVCO Corporation
Lycoming Division
550 South Main Street
Stratford, CT 06497
    Attn: E. Twarog, Mgr.
              Electronics and Instr.
        Copy # 97

Thermonetics Corporation
1028 Garnet Avenue
San Diego, CA 92109
    Attn: H. F. Poppendiek
        Copy # 98

Battelle Columbus Laboratories
505 King Avenue
Columbus, OH 43201
    Attn: M. M. Lemcoe
        Copy # 99

Peter K. Stein
5602 East Monterosa
Phoenix, AZ 85018
Copy # 100

Pratt & Whitney
Main Plant
P.O. Box 2691
West Palm Beach, FL 33402
    Attn: John Prosser (MS C-04)
           William Watkins
           Copy # 101

National Bureau of Standards
Washington, DC 20234
    Attn: Ken Kreider
           Copy # 102

National Bureau of Standards
Washington, DC 20234
    Attn: George Burns
           Inst. for Basic Research
           Copy # 103

General Electric Company
P.O. Box 8
Schenectady, NY 12301
    Attn: Dr. David Skelley
           Bldg. K-1, Rm. 3B24
           Copy # 104

Mechanical Technology, Inc.
968 Albany-Shaker Road
Latham, NY 12110
    Attn: R. Hohenberg
           Copy # 105

Boeing Aerospace Company
Engineering Laboratories
Seattle, WA 98124
    Attn: Darrell R. Harting
           Copy # 106

Engelhard
Engelhard Industries Div.
228 East 10th Street
Newport, KY 41075
    Attn: Ronald G. Braun
           Copy # 107

Williams International
2280 West Maple Road
Walled Lake, MI 48088
    Attn: Henry Moore, Head
           Instr. Dept.
           J. H. Johnston
           Copy # 108

Virginia Polytechnic Institute
  and State University
Mechanical Engineering Dept.
Blacksburg, VA 24061
    Attn: W. F. O'Brien, Jr.
           Copy # 109

Naval Post Graduate School
Department of Aeronautics (Code 67)
Monterey, CA 93940
    Attn: Prof. R. P. Shreeve
           Copy # 110

Pennsylvania State University
233 Hammond Building
University Park, PA 16802
    Attn: Prof. B. Lakshminarayana
           Copy # 111

Kulite Semiconductor Products, Inc.
1039 Hoyt Avenue
Ridgefield, NJ 07657
    Attn: John R. Hayer
           Copy # 112

Bolt Beranek and Newman, Inc.
50 Moulton Street
Cambridge, MA 02138
    Attn: Richard E. Hayden
           Copy # 113

Caterpillar Tractor Company
Technical Center, Building F
100 Northeast Adams Street
Peoria, IL 61629
    Attn: Mr. Donald Wilson
           Copy # 114

Air Force Wright Aeronautical
  Laboratory
Wright Patterson AFB, OH 45433
    Attn: Mr. Charles Bentz/POTC
          Hot Section Technology
          Copy # 115

AVCO Corporation
Lycoming Division
550 South Main Street
Stratford, CT 06497
    Attn: Mr. K. Collinge
          IRAD Mechanical Projects
          Manager
          Copy # 116

Eaton Corporation
Box 766
Southfield, MI 48037
    Attn: Mr. Lamont Eltinge
          Director of Research
          Copy # 117

Public Service Electric & Gas Company
80 Park Plaza
Newark, NJ 07101
    Attn: Dr. Melvin L. Zwillenberg
          Research & Development Dept.
          Copy # 118

Raychem Corporation
300 Constitution Drive
Menlo Park, CA 94025
    Attn: Dr. David C. Chappelear
          Director of Corporate
            Research & Development
          Copy # 119

Fabrication Development Laboratory
Owens/Corning Fiberglas
Technical Center
Granville, OH 43023
    Attn: Mr. Hugh W. Bradley, Jr.
          Copy # 120

Xerox Electro-Optical Systems
1616 North Fort Myer Drive, 16th Floor
Arlington, VA 22209
    Attn: Mr. Clifford I. Cummings
          Manager, Intelligence &
            Reconnaissance
          Copy # 121

Construction Materials Support Group
Owens/Corning Fiberglas
CMG Process Technology Laboratory
Granville, OH 43023
    Attn: Mr. J. W. Scott
          Copy # 122

NASA Headquarters
Washington, DC 20546
    Attn: M/Paul N. Herr
          Copy # 123

Massachusetts Institute of Technology
Cambridge, MA 02139
    Attn: Dr. Alan Epstein
          Rm. 31-266
          Copy # 124

Sverdrup (AEDC)
Arnold AFB, TN 37389
    Attn: Paul McCarty
          Copy # 125

Rosemont, Inc.
Mail Stop F-15
P.O. Box 959
Burnsville, MN 55337
    Attn: Mr. Larry N. Wolfe
          Copy # 126

Thermogage, Inc.
330 Allegany Street
Frostburg, MD 21532
    Attn: Charles E. Brookley
          Copy # 127

Hycal Engineering
12105 Los Nietos Road
Sante Fe Springs, CA 90670
    Attn: William Clayton
          Copy # 128

Medtherm Corporation
P.O. Box 412
Huntsville, AL 35804
    Attn: Larry Jones
        Copy # 129

Rocketdyne
6633 Canoga Avenue
Canoga Park, CA 91304
    Attn: Dr. John C. Lee
        Copy # 130

Combustion Engineering
Dept. 9005-03D1
Windsor, CT 06095
    Attn: John Fishburn
        Copy # 131

RdF Corporation
23 Elm Avenue
Hudson, NH 03051
    Attn: Frank Hines
        Copy # 132

Babcock & Wilcox R&D Division
P.O. Box 835
Alliance, OH 44601
    Attn: Harold Wahle
        Copy # 133

JEC Lasers, Inc.
253 Crooks Avenue
Patterson, NJ
    Attn: Mr. John Wasko
        Copy # 134

NASA Langley Research Center
Hampton, VA 23665
    Attn: R. E. Wright, JR, (MS-234)
           S. L. Ocheltree (MS-235A)
        Copy # 135

Babcock & Wilcox R&D Division
P.O. Box 835
Alliance, OH 44601
    Attn: John Berthold
        Copy # 136

Applied Sensors International
7834 Palace Drive
Cincinnati, OH 45242
    Attn: Richard Stillmaker
        Copy # 137

Carnegie-Mellon University
Dept. of Mechanical Engineering
Pittsburgh, PA 15213
    Attn: Dr. Norman Chigier
        Copy # 138

Calspan Field Services, Inc./AEDC Div.
Arnold Air Force Station, TN 37389
    Attn: C. T. Kidd
        Copy # 139

Physical Sciences Dept.
Arvin/Calspan Adv. Tech. Ctr.
Buffalo, NY 14225
    Attn: M. G. Dunn
        Copy # 140

Eaton Corporation
Electronic Instrumentation Division
(Ailtech Strain's Sensors)
5340 Alla Road
Los Angeles, CA 90066
    Attn: Howard K. Cooper
        Copy # 141

Naval Air Propulsion Test Center
Trenton, NJ 08628
    Attn: Guy Mangano/Code PE42
        Copy # 142

Internal Distribution

UTRC E. Hartford

C. O. Hulse
M.S. 24
Copy # 143

J. G. Smeggil
M.S. 22
Copy # 144

R. B. Graf
M.S. 22
Copy # 145

G. A. Peterson
M.S. 73
Copy # 146

F. A. Otter
M.S. 22
Copy # 147

E. L. Paradis
M.S. 31
Copy # 148

P&W ED-Co.

H. P. Grant
M.S. 116-01
(5) Copy #'s 149-153

W. G. Alwang
M.S. 162-29
Copy # 154

J. H. Elwood
M.S. 162-29
Copy # 155

J. S. Przybyszewski
M.S. 165-46
Copy # 156

R. G. Claing
M.S. 165-46
Copy # 157

W. L. Anderson
M.S. 116-01
Copy # 158

H. J. Kocar
M.S. 118-19
Copy # 159

AFPRO/TM
104-08
Copy # 160